

Modelling and Analysis of Individual Animal Movement

Joseph David Bailey



A thesis submitted for the degree of Doctor of Philosophy in Mathematical Biology

Department of Mathematical Sciences

University of Essex

December 2019

Abstract

Movement is ubiquitous to almost all life with most individuals undergoing some spatial change across their lifespans. Understanding how and why animals move through and interact with their environment is therefore key in understanding some of the most open and pressing questions in science; from the effects of climate and environmental change on local species, to preventing the spread of disease and infection.

In this Thesis we show how theoretical approaches to modelling individual animal movement can lead to a better understanding of the processes behind movement. By using the framework of random walk (RW) theory we analyse observed movement data to predict and interpret movement behaviour of individuals.

Chapters 2 and 3 introduce the field of Movement Ecology and concentrate on recent developments within the subject along and include derivations of key mathematical properties of RW theory which will be the analytical framework for analysing movement used throughout the Thesis. Chapter 4 uses a biased and correlated random walk (BCRW) as a model of individual animal movement to demonstrate efficiency in navigation. Chapter 5 explores the variation in movement of individual ground beetles (*Poecilus cupreus*) and demonstrates how this variation effects predictions of important population level movement dynamics, such as the expected displacement. Chapter 6 demonstrates that a highly peaked, heavy-tailed distribution found in the distribution of turning angles across an individual's movement path can arise from the mixing of two distinct normal-type distributions, and provides an example of how this can indicate the presence of multiple behaviours in the movement path. Finally, Chapter 7 considers how animal 'personality' can effect individual movement behaviour by considering the movement of stickleback fish (*Gasterosteus aculeatus*) across three differing experimental environments.

Declaration

The work in this Thesis is based on research carried out at the Department of Mathematical Sciences, University of Essex. No part of this thesis has been submitted elsewhere for any other degree or qualification, and unless referenced to the contrary in the text it is all work of the author.

Acknowledgements

There are many people without whom this work would neither have been possible nor enjoyable and whilst listing them all would make this work even longer, there are some who require a special mention.

All the members of the Department of Mathematical Sciences at the University of Essex who have made working in the department a welcome experience. With a special mention for Chris Antonopolous for his input during the Supervisory Board meetings and also for all the members of the Admin team who are always on hand to hep out a flagging research student, regardless of how inane a question or request might be.

Friends and family who have encouraged me through the tough periods of research and the seemingly never ending writing-up, and who have also listened patiently whilst I talked at great length about recent findings or problems.

Much of this thesis has greatly benefited from input from external collaborators all of whom have helped inform this body of work; Carly Benefer, Rod Blackshaw, Jamie Wallis and Andrew King.

None of this would have been possible without receiving funding from the Department Doctoral Scholarship, for which I am incredibly grateful and to the scholarship committee for taking a chance on my application.

Finally, and most importantly, a thank you to Edd for his supervision. Simply put there is nothing more one could ask for in a Supervisor.

Contents

Contents	iv
List of Figures	x
List of Tables	xiv
List of Initialisations	xvi
1 Introduction	1
1.1 Movement Ecology Overview	1
1.2 Thesis Objectives and Structure	3
2 Historical background and foundations of Mathematical Ecology	5
2.1 Historical Background	5
2.2 Modern Movement Ecology	5
2.3 Movement Data Capture	7
2.4 Mathematical Tools	10
2.4.1 Continuous Time Models	11
2.4.2 Discrete Time Models	12
2.5 Use of Random Walks in Animal Movement	13
2.6 RW as a ‘step-and-turn’ Process	15
2.7 Extensions to SRW, CRW and BRW models	17
2.7.1 Biased & Correlated Random Walk	17
2.7.2 Lévy Walk	18
2.8 Common Descriptive Characteristics of RW Paths	19
2.9 Limitations of RW Theory in Movement Analysis	21
3 Mathematics of Random Walks	24
3.1 Simple Random Walk	25
3.1.1 SRW in Discrete Time and Space	25

3.1.2	SRW in Higher Dimensions	28
3.2	Biased Random Walk	29
3.2.1	BRW in Higher Dimensions	29
3.3	Correlated Random Walk	33
3.3.1	CRW in Higher Dimensions	35
3.4	Diffusion, sub-diffusion and super-diffusion	39
3.5	Circular Statistics and Distributions	40
3.6	Circular Data	40
3.7	Circular Distributions	41
3.7.1	Wrapped Distributions	41
3.7.2	Non-Wrapped Distributions	43
3.8	Trigonometric moments	44
4	Navigational efficiency in a biased and correlated random walk model of individual animal movement	47
4.1	Introduction	48
4.2	Mathematical model	50
4.2.1	First Analytical Approximation	52
4.2.2	Second Analytical Approximation	54
4.2.3	Maximum Efficiency and Optimal Weighting	57
4.2.4	95% Maximum Efficiency	60
4.3	Results	60
4.3.1	Comparison of analytical methods	60
4.3.2	Simulated results and comparison with analytical method	65
4.4	Discussion	69
4.5	Conclusions	75
4.6	Appendices	77
4.6.1	Appendix A1 - Eq. 4.12 has precisely one root for c_θ in the interval $[0, 1]$	77

4.6.2	Appendix A2 - Eq. 4.12 implies that the navigation efficiency, $c_\theta \rightarrow 1$ as $w \rightarrow 1$ when $c_\delta = 1$	80
4.6.3	Appendix A3 - Eq. 4.13, considered as a function of w , has precisely one turning point in $[0, 1]$ for all w, c_ϕ, c_δ	81
4.6.4	Appendix A4 - Navigational efficiency of the BCRW model with $c_\delta < 1$ is relatively unaffected by the number of steps	85
5	Walking behaviour in the ground beetle <i>Poecilus cupreus</i>: individual variation, intermittency, and dispersal potential	87
5.1	Background	87
5.2	Methods	91
5.2.1	Sample Collection	91
5.2.2	Tracking Beetle Walking Behaviour	91
5.3	Data Analysis	94
5.3.1	Initial Processing of Movement Path data	94
5.3.2	Path Analysis Measures	95
5.3.3	Statistical analysis	96
5.3.3.1	Intra- & inter- individual variation	96
5.3.3.2	Correlation in movement parameters	97
5.3.3.3	Analysis of population level movement dynamics	98
5.3.3.4	Comparison of paths as a CRW or BRW	99
5.4	Results	100
5.4.1	Basic Path Analysis Measures	100
5.4.2	Intra- and Inter-Individual Variation	101
5.4.3	Global Movement Direction	106
5.4.4	Turning Angles	107
5.4.5	Step-lengths (Instantaneous Speeds)	107
5.4.6	Intermittency (movement and non-movement bouts)	108
5.4.7	CRW v BRW Behaviour	108
5.5	Discussion	111

5.6	Conclusions	116
5.7	Appendices	117
5.7.1	Appendix B1 - Bout classification	117
5.7.2	Appendix B2 - Comparison of Summary Statistics	121
5.7.3	Appendix B3 - Complete data analysis for all sampling rates and speed thresholds	124
5.7.4	Appendix B4 - Analysis of data when including truncated bouts .	137
5.7.5	Appendix B5 - Categorisation of movement paths as a BRW or a CRW	139
6	Potential misinterpretation of directional data: apparent emergence of a heavy-tailed distribution from an underlying mixed distribution	144
6.1	Introduction	144
6.2	Background: Circular Statistics and Distributions	148
6.2.1	Symmetric Wrapped Stable Distributions	148
6.2.2	Mixed wrapped distributions	149
6.2.3	Determining between best-fit circular distributions	149
6.3	Fitting individual wrapped distributions to a mixed distribution	150
6.3.1	Statement of main claim	150
6.3.2	Demonstration of main claim	151
6.4	Results	154
6.5	Example: analysis of elephant movement	156
6.6	Discussion	158
6.7	Conclusions	162
6.8	Appendices	164
6.8.1	Appendix C1 - Alternative methods of calculating the distance between two PDFs	164
6.8.2	Appendix C2 - Considering mixed distributions formed from (i) two wrapped Cauchy distributions; (ii) a wrapped Cauchy and a wrapped normal distribution	169

6.8.3	Appendix C – Detailed Proof of Lemma 2 from the Main Text . . .	173
-------	---	-----

7	Intraspecific movement specialisations and their implications for ‘personality’ and movement ecology research	176
7.1	Introduction	176
7.2	Methods	179
7.2.1	Subjects and Housing	179
7.2.2	Behavioural Tests	180
7.2.3	Movement Data	181
7.2.4	Statistical Analyses	182
7.2.5	Movement Model	184
7.3	Results	187
7.3.1	Comparing Between Fish per Environment	187
7.3.2	Comparing Fish across Environments	188
7.3.2.1	Population Level	188
7.3.2.2	Individual level	189
7.3.3	Comparing Fish disregarding environments	192
7.3.4	Movement Model	199
7.3.4.1	Model Selection	199
7.3.4.2	Comparison between observed data and model	202
7.4	Discussion	203
7.5	Conclusions	209
7.6	Appendices	211
7.6.1	Appendix D1– Initial processing of data and population level analyses	211
7.6.2	Appendix D2 - Effect of using a different array size for determining space use	217
7.6.3	Appendix D3 - Effect of using a different value for dividing tank into regions of Free Water, Near the Wall and Near an Object	219
7.6.4	Appendix D4 - ANOVA Results between fish per environment	221

7.6.5	Appendix D5 - MANOVA Results	225
7.6.6	Appendix D6 - Movement Model Comparison and Selection	227
8	Conclusion	232
8.1	Extending the BCRW model in Chapter 4 to include group dynamics	232
8.2	Integrating animal ‘personality’ and movement ecology	233
8.3	Understanding and analysing large data sets	234
8.4	Extending the work in Chapter 6 for use in data analysis	235
9	References	237

List of Figures

2.1	Demonstrating the number of publications found on Web of Science under the keyword of “movement ecology” from 2007-2018 (Web of Science, 2019)	7
2.2	Example paths for types of random walks	15
2.3	Comparison of the final positions of different types of random walks . . .	16
2.4	Discrete movement path as a step-and-turn process	17
3.1	Calculating successive step locations using a step-and-turn process with headings taken from the positive y -axis	31
3.2	Comparison of the predicted MSD against simulations for a BRW with 300 steps.	34
3.3	Comparison of the observed MSD of a CRW against the predicted results	37
3.4	Evolution of the locations of 2D CRW as time increases	38
3.5	Comparison of the MSD for a SRW, CRW, BRW and ballistic motion . .	40
4.1	Efficiency against weighting factor comparing predictions from the first analytical model with the results of simulations for the BCRW model . .	55
4.2	Efficiency against weighting factor comparing predictions from the second analytical model with the results of simulations for the BCRW model . .	58
4.3	Directly comparing the results from Fig. 4.1 & Fig. 4.2	59
4.4	Heat maps showing the weighting factor, w , that leads to the maximum navigation efficiency, (‘optimal w ’), and the corresponding maximum navigation efficiency	61
4.5	Plots showing the weighting factor, w , against the error on persistence, c_δ	62
4.6	Comparing the optimal w against values of the error on navigation c_ϕ . .	66
4.7	Heat maps for the parameter space of c_ϕ and c_δ showing the absolute difference between the simulated results and the two analytical methods for both the optimal w and maximum efficiency	67
4.8	Plots demonstrating that the efficiency of the BCRW with $c_\delta < 1$ is unaffected by the number of steps	86

5.1	TrackSphere LC 300 locomotion compensator and image of an adult <i>Poecilus cupreus</i> beetle	92
5.2	Movement paths, net displacement, turning angles and global orientations of beetles.	93
5.3	Comparison of displacement, mean speed, mean cosine & number of bouts	102
5.4	Distributions of turning angles, instantaneous speeds and lengths of bouts of movement and stationarity	109
5.5	Comparison of net displacement and mean cosine of turning angles for the beetles and the predictive models	112
5.6	Demonstration of the bout classification algorithm	118
5.7	Comparison of time spent moving, bout duration & average length of bouts	122
5.8	Comparing the lengths of following bouts from the observed data against possible distributions for the distribution of bout lengths	126
5.9	Comparison of initial heading of individual trial and the final location of the trial	140
6.1	Plots demonstrating the parameter space for where a single WC or WN is the favoured distribution in comparison to a mixed distribution formed from two WN distributions	155
6.2	Movement data analysis of African elephant	159
6.3	Similar to Fig. 6.1 except using the Bhattacharyya metric	166
6.4	Similar to Fig. 6.1 except using the Kullback-Leibler metric	167
6.5	Similar to Fig. 6.1 except using the Wasserstein metric	168
6.6	Plots demonstrating the parameter space for where a single EC or WN distribution is the favoured distribution in comparison to a mixed distribution formed from two WC distributions	171
6.7	Plots demonstrating the parameter space for where a single EC or WN distribution is the favoured distribution in comparison to a mixed distribution formed from one WN and one WC distribution	172
7.1	Adult <i>Gasterosteus aculeatus</i>	179

7.2	(a) Top-down schematic of the tank setup. (b) Experimental arena setup.	180
7.3	Examples of movement paths for 5 individual fish across the simple environment (black), moderate environment (red) and complex environment (green)	183
7.4	Method for calculating the new location in the movement model if a step took the fish out of the bounds of the tank, or into an object.	187
7.5	Boxplots of calculated statistics for every individual run compared across environments.	191
7.6	Line plots demonstrating how the calculated statistics varied for individual fish across environments	194
7.7	Boxplots indicating the difference between the mean value for an individual fish across all six individual trials and each individual trial.	196
7.8	Box plots indicating the spread of the calculated statistics for each individual fish across all environments (red = Simple, blue = Moderate, green = Complex)	201
7.9	Distance Travelled against Time Spent Stationary (%) for the simulated model, the observed data	204
7.10	Comparing the Occupation Time (%) of the simulations (A-C) and the observed data (D-F) as functions of Time Spent Stationary (%).	205
7.11	Space Use (%) against Time Spent Stationary (%) for the simulated model and the observed data	206
7.12	Distribution of turning angles for the raw data	211
7.13	Step-length (x-axis) against the preceding cosine of the turning angle (y-axis)	212
7.14	A zoomed in segment of an individual path. The points are the location found at the recorded level of 25Hz	213
7.15	Distribution of turning angles after the data had been sampled at a rate of 2.5Hz and a speed threshold of 5mm/s had been introduced.	213

7.16	Demonstrating the locations of large turns with magnitude ($> \pi/2$) in the Simple environment	214
7.17	Distribution of turning angles with a sub-sampling rate of 2.5Hz, a speed threshold of 5mm/s and the removal of turns close to the border of the experimental tank.	215
7.18	Distribution of step-lengths for each environment	216
7.19	Distribution of turning angles for each environment	216
7.20	The effect of array size (n) against calculated Space Use (%)	218
7.21	Demonstrating how distance for determining if fish were 'near' to a part of the environment (x-axis) effects the % of time spent in that section of the environment.	220
7.22	Scatter-plots of the calculated statistics of Distance Moved, Space Use & Occupation Time, comparing between the simulations for model (i) a SRW (orange) and the observed data (black)	228
7.23	Scatter-plots of the calculated statistics of Distance Moved, Space Use & Occupation Time, comparing between the simulations for model (ii) a CRW (blue) and the observed data (black)	229
7.24	Scatter-plots of the calculated statistics of Distance Moved, Space Use & Occupation Time, comparing between the simulations for model (iii) a CRW with waiting times (gold) and the observed data (black)	230
7.25	Example movement paths from a simulation of model (iii) a CRW with waiting times, over the complex environment (featuring 5 objects) for a range of values of Time Spent Stationary (ν)	231

List of Tables

2.1	Various methods of determining the tortuosity of discrete movement paths	20
4.1	Absolute difference between curves for the simulated results and the First and Second analytical solutions respectively.	63
4.2	Absolute difference between curves representing the simulated results and those given by the first and second analytical solutions for the optimal w , with fixed c_δ	64
5.1	Values of the ICC for the calculated parameters	104
5.2	Correlations for parameters at both within- and between- individual level	105
5.3	Parameters for best fit distribution of instantaneous speeds with ϵ value in the smoothing algorithm fixed at $\epsilon = 7$	119
5.4	Results of the statistical tests for each best fitting distribution when the median ϵ value was used in the smoothing algorithm	120
5.5	Repeated measures ANOVA test results	121
5.6	One-way ANOVA and Kruskal-Wallis (KW) test for inter-beetle variances	123
5.7	Statistical test results for the turning angle distributions at all considered sampling rates and speed threshold values.	127
5.8	MLE for the parameters of the Wrapped Cauchy and von Mises distributions when considering the turning angle distribution for all considered sampling rates and speed threshold values.	128
5.9	Statistical test results for the instantaneous speed distribution at every considered sampling rate and speed threshold value, for the tail of the data only	129
5.10	Similar to Table 5.9, results of the G-Test for the distribution of instantaneous speed. Results are for the tail of the data only.	130
5.11	Parameter values calculated for the instantaneous speed distribution for the tail of the data only.	131

5.12	Statistical test results for the speed distribution at every sampling rate and speed threshold value, without removing the tail of the data	132
5.13	Similar to Table 5.12, with additional results of the G-Test	133
5.14	Parameter values calculated for the speed distribution for the whole data set, without removing the tail of the data.	134
5.15	Statistical test results for the bout distributions	135
5.16	MLE for the parameters of the four distributions considered for the distribution of the bout lengths.	136
5.17	MLE for the parameters of the four distributions considered for the bout distributions when including truncated bouts	137
5.18	Test results for the bout distributions when truncated bouts were included	138
5.19	The Δ statistic calculated from the observed movement paths	143
7.1	Summary of statistical tests used in the analysis of the fish movement . .	185
7.2	Results of the Wilcoxon-paired test comparing means between pairs of environments	189
7.3	Results of Levene's Test comparing between fish disregarding the change in environment	197
7.4	Results of the ANOVA comparing between fish disregarding the change in environment.	198
7.5	Results of calculating the ICC for the calculated statistics, along with the 95% CIs and the associated p-value	199
7.6	Results of the ANOVA comparing between individuals for the Simple environment	222
7.7	Results of the ANOVA comparing between individuals for the Moderate environment	223
7.8	Results of the ANOVA comparing between individuals for the Complex environment	224
7.9	Results of the MANOVA comparing within individuals as the environment changed	226

List of Initialisations

- BCRW** Biased & Correlated Random Walk
- BRW** Biased Random Walk
- CRW** Correlated Random Walk
- HMM** Hidden Markov Model
- i.i.d** Independent and Identically Distributed
- ICC** Intra-class Coefficient
- LMM** Linear Mixed Model
- LW** Lévy Walk
- MeM** Mixed-effect Model
- MLE** Maximum Likelihood Estimation
- MSD** Mean Square Displacement
- PDF** Probability Density Function
- RW** Random Walk
- SL** Step-lengths
- SSM** State-Space Models
- SWS** Symmetric Wrapped Stable Distribution
- TA** Turning Angles
- vM** Von-Mises Distribution
- WC** Wrapped Cauchy Distribution
- WN** Wrapped Normal Distribution

1 Introduction

1.1 Movement Ecology Overview

Understanding how and why animals move through, and interact with, their environment is fundamental to our understanding of some of the most important open questions in science (Nathan et al, 2008); from how climate change will affect habitat use and home range-shifts (Russell et al, 2014, 2016; Riotte-Lambertt, 2015) to better control and prevention of infectious disease spread and of invasive species (Petroksvii et al, 2014; Boulinier et al, 2016; Dougherty et al, 2018).

The processes which cause individuals to move through space are many and diverse but movement itself is fundamental to all life, both animal and plant alike with almost all organisms undergoing some spatial change across their lifespan (Holyoak et al, 2008). Movement ecology is the field which aims to understand, describe and quantitatively model animal movement. It strives to demonstrate how movement affects and relates to key processes in individual and group level movement dynamics such as reaction to predation risk, interaction behaviour, resource use and navigation.

Traditionally movement ecology studies were focused on understanding the spaces within an environment visited by an animal in order to improve management and welfare strategies and were largely informed by either capture-recapture techniques or by simply visually tracking individuals. However, over the past 30 years the field has undergone a rapid expansion, in large due to the increase in availability, affordability and accuracy of electronic tagging devices; allowing for ever increasing levels of precision in monitoring the movement of individual animals (Patterson et al, 2017). This has moved the field from simple studies investigating where animals go, to describing the underlying mechanisms behind animals' behaviour and movement processes.

In general movement ecology takes a 'bottom-up' approach to population movement dynamics, by seeking to model individual-level behaviour and then extrapolating up to group or population level (Jeltsch et al, 2013; Patterson et al, 2017). Therefore, understanding and modelling individual animal movement is crucial to the field. Along

with the expansion in recorded data, the number of statistical techniques and models available to movement ecologists has also dramatically increased within recent times, ranging from simple explicit models of individual movement, such as random walk models (Kareiva & Shigesada, 1983; Codling et al, 2008) to more complex statistical structures such as hidden Markov Models (Parton & Blackwell, 2017; McClintock & Michelot, 2018). Whilst these developments in analytical approaches have potentially given greater insights into animal movement, care must be taken when seeking to analyse data to ensure that the statistical tools are appropriate for the type of data and for what is sought from the data (Patterson et al, 2017). Movement is a composite process which is known to be formed from many internal and external cues (Nathan et al, 2008), therefore whilst simple models benefit from being easy to implement and cheap in terms of computation cost, they will not in general pick up more intricate movement behaviours. Whereas more complex models become less tractable for non-experts to utilise and can also lead to overly complex behaviour being wrongly assigned to a simple movement process. This can particularly be the case for small studies with limited individuals over short time scales; as is often inherent in laboratory based experimental setups. As such extensions to simple movement models can allow for intuitive aspects of movement to be encapsulated within the framework of the model whilst simultaneously letting more advanced and complex behaviour be captured, with random walks being a good example of this.

Random walks have an established history with animal movement (Levin, 1986; Getz & Saltz, 2008; Codling et al, 2008; Miller et al, 2019) in part due to the nature of movement data often being recorded as a series of discrete locations. Since the work of Kareiva & Shigesada (1983), correlated random walks (CRW), which are random walks that incorporate an animal's expected inherent ability to have some persistence in their movement path (Patlak 1953), that is knowledge of their previous direction, have frequently been used as null models to which real movement can be compared (McCulloch & Cain, 1989; Fagan & Calabrese, 2014; Miller et al, 2019). The benefits of such a model are that the parameters required to inform the model can be calculated straightforwardly

without the use of lengthy computation (Fagan & Calabrese, 2014). Recently, these null models are being replaced by more complex models (such as biased and correlated random walks (BCRW); Benhamou & Bovet, 1992; McClintock et al, 2012; Duchesne et al, 2015) which can more accurately account for the complexities inherent within an animals movement and behaviour, for example switches in behaviour possibly due to changes with the local environment or landscape (Schultz & Crone, 2001; McClintock et al, 2012). RW theory also underpins many advanced statistical models used in modern movement ecology including state-space models (SSM) and hidden Markov models (Patterson et al, 2017), therefore further development in the models utilising RW theory as well as completing a more thorough mathematical understanding of RW theory will continue to benefit and push forward the movement ecology field.

1.2 Thesis Objectives and Structure

This thesis is formed of two introductory chapters and four research chapters. Each research chapter is distinct in their content as they are taken from work which has either been published or is in preparation for submission featuring a mix of theoretical results based on RW theory, with analysis of real world data and individual based models.

Chapter 2 introduces the historical background of movement ecology and outlines the current research being undertaken within the field, explaining how the biological and mathematical aspects of the field work together in informing modern movement ecology.

Chapter 3 focuses on deriving some of the key mathematical properties of random walk theory and introduces the concept of circular data and statistics. Both of which are the key mathematical tools used throughout the research chapters.

Chapter 4 considers a BCRW movement model for an individual, which is an extension of a model first analysed by Bovet & Benhamou (1999). It is demonstrated that in the case where the error on persistence is small (that is the animal has good knowledge of its previous heading) then for long term motion, heading towards a preferred direction (or point at infinity) the most efficient method of moving is to put more weight

into following the direction of the previous step than into the navigation. An analytical approximation to the long term behaviour of the model is given and the uses of such a model and the findings in the wider movement ecology field are discussed.

Chapter 5 looks at the analysis of the movement paths of the ground beetle *Poecilus cupreus*. The movement paths were recorded in a featureless, homogeneous laboratory setting at high frequency. The beetles were found to have the ability to disperse much more rapidly than predicted by simple CRW models and demonstrate high individual variability in movement behaviour. The findings demonstrate the importance of considering individual movement traits rather than aggregated population movement dynamics, as important characteristics, such as the net displacement, can be greatly affected.

Chapter 6 concerns the distribution of turning angles found in movement data. It is shown that the apparent presence of a heavy-tailed distribution (such as a wrapped Cauchy distribution) can be due to the erroneous assumption that the observed movement includes turning angles drawn from one probability distribution. This is demonstrated analytically by considering the probability distribution formed by a mixing two normal-type distributions and comparing this to a heavy tailed distribution (a wrapped Cauchy distribution).

Chapter 7 looks at how changes in an environment can affect the movement behaviour of stickleback fish (*Gasterosteus aculeatus*). High-resolution image-tracking was used to repeatedly record the movements of individual three-spined stickleback fish in a simple environment that had either two, three or five shelters present. Subsequent analyses of the movement paths indicated that changes in the environmental setup did not explain variability in our sample, whereas a significant proportion of the observed variation was attributed to individuality. The findings demonstrate the link between animal 'personality' theory and movement ecology and highlight the importance of including such individuality when attempting to scale up individual models to inform group level movement behaviour.

2 Historical background and foundations of Mathematical Ecology

2.1 Historical Background

Perhaps the earliest documented interest into the movement of animals comes from Aristotle in the 4th Century BC where he stated in his text *On the motion of Animals* (Aristotle)

- “*We have inquired elsewhere into the details of the movement of the various kinds of animals, the differences between these movements, and the causes of the characteristics which each exhibit; we must now inquire generally into the common cause of animal movement of whatever kind*”

Despite this it took until the 19th Century for the seasonal migration of birds to be noted, in part due to the discovery of the Rostocker Pfeilstorch found in 1822 (Berthold, 2001). Even noted Biologists such as Charles Darwin, despite writing in *On the Origin of species* that animals tended to restrict their movement to small, local areas or ranges, did not explore the importance of studying the methods and movement paths of animals (Darwin, 1859).

2.2 Modern Movement Ecology

Modern research has come to realise the importance of understanding animal movement as there are aspects in many of fields of science which inherently rely upon an understanding of movement ecology including; ecosystem management (Berkes et al, 2008), animal behaviour (King et al, 2018), evolutionary science (Peck, 2001), population dynamics (Patterson et al, 2008; Holyoak et al, 2008), epidemiology (Boulinier et al, 2016) and conservation science (McLane et al, 2011). A thorough knowledge of the expected movement behaviour of animals is vital for controlling and managing the spread of diseases and infestations as well as protecting degraded ecological areas and in protecting

animal welfare whilst also allowing for sustainability in agriculture.

The modern field of movement ecology came into existence around the beginning of the 21st century where work focused on testing empirical data with theoretical models and, subsequently, using the theoretical models to predict animal movement and behaviour (Holden, 2006). Since then movement can be, and has been, classified in numerous ways. It can be passive, such as spread caused by currents or the wind, or purposeful and serve as relocationary, exploratory, fleeing, patrolling etc. and can take place across time scales from minutes and hours to days and months, over spatial scales of small home-ranges and patches (Schultz & Crone, 2001; Jonsen et al, 2005; Fortin et al, 2005; McClintock et al, 2012; Riotte-Lambert, 2015; Blackwell et al, 2016) to large inter-continental migrations (Gardiner et al, 2015; Nicosia et al, 2017; Muheim et al, 2018). Purposeful movement of animal is often, if not always, affected by the internal state of the individual influenced by such things as levels of hunger, predation risk, stress, body condition and health (Nathan et al, 2008). These internal states are hard to empirically quantify, however, with advances in technology these can now be measured (Spiegel et al, 2013, Fürtbauer et al, 2015; Cox et al, 2016; Vazquez Diosdado et al, 2018). Due to this wide range of movement types, over varying spatial and temporal scales, along with the rapid expanse of the field there was no common terminology or best practice appropriated by the community and, as is pointed out by Nathan et al (2008), this idiosyncratic classification is further compounded by differing taxonomic groups using differing movement models and studies despite clear overlaps. Hence, Nathan et al (2008) presented a framework to unify the field by stating that any such model of animal movement should include expressions for internal state w_t , ability to move, Ω , navigational ability, Φ and environmental factors r_t . Giving the potential of moving to a new location u_{t+1} from a current location u_t , at a given time, t , as a function of these variables:

$$u_{t+1} = F(\Omega, \Phi, r_t, w_t, u_t) \quad (2.1)$$

This approach to integrating the separate factions of research into movement is in essence what modern movement ecology has entailed over the past 10-15 years, and proved timely

as the field underwent a dramatic increase in the number of publications listed under the key word of “movement ecology” since 2007 (Fig. 2.1).

Perhaps the major development within the field in the last two decades has hinged upon

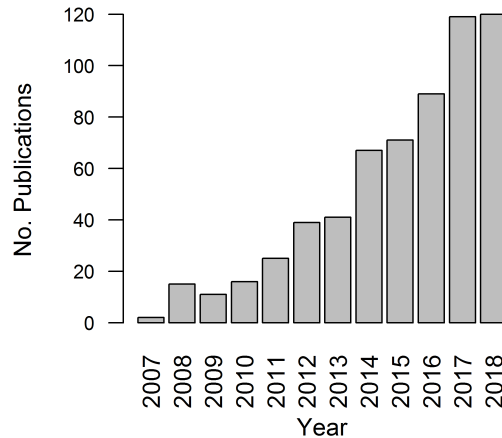


Figure 2.1: Demonstrating the number of publications found on Web of Science under the keyword of “movement ecology” from 2007-2018 (Web of Science, 2019)

advancements within tagging technology and other methods of recording animal locations (Robinson et al, 2010; Hazen et al, 2012; Cooke et al, 2013), as well as the dramatic increase in computational power and advances in mathematical and analytical techniques which have allowed researchers to exploit the increase in raw data. This has resulted in a better and more robust understanding of animal behaviour and in greater detail than was previously possible. Traditionally, acquiring accurate and quality movement data was challenging involving great expense, both economically and in terms of field work, however, with the aid of the advances in tagging technology and the increase in raw computer power, it has become possible to record movement data at a high degree of accuracy across longer time scales without burdening or obviously effecting the natural movement of the animal in question.

2.3 Movement Data Capture

Data capture techniques have dramatically improved over recent years, not just in the volume of data which can be recorded but also in the accuracy and the ability to record

data other than simple location, such as temperature, pressure, humidity and depth. This coupled with the relative inexpensiveness of such devices has caused an explosion in the size and number of data sets, with data repositories now dedicated in storing vast amounts of open access data; such as MoveBank (Movebank.org, 2019) and Dryad (Datadryad.org, 2019). However, care must be taken when attempting to tag individuals ensuring that any affect of a device upon an individual does not affect nor inhibit its usual movement behaviour, similarly, care must be taken when attaching any device to prevent any distress or harm; McMahon et al (2011) detail common potential effects of tagging individuals and suggest best practice methods.

Commonly used tracking devices in the wild include global positioning system (GPS) tags, which give highly accurate readings of global location as well as height, however, such tags are usually larger and bulkier than alternative methods (Cagnacci et al, 2010; Recio et al, 2011) and as such are best suited for larger animals, such as sunfish, *Mola mola*, (Sims et al, 2009), elk, *Cervus canadensis*, (Fortin et al, 2005), green turtle *Chelonia mydas* (Dujon et al, 2014) golden eagle, *Aquila chrysaetos*, and turkey vulture, *Cathartes aura* (Bohrer et al, 2012). Smaller and cheaper alternatives exist, such as the ARGOS Doppler tags, which will give locations most places on the globe, however, whilst they are lighter than the GPS tags, the trade-off is in accuracy of data. These tags have been used in tracking a wide range of animals, from smaller lightweight birds such as snowy owl, *Bubo scandiacus*, (Therrien et al, 2015), African cuckoo *Cuculus gularis* (Iwajomo et al, 2018) and Grasshopper Sparrows *Ammodramus savannarum* (Hill & Renfrew, 2019) to larger mammals such as blue whale, *Balaenoptera musculus*, (Bailey et al, 2009) and both the bearded seal *Erignathus barbatus* and Hawaiian monk seal *Monachus schauinslandi* (McClintock et al, 2015). Finally, smaller and inexpensive alternatives like VHF (Very high frequency) radio tags can be used, which are light and unobtrusive enough to be attached to small birds, mammals and even insects, however in general these require the animal to be within a short distance (order of kilometres) of the recording receiver. These are often used to track populations where the home range is known and as they have a long battery life they have been used in data recording

of both brown bats, *Eptesicus fuscus*, and hoary bats, *Lasiurus cinereus*, (Castle et al, 2015), juvenile Eagle owls, *Bubo bubo* (Aebischer et al, 2010) and across a wide range of insects (Gourret et al, 2011).

Other common tracking methods used include capture-recapture techniques. These involve placing a series of traps across a given area and recording the presence of an animal when it engages the trap. The individual will often be labelled then released and as it engages with future traps, information about its movement can be extrapolated from the occurrences of appearances in the traps. This technique has been extensively studied in terms of conservation and population management (Williams et al, 2002; King, 2012) and whilst modelling specific movement paths from this data is not usually attempted due to the heavily discretised spatial and temporal nature of the data, it is an important and commonly used practice in movement ecology as it allows for estimations of important population level statistics such as animal density (Efford, 2011) and survival probabilities (King, 2012).

Data is often also recorded in a laboratory setting where the environmental effects can be carefully controlled and monitored. For obvious reasons these laboratory settings are best suited for smaller animals and cannot be used to reproduce large scale, migratory type movement. Data here can be found by live tracking the animal, such as through a tracking sphere as is discussed in Chapter 5 and has been used for desert ants in Dahmen et al (2016). Or this can be done via video tracking devices, where a video recording of the movement path is analysed by computational programmes tracking the movement of individuals by considering the centre of mass of the animal and returning a simple time series of location points (see Chapter 7) (Noldus et al, 2001, 2002; Qian et al, 2016; Madan & Spetch 2014). Whilst these experimental setups benefit from the inclusion of controlled and repeatable settings, care must always be taken when extrapolating results into the real world setting (Englund & Cooper, 2003; Miller et al, 2004).

These advances in data capture techniques along with the explosion of interest of applying mathematics to biology in the 20th and 21st century has given rise to many new theoretical mathematical frameworks, which can be used in spatial ecology to help

understand, interpret and predict animal movement and behaviour.

2.4 Mathematical Tools

Movement data which has been obtained and processed using computational methods are usually stored as a time series of individual location points. This discrete process is often recorded at regular intervals, although this is not always the case perhaps due to loss of signal with tagging equipment or by the use of less dynamic forms of data capture, such as fixed location traps or visual recordings.

A simple piece-wise linear reconstruction of the movement path can be made by connecting the spatial locations in temporal order, which allow for the calculation of descriptive statistics that are readily available from such data and are often used in movement analysis including:

- step-lengths; the distance between two successive spatial locations. Usually this is the standard Euclidean distance, but in large scale movements, such as migrations, this might be measured by the orthodromic distance.
- instantaneous-speeds; these take the step-length and divide by the temporal difference between two points. These are often used in high frequency data as they give a sense of the speed at which an individual is moving at a given point, despite not working with continuous data.
- turning angles; the relative angle between direction of movement for successive locations.
- headings/global orientations/bearings; the change in direction between two successive locations taken from some absolute direction (magnetic North in the case of bearings).
- intermittency; periods of time when the animal is stationary

It should be clear that the choice of which statistics to use is determinate upon both the temporal and spatial scale of the data. High frequency data, recorded at multiple

counts per second, will therefore need to be treated and analysed differently to data which is recorded at timescales of hours or days.

Therefore, when analysing any such data, the type of data recorded, whether temporally regular, spatially regular or intermittent in both spatio-temporal scales needs to be taken into account (Patterson et al, 2017).

2.4.1 Continuous Time Models

In the case when data has not been recorded at regular time intervals it is often necessary to use continuous time models as these assume data has only been recorded at certain temporal or spatial points with missing data in between. This allows the data to be modelled without interpolation, sampling or aggregation (Johnson et al, 2008). Such models are usually derived from some diffusive stochastic process, such as the Wiener or Ornstein-Uhlenbeck process (OU). Johnson et al (2008) used a continuous time correlated random walk (CTCRW) derived from an OU process to model the movement and space-use of harbour seals (*Phoca vitulina*) and northern fur seals (*Callorhinus ursinus*). This method accounts for the irregularity in the recorded data and therefore prevents researchers from the sometimes arbitrary, decision of the temporal scale of data capture beforehand. Continuous time models utilising the OU process have been used in a range of movement processes including; estimating home ranges (Nations & Anderson-Sprecher, 2006), group movement (Niu et al, 2016) and the movement of central place foragers (Fleming et al, 2015). Models utilising different continuous processes such as velocity jump processes, which model the velocity at a given time as a random walk rather than the spatial location (Codling & Hill, 2004), have been used in describing the movement of a diverse range of animals from the ‘run and tumble’ movement of bacteria such as *Escherichia coli* and *L. fuscus* (Berg, 1990; Hill & Hader, 1997; Taylor-King et al, 2015) to the migration of the lesser black-backed gull (*Larus fuscus*) (Taylor-King et al, 2015). A more general approach than using an OU process is to describe movement as a stochastic differential equation (SDE). These can model more complex behaviour than the OU process, such as by including a term which models the drift in movement

towards (or away from) a certain direction or point. This drift term can be included in a variety of ways, Bengtsson et al (Bengtsson et al, 2002) showed that by calculating the drift as a function of the distance between individuals, the dispersal patterns in soil-living invertebrates (*Onychiurus armatus*) could be modelled and characterised, whereas, Preisler et al (2001) used the angle between the heading of an individual and a point source emitting male pheromones to model the movement of female bark beetles (*Ips paraconfusus*). Whilst SDEs are more flexible than other continuous time models, their flexibility does come at a cost of increased computational time and decreased statistical tractability (Patterson et al, 2017).

2.4.2 Discrete Time Models

Modern approaches for the analysis of data recorded at regular time intervals has relied on advanced statistical tools such as Hidden Markov Models (HMMs) and state-space models (SSMs), as these allow for efficient and accurate analysis of the large data sets that modern movement ecology now entails (Cagnacci et al, 2010).

HMMs are especially effective in the case where the latent error in the location measurement is small (Patterson et al, 2017), and can identify important aspects of movement data such as auto-correlation, as well as identifying when animals switch movement behaviour (perhaps from more active to more sedantary behaviour) and have been used in the analysis of a variety of animals, including elephants *Loxodonta africana* (McClintock & Michelot, 2018), grey seal *Halichoerus grypus* (Whoriskey et al, 2017), woodpeckers *Picoides borealis* (McKellar et al, 2016), cheetah *Acinonyx jubatus* (Grünewälder et al, 2012) and *Drosophila* fruit flies (Holzmann et al, 2006). The popularity of using HMM techniques has been furthered by the relative ease of applying the methodology due to readily available computational programme packages, such as the *moveHMM* (Michelot et al, 2016) and *momentuHMM* (McClintock & Michelot, 2018), which can both be implemented straightforwardly in *R* (R Team, 2019)

State-space models (SSM) combine a process model for the movement, as would be used in an HMM, with a model for the accuracy of the observations that could take the

form of the Gaussian error function, for example. In this way, an SSM can be thought of as an extension of an HMM which allows for inaccuracies in the data recording, or similarly, an HMM can be thought of as an SSM which assumes that the recorded data comes from a discrete number of unobservable or hidden states (Patterson et al, 2008). Parameters for both the movement and observation models are found from the data itself, usually by either Bayesian or maximum-likelihood methods (Jonsen et al, 2005; Johnson et al, 2008; Patterson et al, 2008; Pederson & Weng, 2013; McClintock et al, 2012; Alberrrtsen et al, 2015). These models are particularly useful when data has been recorded from the ARGOS system due to the known error in the recorded data, which can be modelled as a stochastic process (Johnson et al, 2008; McClintock et al, 2012; Alberrrtsen et al, 2015).

Both HMMs and SSMs require an underlying model for which the movement data is to be described, with perhaps the most commonly used model being a discrete random walk (RW) (Patterson et al, 2017). Discrete random walks assume that animals travel by a discrete path given as a time series of individual spatial locations and as such are well suited for analysing, exploring and interpreting movement data. Random walks have been used extensively within the field of movement ecology as models can, in general, be informed by two parameters; a measure of distance travelled between locations (step-lengths or instantaneous speeds) and a direction at each step (turning angle or global orientation/bearing).

2.5 Use of Random Walks in Animal Movement

Random walk theory has a long history of being used to model individual animal movement and navigation (Levin, 1986), and as a tool to classify and interpret observed movement data using various path analysis techniques. RWs have been used to describe and analyse the movement of insects such as cabbage white butterflies *Pieris rapae* (Kareiva & Shigesada, 1983) and *Cataglyphis* desert ants (Dahmen et al, 2015) to large mammals such as elk *Cervus elaphus* (Frair et al, 2005) and grey seal *Halichoerus grypus* (McClintock et al, 2012). McLane et al (2011) gives a list of examples of recorded animal

movement which were described by various types of RW.

One of the reasons for the tractability of RW theory in movement analysis is that measures such as the distributions of the turning angles, step-lengths and bearings can be readily calculated directly from recorded data and simple descriptive statistics useful for practising ecologists can be freely obtained, such as mean square displacement (MSD), sinuosity, preferred direction in movement and space-use.

In terms of movement modelling the three most commonly used types of RW are; the isotropic simple random walk (SRW) in which the direction of a step is equally likely across all possible directions at any given point in time or space; the biased random walk (BRW) which differs from the SRW by featuring a preference towards a certain direction at each time step. This can be towards a specific point in space, in which case the orientation of the preferred direction will depend upon the location of the walker at each step, or it can be towards a specific direction, for example magnetic North and it can be consistent across time and space or vary depending upon location and/or time. Finally, the correlated random walk (CRW), which assumes the direction of movement at any given point is correlated to the previous movement direction (Kareiva & Shigesada, 1983; Codling et al, 2008). Fig. 2.2 demonstrates the difference in movement paths of each of these types of RW and Fig. 2.3 compares of the final positions of a group of walkers using each type of RW of a fixed length.

Since the work of Kareiva & Shigesada (1983), the CRW has often been treated as a null model for animal movement (Proulx et al, 2013; Fagan & Calabrese, 2014) as closed expressions for the mean square displacement (MSD) can be derived (see section 3.3) which rely solely on the mean trigonometric and mean step lengths, values which can be easily obtained from the observed data, therefore, giving a quick and simple check for ecologists as to how well the standard CRW model fits observed data (Fagan & Calabrese, 2014). However, as noted by Kareiva & Shigesda (along with others; Fortin & Dale (2005), Shimatani et al, (2012), Fagan & Calabrese (2014)) whilst the CRW may work well as a null model it is a poor simplification of real animal movement and

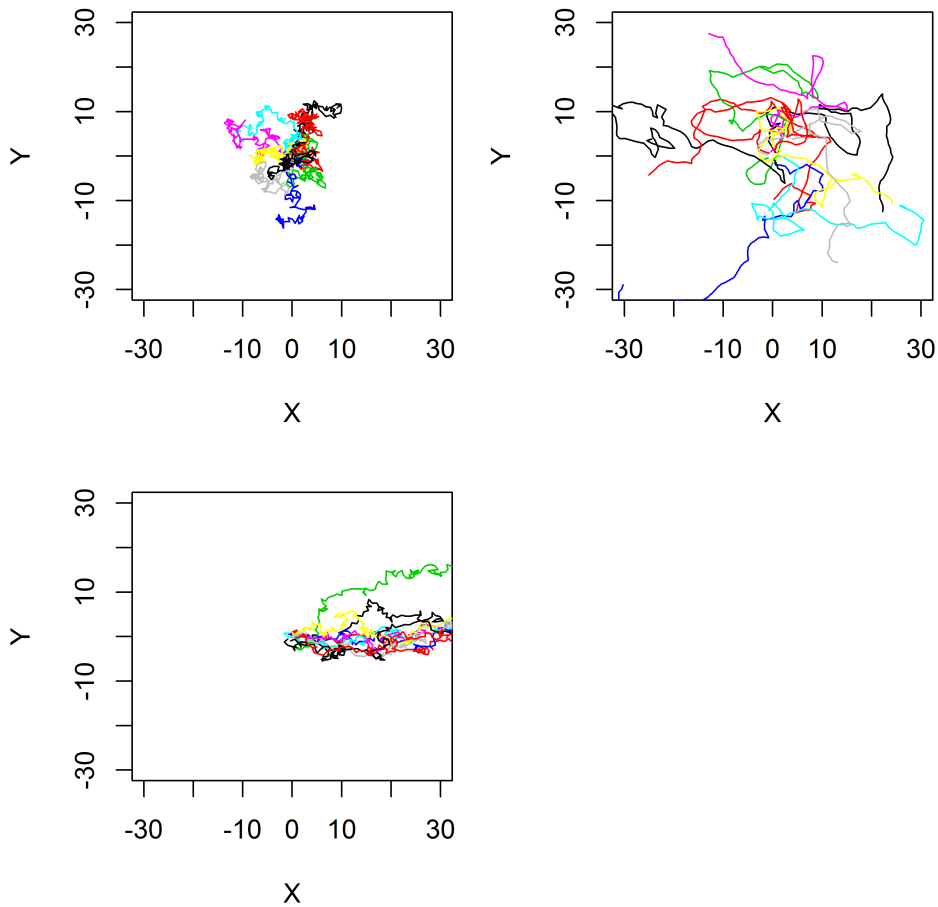


Figure 2.2: Example paths for (a) SRW; (b) CRW; (c) BRW. Each with 10 walkers after 50 steps each of unit length.

explains none of the underlying motives for movement behaviour, as required for a deeper understanding of animal movement (Nathan et al, 2008).

2.6 RW as a ‘step-and-turn’ Process

One common method of describing a RW is as a series of step-lengths, l_i , drawn from some positive distribution, Λ , and angles (either global orientations/headings, ϕ_i drawn from some distribution Φ with domain $(-\pi, \pi]$, or turning angles θ_i drawn from some distribution Θ also with domain $(-\pi, \pi]$; see section 3.7 for a discussion of such distributions) (Fig. 2.4). It is by viewing the RW process in such a manner that allows for many important and useful mathematical properties of RWs to be calculated, such as mean location and mean square displacement, therefore allowing for direct comparisons of these abstract models with observed data (Kareiva & Shigesada, 1983; Cheung et al,

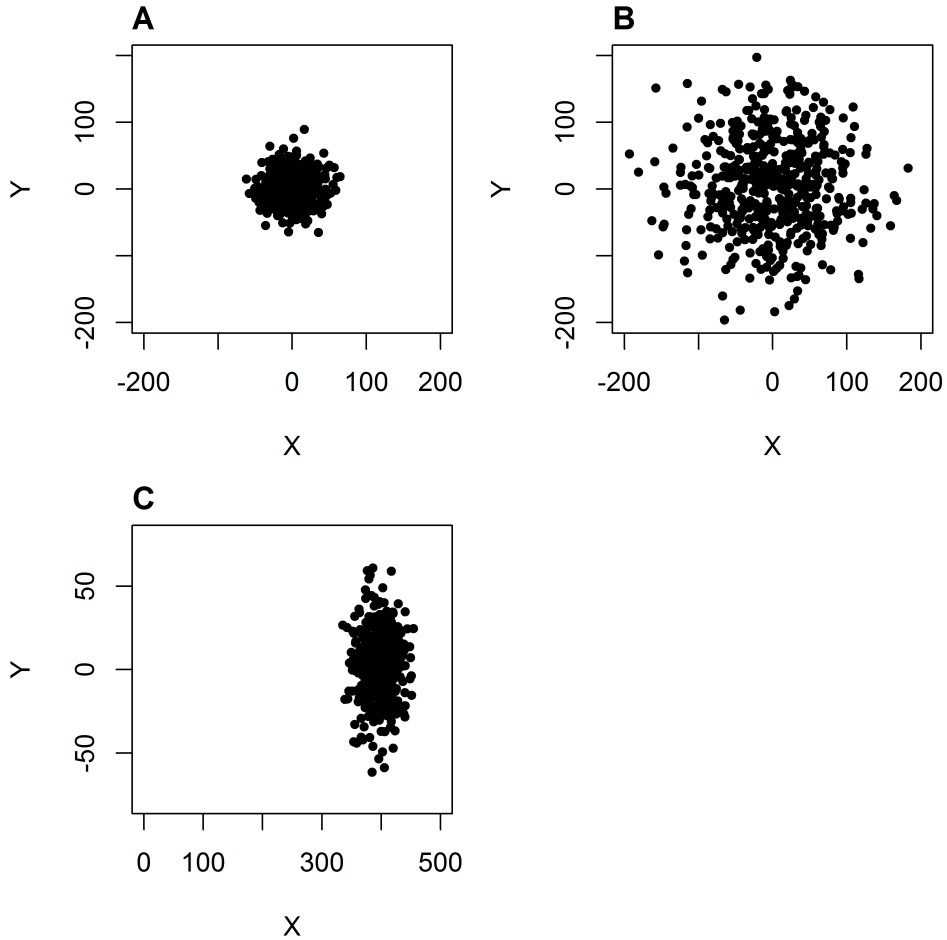


Figure 2.3: Final position of 1000 walkers for (a) SRW; (b) CRW; (c) BRW after 100 steps each of unit length. All starting positions were the origin, $(0, 0)$.

2007; Fagan & Calabrese, 2014).

Using this definition of a RW we can classify an isotropic SRW as one in which the distribution of the angles is uniform (this will be the case for both the distribution of headings, Φ , and for turning angles, Θ).

For a CRW we would expect the distribution of turning angles, Θ , to be stable over time (that is the distribution tends to a stable state as time increases) and symmetric around 0 (assuming the walker is equally likely to take left and right turns). With a taller peak at 0 corresponding to a walk with high persistence and a lower peak giving a near isotropic SRW.

For a BRW with a *global* bias (that is a preference to always move in a certain direction or to a point at infinity), we would expect the distribution of the global orientations/headings, Φ , to be stable over time and centred around the angle of the preferred

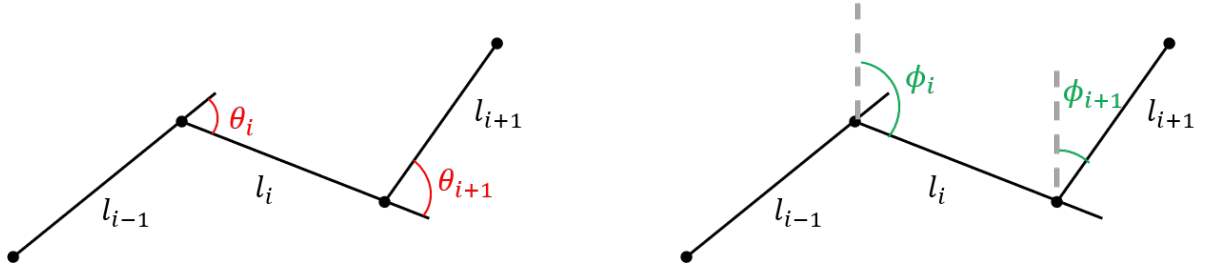


Figure 2.4: Discrete movement path as a step-and-turn process. Successive locations are given by closed black circles with steps of length l , turning angles, θ , and headings, ϕ .

direction when compared to the direction from which the global orientation/heading is taken (e.g. North). With a higher peak corresponding to a stronger bias and a flatter distribution giving near isotropic SRW movement. This is only the case for global bias, if the bias in direction is towards a specific point in space then then direction of the bias at any other given point will depend upon the relative positions of the current position and the goal position. Therefore, the distribution of angles will not necessarily stabilise to a fixed distribution over time.

2.7 Extensions to SRW, CRW and BRW models

The three models described above are among the most straight forward versions of random walks and as such are the most commonplace within the movement ecology literature. However, simple extensions which add extra realism in specific animal ecological problems can also be calculated. Those which have been used specifically in animal movement are briefly mentioned below.

2.7.1 Biased & Correlated Random Walk

Though pure CRW or BRW have been reported as models for animal movement, other extensions to these models which take into account some of the short comings noted by Kareiva & Shigesada (1983) and Fagan & Calabrese (2014) have recently been incorporated. One can consider a random walk which has both a biased and correlated component, such biased and correlated random walks (BCRW) can be expressed in various ways but include an additional term which controls the weight, or preference, the walker puts into the correlated and biased terms. Benhamou & Bovet (1992) considered

a weighted vector sum to describe a BCRW, where the length and direction of steps are formed by a weighted sum of the vectors formed by pure CRW and BRW. A similar form of the BCRW considers the angle at each step to be calculated by a weighted sum (Schultz & Crone, 2001; Fortin et al, 2005), although this gives differing results to those calculated utilising the vector sum method due to the periodicity of the trigonometric functions.

2.7.2 Lévy Walk

A Lévy walk (LW) is essentially a SRW where the distribution of step lengths, $\Lambda(l)$, is given by a power law, $\Lambda(l) \sim l^{-\alpha}$, where for some $\alpha > 1$. This distribution for step-lengths gives an infinite variance allowing for the unrealistic effect of instantaneous propagation over an infinite domain. Technically this stochastic model is known as a Lévy flight, whereas a Lévy walk assumes a finite constant velocity at each step causing longer step-lengths to take proportionally longer time (Zaburdaev et al, 2015), however, assuming that we have a free boundary condition then Lévy flights can accurately model Lévy walks (Dybiec & Gudowska-Nowak, 2017) and hence are often referred to interchangeably in the literature.

Qualitatively a LW resembles periods of random movement concentrated in a small area followed by a sudden large relocation to a new area and the process repeats. Such heavy-tailed behaviour of the step-lengths is the indicative characteristic of Lévy behaviours and as such is usually the method for which movement is classified as Lévy or not (Bartumeus et al, 2005; Viswanathan et al, 2011; Plank et al, 2013). Evidence for Lévy type movement has been reported in various animals including wandering albatrosses, *Diomedea exulans*, (Viswanathan et al, 1996), black bean aphids, *A. fabae Scopoli*, (Mashanova et al, 2009) and humans (Raichlen et al, 2014). Theoretical approaches have also been developed to show that Lévy behaviour can optimise search and foraging movement (Bartumeus et al, 2002; Sims et al, 2012). However, the validity of determining the presence of Lévy behaviour is a contentious topic (Pyke, 2015). It has been shown that heavy tailed behaviour in step-lengths can be recovered by con-

sidering a composite correlated random walk (CCRW) which consists of two distinct phases of movement behaviour, one of intensive foraging involving movement in a small localised area, and another of large displacement representing exploratory behaviour (Plank & Codling, 2009; Auger-Méthé et al, 2014). Evidence to suggest the manner in which movement paths are sampled can also cause apparent emergence of power laws (Codling & Plank, 2011; Auger-Méthé et al, 2011). As Tilles et al (2017) highlights, data which was initially classified as exhibiting heavy tailed step length distribution has since been re-classified as “ ‘thin-tailed’ Brownian walkers”, notably wandering albatrosses, *Diomedea exulans* (original analysis, Viswanathan et al, 1996; subsequent analysis Edwards et al, 2007), mussels *Mytilus edulis* (de Jager et al, 2011; Jansen et al, 2012) and Tenebrio beetles, *Tenebrio molitor*, (Reynolds et al, 2013; Bearup et al, 2016). The presence of power laws is in general a non-trivial task to determine (Virkar & Caluset, 2014); it has long been held that power laws are present in almost all complex networks, ranging from areas of computer and data science (Albert et al, 1999; Mislove et al, 2007) to biology and the social sciences (Ichinose & Sayama 2017; Agler et al, 2017) and had been widely reported on over the last couple of decades, however, recent work by Broido & Clauset (2018), has demonstrated that such networks are in fact highly uncommon when using recent advances in statistical methodology and tools.

2.8 Common Descriptive Characteristics of RW Paths

Directly comparing between movement paths is difficult, therefore, summary descriptive statistics are often used to characterise paths of RWs. The most common of these are the mean square displacement, which gives the square of the distance from the current location to a certain reference point (often the initial starting point), and a measure of *tortuosity*, which gives a measure of the amount of turning across the path. As mentioned in section 2.2, movement ecology has a habit of including terminology with no strict definition and this is true here as there are various methods for calculating the *tortuosity* each of which are applicable and helpful in certain situations (Codling et al, 2008). However, certain specific types of tortuosity are well-defined, with common ones

being listed in Table 2.1 (taken and adapted from Almeida et al, (2010) and Edelhoff et al, (2016)). Almeida et al (2010) gives a complete comparison between five measures, detailing how they compare with errors in recorded locations, sample sizes and scalings.

Measure	Equation	Parameters	Refs
Straightness	$\frac{dE}{L}$	dE = Euclidean distance between beginning and end of movement path, L = Total path length	Batschelet (1981), Gurarie et al (2016)
Sinuosity	$\left[\frac{\mathbb{E}[l]}{4} \left(\frac{1-c^2-s^2}{(1-c)^2+s^2} \right) + b^2 \right]^{-0.5}$	$\mathbb{E}[l]$ = mean step length, c = mean cosine of turning angles, s = mean sine of turning angles, b = coefficient of variation of step length (see Eq. 3.27)	Bovet & Benhamou (1988), Benhamou (2004), Codling et al (2008)
Intensity use	$\frac{L}{\sqrt{A}}$	L = total path length, A = area of movement	Hailey & Coulson (1996), Loretto & Vieira (2005), Ferreira et al (2017)
Fractal dimension, D	various computational methods but always with $D \in [1, 2]$	Usually requires the length of path and some measure of the area through which the path has traversed.	Benhamou (2004), Turchin (1996), Mårell et al (2002), Tremblay et al (2007)

Table 2.1: Various methods of determining the tortuosity of discrete movement paths

It should be mentioned that the use of the term *fractal dimension* (Table 2.1) is not technically correct as the random walks and data discussed here and in the movement literature are not strictly fractal in nature, since they have a minimum scale size. Also it has been shown that at the scale of the animal itself movement is effectively linear (Turchin 1996), however, measures of “fractality” have been successfully used in comparing movement paths for animals such as grey teal *Anas gracilis* (Roshier et al, 2008), migrating wandering albatross *Diomedea exulans* (Fritz et al, 2003) and zooplankton

(Seuront, 2015); see also Table 1 in Seuront (2015) for a list of studies on Fish and Crustaceans.

True fractal analysis requires self-similarity across scales, however, as this is not the case in animal movement, comparisons of paths using a measure of fractal dimension can only be used at the same scales (paths considered to be Lévy in nature can be compared across scales as, by definition, they are scale invariant due to the inherent power law, however as discussed in section 2.8.2 the viability and existence of such scale free movement paths is up for debate).

Almeida et al (2010) and Codling et al (2008) both highlight the importance of using the correct measure of tortuosity in attempting to compare movement paths as each of the suggested measures has limitations in certain contexts and can be affected by factors such as error in data recording, sampling rate of movement and the scale at which the data has been captured.

2.9 Limitations of RW Theory in Movement Analysis

Whilst the uses of RW theory in movement ecology have been discussed, there are limitations to this modelling framework. Notably, analysis of the step length and turning angle distributions requires accurate recording of the location data. Though this has rapidly improved in recent years (see section 2.3) errors in the recording of data can give rise to the incorrect use of models. For example, when considering the analysis of the distribution of turning angles the temporal scale at which the data is recorded can have a drastic effect. Consider an insect or fish whose natural movement emits a sinusoidal motion, either through the tripod rocking of walking (Hughes, 1952; Holmes et al, 2006) or by the wave like motion the body a fish uses for forward movement (Gray, 1933; Stephens et al, 2003). If the data are recorded at a high frequency this rocking motion will be assumed part of the movement path of the individual, despite the animal attempting to walk in a straight line, and the rocking motion will cause the recorded path to appear highly sinuous (Delcourt et al, 2013; Qian et al, 2016). Conversely, too large a temporal scale, for example long term migrations where data can only be captured a few times

a day, risks omitting the local level movement behaviour and can lead to non-sensical descriptions of turning angle behaviour as changes in directions are considered to occur only a few times a day. It has also been shown that the method for recording locations can cause inaccuracies in the subsequent analyses with errors in GPS data locations producing contrived large and 180° turns, which would falsely enhance the heavy-tailed nature of recorded turning angles (Hurford, 2009). As mentioned previously (section 2.4) methods to address the inherent error in movement data have been developed, for example with the use of state-space models (SSM).

It is also assumed by the RW model that the animal moves between data points in a straight-line, again at large temporal scales this is an unreliable assumption. Modern methods which allow for the continuous nature of movement in connecting discrete locations rely on Bayesian inference and usually require heavy computational implementation of advanced statistical techniques such as Markov chain Monte Carlo (MCMC) algorithms (Blackwell et al, 2016) or Kalman filters (Fleming et al, 2017). An alternative would be to employ spline techniques, which are used frequently in discrete point analysis in computer sciences and have been seen in animal movement such as in Buderman et al (2016) who used spline techniques to give best fit curves between data points in the analysis of Colorado Canada lynx (*Lynx canadensis*), providing a Bayesian based model which could be used across temporal scales in order to obtain behavioural change point locations in continuous time.

In fact the method of Buderman et al (2016) method takes into account the non-trivial problem of the effects of missing data. Missing data can be corrected by simple interpolation via generalised linear models (GLMs) which can infer the location of missing data (Hanks et al, 2015), or through other techniques such as cluster analysis (Hanks et al, 2011) or data augmentation (Johnson, London & Kuhn 2011), although as noted in Buderman et al (2016) these techniques are not suitable for multiple data sources and so in the case of data coming from multiple individuals other methods such as that described by Buderman et al (2016) need to be incorporated.

Similarly, as data are usually recorded at specific time intervals the assumption in

the framework of discrete RW models is that the change in direction or speed/step-length of an animal occurs at these precise discrete time points. Rosser et al (2013) showed that the rate at which a movement path is sampled significantly affects the statistics used in RW framework, such as the mean trigonometric moments and mean step length. This is reinforced by the findings of Postlethwaite & Dennis (2013) who showed that varying the sub-sampling rate from between 10-60 minutes substantially changed the calculated mean trigonometric moments and mean step length, specifically the turning angle distribution went from highly peaked at finer scales to broader and closer to uniform at larger scales. Similar findings have been reported by Codling & Hill (2004) who give a mathematical analytical justification for the change in value for the parameters across scales, providing a method for estimating the values of the parameters used in the original RW from the sub sampled path by assuming a linear relation between sampling time step and the parameter values. However, Fryxell et al (2008) reported in the movement of free ranging elk (*Cervus elaphus*) that at varying spatiotemporal scales, whilst the parameters used to describe the movement behaviour may change, the number of movements modes/strategies was apparent at all scales indicating that mutliphase behaviour may still be captured and retained at varying scales using RW framework.

Having discussed the importance of RW in movement ecology, we now look at the mathematical framework of RW theory and demonstrate some of the key measures which can be analytically calculated from the most useful and common forms of random walks used within the field.

3 Mathematics of Random Walks

Perhaps the first example of a random walk was famously introduced into the scientific literature by the botanist Brown (Brown, 1828) who, whilst studying the movement of pollen on an apparent still body of water, noted the random movement of the grains of pollen across the meniscus. This random movement behaviour became known as *Brownian motion* and was given a mathematical explanation by the French mathematician Bachelier in his PhD thesis (Bachelier, 1900). Due to Bachelier's work, the first use of Brownian motion was applied to the stock market in an attempt to understand the movement of stock prices in the early 20th Century, however, it wasn't until the work of physicists von Smoluchowski (von Smoluchowski, 1906) and Einstein (Einstein, 1905) who, amongst other discoveries, derived the diffusion equation from the model of Brownian motion and showed the mathematical and predictive power of random processes when modelling averaged behaviour across systems with many particles. Although, at a similar time to Einstein's and von Smoluchowski's discoveries, the great English mathematician and statistician Karl Pearson wrote in a letter to *Nature* (Pearson, 1905)

- *A man starts from a point \mathbf{O} and walks l yards in a straight line; he then turns through any angle whatever and walks another l yards in a straight line. He repeats this process n times. I require the probability that after these n stretches he is at a distance between r and $r + \delta r$ from his starting point \mathbf{O} .*

This was answered by Lord Rayleigh in the same issue whose work on the superposition of light waves some years previous had yielded equivalent and analogous results (Rayleigh 1905).

The link here for the use of RW in analysis of movement data seems now to be clear, however, the initial models used were based on pure Brownian motion and as such treated every step in the process to be independent of the previous one, giving no preference for direction nor indeed the orientation of a walker at any specific step, hence providing a purely Markovian process (Weiss 1994).

Movement which is akin to Brownian motion is referred to as an isotropic simple ran-

dom walk (SRW), since the walker is equally like to step in any direction at any point in time or space and, importantly, the direction of each successive step is uncorrelated, that is the directions chosen are all statistically independent. In terms of animal movement, this is an assumption which appears unrealistic as certainly in the terms of purposeful movement (movement concerned with dislocation) a purely random direction selection would seem nonsensical, with animals often wishing to move towards a specific target or direction and most plausibly having knowledge of the direction from which they have just travelled. These observations give rise to the two other important types of RW which have become common in movement data analysis; the correlated random walk (CRW) in which there is a correlation between successive steps described as *persistence* by Patlak (1953), and the biased random walk (BRW), where there is a preference in direction (be that towards a specific point in space or a perceived directional gradient).

We now consider the three discussed types of RW in detail and derive some of the fundamental mathematical properties of each, which can be used to discern between them.

3.1 Simple Random Walk

Here we briefly introduce some standard results from random walk theory, which will be assumed in subsequent chapters.

3.1.1 SRW in Discrete Time and Space

If we assume we are in 1-dimensional discrete space with time steps from the index set $T = \{1, 2, 3, \dots\}$, then we can think of a SRW as a stochastic process S_n such that $\{S_n, n \in T\}$ given by

$$S_n = S_0 + \sum_{t=1}^n X_t \quad \text{for all } n \geq 1,$$

where S_0 is a constant and the random variables X_t are independently and identically distributed (*i.i.d.*) for all $n \in \{1, 2, \dots\}$, with $\Pr(X_t = 1) = p$ and $\Pr(X_t = -1) = q = 1 - p$.

Using this formulation of a SRW starting at $S_0 = 0$ we can calculate the expected

value of a SRW as,

$$\begin{aligned}\mathbb{E}[S_n] &= \mathbb{E}\left[S_0 + \sum_{t=1}^n X_t\right] \\ &= S_0 + \sum_{t=1}^n \mathbb{E}[X_t] \\ &= n \cdot \mathbb{E}[X_t] \\ &= n \cdot (p - q)\end{aligned}$$

where $\mathbb{E}[X_t] = 1 \cdot p + (-1) \cdot q = p - q$.

Similarly, we can find the variance of a SRW after n steps to be

$$\begin{aligned}\text{Var}[S_n] &= \text{Var}\left[S_0 + \sum_{t=1}^n X_t\right] \\ &= \text{Var}\left[\sum_{t=1}^n X_t\right] \\ &= \sum_{t=1}^n \text{Var}[X_t] \\ &= n \cdot \text{Var}[X_t] = 4npq\end{aligned}$$

where

$$\begin{aligned}\text{Var}[X_t] &= \mathbb{E}[X_t^2] - (\mathbb{E}[X_t])^2 \\ &= (1^2 \cdot p + (-1)^2 \cdot q) - (p - q)^2 = 4pq\end{aligned}$$

Hence, the MSD, $\mathbb{E}[S_n^2]$ of a SRW is given by

$$\mathbb{E}[S_n^2] = \text{Var}[S_n] + \mathbb{E}[S_n]^2 = 4npq + n^2(p - q)^2$$

In the specific case for the SRW being isotropic, that is $p = q = \frac{1}{2}$, the expected

value, MSD and variance becomes

$$\mathbb{E}_{\text{iso}}[S_n] = n(p - q) = 0 \quad \mathbb{E}_{\text{iso}}[S_n^2] = 4npq = \text{Var}_{\text{iso}}[S_n] = n \quad (3.1)$$

This shows that in the case of the isotropic SRW the expected location after n steps is in the initial starting location and that the MSD increases linearly with time.

It be shown that in continuous time and space, that the probability of a walker having location, x , at time, t , is given by the Gaussian probability distribution

$$P(x, t) = \frac{1}{\sqrt{4\pi Dt}} \exp\left(-\frac{(x - vt)^2}{4Dt}\right) \quad (3.2)$$

where v is known as the *drift velocity*. Here, the initial condition is given by $P(x, t) = \delta(x)$, where $\delta(x)$ is the Dirac delta function (Codling, 2003).

Considering the specific case of an isotropic random walk, with $p = q = 1/2$ we have the drift velocity v equal to 0 in the exponential of Eq. 3.2 and hence, the expression for the probability distribution of a walker being at location, x , after time t , in continuous time and space when moving under an isotropic SRW is

$$P(x, t) = \frac{1}{\sqrt{4\pi Dt}} \exp\left(-\frac{x^2}{4Dt}\right) \quad (3.3)$$

which is the fundamental solution to the *diffusion equation*

$$\frac{\partial P}{\partial t} = D \left(\frac{\partial^2 P}{\partial x^2} \right) \quad (3.4)$$

where D is defined as the *diffusion coefficient*.

Hence the expected mean location and MSD of an isotropic SRW in continuous time and space is simply the first and second moments of the Gaussian distribution given in Eq. 3.3

$$\mathbb{E}[x] = 0, \quad \mathbb{E}[x^2] = 2Dt \quad (3.5)$$

Therefore, a 1-dimensional isotropic random walk in continuous time and space has the

expected location of the initial starting point, 0 and MSD which grows linearly with time. Although it should be noted these values are valid only as $n \gg 1$ or equivalently as $t \rightarrow \infty$.

3.1.2 SRW in Higher Dimensions

One can find an expression for $P(\mathbf{x}, t)$ where $\mathbf{x} = (x_1, \dots, x_n)$ is an n -dimensional vector by considering a random walk in continuous n -dimensional space (\mathbb{R}^n). The resulting expression is given by finding the fundamental solution to the n -dimensional diffusion equation (Codling, 2003; Codling et al, 2008)

$$\frac{\partial P}{\partial t} = D \left(\frac{\partial^2 P}{\partial^2 x_1} + \dots + \frac{\partial^2 P}{\partial^2 x_n} \right) \quad (3.6)$$

which is given by

$$P(\mathbf{x}, t) = \frac{1}{(4\pi Dt)^{n/2}} \exp\left(-\frac{r^2}{4Dt}\right) \quad (3.7)$$

where $r^2 = x_1^2 + \dots + x_n^2$, with initial condition of $P(\mathbf{x}, 0) = (\delta(x_1), \dots, \delta(x_n))$.

In the specific 2-dimensional case we have the expected position of a walker at any given time to be $\mathbb{E}[\mathbf{x}, t] = \mathbb{E}[(x, y), t] = (0, 0)$ and the MSD to be given as $\mathbb{E}[R_t^2] = \mathbb{E}[r^2] = \mathbb{E}[x^2 + y^2] = 4Dt$ (Codling, 2003), which increases linearly with time as in the one-dimensional case.

In general solutions for the mean location and MSD can be generalised for any dimension, n , given as

$$\mathbb{E}[(\mathbf{x}, t)] = \mathbf{0} \quad \mathbb{E}[R_t^2] = 2nDt \quad (3.8)$$

where \mathbf{x} is a n -dimensional vector and $\mathbf{0}$ is the origin (initial starting point) of the walk. As with the one-dimensional case it should be noted that these solutions are only asymptotic approximations for the values of mean location and MSD as we assumed in the derivation that $N \rightarrow \infty$, therefore these values are not valid at short time scales.

3.2 Biased Random Walk

As discussed, the biased random walk (BRW) differs from the SRW by featuring a preference towards a certain direction at each time step. This can be towards a specific point in space, in which case the orientation of the preferred direction will depend upon the location of the walker at each step, or it can be towards a specific direction, for example magnetic North. The latter of these allows for summary statistics such as the MSD and expected location to be readily calculated, as the direction of the bias is considered homogeneous across all space.

In the 1-dimensional case the expected location and the MSD of a BRW at time t is given by

$$\mathbb{E}[x] = vt, \quad \mathbb{E}[x^2] = 2Dt + v^2t^2 \quad (3.9)$$

which are derived by finding the first and second moments of the probability distribution function given in Eq. 3.2. In our case, as we have taken the probability of moving right at any time step to be p then a bias towards the right direction will be given by having $p > q$, and vice-versa for preference to head towards the left. Eq. 3.9 shows that the expected location of a walker under a biased random walk increases linearly with time towards the direction of the bias, whereas the MSD increases quadratically with time. It's worth noting here that the MSD in this case is calculated around the initial starting point whereas a more sensible measure of spread would be to use the variance, since this measures the spread around the mean location (Codling et al, 2008). Eq. 3.9 gives us that the value for the variance, $\mathbb{E}[x^2] - \mathbb{E}[x]^2$, is $2Dt$; an expression which increases linearly with time and is therefore similar to the standard diffusion process.

3.2.1 BRW in Higher Dimensions

Throughout this thesis we will be focusing on random walks as a model for terrestrial movement, therefore we look to calculate the expected mean location and MSD of a BRW in two dimensions. Specifically, in accordance with movement data being recorded at discrete intervals we focus on a BRW in continuous 2-dimensional space \mathbb{R}^2 but in

discrete time.

To do this we consider a RW as a step-and-turn process. Recalling from section 2.6 this allows us to consider the walk as a series of step-lengths, l_i drawn from some positive distribution Λ , and angles, ϕ_i drawn from a distribution Φ with domain $(-\pi, \pi]$. Here we also include the conditions that angles and step-lengths are not correlated, nor are successive step-lengths and nor are successive angles. As we are considering a BRW we use global orientations/headings rather than turning angles, where the angle for the heading is taken clockwise from the positive y -axis (see Fig. 3.1). Section 2.6 stated that if the bias in movement is towards a specific point in space then the distribution of the headings is not stable over time, as the preferred direction is dependent upon the current location of a walker. Therefore, in this case deriving closed expressions for the expected location and MSD are not possible; although they can be found via simulation. Instead we consider the case in which the bias is towards a global direction (or a point at infinity).

We first introduce terms which are used in describing the distributions found in step-and-turn processes; mean cosine, $\mathbb{E}[\cos \omega]$, and mean sine, $\mathbb{E}[\sin \omega]$, which give the expected cosine and sine values of the probability distribution, Ω , used to describe the angles in the process, whether turning angles or global orientations/headings, and are linked to the moments of such distributions (these are discussed further in sections 3.7 & 3.8), as well as the mean cosine-squared, $\mathbb{E}[\cos^2 \omega]$ and mean sine-squared, $\mathbb{E}[\sin^2 \omega]$ along with the mean step length, $\mathbb{E}[l]$ and the mean square step length, $\mathbb{E}[l^2]$; all of which

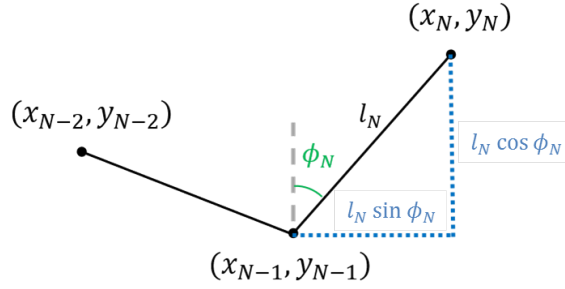


Figure 3.1: Calculating successive step locations using a step-and-turn process with headings taken from the positive y -axis

are given by the expressions:

$$\mathbb{E}[\cos \omega] = \int_{-\pi}^{\pi} \cos \omega \Omega(\omega) d\omega \quad (3.10)$$

$$\mathbb{E}[\sin \omega] = \int_{-\pi}^{\pi} \sin \omega \Omega(\omega) d\omega \quad (3.11)$$

$$\mathbb{E}[\cos^2 \omega] = \int_{-\pi}^{\pi} \cos^2 \omega \Omega(\omega) d\omega \quad (3.12)$$

$$\mathbb{E}[\sin^2 \omega] = \int_{-\pi}^{\pi} \sin^2 \omega \Omega(\omega) d\omega \quad (3.13)$$

$$\mathbb{E}[l] = \int_0^{\infty} l \Lambda(l) dl \quad (3.14)$$

$$\mathbb{E}[l^2] = \int_0^{\infty} l^2 \Lambda(l) dl \quad (3.15)$$

To calculate the expected location and MSD for a BRW in continuous 2-space with discrete time, let us consider that after $N - 1$ steps a walker is at position (x_{N-1}, y_{N-1}) (Fig. 3.1). The walker will move to position (x_N, y_N) given by

$$(x_N, y_N) = (x_{N-1}, y_{N-1}) + (l_N \sin \phi_N, l_N \cos \phi_N) \quad (3.16)$$

We can continue this process iteratively on the RHS allowing us to write (x_N, y_N) as

$$(x_N, y_N) = \left(\sum_{i=1}^N l_i \sin \phi_i, \sum_{i=1}^N l_i \cos \phi_i \right) \quad (3.17)$$

Therefore the mean location after N steps is found by taking the expectation of Eq.

3.17, giving

$$\mathbb{E}[\mathbf{x}] = \mathbb{E}[(x, y)] = \left(\mathbb{E} \left[\sum_{i=1}^N l_i \sin \phi_i \right], \mathbb{E} \left[\sum_{i=1}^N l_i \cos \phi_i \right] \right) \quad (3.18)$$

with starting location assumed to be the origin, $(x_0, y_0) = (0, 0)$.

Due to the expectation function being linear and recalling that the step-lengths and angles are independent, Eq. 3.18 becomes

$$\mathbb{E}[(x, y)] = \left(\sum_{i=1}^N \mathbb{E}[l_i] \mathbb{E}[\sin \phi_i], \sum_{i=1}^N \mathbb{E}[l_i] \mathbb{E}[\cos \phi_i] \right) \quad (3.19)$$

as all the step-lengths and angles are i.i.d we have that $\mathbb{E}[l_i] = \mathbb{E}[l]$, $\mathbb{E}[\cos \phi_i] = \mathbb{E}[\cos \phi]$ and $\mathbb{E}[\sin \phi_i] = \mathbb{E}[\sin \phi]$, hence Eq. 3.19 becomes

$$\mathbb{E}[(x, y)] = \left(\sum_{i=1}^N \mathbb{E}[l] \mathbb{E}[\sin \phi], \sum_{i=1}^N \mathbb{E}[l] \mathbb{E}[\cos \phi] \right) = N \mathbb{E}[l] (\mathbb{E}[\sin \phi], \mathbb{E}[\cos \phi]) \quad (3.20)$$

We note that this is similar to the 1-dimensional case with the drift velocity, v , now a 2-dimensional vector given by $(\mathbb{E}[l] \mathbb{E}[\sin \phi], \mathbb{E}[l] \mathbb{E}[\cos \phi])$

The MSD, $\mathbb{E}[R_N^2]$, after N steps can be calculated in a similar method. As the MSD at any given point is $R_i^2 = x_i^2 + y_i^2$ we can use Eq. 3.17 to give

$$R_N^2 = x_N^2 + y_N^2 = \left(\sum_{i=1}^N l_i \sin \phi_i \right)^2 + \left(\sum_{i=1}^N l_i \cos \phi_i \right)^2 \quad (3.21)$$

and hence

$$\begin{aligned} \mathbb{E}[R_N^2] &= \mathbb{E} \left[\left(\sum_{i=1}^N l_i \sin \phi_i \right)^2 + \left(\sum_{i=1}^N l_i \cos \phi_i \right)^2 \right] \\ &= \mathbb{E} \left[\left(\sum_{i=1}^N l_i \sin \phi_i \right)^2 \right] + \mathbb{E} \left[\left(\sum_{i=1}^N l_i \cos \phi_i \right)^2 \right] \end{aligned} \quad (3.22)$$

Using the linearity of the expectation and recalling that successive step-lengths and

angles are uncorrelated we can write the expected MSD after N steps as

$$\begin{aligned}\mathbb{E}[R_n^2] &= N \mathbb{E}[l^2] (\mathbb{E}[\sin^2 \phi] + \mathbb{E}[\cos^2 \phi]) + N(N-1) \mathbb{E}[l]^2 (\mathbb{E}[\sin \phi]^2 + \mathbb{E}[\cos \phi]^2) \\ &= N \mathbb{E}[l^2] + N(N-1) \mathbb{E}[l]^2 (\mathbb{E}[\sin \phi]^2 + \mathbb{E}[\cos \phi]^2)\end{aligned}\tag{3.23}$$

Finally if we assume we are in the long-term limit with $N \gg 1$ then this will tend asymptotically to

$$\mathbb{E}[R_n^2] = N \mathbb{E}[l^2] + N^2 \mathbb{E}[l]^2 (\mathbb{E}[\sin \phi]^2 + \mathbb{E}[\cos \phi]^2)\tag{3.24}$$

which is analogous to the 1-dimensional case with the drift velocity, v , now a 2-dimensional vector given as before to be $(\mathbb{E}[l] \mathbb{E}[\sin \phi], \mathbb{E}[l] \mathbb{E}[\cos \phi])$, and therefore $v^2 = (|v|)^2 = \mathbb{E}[l]^2 (\mathbb{E}[\sin \phi]^2 + \mathbb{E}[\cos \phi]^2)$

As in the 1-dimensional case the MSD increases quadratically with time, unlike the SRW. Fig. 3.2 demonstrates how the analytical solution for the MSD compares to a simulation of one individual random walker across varying degrees of strength in the bias term, due to the asymptotic nature of the solution the accuracy increases as the number of steps increase.

3.3 Correlated Random Walk

Both RW discussed previously have assumed that the orientations of successive steps are independent of each other. However, in a correlated random walk (CRW) it is assumed that a correlation exists between the directions of successive steps, often referred to as persistence (Patlak, 1953; Bovet and Benhamou, 1988, Wu et al, 2000; Codling et al, 2008).

This will produce a small scale local bias in preferred direction as the walker attempts to follow the heading of the previous direction.

In the 1-dimensional case the expected mean location of a CRW with N steps in which each step is of constant length, Δx , starting at the origin and with $N \gg 1$ is the origin

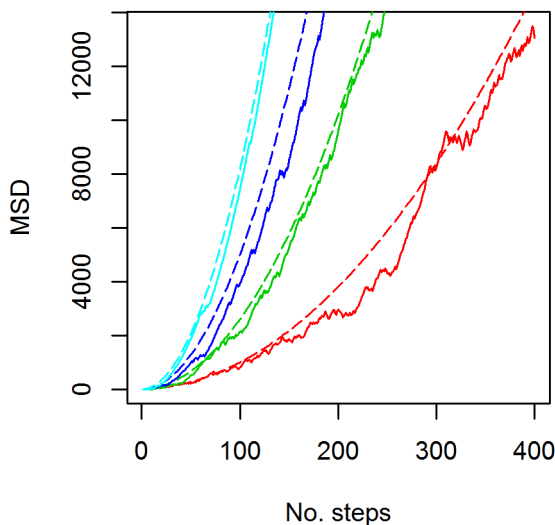


Figure 3.2: Comparison of the predicted MSD against simulations for a BRW with 300 steps. Dashed lines are the predicted results and the solid lines are the simulated results. The level of bias was given by the mean cosine, c , value of the distribution of angles (the distribution was symmetric around 0 and hence the mean sine value was 0; see section 3.8) with $c = 0.3$ (red), $c = 0.5$ (green), $c = 0.7$ (blue) & $c = 0.9$ (cyan). Simulations were for one random walker over 300 time steps.

itself. The MSD for a correlated walk tends asymptotically to

$$\mathbb{E}[x_N^2] \sim N(\Delta x)^2 \frac{1+\gamma}{1-\gamma} \quad (3.25)$$

where $\gamma = \frac{\mathbb{E}[x_i x_{i+1}]}{(\Delta x)^2}$. As we assumed each step was of constant length then the term in the numerator of γ must lie between 0 and $(\Delta x)^2$ and hence we have that $0 < \gamma < 1$. The specific cases for $\mathbb{E}[x_i x_{i+1}] = 0, 1$ are precisely the cases for the isotropic SRW and straight-line (ballistic) movement respectively. For all other values of γ Eq. 3.25 indicates that the MSD of a 1-dimensional CRW increases linearly with time but scaled by the factor $\frac{1+\gamma}{1-\gamma}$. As $\gamma \rightarrow 0$ the MSD reduces to $\mathbb{E}[x_N^2] \approx N(\Delta x)^2$, a result which is comparable to the result found for standard diffusion in continuous time, $\mathbb{E}[x^2] = 2Dt$ (Eq. 3.5), however this will only happen for very large N as the local bias in the initial orientation slowly decays.

3.3.1 CRW in Higher Dimensions

Similar to the BRW in higher dimensions we consider a CRW in 2-dimensions, in continuous space but discrete time using the step-and-turn process.

Kareiva & Shigesada (1983) used this model of a CRW to compute the MSD in a similar method to that used in the derivation of the BRW except here the correlation between steps needs to be taken into account. Kareiva & Shigesada (1983) showed that after N steps, $\mathbb{E}[R_N^2]$ is given by

$$\mathbb{E}[R_N^2] = N \mathbb{E}[l^2] + 2 (\mathbb{E}[l])^2 \left(\frac{N(c - c^2 - s^2) - c}{(1 - c)^2 + s^2} + \frac{2s^2 + (c^2 + s^2)^{(n+1)/2}\gamma}{((1 - c)^2 + s^2)^2} \right) \quad (3.26)$$

where $\gamma = ((1 - c)^2 - s^2) \cos((N + 1)\theta_0) - 2s(1 - c) \sin((N + 1)\theta_0)$ and θ_0 is the mean turning angle, defined as $\tan \theta_0 = s/c$.

In certain specific cases Eq. 3.26 becomes easier to handle, such as in the case for Θ being the uniform distribution (that is where $p(\theta) = \frac{1}{2\pi}$ for all $\theta \in [-\pi, \pi)$; see section 3.7) we would expect Eq. 3.26 to return the MSD for a 2-dimensional isotropic SRW. Using the uniform distribution we have $s = c = 0$ and therefore, $\mathbb{E}[R_N^2] \propto N \mathbb{E}[l^2]$ as $N \gg 1$, which is equivalent to the expression for the MSD of a 2-dimensional SRW given in Eq. 3.8 (with $n = 2$).

We can also consider the case for when the distribution, Θ , is symmetric around the mean value, $\mathbb{E}[\theta] = \mu$, which in terms of a random walker implies that clockwise turns are equally likely to anti-clockwise turns of the same magnitude. This is a reasonable assumption when considering animal movement in general, although there are specific cases when this is not a valid assumption. In this case the symmetry of the probability distribution reduces the mean sine term to $s = 0$ as $\sin \theta$ is an odd function. 3.11. Thus Eq. 3.26 reduces to

$$\mathbb{E}[R_N^2] = (\mathbb{E}[l])^2 \left(N \left(\frac{1 + c}{1 - c} + b^2 \right) - \frac{2c(1 - c^N)}{(1 - c)^2} \right) \quad (3.27)$$

where $b^2 = (\mathbb{E}[l^2]/\mathbb{E}[l]^2) - 1$, which is known as the coefficient of variation of the step

length. Eq. 3.27 shows the effect on the MSD varying the distribution of step lengths can have; in the simplest case with fixed step lengths we have $\mathbb{E}[l^2] = \mathbb{E}[l]^2$ and hence $b = 0$.

Assuming we are in the long term limit, with $N \rightarrow \infty$, we have

$$\mathbb{E}[R_N^2] \sim N \mathbb{E}[l^2] + 2N \mathbb{E}[l]^2 \frac{c}{1-c}, \quad c \neq 1 \quad (3.28)$$

This indicates that the MSD increases linearly with time and that distributions with a value of c close to 1 gives a larger MSD value, which is to be expected since $c \rightarrow 1$ implies that movement approaches straightline, ballistic behaviour.

Kareiva & Shigesada (1983) discuss the usefulness of these expressions for calculating MSD using a CRW as they give a simple method for whether or not movement can be interpreted as a CRW. By directly analysing the movement data, values for $\mathbb{E}[l]$, $\mathbb{E}[l^2]$, mean sine, s , and mean cosine, c , can be found which in turn can be substituted into Eq, 3.26 in order to predict the MSD as time increases. This can be directly compared to the observed data allowing for a simple indicative check that movement can be considered as a CRW. Fig. 3.3 shows the comparison of how the MSD of a CRW increases with time for simulated results (solid lines) against the predicted results (dashed lines), for a range of values representing the level of correlation between successive steps. Similar to the γ term described in the 1-dimensional case (Eq. 3.25) the mean vector length, r , defined as $r = (c^2 + s^2)^{1/2}$, gives a measure of the correlation of movement. Values close to 1 represent highly correlated movement and values close to 0 describe movement with almost no correlation. The mean vector length can be used to give the directional correlation between steps which are k places apart as r^{k+1} , and if we exclude the case for straight-line movement given when $r = 1$ then $r \in [0, 1)$ which tends to 0 as k gets very large for all values of r , indicating that a CRW sub-sampled at increasingly large intervals appears similar to a SRW. This demonstrates that the mean location, $\mathbb{E}[(\mathbf{x}, t)]$, for a CRW tends to the initial starting point of the walk, the same for the isotropic SRW. Note that this does require we are in the long term limit and $t \rightarrow \infty$, for example if we assume a group of walkers all starting moving in the same direction then if the level of

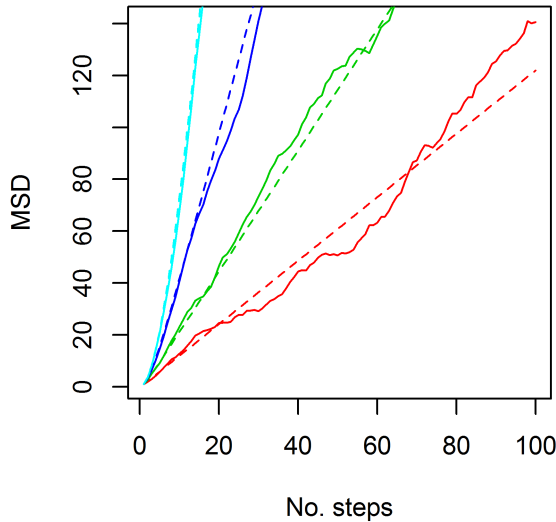


Figure 3.3: Comparison of the observed MSD of a CRW against the predicted results given in Eq. 3.28. Solid lines show the simulated results and the dashed lines are the predicted results. Results are for varying levels of correlation given by values of the mean cosine, c as 0.9 (cyan), 0.7 (blue), 0.4 (green) & 0.1 (red). Simulations were calculated by averaging over a group of 100 walkers

persistence is high (that is the ability to follow the previous direction is high, giving r close to 1) the early movement will appear to drift in the initial direction of movement, however, as time increases this apparent bias in movement direction will fall off and the walk will appear closer to that of an isotropic SRW (Fig 3.4).

Generalising the expressions for the MSD of a CRW in 3-dimensions or above using the methods of Kareiva & Shigesada is complex due to the need for spherical distributions (or the higher dimensional analogues), however, closed expressions do exist for the specific case where the distribution of turning angles are symmetric with respect to cylindrical coordinates (Sadjadi et al, 2015). Note this is the 3-dimensional equivalent of 2-dimensional case with a symmetric distribution in the turning angles, interpreted as a left turn and right turn of the same magnitude are equally likely.

Sadajadi et al (2015) derived the expression for the MSD in 3-dimensions as

$$\mathbb{E}[R_N^2] = N \mathbb{E}[l^2] + \mathbb{E}[l]^2 \frac{2\mathcal{E}}{1-\mathcal{E}} \left(N - \frac{1-\mathcal{E}^N}{1-\mathcal{E}} \right) \quad (3.29)$$

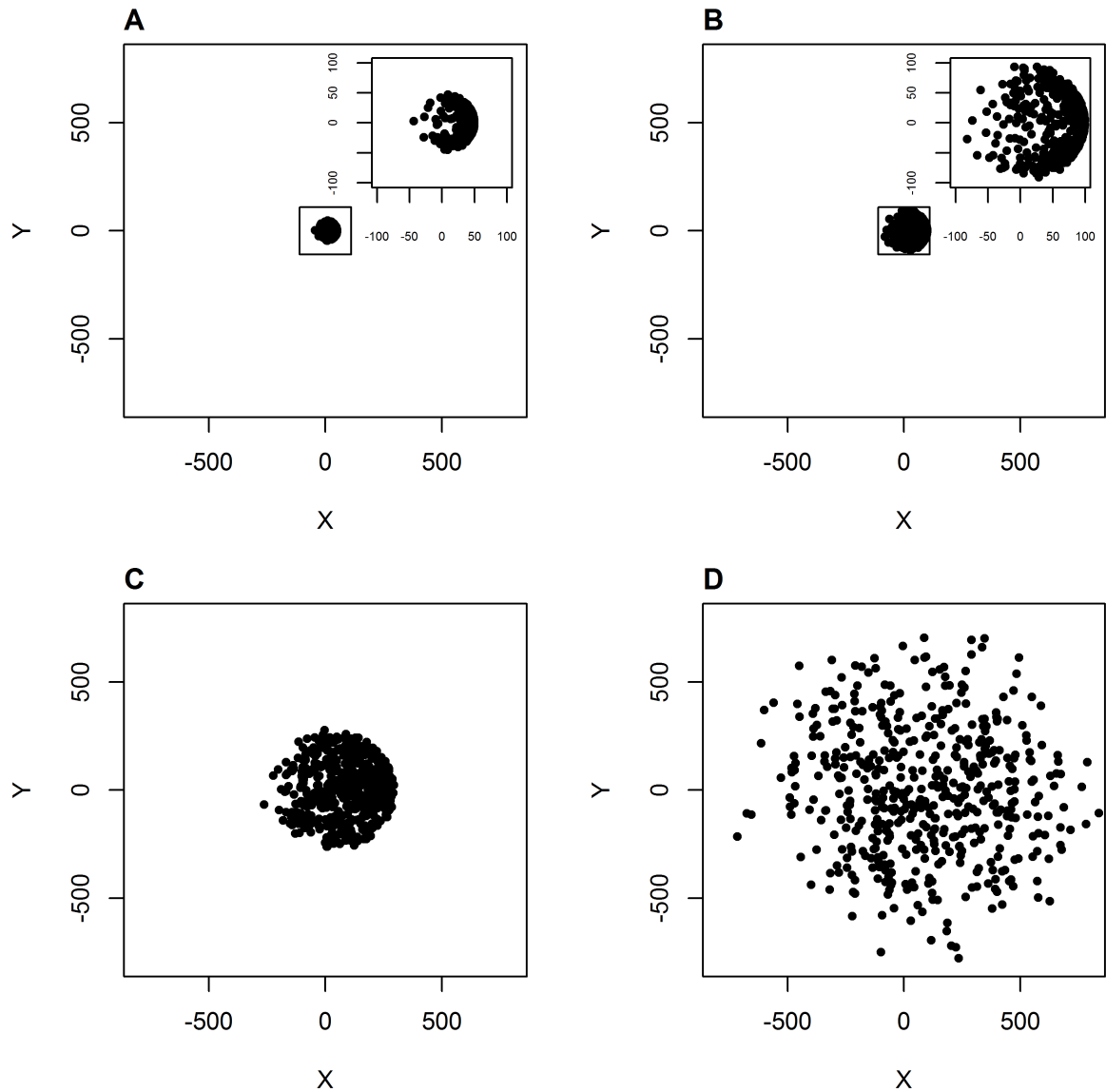


Figure 3.4: CRW in 2-dimensions with 100 walkers after (a) 10 steps; (b) 50 steps; (c) 100 steps; (d) 300 steps. The turning angles were drawn from a wrapped normal distribution centred at 0 with concentration value $\rho = 0.8$. All walkers had initial direction of movement towards the infinity in the positive x-direction. Step lengths were all of unit length

where

$$\mathcal{E} = \int_0^\pi \cos(\phi) \sin(\phi) \Phi(\phi) d(\phi) \quad (3.30)$$

Here, $\Phi(\phi)$, is the probability distribution for turning angle ϕ (the azimuth angle). With the polar angle ψ (the angle which lies in the xy -plane) considered to be uniformly distributed across ϕ , that is $p(\psi_1|\phi) = p(\psi_2|\phi)$ for all $\psi_1, \psi_2 \in [-\pi, \pi)$ and $\phi \in [0, \pi]$.

It should be noted that Benhamou (2018) derived the equivalent result using spherical coordinates in a method echoing that of Kareiva & Shigesada (1983).

3.4 Diffusion, sub-diffusion and super-diffusion

As seen in sections 3.1-3.3 the rate at which the MSD of a RW increases is proportional to some power of the time passed, $\mathbb{E}[R_t^2] \propto t^\beta$ (Fig. 3.5). The cases in which the MSD does not increase linearly with time ($\beta \neq 1$) are known as *anomalous diffusion* processes. The specific value of β can help identify between types of RW and give rise to 5 cases:

- $\beta = 0$. This is the trivial case in which no movement occurs,
- $0 < \beta < 1$. This case is known as *sub-diffusion* as the increase in MSD is less than with the linear relationship of standard diffusion. This slower increase in MSD can be seen in RWs with stopping times (Codling et al, 2008) and models of “run-and-tumble” motion in bacteria such as *E. coli* (Thiel et al, 2013).
- $\beta = 1$. This is the case for standard diffusive behaviour, as is the case for an isotropic SRW and a CRW (in the long term-limit) (see section 3.1 & 3.3)
- $1 < \beta < 2$. This case is known as *super-diffusion* as the increase in MSD is greater than the linear relationship of standard diffusion. This has been demonstrated to be the case for Lévy walks (Viswanathan, 2008) due to the variance in step-lengths being non-finite (Codling et al, 2008)
- $\beta = 2$. This is known as *ballistic* behaviour as the MSD increases at the greatest possible rate with time, and is equivalent to an individual moving in a constant direction away from the initial starting location.

Remark. The case for $\beta > 2$ is not considered as having a value greater than 2 does not make sense in terms of animal displacement.

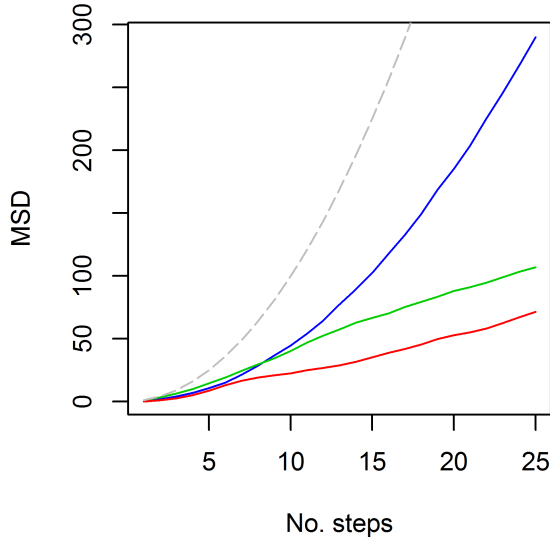


Figure 3.5: Comparison of the MSD against number of time steps for SRW (red), CRW (green), BRW (blue) and pure ballistic movement (grey). Simulations were run across 1000 walkers for 25 time steps, with each step having unit length

3.5 Circular Statistics and Distributions

Clearly the analysis of angular data is important in the RW model framework. Recorded data gives rise to a time series of discrete angles, and due to the periodicity of angular data traditional statistical techniques cannot be used, instead we introduce the notion of circular statistics.

3.6 Circular Data

Discrete angular data can be described by various summary statistics, as fully described in Fisher (1993); Mardia & Jupp (2000); Jammalamadaka & SenGupta (2011). Let $\boldsymbol{\theta} = (\theta_1, \dots, \theta_n)$ be a series of n angles then we define the p th cosine moment, \bar{C}_p , and p th sine moment, \bar{S}_p values as

$$\bar{C}_p = \frac{1}{n} \sum_{i=1}^n \cos p\theta_i, \quad \bar{S}_p = \frac{1}{n} \sum_{i=1}^n \sin p\theta_i \quad (3.31)$$

where the specific case for $p = 1$ gives the mean cosine, \bar{C} , and mean sine \bar{S} values respectively.

Using the mean cosine and sine values we can define the *mean resultant length* \bar{R} , which is given by

$$\bar{R} = (\bar{C}^2 + \bar{S}^2)^{1/2} \quad (3.32)$$

The mean angle $\bar{\theta}$ is given by

$$\bar{\theta} = \begin{cases} \arctan(\bar{S}/\bar{C}) & \text{if } \bar{C} \geq 0 \\ \arctan(\bar{S}/\bar{C}) + \pi & \text{if } \bar{C} < 0 \end{cases} \quad (3.33)$$

note here that $\bar{\theta}$ is not defined when $\bar{R} = 0$ and importantly $\bar{\theta} \neq (\theta_1 + \dots + \theta_n)/n$ due to the periodicity of angular data.

The value of \bar{R} gives information as to the spread of angles around the unit circle, values close to 1 indicate that the angles are clustered close together whereas a value closer to 0 indicates a near uniform distribution on the unit circle.

3.7 Circular Distributions

3.7.1 Wrapped Distributions

One can form a distribution around the unit circle by taking distributions along the real line and transforming the real-valued random variable, X , into a circular random variable, θ by reducing it modulo 2π (Mardia & Jupp, 1999; Jammalamadaka & SenGupta, 2001)

$$\theta \equiv X \pmod{2\pi} \quad (3.34)$$

in particular this allows the distribution of the wrapped analogy of a linear distribution, $f_{\circ}(\theta)$, to be written in terms of the linear distribution $f(X)$ as

$$f_{\circ}(\theta) = \sum_{m=-\infty}^{\infty} f(\theta + 2\pi m), \quad \theta \in [-\pi, \pi), \quad m \in \mathbb{N} \quad (3.35)$$

The most straightforward of these distributions is the circular uniform distribution which is the circular analogy of the uniform distribution on the reals.

Definition 3.1. Circular Uniform Distribution

The circular uniform distribution is given by

$$f_{\text{CU}}(\theta) = \frac{1}{2\pi} \quad (3.36)$$

where $\theta \in [-\pi, \pi)$

Two other examples which will be used throughout are the wrapped normal and the wrapped Cauchy distributions, respectively formed by wrapping the usual normal (Gaussian) and the Cauchy distributions, on the real numbers around the unit circle.

Definition 3.2. Wrapped Cauchy distribution

A wrapped Cauchy (WC) distribution is given by the density

$$f_{\text{wc}}(\theta; \sigma, \mu) = \frac{1}{\pi} \sum_{m=-\infty}^{\infty} \frac{\sigma}{\sigma^2 + (\theta - \mu + 2m\pi)^2} \quad m \in \mathbb{N} \quad (3.37)$$

where $\theta \in [-\pi, \pi)$. The location and dispersion parameters are given respectively by $\mu \in [-\pi, \pi)$, $\sigma > 0$.

A useful trait of the WC distribution is that it can be written in closed form

$$f_{\text{wc}} = \frac{1}{2\pi} \frac{1 - \rho^2}{1 + \rho^2 - 2\rho \cos(\theta - \mu)} \quad (3.38)$$

where $\rho = e^{-\sigma}$ is defined as the concentration parameter of the distribution.

Definition 3.3. Wrapped Normal Distribution

A wrapped normal (WN) distribution is given by the density

$$f_{\text{wn}}(\theta; \sigma, \mu) = \frac{1}{\sigma\sqrt{2\pi}} \sum_{m=-\infty}^{\infty} \exp\left(-\frac{(\theta - \mu + 2m\pi)^2}{2\sigma^2}\right) \quad m \in \mathbb{N} \quad (3.39)$$

where $\theta \in [-\pi, \pi)$. The location and dispersion parameters are given respectively by $\mu \in [-\pi, \pi)$, $\sigma > 0$.

A more general family of wrapped distribution, known as the symmetric wrapped stable (SWS) distributions, includes distributions which are symmetric about their mean value and can be defined as;

Definition 3.4. Symmetric Wrapped Stable Distribution

A symmetric wrapped stable (SWS) distribution has the density function given by:

$$f_{\text{sws}}(\theta; \rho, \mu, a) = \frac{1}{2\pi} \left(1 + 2 \sum_{n=1}^{\infty} \rho^{n^a} \cos n(\theta - \mu) \right), \quad n \in \mathbb{N} \quad (3.40)$$

where $\rho \in [0, 1]$ is the concentration parameter of f_{sws} , $\mu \in [-\pi, \pi)$ is the location parameter around which the distribution is symmetric and $a \geq 0$ (Jammalamadaka & Sengupta, 2001; Chapter 2).

It can be shown that both the WC and WN distributions are SWS distributions with (Jammalamadaka & Sengupta, 2001; Chapter 2);

- $a = 1$, for the wrapped Cauchy distribution with a concentration parameter calculated by $\rho_{\text{wc}} = e^{-\sigma_{\text{wc}}}$
- $a = 2$, for the wrapped normal distribution with a concentration parameter calculated by $\rho_{\text{wn}} = e^{-\sigma_{\text{wn}}^2/2}$

3.7.2 Non-Wrapped Distributions

Another important circular distribution which is not a member of the SWS distribution family and therefore cannot be formed by wrapping a distribution on the real line around the unit circle is the von Mises (vM) or Circular Normal (CN) distribution (Stephens, 1963; Mardia & Jupp, 1999; Jammalamadaka & Sengupta, 2001)

Definition 3.5. Von Mises Distribution

A von Mises distribution is given by the density function

$$f_{\text{vM}}(\theta; \mu, \kappa) = \frac{1}{2\pi I_0(\kappa)} e^{\kappa \cos(\theta - \mu)} \quad (3.41)$$

where $\theta \in [-\pi, \pi)$ and I_0 is the modified Bessel function of the first kind with order 0. The location and dispersion parameters are given respectively by $\mu \in [-\pi, \pi), \kappa \geq 0$.

The concentration parameter of the von Mises distribution, ρ_{vM} , is found using the relation $\rho_{\text{vM}} = \frac{I_1(\kappa)}{I_0(\kappa)}$ where I_1 is the modified Bessel function of the first kind with order 1.

It is well known that for any given WN distribution a vM can be found as an accurate approximation (Stephens, 1963; Collett & Lewis 1981; Jammalamadaka & Sengupta, 2001). Hence, both give qualitatively similar results when used in random walk (RW) models (Codling et al, 2010).

3.8 Trigonometric moments

Trigonometric moments of circular distributions are analogous to the conventional real-valued moments of general probability distribution functions ($\mathbb{E}[X^n]$ for $n \in \mathbb{Z}^+$),

Definition 3.6. Trigonometric Moments

The n th trigonometric moment of a random variable θ with circular density function f_\circ is given by

$$\phi_n(\theta) = \mathbb{E}[e^{in\theta}] = \int_{-\pi}^{\pi} e^{in\theta} f_\circ(\theta) d\theta, \quad n \in \mathbb{N} \quad (3.42)$$

Using the properties of complex numbers $\phi_n(\theta)$ can be written in terms of cosine and sine, as

$$\phi_n(\theta) = \mathbb{E}[e^{in\theta}] = \mathbb{E}[\cos n\theta + i \sin n\theta] = \mathbb{E}[\cos n\theta] + i \mathbb{E}[\sin n\theta] =: \alpha_n + i\beta_n \quad (3.43)$$

Remark. In the specific case where f_\circ is symmetric around the centre value $\mu = 0$, we have $\beta_n = 0$ for all n since

$$\beta_n = \int_{-\pi}^{\pi} \sin n\theta f_\circ(\theta) d\theta = 0 \quad (3.44)$$

by the properties of $\sin n\theta$ being an odd function and f_\circ symmetric around 0. Hence, all the trigonometric moments of a zero centred symmetric circular distribution (such as

the SWS family with $\mu = 0$; Def. 3.44) are real and involve only cosine terms.

The concentration parameter, ρ , of a SWS is linked to the trigonometric moments by

$$\rho^{n^a} = \sqrt{\alpha_n^2 + \beta_n^2} \quad (3.45)$$

(Jammalamadaka & SenGupta, 2001; Chapter 1) Eq. 3.44 shows that the *first trigonometric moment* of a symmetric distribution centred around 0 is given by $\phi_1(\theta) = \alpha_1$ and, therefore, from Eq. 3.45 we see that $\alpha_1^{\{\text{wn}\}} = \rho_{\text{wn}}$ and $\alpha_1^{\{\text{wc}\}} = \rho_{\text{wc}}$ demonstrating that the concentration parameters for both WC and WN distributions are precisely the first trigonometric moments of the distributions.

Using these and the definition of a SWS distribution (Def 3.4) we can write a SWS distribution as

$$f_{\text{sws}}(\theta; \rho_{\text{sws}}, \mu_{\text{sws}}) = \frac{1}{2\pi} \left(1 + 2 \sum_{n=1}^{\infty} \alpha_n \cos n(\theta - \mu_{\text{sws}}) \right) \quad (3.46)$$

where α_n is the n th cosine moment of f_{sws} given as $\rho_{\text{sws}}^{n^a} = \alpha_n$ as in Eq. 3.45.

Similarly WC and WN distributions can be written as

$$f_{\text{wc}}(\theta; \rho_{\text{wc}}, \mu_{\text{wc}}) = \frac{1}{2\pi} \left(1 + 2 \sum_{n=1}^{\infty} \rho_{\text{wc}}^n \cos n(\theta - \mu_{\text{wc}}) \right) \quad (3.47)$$

$$f_{\text{wn}}(\theta; \rho_{\text{wn}}, \mu_{\text{wn}}) = \frac{1}{2\pi} \left(1 + 2 \sum_{n=1}^{\infty} \rho_{\text{wn}}^{n^2} \cos n(\theta - \mu_{\text{wn}}) \right) \quad (3.48)$$

The trigonometric moments of the von Mises distribution are given by

$$\begin{aligned} \phi_n^{\text{vM}} &= \frac{1}{2\pi I_0(\kappa)} \int_{-\pi}^{\pi} \cos n(\theta - \mu) e^{\kappa \cos(\theta - \mu)} d\theta \\ &= \frac{I_n(\kappa)}{I_0(\kappa)} \end{aligned} \quad (3.49)$$

where I_n is the modified Bessel function of the first kind of order n (Jammalamadaka & SenGupta, 2001).

This allows the von Mises distribution to be written in a similar form to the WC and WN in Eqs. 3.47 & 3.48 as

$$f_{\text{vM}}(\theta; \kappa, \mu_{\text{vM}}) = \frac{1}{2\pi I_0(\kappa)} \left(I_0(\kappa) + 2 \sum_{n=1}^{\infty} I_n(\kappa) \cos n(\theta - \mu_{\text{vM}}) \right) \quad (3.50)$$

For a complete discussion of circular distributions and trigonometric moments see Mar-dia & Jupp (2000) and Jammalamadaka & Sengupta (2001).

The previous Chapters have introduced and given an overview of the themes and topics used throughout the thesis. The following Chapters represent the research portion of the thesis.

4 Navigational efficiency in a biased and correlated random walk model of individual animal movement

This chapter is adapted from work which was published in *Ecology* (Bailey et al, 2018) and includes contributions from J. Wallis (JW) (University of Oxford) and E.A. Codling (EC) (University of Essex). JW and EC considered the derivation and analysis of the basic model in section 4.2.1. EC contributed towards the writing of the published manuscript (Bailey et al, 2018).

As discussed in the introductory chapter, understanding how an individual animal is able to navigate through its environment is a key question in movement ecology as it can give an insight into observed movement patterns and the mechanisms behind them. Efficiency of navigation is important for behavioural processes at a range of different spatio-temporal scales, including foraging and migration. Chapters 2 & 3 discussed that a standard framework for modelling individual animal movement and navigation uses random walk models. In this chapter we consider a vector-weighted biased and correlated random walk (BCRW) model for directed movement (taxis), where external navigation cues are balanced with forward persistence. We derive mathematical approximations of the expected navigational efficiency for any BCRW of this form and confirm the model predictions using simulations. We demonstrate how the navigational efficiency is related to the weighting given to forward persistence and external navigation cues, and highlight the counter-intuitive result that for low (but realistic) levels of error on forward persistence, a higher navigational efficiency is achieved by giving more weighting to this indirect navigation cue rather than direct navigational cues. We discuss and interpret the relevance of these results for understanding animal movement and navigation strategies.

4.1 Introduction

Animal navigation can occur across various spatio-temporal scales corresponding to a wide variety of behavioural processes, ranging from short-term foraging and home-range exploration (Schultz & Crone, 2001; Jonsen et al, 2005; Fortin et al, 2005; McClintock et al, 2012) to large-scale migration events (Gardiner et al, 2015; Nicosia et al, 2015).

Chapters 2 & 3 demonstrated that random walk (RW) theory has a long history of being used to model individual animal movement and navigation, and as a tool to interpret observed movement data using various path analysis techniques (Jonsen et al, 2005; Codling et al, 2008; Langrock et al, 2012; McClintock et al, 2012). RW models that incorporate a directional preference (e.g. preference to navigation towards a specific target, or towards a specific direction) were termed as biased random walks (BRW) (Marsh & Jones, 1988; Benhamou, 2006; Codling et al, 2008; Codling et al, 2010) and those which had a correlation in the direction of concurrent steps were termed correlated random walks (CRW), with this preference to follow the previous heading referred commonly as persistence (Patlak, 1953; Kareiva & Shigesada, 1983; Bovet & Benhamou, 1988; Benhamou, 2004; Codling et al, 2008). Movement processes that contain both a short-term localised forward persistence and a global target can be modelled as biased and correlated random walks (BCRW). In a BCRW the external navigation and forward persistence components can be combined in a simple weighted vector sum (Benhamou & Bovet, 1992; Benhamou, 2004; Codling et al, 2008), but other models are also possible (Schultz & Crone, 2001; Codling et al, 2005; Peleg & Mahadevan, 2016).

Common navigation orientation mechanisms include taxis, where an animal directly orientates in response to external directional cues, and differential klinokinesis (DKK), where the level of turning in the movement path (sinuosity) depends on variations in the magnitude of an external stimulus; both taxis and DKK lead to a long-term directional drift (bias) towards the target (Benhamou & Bovet, 1992). Empirical studies have considered how a variety of different animals may balance taxis and persistence mechanisms in order to navigate within their local environment, including butterflies (Schultz & Crone, 2001), elk (Fortin et al, 2005), and grey seals (McClintock et al, 2012). Hence

it is important to consider a theoretical basis for animal navigation and the underlying mechanisms that may lead to improved navigational efficiency.

Benhamou & Bovet (1992) combined taxis and forward persistence to form a vector-weighted BCRW model of movement, and found in a 1000-step random walk that the best navigational strategy was to give approximately 10% weighting to external navigation cues (taxis) and approximately 90% weighting to forward persistence. Such a navigation strategy gave higher navigational efficiency than a movement process based on taxis alone (a pure BRW), although it should be stressed that Benhamou & Bovet (1992) only included error in their external navigation term and not in their forward persistence term. The fact that the most efficient navigation strategy involved giving a high weighting to persistence rather than taxis may seem to be a counter-intuitive result, since movement based purely on persistence is known to be an inefficient navigation strategy when compared to pure taxis (Cheung et al, 2007). A similar result to Bovet & Benhamou (1992) was obtained by Codling & Bode (2014) who found that, in the context of a collective movement model for navigating animal groups, the most efficient navigational strategy was to give a high weighting to indirect navigational cues (copying the movement of other group members) and a low (but non-zero) weighting to direct individual navigational cues (taxis). In a follow-up study, Codling & Bode (2016) included individual forward persistence in the collective movement model and showed that giving a high weighting to indirect cues (copying neighbours or using forward persistence) rather than relying on direct navigational cues gave the highest navigational efficiency.

The findings of Benhamou & Bovet (1992) and Codling & Bode (2014, 2016) were based on simulations only and the authors did not give a mathematical explanation for these results. Here we consider a generalised form of the Benhamou & Bovet (1992) BCRW navigation model, that includes error on the persistence term, and derive a mathematical approximation for the expected navigational efficiency. The model predicts that for a reasonably large (and realistic) range of navigation and persistence errors, the highest navigational efficiency is achieved by giving a low weighting to direct navigational

cues. We discuss the relevance and implications of these findings in the wider movement ecology context.

4.2 Mathematical model

The BCRW model of Benhamou & Bovet (1992) assumes a single random walker starts at the origin, $(0, 0)$, and moves through an featureless, homogeneous two-dimensional environment. For simplicity, the target is assumed to be a ‘point at infinity’ located along the positive x-axis (this effectively means we are only considering the large-scale part of the navigation process when the animal is far from the target). Orientation angles are measured counter-clockwise from the x-axis, and hence the target direction is given by $\Omega_T = 0$. We assume the walker initially starts with no information about the target direction; an initial movement direction, θ_0 , is randomly drawn from a uniform circular distribution (this assumption does not affect our results as we will show that the long-term navigational efficiency is independent of θ_0). At each random walk step the components of movement in each direction are given by a weighted vector sum of a navigation term and a persistence term (Benhamou & Bovet, 1992):

$$\Delta x_{n+1} = r_{n+1} (w \cos(\Omega_T + \phi_n) + (1 - w) \cos(\theta_n + \delta_n)) \quad (4.1)$$

$$\Delta y_{n+1} = r_{n+1} (w \sin(\Omega_T + \phi_n) + (1 - w) \sin(\theta_n + \delta_n)) \quad (4.2)$$

Where r_{n+1} is the step length (distance moved) in the current step, $\Omega_T = 0$ is the target direction (which is fixed as the x-axis for all steps), θ_n is the direction of movement in the previous step (which varies at each step), δ_n is a persistence error term, ϕ_n is a navigation error term, and $w \in [0, 1]$ is the weighting given to navigation (and hence $(1-w)$ is the weighting given to persistence). In contrast to Benhamou & Bovet (1992) (who only included an error in the navigation term), we include errors on both the navigation and persistence terms. In principle it would be possible to have an even more general BCRW model that includes an additional ‘output noise/error’ term in addition to the navigation and persistence error terms. This output noise could represent either

additional movement error because of environmental factors (e.g. turbulence) or could represent a form of ‘voluntary’ error that the animal may use to modulate its behaviour between behavioural states. However, these more complex model features are beyond the scope of the current work.

The additive navigation and persistence random error terms, ϕ_n and δ_n , are drawn from separate zero-centred symmetric circular distributions with respective mean cosine values given by $c_\phi \in [0, 1]$ and $c_\delta \in [0, 1]$. The level of navigation and/or persistence error is determined by the mean cosine values, c_ϕ and c_δ : a value close to 0 corresponds to very high error, and a value close to 1 corresponds to very low error. We assume that c_ϕ and c_δ are fixed for all steps of the random walk, which implies that direction and persistence errors are independent (no correlation of errors between successive steps) and are not related to spatial location or any other external factor. Hence we do not consider possible changes in navigation cue strength as the animal approaches the target, interactions with other animals, or changes in behaviour and interactions with the environment such as foraging or resting during the navigation process. Note that, as long as c_ϕ and c_δ are defined, the choice of which circular distribution to use is not important since the results only depend on the first trigonometric moment (the mean cosine value); the same results are obtained using common circular distributions such as the wrapped normal, von Mises and wrapped Cauchy (Section 3.7; Mardia & Jupp, 1999).

Similar to Benhamou & Bovet (1992), we define the navigational efficiency of a single step of the movement process as:

$$\text{Navigational efficiency} = \frac{\text{Net distance moved towards target in } x \text{ direction}}{\text{Total distance moved}} \quad (4.3)$$

Hence, for the BCRW given by Eqs. 4.1 and 4.2 the expected navigational efficiency at a given step is given by $\mathbb{E}[\cos \theta_{n+1}]$ since the target direction is the x-axis ($\Omega_T = 0$). In the extreme case of a pure BRW ($w = 1$), navigational efficiency is given exactly by $\mathbb{E}[\cos \phi_n] = c_\phi$, while for a pure CRW ($w = 0$), navigational efficiency is given exactly by $\mathbb{E}[\cos(\theta_n + \delta_n)] = 0$, since we assume a uniform initial orientation and there is no external navigation cue.

We now look to find a direct expression for the navigational efficiency at each step, $\mathbb{E}[\cos \theta_{n+1}]$ the general case of $0 < w < 1$.

4.2.1 First Analytical Approximation

In this first method of analytically solving the model we first normalise Eq. 4.1 and rewrite using standard trigonometric identities to give

$$\cos \theta_{n+1} = \frac{w \cos \phi_n + (1 - w) \cos(\theta_n + \delta_n)}{\sqrt{w^2 + (1 - w)^2 + 2w(1 - w) \cos(\phi_n - (\theta_n + \delta_n))}} \quad (4.4)$$

which it should be noted is independent of the step length, r_{n+1} . Taking the expectation of Eq. 4.4 then gives

$$\mathbb{E}[\cos \theta_{n+1}] = \mathbb{E} \left[\frac{w \cos \phi_n + (1 - w) \cos(\theta_n + \delta_n)}{\sqrt{w^2 + (1 - w)^2 + 2w(1 - w) \cos(\phi_n - (\theta_n + \delta_n))}} \right] \quad (4.5)$$

The expression on the right-hand side of Eq. 4.5 is non-linear so we cannot directly calculate the expectation. Hence we assume we can approximate a solution using a similar argument as given in Wu et al (2000) (equation 10), and we proceed by treating the right-hand side of Eq. 4.5 as if it were linear. This approximation, along with the fact that w is a constant, means Eq. 4.5 can be written as

$$\mathbb{E}[\cos \theta_{n+1}] \approx \frac{w \mathbb{E}[\cos \phi_n] + (1 - w) \mathbb{E}[\cos(\theta_n + \delta_n)]}{\sqrt{w^2 + (1 - w)^2 + 2w(1 - w) \mathbb{E}[\cos(\phi_n - (\theta_n + \delta_n))]}} \quad (4.6)$$

If we assume θ_n, ϕ_n and δ_n are all independent, then

$$\mathbb{E}[\cos(\theta_n + \delta_n)] = \mathbb{E}[\cos \theta_n] \mathbb{E}[\cos \delta_n] \quad (4.7)$$

and

$$\mathbb{E}[\cos(\phi_n - (\theta_n + \delta_n))] = \mathbb{E}[\cos \theta_n] \mathbb{E}[\cos \phi_n] \mathbb{E}[\cos \delta_n] \quad (4.8)$$

since

$$\mathbb{E}[\sin \phi_n] = \mathbb{E}[\sin \delta_n] = 0 \quad (4.9)$$

(as δ_n and ϕ_n are drawn from symmetric circular distributions centred on zero; see section 3.8). Under this assumption of independence and using standard trigonometric identities, Eq. 4.6 can then be written as

$$\mathbb{E}[\cos \theta_{n+1}] \approx \frac{w \mathbb{E}[\cos \phi_n] + (1-w) \mathbb{E}[\cos \theta_n] \mathbb{E}[\cos \delta_n]}{\sqrt{w^2 + (1-w)^2 + 2w(1-w) \mathbb{E}[\cos \phi_n] \mathbb{E}[\cos \theta_n] \mathbb{E}[\cos \delta_n]}} \quad (4.10)$$

We now consider the long-term limit as n gets large. Hill & Häder (1997) demonstrated that, in the long-term limit, the distribution of movement directions in a BCRW is stable and symmetric around the target direction. Hence, we assume that for large n in our model we have $\mathbb{E}[\cos \theta_{n+1}] = \mathbb{E}[\cos \theta_n] = \mathbb{E}[\cos \theta_\infty]$, where $\mathbb{E}[\cos \theta_\infty]$ represents the expectation of the long-term limit directional cosine in the target movement direction. Hence from Eq. 4.3, $\mathbb{E}[\cos \theta_\infty]$ is exactly equivalent to the long-term navigational efficiency. Under this assumption and using the fact that $\mathbb{E}[\cos \phi_n] = \mathbb{E}[\cos \phi] = c_\phi$ and $\mathbb{E}[\cos \delta_n] = \mathbb{E}[\cos \delta] = c_\delta$ we can rewrite Eq. 4.10 as

$$\mathbb{E}[\cos \theta_\infty] = \frac{w c_\phi + (1-w) c_\delta \mathbb{E}[\cos \theta_\infty]}{\sqrt{w^2 + (1-w)^2 + 2w(1-w) c_\phi c_\delta \mathbb{E}[\cos \theta_\infty]}} \quad (4.11)$$

Now defining $c_\theta = \mathbb{E}[\cos \theta_\infty]$, and rearranging; Eq. 4.11 leads to a cubic polynomial for c_θ :

$$2w(1-w)c_\phi c_\delta c_\theta^3 + (w^2 + (1-w)^2(1-c_\delta^2)) c_\theta^2 - 2w(1-w)c_\phi c_\delta c_\theta - w^2 c_\phi^2 = 0 \quad (4.12)$$

It is possible to show that this polynomial has precisely one root in $[0, 1]$ for all feasible values of c_ϕ, c_δ and w (see Appendix A1). This root can be calculated using Cardano's method, which gives a solution in the form

$$c_\theta = \sqrt[3]{A + \sqrt{A^2 + B^3}} + \sqrt[3]{A - \sqrt{A^2 + B^3}} - C \quad (4.13)$$

where

$$\begin{aligned}
A &= - \left[\frac{w^2 + (1-w)^2(1-c_\delta^2)}{6w(1-w)c_\phi c_\delta} \right]^3 - \frac{w^2 + (1-w)^2(1-c_\delta^2)}{12w(1-w)c_\phi c_\delta} + \frac{wc_\phi}{4(1-w)c_\delta} \\
B &= - \left[\frac{w^2 + (1-w)^2(1-c_\delta^2)}{6w(1-w)c_\phi c_\delta} \right]^2 - \frac{1}{3} \\
C &= \frac{w^2 + (1-w)^2(1-c_\delta^2)}{6w(1-w)c_\phi c_\delta}
\end{aligned} \tag{4.14}$$

Figure 4.1 shows the results of plotting the navigational efficiency, c_θ , against weighting factor on navigation, w , for a range of navigation error levels, $c_\phi = 0.1$ (black), $c_\phi = 0.3$ (cyan), $c_\phi = 0.6$ (gold) & $c_\phi = 0.9$ (blue) with the value of the error on persistence varying from $c_\delta = 1$ (the specific case for perfect persistence, as discussed in Benhamou & Bovet (1992)) to $c_\delta = 0.1$, corresponding to a large error on navigation. In all plots the solid lines represent the theoretical model predictions and the dashed lines represent the results from simulations.

4.2.2 Second Analytical Approximation

Similar to the previous approach we start by normalising Eq. 4.1 to give

$$\cos \theta_{n+1} = \frac{w \cos \phi_n + (1-w) \cos(\theta_n + \delta_n)}{\sqrt{w^2 + (1-w)^2 + 2w(1-w) \cos(\phi_n - (\theta_n + \delta_n))}} \tag{4.15}$$

We now square both sides and rearrange to give

$$\begin{aligned}
\cos^2 \theta_{n+1} [w^2 + (1-w)^2 + 2w(1-w) \cos(\phi_n - (\theta_n + \delta_n))] = \\
(w \cos \phi_n + (1-w) \cos(\theta_n + \delta_n))^2 \tag{4.16}
\end{aligned}$$

Expanding and using standard trigonometric identities, then taking the expectation of both sides and recalling that as before we consider ourselves in the long term limit and

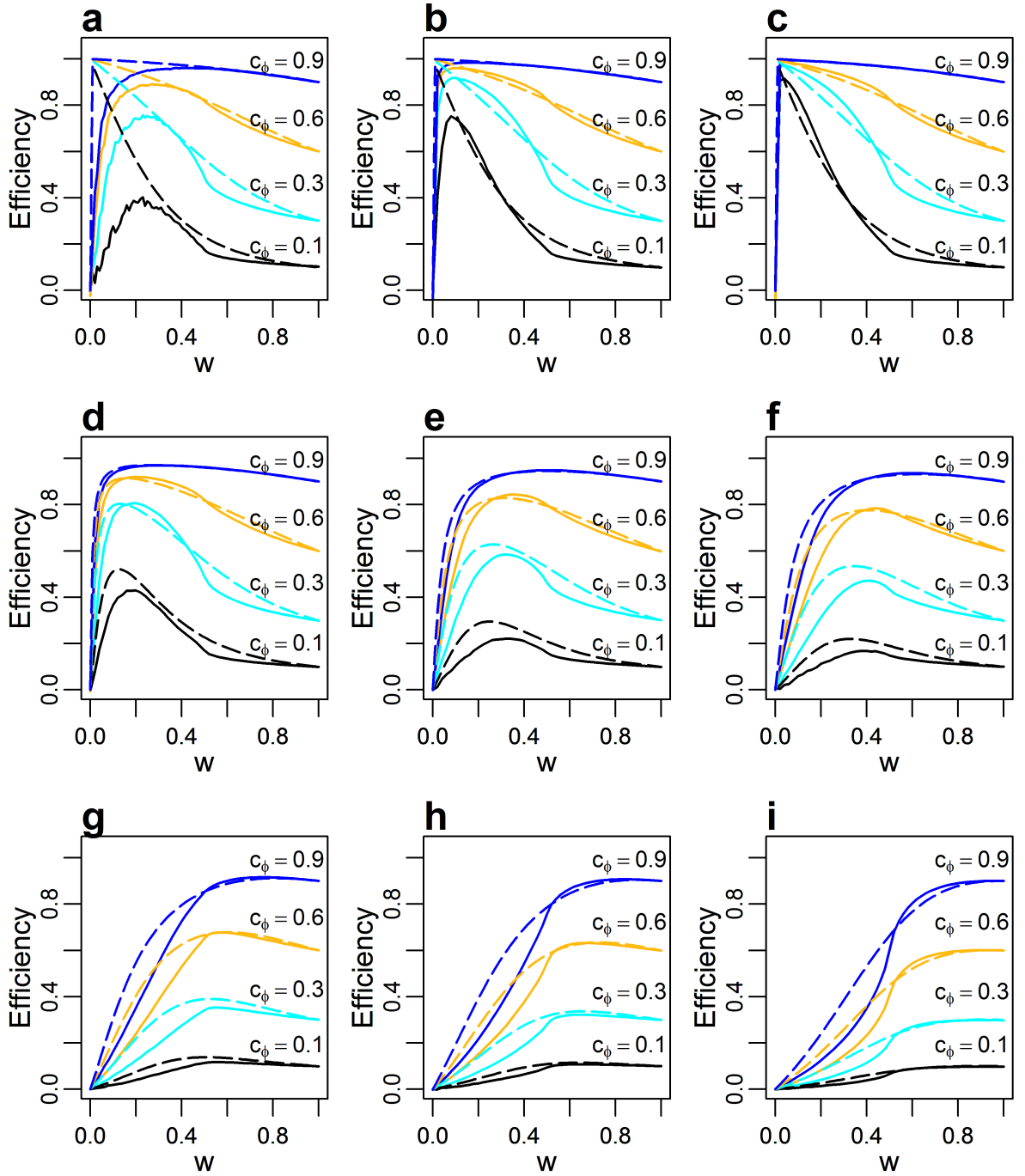


Figure 4.1: Plots of efficiency against weighting factor, w , for error on navigation, c_ϕ , taking values of 0.9 (blue), 0.6 (gold), 0.3 (cyan) & 0.1 (black). Error on persistence, c_δ , has value 1 (a)-(c) (equivalent to Benhamou & Bovet (1992) results), 0.99 (d), 0.95 (e), 0.9 (f), 0.7 (g), 0.5 (h) & 0.1 (i). Dashed lines show predictions from first analytical model, solid lines are results of simulations. Plots (a)-(c) were run for simulations of 100, 1000, 10000 time-steps respectively all others ran for 1000 time-steps.

hence

$$\mathbb{E}[\cos \theta_{n+1}] = \mathbb{E}[\cos \theta_n] = \mathbb{E}[\cos \theta_\infty] \quad (4.17)$$

$$\mathbb{E}[\cos \phi_n] = \mathbb{E}[\cos \phi], \quad \mathbb{E}[\cos \delta_n] = \mathbb{E}[\cos \delta] \quad (4.18)$$

and

$$\mathbb{E}[\sin \theta_\infty] = \mathbb{E}[\sin \delta_n] = \mathbb{E}[\sin \phi_n] = 0 \quad (4.19)$$

gives

$$\begin{aligned} 0 = & 2w(1-w) \mathbb{E}[\cos \phi] \mathbb{E}[\cos \delta] \mathbb{E}[\cos^3 \theta_\infty] \\ & + (w^2 + 2(1-w)^2(1 - \mathbb{E}[\cos^2 \delta])) \mathbb{E}[\cos^2 \theta_\infty] \\ & - 2w(1-w) \mathbb{E}[\cos \phi] \mathbb{E}[\cos \delta] \mathbb{E}[\cos \theta_\infty] \\ & - (w^2 \mathbb{E}[\cos^2 \phi] + (1-w)^2(1 - \mathbb{E}[\cos^2 \delta])) \end{aligned} \quad (4.20)$$

Here we note we have terms of the form $\cos^n X$, and so we apply the trigonometric identities of $\cos^3 X \equiv \frac{1}{4} \cos 3X + \frac{3}{4} \cos X$ and $\cos^2 X \equiv \frac{1}{2}(1 + \cos 2X)$ with the approximation of $\mathbb{E}[\cos nX] \approx \mathbb{E}[\cos X]^n$. Finally, using the linearity of the expectation function and employing the notation from the previous section of $\mathbb{E}[\cos X] = c_X$, gives a cubic in terms of c_θ

$$w(1-w)c_\phi c_\delta c_\theta^3 + (w^2 + (1-w)^2(1 - c_\delta^2)) c_\theta^2 - w(1-w)c_\phi c_\delta c_\theta - w^2 c_\phi^2 = 0 \quad (4.21)$$

Note, we apply the approximation of $\mathbb{E}[\cos nX] \approx \mathbb{E}[\cos X]^n$ to both ϕ and δ despite knowing the precise distributions they are drawn from, since we wish to keep this approximation valid for all circular distributions and, hence, require using the first cosine moment only.

Upon initial inspection, this cubic differs only slightly from the one discussed in the previous section (Eq. 4.12) with the coefficients of c_θ^3 and c_θ terms being halved. As such the method for solving the cubic are precisely the same as described in section

4.2.1; using Caradano's solution given in Eq. 4.13 with slight modifications to the terms A, B, C given in Eq. 4.14, which are now given as

$$\begin{aligned}
A &= - \left[\frac{w^2 + (1-w)^2(1-c_\delta^2)}{3w(1-w)c_\phi c_\delta} \right]^3 - \frac{w^2 + (1-w)^2(1-c_\delta^2)}{6w(1-w)c_\phi c_\delta} + \frac{wc_\phi}{2(1-w)c_\delta} \\
B &= - \left[\frac{w^2 + (1-w)^2(1-c_\delta^2)}{3w(1-w)c_\phi c_\delta} \right]^2 - \frac{1}{3} \\
C &= \frac{w^2 + (1-w)^2(1-c_\delta^2)}{3w(1-w)c_\phi c_\delta}
\end{aligned} \tag{4.22}$$

Figure 4.2 shows the results of plotting the navigational efficiency, c_θ , against weighting factor on navigation, w , for a range of navigation error levels, $c_\phi = 0.1$ (black), $c_\phi = 0.3$ (cyan), $c_\phi = 0.6$ (gold) & $c_\phi = 0.9$ (blue). With the value of the error on persistence varying from $c_\delta = 1$ (the specific case for perfect persistence, as discussed in Benhamou & Bovet (1992)) to $c_\delta = 0.1$, corresponding to a large error on navigation. In all plots the solid lines represent the theoretical model predictions and the dotted lines represent the results from simulations.

An interesting question raised from the BCRW model is how maximum efficiency can be achieved; that is, for any given values of the error terms, c_ϕ, c_δ what weighting value, w , should be chosen in order to maximise the efficiency.

4.2.3 Maximum Efficiency and Optimal Weighting

The maximum navigational efficiency can be found by locating the peak of each of the curves in Figs 4.1(d)-(i) and 4.2(d)-(i). For the simulated results (solid lines Figs 4.1 & 4.2) this value can be found by directly considering the results of the simulations for fixed values of c_ϕ and c_δ , and simply choosing the largest value of c_θ as w varies. The optimal weighting will then be given by the precise value of w which gave the largest c_θ . Repeating this across all combinations of c_ϕ and c_δ will give the value of the maximum efficiency along with the optimal value of w at which this occurs. However, for the analytical solutions precise values for the maximum efficiency and optimal w can be calculated directly from Eq. 4.12 for the first method and Eq. 4.21 for the second

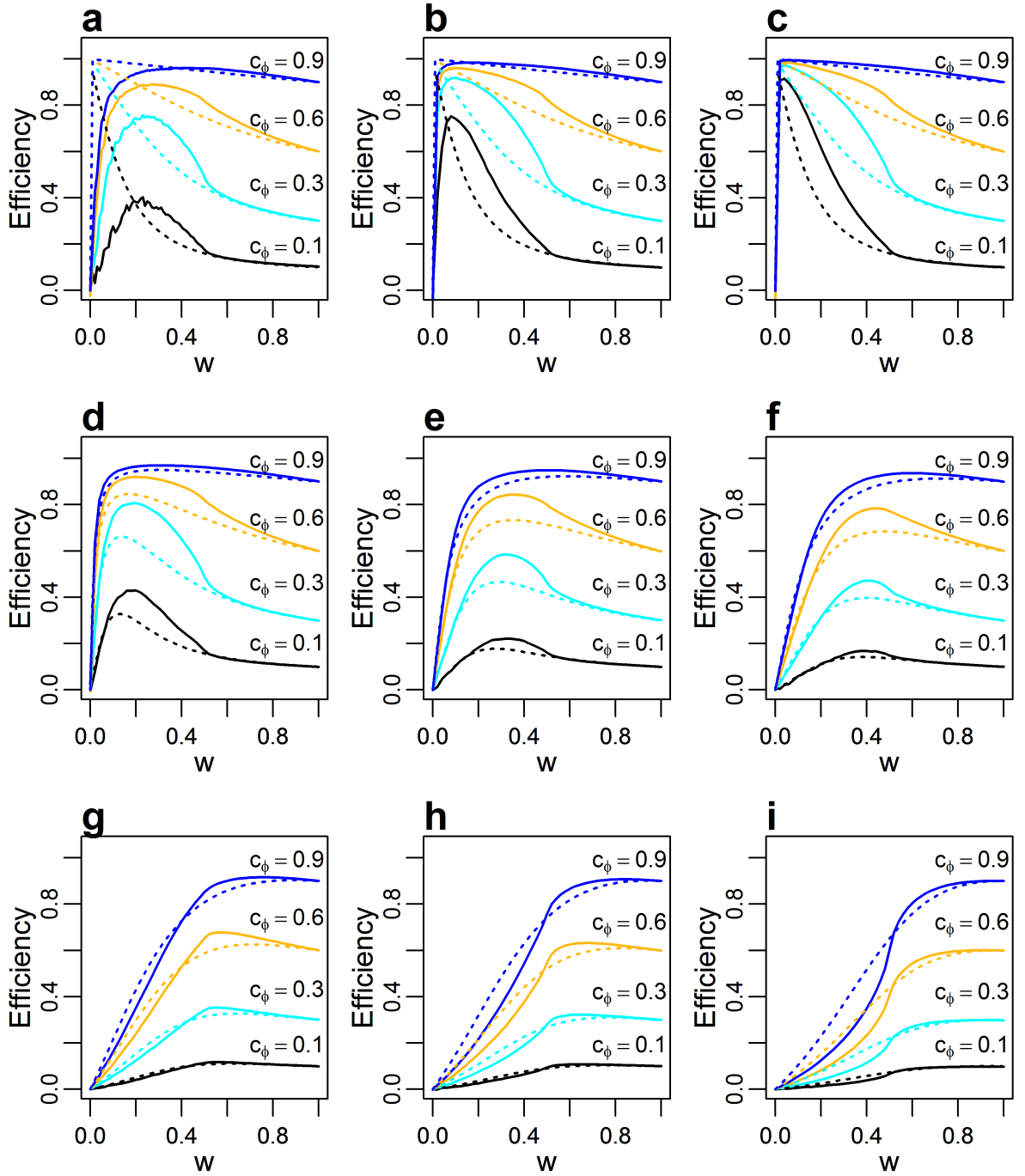


Figure 4.2: Plots of efficiency against weighting factor, w , for error on navigation, c_ϕ , taking values of 0.9 (blue), 0.6 (gold), 0.3 (cyan) & 0.1 (black). Error on persistence, c_δ , has value 1 (a)-(c) (equivalent to Benhamou & Bovet (1992) results), 0.99 (d), 0.95 (e), 0.9 (f), 0.7 (g), 0.5 (h) & 0.1 (i). Dotted lines show predictions from second analytical model, solid lines are results of simulations. Plots (a)-(c) were run for simulations of 100, 1000, 10000 time-steps respectively all others ran for 1000 time-steps.

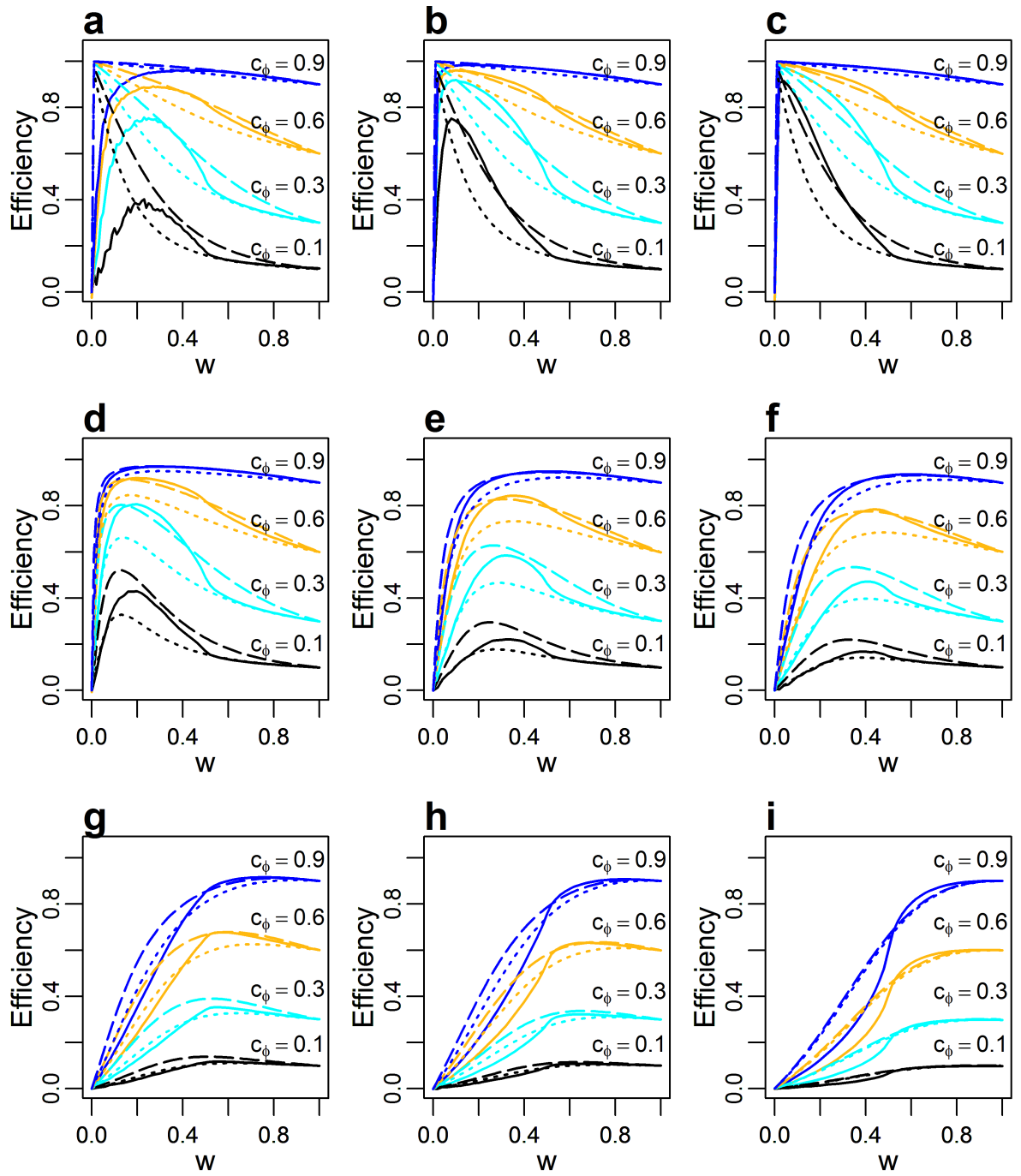


Figure 4.3: Directly comparing the results from Fig. 4.1 & Fig. 4.2. Solid lines are the results from simulations, dashed lines are the predictions from the first analytical model and dotted lines are the predictions from the second analytical model.

method, by finding the turning point of the dashed curves given in Fig 4.1 and the dotted curves in Fig 4.2. This can be done by showing that Eqs. 4.12 & 4.21 when considered as functions of w , have precisely one turning point in $[0, 1]$ for all w, c_ϕ, c_δ (See Appendix A3 for a complete proof of this).

Figure 4.4 shows heat maps of the optimal weighting factor, w , and the corresponding maximum navigation efficiency values. Panels (a) and (b) show the respective simulated results, (c) and (d) show the results for the first analytical method and (e) and (f) show the results for the second analytical method.

4.2.4 95% Maximum Efficiency

Whilst achieving maximal efficiency is always preferable, it depends on precise knowledge of the error value for navigation and persistence and as such it may be sensible instead to consider the range of values of w which would yield near-maximal efficiency. These values can be found by direct calculation; that is by calculating the maximum efficiency for fixed c_ϕ and c_δ then finding the range of w whose corresponding efficiency values lie within 95% of the maximum efficiency.

Fig. 4.5 indicates the range of values of the weighting factor, w , for which 95% maximum efficiency is reached depending on the values of c_ϕ and c_δ . Panels a_{1-3} show the results for simulated data whereas panels b_{1-3} show the results from the first analytical solution. Figures plot the weighting value, w , against the error on persistence c_δ with the error on navigation taking values $c_\phi = 0.1, 0.5, 0.9$; for plots with subscripts 1, 2, 3 respectively. The shaded areas represent the values of w for which an efficiency of over 95% of the maximum efficiency is reached, with the red line representing the optimal value w returning the maximum efficiency.

4.3 Results

4.3.1 Comparison of analytical methods

Comparing the results of the first analytical method (described in section 4.2.1) with the simulated results (Fig 4.1) show that this method appears to consistently over predict

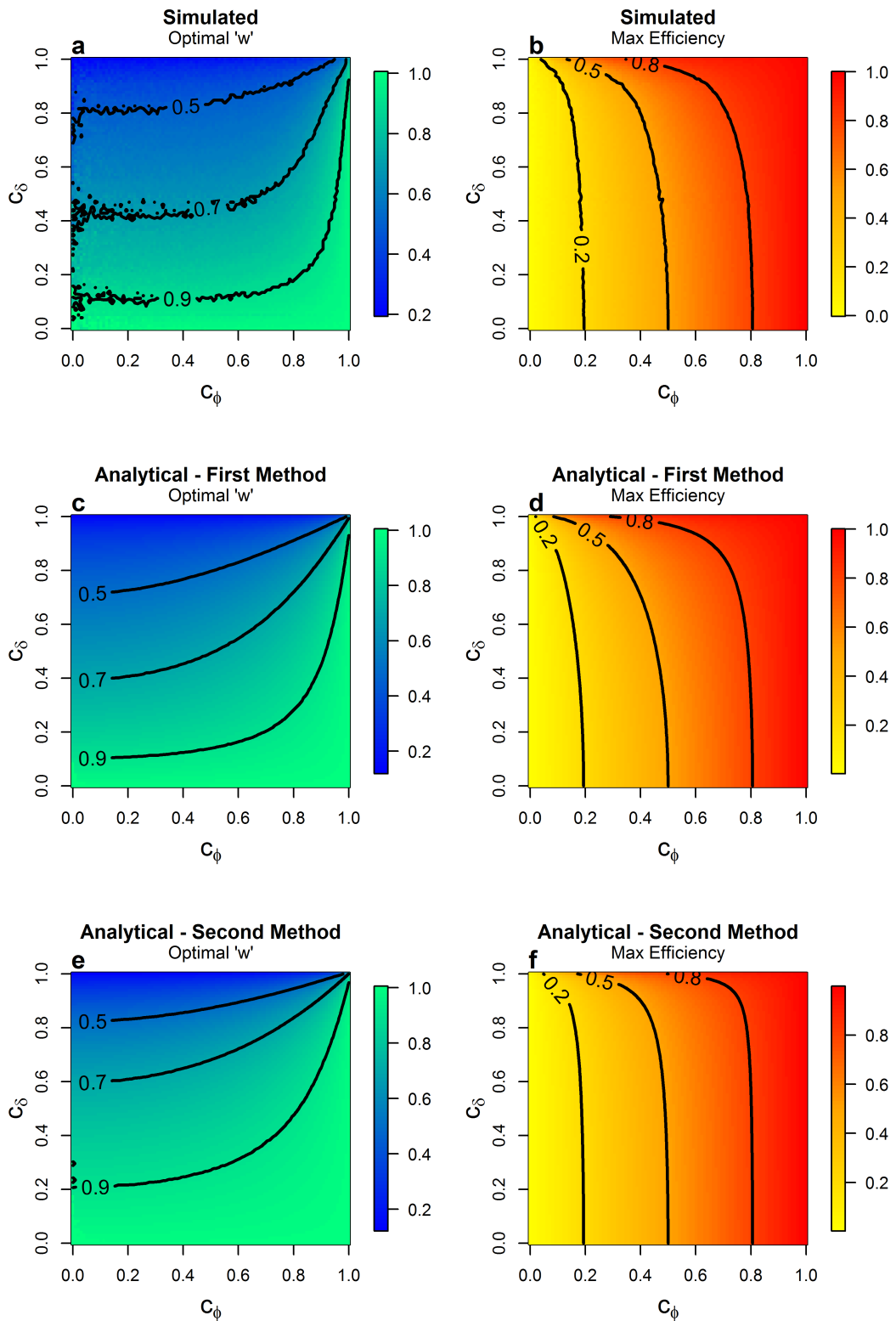


Figure 4.4: Heat maps showing (a) the weighting factor, w , that leads to the maximum navigation efficiency, ('optimal w '), and (b) the corresponding maximum navigation efficiency; calculated from simulations of 1,000 walkers moving for 1,000 steps. (c)-(d) & (e)-(f) show the predicted results for the first and second analytical models respectively. In each, c_δ and c_ϕ range from 0 to 1 at 0.01 intervals.

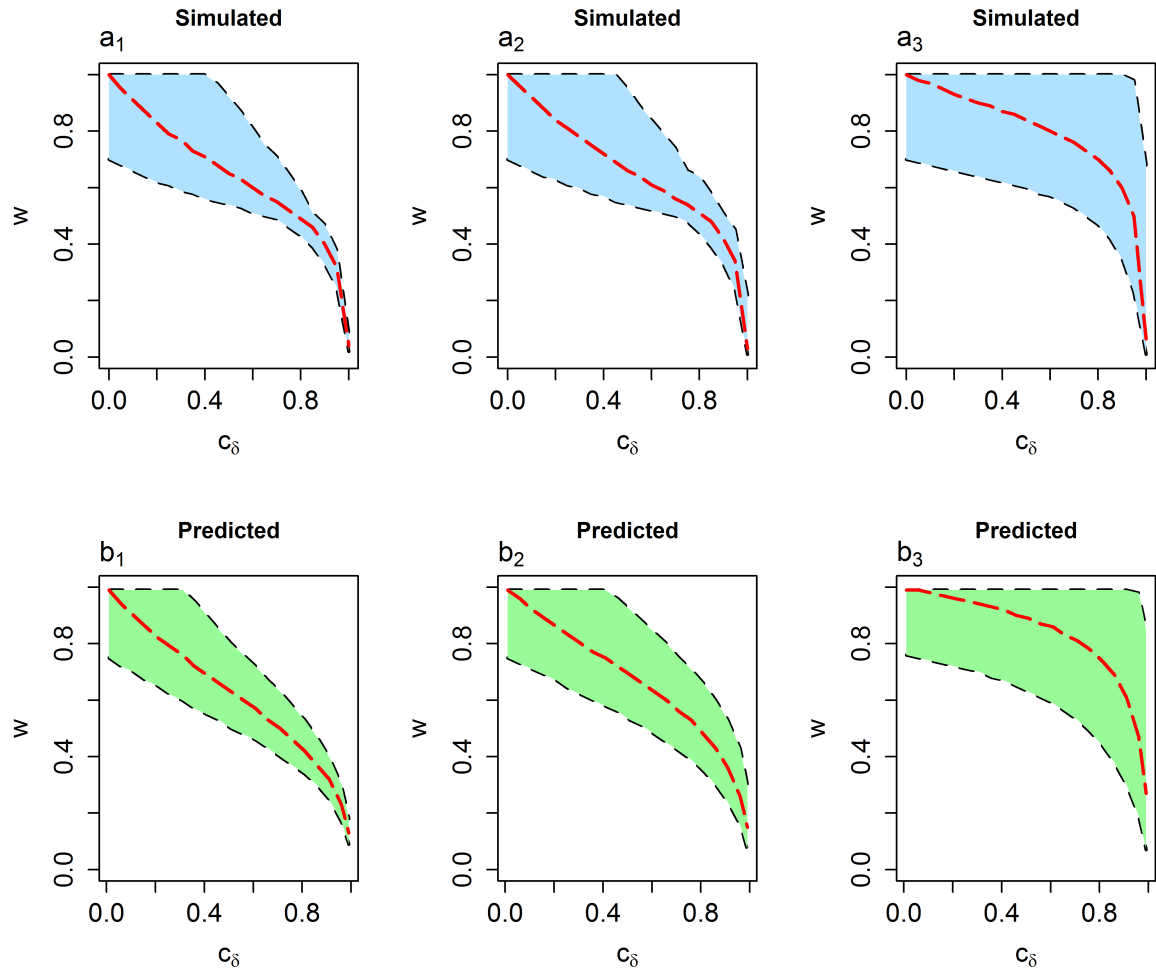


Figure 4.5: Plots showing the weighting factor, w , against the error on persistence, c_δ . The error in navigation c_ϕ takes values of 0.1, 0.5, 0.9 in subscripts (1)-(3) respectively. The red dashed line represents the optimal w . Shaded regions between the black dashed lines give values for w which return $\geq 95\%$ maximum efficiency. Top row (a) gives results from simulations and the bottom row (b) are the predictions from the first analytical method

<i>First Method</i>		Error in persistence c_δ						
		1^\dagger	0.99	0.95	0.9	0.7	0.5	0.1
Error in navigation c_ϕ	0.1	1.625*	2.367	2.229	1.796	1.035	0.633	0.386
	0.3	2.202*	2.322*	2.976	3.403	2.473	1.794	1.114
	0.6	0.882*	1.104*	1.747*	2.193	2.866	2.664	2.235
	0.9	0.045*	0.334*	1.013*	1.625	3.053	3.521	3.335

<i>Second Method</i>		Error in persistence c_δ						
		1^\dagger	0.99	0.95	0.9	0.7	0.5	0.1
Error in navigation c_ϕ	0.1	3.841	1.917*	0.626*	0.345*	0.235*	0.301*	0.346*
	0.3	3.716	3.405	1.969*	1.089*	0.755*	0.970*	1.059*
	0.6	2.381	2.657	2.631	2.160*	1.674*	1.897*	2.157*
	0.9	0.582	0.931	1.336	1.274*	1.670*	2.478*	3.155*

Table 4.1: Absolute difference between curves for the simulated results and the First and Second analytical solutions respectively. Values marked with an asterisk (*) indicate the method with the closer fitting solution

the efficiency value, whereas, comparing the second analytical method (section 4.2.2) and the simulated results (Fig 4.2) gives results which consistently under-predict. Directly comparing both methods with the simulated results (Fig 4.3) indicates that neither method gives a perfect match with the simulated results often lying between the two analytical results. As a simple measure of ‘best-fit’ the sum of the absolute differences between the analytical curves and the simulated results was calculated for each plot. Table 4.1 shows the results of the distance measure. Smaller values, corresponding to the closer fitting curve, are marked with an asterisk (*). These results indicate that the second method was generally the closer fitting curve, with it always giving the better fitting result for all values of c_ϕ whenever $c_\delta \leq 0.9$. However, for large values of c_δ (corresponding to near perfect persistence) the first method gives the better fitting results, particularly as c_ϕ increases towards 1. Therefore, whilst neither method recreates the simulated curves precisely, the second method appears to give consistently closer results.

Considering the maximum efficiency and corresponding optimal weighting for the simulated results and both analytical methods, Fig 4.4, we see a good fit for both mathematical approaches when visually compared to the simulated results. However, if we

	Error in persistence c_δ						
	1[†]	0.99	0.95	0.9	0.7	0.5	0.1
First Method	0.794*	1.587*	2.987*	3.411*	3.614*	4.987	10.199
Second Method	1.668	4.169	9.646	12.105	11.046	4.353*	8.904*

Table 4.2: Absolute difference between curves representing the simulated results and those given by the first and second analytical solutions for the optimal w , with fixed c_δ letting c_ϕ vary. Results marked with an asterisk (*) indicate the analytical method with the closer fitting solution curve

consider certain ‘slices’ of the heatmaps at specific values of the error on persistence, c_δ , to see how the two methods compare with the simulated results we can get a better idea which fits the simulated results closer. Fig 4.6 shows the values of the optimal weighting, w , which corresponds to the maximum efficiency, found for fixed values of c_δ in $(0.1, 0.5, 0.7, 0.9, 0.95, 1)$ (the same values for c_δ used in Figs 4.1-4.3) as the error on navigation, c_ϕ varies across $[0, 1]$. Here the simulated results are given by the green line, the first analytical method by the black line, and by the second analytical method by the red line. As before, visual inspection indicates that neither are perfect matches for the simulated results and therefore, we consider the sum of the absolute differences between the simulated and the analytical curves to find the closer fitting.

Table 4.2 indicates that by fixing c_δ and letting c_ϕ vary across $[0, 1]$ then the first method is the closer fitting for $c_\delta > 0.5$ and the second method is the closer fitting for $c_\delta \leq 0.5$. Whilst this shows that both methods can give the most accurate results over roughly equal amounts of the parameter space, as we are mainly concerned with high values of c_δ , corresponding to good knowledge of previous step direction and hence good persistence (see Discussion – Section 4.4), then the first method would give us the most apposite results.

Another simple way to compare between the methods is to simply find the absolute difference of the predicted results and the simulated results across the c_δ, c_ϕ parameter space (the absolute errors) seen in Fig. 4.4. Fig 4.7 shows the results of calculating this absolute difference for the optimal weighting (a) & (b) and the corresponding maximum efficiency (c) & (d) for both the first and the second analytical methods respectively. The darker the hue the larger the absolute value and the further away the prediction from

the simulated value. Visual inspection appears to indicate that the first method differs less than the second, shown by the lighter overall hue in both optimal weighting and maximum efficiency plots, and simply summing across the entire parameter space verifies this with $\epsilon_{w,1} = 349.76$, $\epsilon_{w,2} = 827.37$, $\epsilon_{\text{eff},1} = 111.46$, $\epsilon_{\text{eff},2} = 199.81$; where $\epsilon_{w,i}$ and $\epsilon_{\text{eff},i}$ are the sum of the absolute differences across the parameter space for the optimal w and maximum efficiency respectively, when comparing the simulated results with analytical method i . Therefore, neither analytical method matches the simulated results perfectly and neither are consistently the closest fitting. However, an important aspect of the model is to accurately reproduce the optimal weighting value (see Discussion - section 4.4) and therefore we chose the first method as the one which most accurately predicts the simulated behaviour and is the one considered in direct comparison when comparing the simulated and predicted results.

4.3.2 Simulated results and comparison with analytical method

We first consider the specific case of zero error on forward persistence, $c_\delta = 1$, which was considered originally by Benhamou & Bovet (1992). In this case Eq. 4.12 can be simplified and a limiting argument can be used to show that for all $c_\phi > 0$ (i.e. as long as external navigation cues are present) then $c_\theta \rightarrow 1$ as $w \rightarrow 1$ (see Appendix A2 and Fig. 4.1(a)-(c)). It may seem counter-intuitive that more efficient navigation can be obtained by giving a vanishingly small (but strictly non-zero) weighting to direct navigational cues but this is explained by the fact that once a navigating animal is oriented towards the target direction (which is always eventually possible if w is strictly non-zero), it can then maintain this direction of movement indefinitely since there is no persistence error, and hence no further external navigation cues are required. Nevertheless, the higher the level of navigation error (i.e. the lower the value of c_ϕ) the longer it will take (on average) for the animal to orientate itself towards the target direction. Consequently, the apparent navigational efficiency is highly dependent on the number of steps in the observed movement process when there is zero persistence error (Fig. 4.1(a)-(c)). Benhamou & Bovet (1992) only considered simulation results for a 1000-step BCRW and

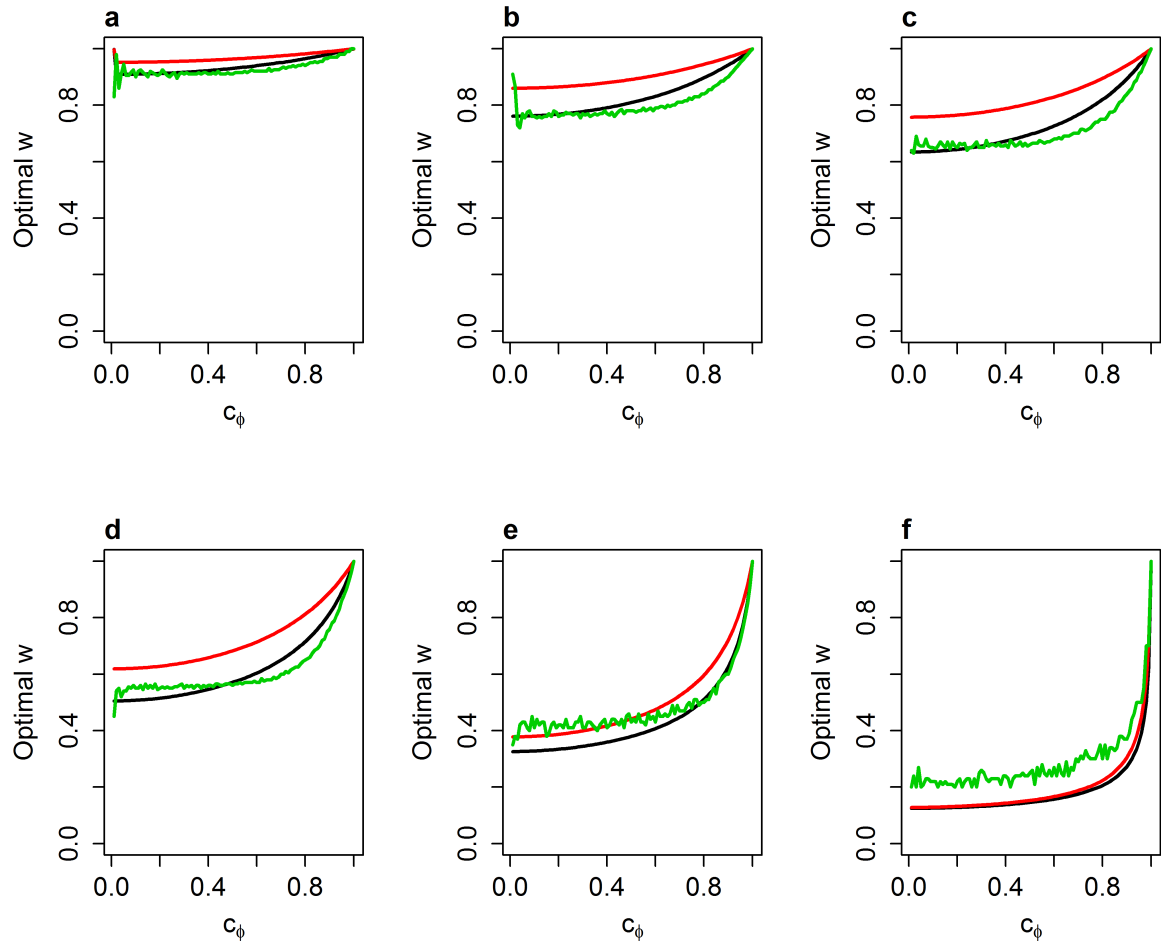


Figure 4.6: Plots comparing the optimal w against values of the error on navigation c_ϕ . Error on persistence, c_δ , takes values of 0.1, 0.5, 0.7, 0.9, 0.95 & 0.99 in (a)-(f) respectively. Green lines show results from simulations, black lines show predictions from the first analytical model and red lines show predictions from the second analytical model.

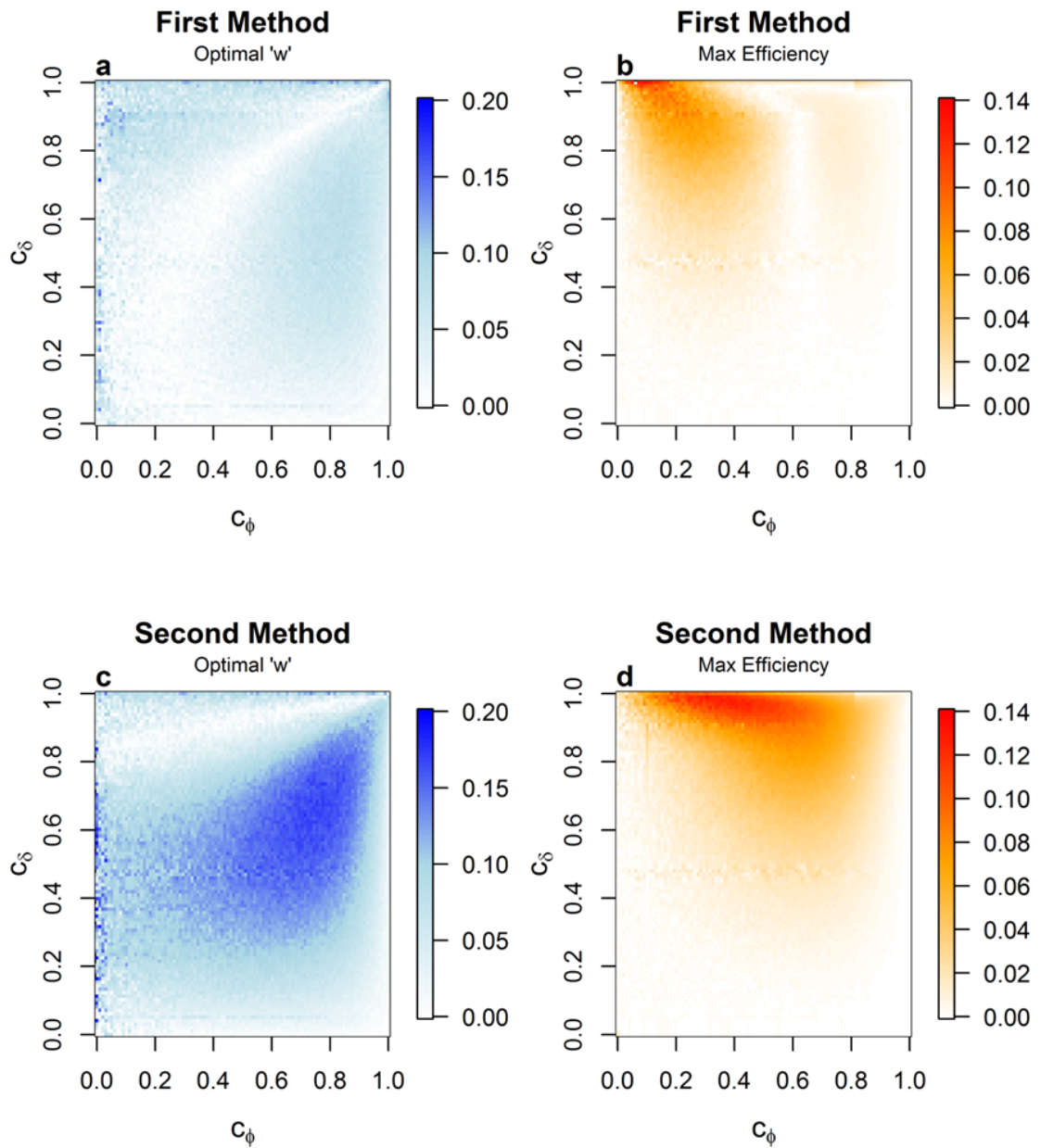


Figure 4.7: Heat maps for the parameter space of error on navigation, c_ϕ , and error on persistence, c_δ , showing the absolute difference between the simulated results and the two analytical methods for values of optimal w (a & c) and corresponding maximum efficiency (b & d). Top row is for the first analytical method and the bottom row is for the second analytical method. In all plots c_ϕ, c_δ takes values from 0 to 1 at 0.01 intervals. The darker the colour the larger the absolute difference, indicating the analytical model did not closely match the simulated results.

hence did not report this long-term limit result directly. For $w > 0$, the predicted long-term navigational efficiency, c_θ , monotonically decreases as w increases, indicating that lower long-term navigational efficiency is obtained when giving a higher weight to external navigation cues. This result is confirmed with the simulation results for the 10,000 step BCRW shown in Fig. 4.1c. In Fig. 4.1a and 4.1b where the BCRW runs for only 100 or 1000 steps respectively, the curves showing the simulated navigational efficiency are non-monotonic: the navigational efficiency is dependent on c_θ with a peak for $0 < w < 0.2$ similar to the result reported by Benhamou & Bovet (1992). This indicates that even with zero error on forward persistence, a BCRW with a small number of steps requires external navigational cues for efficient navigation.

In the case where there is error on both the navigation and persistence components of the movement process (i.e. $c_\delta, c_\phi < 1$), the solution given in Eq. 4.13 predicts that as the persistence error increases (c_δ decreases), the navigational efficiency also decreases for all c_ϕ (solid lines in Fig 4.1(c)-(f)). The predicted solution curves are (in general) non-monotonic with a peak indicating a maximum navigational efficiency for an intermediate value of w . For low persistence errors ($c_\delta = 0.99, 0.95, 0.9$ in Fig. 4.1d-f) the maximum navigational efficiency occurs for $w < 0.5$, and at lower values of w when c_ϕ is also small (higher navigation error). As the persistence error increases ($c_\delta = 0.7, 0.5, 0.1$ in Fig 4.1g-i) the peak indicating the maximum navigational efficiency shifts to the right corresponding to a larger value of the weighting given to navigation, w (Figure 4.1g-i; Appendix A3). In general, the simulation results shown in Fig 4.1g-i show the same qualitative behaviour as the predicted solution curves from Eq. 4.13. In contrast to the case of zero persistence error, for the values of $c_\delta < 1$ considered here, there is very little difference in the model predictions and simulated results for $n = 100, 1000, 10000$ and 10,000 steps (see Appendix A4: Fig 4.8A). The inclusion of even a small error on the persistence term means the effective long-term limiting solutions for navigational efficiency are reached much faster than the case with zero persistence error.

The location of the peak corresponding to the maximum navigational efficiency for each of the curves in Fig 4.1d-i can be calculated directly from Eqs. 4.12 and 4.13. More

generally, it can be shown that Eq. 4.12 has precisely one turning point for $w \in [0, 1]$, and this turning point corresponds to the maximum predicted navigational efficiency (see Appendix A3). The values of w leading to the theoretical maximum navigational efficiency, together with the predicted values for this efficiency, are calculated from Eqs. 4.12 and 4.13 for a range of c_ϕ and c_δ , and are shown in Fig 4.5c and 4.4d respectively. Fig. 4.4a and 4.5b show the equivalent results from simulations of the BCRW, and show a good qualitative match to the theoretical predictions. Fig. 4.4a and 4.4c highlight the result (also seen in Fig 4.1d-i) that when the persistence error is high ($c_\delta < 0.1$), the maximum navigational efficiency occurs when giving a higher weighting to the navigation term ($w > 0.9$), and when $c_\delta \approx 0$ this efficiency is given exactly by c_δ (Fig 4.4b and 4.4d) which corresponds to pure taxis. However, when the persistence error is low ($c_\delta > 0.9$), the maximum navigational efficiency typically occurs for $w < 0.5$ (more weighting on persistence than direct navigation) even if the navigation error is also low (Figs 4.4a and 4.4c). Figs 4.4b and 4.4d highlight that a high navigational efficiency can be maintained even when the navigation error is large ($c_\phi < 0.5$) because of the weighting given to persistence: the contour corresponding to a long-term navigational efficiency of 0.5 extends well below $c_\phi < 0.5$ (Figs 4.4b and 4.4d).

In considering the range of values w can take for which 95% maximum efficiency is reached, Fig. 4.5 demonstrates that when more weight should be put on navigation (optimal $w > 0.5$) the range of values the weighting can take and still yield 95% maximum efficiency is reasonably large regardless of the values of c_ϕ and c_δ . However, when the optimal value of w favours persistence ($w < 0.5$) this range is comparatively small, indicating that in this case getting close to the optimal value of the weighting is significant.

4.4 Discussion

We have developed the model of Benhamou & Bovet (1992) to include persistence error and derived a mathematical approximation for the long-term navigational efficiency of this form of BCRW. We have demonstrated how navigational efficiency depends on

the weighting given between navigation and persistence at each step of the movement process and the level of error in each term (Eq. 4.12; Fig 4.1d-i). In Fig 4.4a, the area above the contour line corresponding to $w = 0.5$ indicates the region of the parameter space where giving a lower weighting to direct navigation cues and a higher weighting to persistence leads to the maximum long-term navigational efficiency. Interestingly, the predicted contour line corresponding to $w = 0.5$ approaches $c_\phi = 1$ in Fig 4.4a, indicating that even with close to zero error on the navigation cue, there is little loss of navigational efficiency by giving equal weight to persistence. This potentially hints at some interesting evolutionary advantages for animals that balance forward persistence and external navigation cues in this way: giving a high weighting to persistence can improve overall navigation efficiency if the error on navigation cues is high ($c_\phi < 0.5$), and has little detrimental effect if the error on navigation cues is low ($c_\phi > 0.9$).

The vector-weighted BCRW navigation model discussed by Benhamou & Bovet (1992) did not include error on the persistence term and the results given in their paper were for a BCRW with only 1000 steps. We have shown mathematically (Appendix A2 and Fig 4.1c) that in this scenario the long-term maximum navigation efficiency is actually obtained when the weighting on external navigation cues (taxis) tends to zero, i.e. $c_\phi \rightarrow 1$ as $w \rightarrow 0$. This may seem like a counter-intuitive result, given that a movement process based purely on persistence with no taxis is known to be a poor navigation strategy (Cheung, 2007). However, this result holds only for the long-term limiting navigation efficiency, where the fact that there is zero error on persistence means an animal can achieve maximum navigational efficiency simply by continuing in the same direction as previously once it is moving in the target direction. At shorter time-scales navigation will not be as efficient (Fig 4.1a-c), and the observed navigational efficiency is dependent on the number of steps of the BCRW.

A possible further extension of this work would be to derive an expression for the navigational efficiency that is valid for a small number of steps and not just the long-term limit. However, Appendix A4: Fig 4.7A demonstrates how the sensitivity of the navigational efficiency to the number of steps in the BCRW is less when persistence error

is non-zero. When referring to the results in Fig 4.1a-c we are implicitly assuming that a random walk with 1000 steps is 10 times longer than a walk with 100 steps and so on. Instead, an alternative interpretation of the model and results is that the overall path length is fixed and it is the reorientation frequency that changes (so that a single step in a 1000-step path is 10 times shorter than that in a 100-step path). From Fig 4.1a-c, this then implies that in a noisy environment an animal may improve its navigational efficiency by increasing its rate of reorientation (effectively giving a larger sample size in the navigational averaging process).

The BCRW model considered here is deliberately simple but could easily be extended to consider more complex scenarios, although this may come at the expense of analytical tractability, and generalised predictions about navigation efficiency informed by mathematical theory may not subsequently be possible. The BCRW model considered here assumes individuals do not change their behaviour over time or interact with conspecifics. Nevertheless, the overall conclusion is similar to results observed by Codling & Bode (2014; 2016) who used simulations to demonstrate that in a group navigation context, the most efficient navigational strategy was to give a high weighting to indirect cues (copying the movement of other group members or using forward persistence), rather than relying on direct navigational cues. An obvious extension of the present work would be to develop a mathematical model for the efficiency of a navigating group. This is likely to be much more analytically difficult, although one approach would be to use stochastic differential equations (SDE) to model the individual interactions within the group. Binhi (2017) used SDEs to explore the “many wrongs” principle in group navigation, giving analytical solutions which compared accurately with simulated results.

Our model also assumes a homogeneous environment with a fixed target direction where navigation cues do not vary in space or time. Movement through a heterogeneous environment could be modelled as a composition of shorter paths through different homogeneous regions and incorporate different localised behaviour where persistence and navigation may be balanced in different ways over time such as foraging or exploratory behaviour (Jonsen et al, 2005; Barraquand & Benhamou, 2008). However, it is not clear

in such cases how a mathematical approximation for the navigational efficiency could be easily derived. An alternative model structure to the vector-weighted BCRW model proposed by Benhamou & Bovet (1992) could also be considered. For example, Codling & Hill (2005a) considered a BCRW where the strength of the navigation cue was either linearly or sinusoidally dependent on the orientation of the individual walker (to respectively model phototaxis and gyrotaxis in swimming micro-organisms).

In the context of group navigation, Bode et al (2010) considered a model where the behaviour of an individual at each time step was probabilistic and chosen to be either purely persistent or purely local navigation, rather than using a vector-weighted sum as we do here. Many migrating animals will undertake other behaviours during the large-scale navigation process (such as resting, foraging etc), or may change their behaviour in response to their local environment. Peleg & Mahadevan (2015) developed a random walk model which includes periods of purely persistent behaviour followed by a pause to reorient according to external navigational cues. By repeating this behaviour, a walk which appears to be purely persistent (a CRW) in the short term can then be described as a BCRW in the long term. This is in contrast to our model where we assume the animal is continuously balancing persistence and navigation (taxis) at every step of the movement path. Nevertheless, the relative weighting between navigation and persistence in our model (w) can be directly compared to the relative navigation reorientation frequency in the model of Peleg & Mahadevan (2015) since both effectively give a way to balance persistence and navigation. In the context of group navigation, Bode et al (2010) used a similar approach and considered a model where the behaviour of an individual at each step was probabilistic and chosen to be either purely persistent or purely local navigation. The probability of choosing persistence against navigation in this model could be directly compared to the relative navigation weighting (w) in our model.

To derive equation 4.12 a number of key assumptions were made to make analytical progress. Specifically, moving from Eq. 4.5 to Eq. 4.6 we assumed a highly non-linear expression could be treated as linear when taking the expectation, and moving from Eq.

4.10 to Eq. 4.11 we assumed the long-time limit such that the distribution of movement directions is stable. It is the former assumption that is likely the reason for the slight discrepancy between the predicted and simulated results in Fig 4.1d-i. We have explored ways to improve the predicted model to give a better fit to the simulated results but this leads to significantly more complex expressions for the predicted navigational efficiency with only a very slight improvement in the model fit (results not shown). The results in Fig 4.1a-c illustrate how (for zero persistence error) the observed navigational efficiency is highly dependent on the number of steps of the BCRW. A possible further extension of this work would be to derive an expression for the navigational efficiency that is valid for a small number of steps and not just the long-time limit as considered here. However, Fig 4.7A demonstrates how the sensitivity of the navigational efficiency to the number of steps in the BCRW is much less when persistence error is non-zero.

Predictions from our model about how animals should (in theory) balance persistence and external navigation cues (taxi) to give the highest navigational efficiency should be tested and compared to observations from empirical data. One of the most interesting model predictions is shown in Fig 4.4a, where in the parameter region above the $w = 0.5$ contour line (corresponding to values of approximately $c_\delta > 0.8$ for low navigation error, $c_\phi < 0.5$ and $c_\delta > 0.9$ for medium levels of navigation error, $0.5 < c_\phi < 0.9$), it is more efficient to give a higher weighting to persistence than direct navigation cues. Directly comparing empirically reported values of c_δ across the literature is known to be difficult since processing and sampling of the data can change the estimated forward persistence of an observed path (Bovet & Benhamou, 1988; Codling & Hill, 2005). Nevertheless, high values for c_δ have been reported for a wide range of species including insects and nematodes ($0.62 \leq c_\delta \leq 0.94$ in Byers, 2001), elk ($c_\delta = 0.68$ in Fortin et al, 2005), dolphins ($c_\delta = 0.8$ in Bailey & Thompson, 2006), foraging seabirds ($c_\delta = 0.885$ for movement mode 3 in Boyd et al, 2014), and reindeer ($c_\delta = 0.84$ for exploratory movement state 2 in Langrock et al, 2014). Hence, it seems clear that many animal species are capable of moving in a highly persistent manner if they choose to do so.

The relative weighting between navigation and persistence in the movement be-

haviour of a prairie butterfly was considered by Schultz & Crone (2001). They found that when returning to within 10-22m of their home habitat they were observed to use a BCRW movement that balanced persistence with navigation with a weighting of $w = 0.38$ (female) and $w = 0.29$ (male). However, the authors did not explore the levels of navigation and persistence error within the observed butterfly movement paths. Fortin et al (2005) considered the balance between forward persistence and directed movements up-slope in the winter foraging of elk. Using a log-likelihood test, they showed that a BCRW model fitted the data better than the alternative of a pure BRW or a pure CRW, and that the weighting on directional bias was $w = 0.17$, implying that almost five times more weighting was given to persistence than localised up-slope directed movements. The results of Schultz & Crone (2001) and Fortin et al (2005) provide empirical evidence that some animals do give a high weighting to persistence rather than directed movement, although the contexts are slightly different to our abstracted navigation problem. In contrast, McClintock et al (2012) used a multi-state generalised BCRW framework to analyse and describe the movements of grey seals near to localised centres of attraction (foraging areas or haul-out sites), and found that when close to the centres of attraction, movement was almost entirely directed ($w > 0.99$). However, the ecological context of their study (short-term foraging within a familiar territory) is different to our problem (large-scale navigation via an external directional cue). In addition, McClintock et al (2012) did not directly consider that localised forward persistence and directional bias are often misclassified, especially in a short movement path, a fundamental problem highlighted by Benhamou (2006).

A number of studies have considered strategies for maximising movement efficiency in the context of foraging, although these are usually based on minimising energy expenditure rather than optimising navigation efficiency. Fortin et al (2003) demonstrated how theories from optimal foraging related to energy maximisation did not seem to hold across varying temporal scales, with other factors influencing movement behaviour becoming more important at larger time-scales. Bartoń et al (2009) used simulations to explore the survival of animals exploring a patchy landscape using a BCRW movement

model that balanced persistence with biased movement towards patches of suitable habitat. They found that “...when an organism’s ability to detect patches decreases with distance from the patch, dispersal mortality is high if the organism engages in a walk with a low degree of correlation. Thus, even if long distance detection of a patch is poor, an individual can still have a good chance of surviving dispersal if it moves using a more economical, highly correlated walk.” Hence, although the model of Bartoń et al (2009) was based on short-scale localised navigation when foraging, their conclusions seem to be consistent with the findings from our model, which is based on large-scale navigation. Further work is now needed to test our model predictions and to determine in more detail how real animals may balance persistence and taxis (and other possible mechanisms) when navigating efficiently over a range of spatio-temporal scales.

4.5 Conclusions

- In this chapter we have given a method for modelling individual animal movement which includes both a biased and correlated component, and seen how the effect of increasing the error attached to each term affects the efficiency of navigating by such a method.
- Our results suggest that it is more beneficial in the long term for an individual to move towards a target direction putting more weight into following their previous direction (persistence) rather than directly following navigational cues and have given a mathematical justification for these results.
- We have extended the work done by Benhamou and Bovet (1992), showing how the overall efficiency of a BCRW model for animal movement is affected by errors on both the navigational and persistence terms.
- We have given a mathematical approximation which accurately predicts the simulated results for the case of “perfect” persistence running in the long term.
- We have also given mathematical approximations to predict the simulated results when we have an error on the persistence term, which give accurate predictions for

values of $w > 0.5$, however, because of our assumptions and approximations made the accuracy is not as good for $w < 0.5$. Similarly, our approximations are only valid in the long term limit and therefore, not reliable for a small number of time steps.

- The specific values of weighting required to return optimal efficiency have been calculated and have shown to be a close fit to those predicted by our first mathematical approximation method.
- The results show that in general, the maximum efficiency of the model was found when more weight was put onto the navigational component, however, when the error in the persistence is small (which is a realistic assumption for certain animal movement) the optimal value of w is found to decrease implying that one should favour persistence more than navigational ability.
- Questions still remain regarding this model, such as finding solutions which are not based in the long term limit. Our findings could be better understood by a more accurate and complete mathematical solution along with applying these findings to empirical studies

4.6 Appendices

4.6.1 Appendix A1 - Eq. 4.12 has precisely one root for c_θ in the interval $[0, 1]$.

In this appendix we show that Eq. 4.12 in the main text has precisely one root for c_θ in the interval $[0, 1]$. We first show that there is at least one root in this interval and then show that this must be the only root in the interval.

Existence of at least one root in $[0, 1]$

Recall Eq. 4.12 in the main text which is a cubic polynomial, $f(c_\theta)$:

$$2w(1-w)c_\phi c_\delta c_\theta^3 + (w^2 + (1-w)^2(1-c_\delta^2))c_\theta^2 - 2w(1-w)c_\phi c_\delta c_\theta - w^2 c_\phi^2 = 0 \quad (4.23)$$

where $0 \leq w, c_\phi, c_\delta \leq 1$.

This polynomial $f(c_\theta)$ is well defined except for the special case where $c_\delta = 1$ and $w = 0$. In this special case (where there is zero weighting given to navigation) we define the navigational efficiency as $c_\theta = 0$. For all other cases:

- (i) at $c_\theta = 0$, we have $f(0) = -w^2 c_\phi^2 \leq 0$;
- (ii) at $c_\theta = 1$, we have $f(1) = w^2(1 - c_\phi^2) + (1 - w)^2(1 - c_\delta^2) \geq 0$.

Now, if either $f(0) = 0$ or $f(1) = 0$ then we clearly have at least one root for $c_\theta \in [0, 1]$. Otherwise, we must have $f(0) < 0$ and $f(1) > 0$. Now as $f(c_\theta)$ is continuous and must change sign in the interval $[0, 1]$, we can use the intermediate value theorem (specifically Bolzano's theorem) to show that there must exist at least one root in this interval.

Existence of no more than one root in $[0, 1]$

We first rewrite $f(c_\theta)$ as:

$$a(w, c_\phi, c_\delta)c_\theta^3 + b(w, c_\phi, c_\delta)c_\theta^2 + c(w, c_\phi, c_\delta) + d(w, c_\phi, c_\delta) = 0 \quad (4.24)$$

where

$$\begin{aligned} a &= 2w(1-w)c_\phi c_\delta, \\ b &= w^2 + (1-w)^2(1-c_\delta^2), \\ c &= -2w(1-w)c_\phi c_\delta, \\ d &= -w^2c_\phi^2 \end{aligned} \quad (4.25)$$

We first show that only one root exists in $[0, 1]$ when any of a, b, c or $d = 0$. These occur when either (i) $w = 1$; (ii) $w = 0$; (iii) $c_\phi = 0$; (iv) $c_\delta = 0$.

Substituting these values into $f(c_\theta)$ gives:

(i) $w = 1$:

$$c_\theta^2 - c_\phi^2 = 0 \implies c_\theta = c_\phi \in [0, 1] \text{ as required.}$$

(ii) $w = 0$:

$(1 - c_\delta^2)c_\theta^2 = 0 \implies c_\theta = 0$ or $c_\delta = 1$. However, we defined $c_\theta = 0$ when $c_\delta = 1, w = 0$, so we have one root at $c_\theta = 0$.

(iii) $c_\phi = 0$:

$[w^2 + (1-w)^2(1-c_\delta^2)]c_\theta^2 = 0$. Either $c_\theta = 0$ or $w^2 + (1-w)^2(1-c_\delta^2) = 0$. However, we note that $w^2 + (1-w)^2(1-c_\delta^2)$ is strictly positive unless $w = 0$ and $c_\delta = 1$. In this case we defined $c_\theta = 0$. Therefore we have one root at $c_\theta = 0$ as required.

(iv) $c_\delta = 0$:

$$[w^2 + (1-w)^2]c_\theta^2 - w^2c_\phi^2 = 0 \implies \frac{w}{\sqrt{w^2+(1-w)^2}}c_\phi. \text{ Note, that as } \frac{w}{\sqrt{w^2+(1-w)^2}} \in [0, 1] \text{ and}$$

$c_\phi \in [0, 1]$ then clearly $\frac{w}{\sqrt{w^2+(1-w)^2}}c_\phi \in [0, 1]$ and is unique as required.

We now consider the general cases when $a, b, c, d \neq 0$. Clearly $0 < a, b \leq 1$ and $0 > c, d \geq -1$, for all $w, c_\phi, c_\delta \in [0, 1]$ and, hence $f(c_\theta)$ has one change of sign across its coefficients for positive c_θ . From Descartes change of sign rule we know that this implies the existence of at most one positive root.

Combining the general result with the cases where at least one of the coefficients of $f(c_\theta)$ is 0, shows that there exists at most one non-negative root for $f(c_\theta)$ across all values of w, c_ϕ, c_δ .

4.6.2 Appendix A2 - Eq. 4.12 implies that the navigation efficiency, $c_\theta \rightarrow 1$ as $w \rightarrow 1$ when $c_\delta = 1$

We show that in the specific case of $c_\delta = 1$, Eq. 4.12 in the main text implies that the navigation efficiency, $c_\theta \rightarrow 1$ as $w \rightarrow 1$.

Eq. 4.12 in the main text is given by

$$2w(1-w)c_\phi c_\delta c_\theta^3 + (w^2 + (1-w)^2(1-c_\delta^2))c_\theta^2 - 2w(1-w)c_\phi c_\delta c_\theta - w^2 c_\phi^2 = 0 \quad (4.26)$$

where $0 \leq w, c_\phi, c_\delta \leq 1$.

For $w \neq 0$ this simplifies to

$$2(1-w)c_\phi c_\delta c_\theta^3 + \left(w + \frac{(1-w)^2(1-c_\delta^2)}{w} \right) c_\theta^2 - 2(1-w)c_\phi c_\delta c_\theta - w c_\phi^2 = 0 \quad (4.27)$$

Letting $c_\delta = 1$ this simplifies further to

$$2(1-w)c_\phi c_\theta^3 + w c_\theta^2 - 2(1-w)c_\phi c_\theta - w c_\phi^2 = 0 \quad (4.28)$$

Now letting $w \rightarrow 0$ we get

$$\lim_{w \rightarrow 0^+} 2(1-w)c_\phi c_\theta^3 + w c_\theta^2 - 2(1-w)c_\phi c_\theta - w c_\phi^2 = 2c_\phi c_\theta^3 - 2c_\phi c_\theta = 0 \quad (4.29)$$

Finally, assuming $c_\phi \neq 0$ (the case for $c_\phi = 0$ is discussed in Appendix S1) this gives $c_\theta^3 = c_\theta \iff c_\theta = 1$ as required.

4.6.3 Appendix A3 - Eq. 4.13, considered as a function of w , has precisely one turning point in $[0, 1]$ for all w, c_ϕ, c_δ

We wish to show that Eq. 4.13 in the main text, when considered as a function of w , has precisely one turning point in $[0, 1]$ for all w, c_ϕ, c_δ . To show this we prove the existence of precisely one root in $[0, 1]$ for $\frac{dc_\theta}{dw} = 0$.

Recall Eq. 4.12 from the main text, written as in Appendix A1:

$$f(c_\theta) = a(w, c_\phi, c_\delta)c_\theta^3 + b(w, c_\phi, c_\delta)c_\theta^2 + c(w, c_\phi, c_\delta)c_\theta + d(w, c_\phi, c_\delta) = 0 \quad (4.30)$$

Differentiating this with respect to w , gives

$$\begin{aligned} & \frac{d}{dw} (a(w, c_\phi, c_\delta)c_\theta^3 + b(w, c_\phi, c_\delta)c_\theta^2 + c(w, c_\phi, c_\delta)c_\theta + d(w, c_\phi, c_\delta)) = 0 \\ \implies & c_\theta^3 \frac{da}{dw} + 3ac_\theta^2 \frac{dc_\theta}{dw} + c_\theta^2 \frac{db}{dw} + 2bc_\theta \frac{dc_\theta}{dw} + c_\theta \frac{dc}{dw} + c \frac{dc_\theta}{dw} + c_\theta \frac{dc}{dw} + \frac{dd}{dw} = 0 \end{aligned} \quad (4.31)$$

giving

$$\frac{dc_\theta}{dw} = - \left(\frac{a'c_\theta^3 + b'c_\theta^2 + c'c_\theta + d'}{3ac_\theta^2 + 2bc_\theta + c} \right) \quad (4.32)$$

where $a' \equiv \frac{da}{dw}$, $b' \equiv \frac{db}{dw}$, $c' \equiv \frac{dc}{dw}$, $d' \equiv \frac{dd}{dw}$.

Special cases (no turning point exists)

Let us consider the cases when the denominator of Eq. 4.32 is zero (no turning point exists). If such cases existed, then there would have to exist a $c_\theta \in [0, 1]$ satisfying

$$ac_\theta^3 + bc_\theta^2 + cc_\theta + d = 0 \quad \text{and} \quad 3ac_\theta^2 + 2bc_\theta + c = 0 \quad (4.33)$$

where w, c_ϕ, c_δ are fixed. Giving

$$ac_\theta^3 + bc_\theta^2 + cc_\theta + d = 3ac_\theta^2 + 2bc_\theta + c = 0 \quad (4.34)$$

$$\implies ac_\theta^3 + (b - 3a)c_\theta^2 + (c - 2b)c_\theta + (d - c) = 0 \quad (4.35)$$

When $c_\theta = 0$ this reduces to

$$d - c = -w^2c_\phi^2 + 2w(1 - w)c_\phi c_\delta \quad (4.36)$$

However, from Eq. 4.12 in the main text we see that $c_\theta = 0 \implies -w^2c_\phi^2$ and so either $w = 0$ or $c_\phi = 0$ and, therefore, $d - c = 0$.

Hence, we have one solution at $c_\theta = 0$.

We now show there are no other solutions by showing Eq. 4.35 is monotonically decreasing, across $c_\theta \in [0, 1]$.

Differentiating Eq. 4.35 with respect to c_θ we get

$$\begin{aligned} \frac{d}{dc_\theta}ac_\theta^3 + (b - 3a)c_\theta^2 + (c - 2b)c_\theta + (d - c) &= 3ac_\theta^2 + 2(b - 3a)c_\theta + (c - 2b) \\ &= 3ac_\theta(c_\theta - 1) + 2b(c_\theta - 1) + c \\ &\leq 0 \end{aligned} \quad (4.37)$$

as $a, b \geq 0, c \leq 0$ and $0 \leq c_\theta \leq 1$.

Recalling that $a = -c$, this inequality is strict unless (i) $c_\theta = 0, b = 0, a = 0$, (ii) $c_\theta = 1, a = 0$ or (iii) $a = 0, b = 0$.

From Eq. 4.12 in the main text and Appendix A1, we note that

$$a = 0 \implies w = 0, w = 1, c_\phi = 0 \text{ or } c_\delta = 0.$$

$$b = 0 \implies w = 0 \text{ and } c_\delta = 1.$$

$c_\theta = 1 \implies w = 1$ and $c_\phi = 1$ (recalling from Appendix A2 that when $w = 0, c_\delta = 1$ we defined $c_\theta = 0$).

$$c_\theta = 0 \implies w = 0 \text{ or } c_\phi = 0.$$

Therefore, the cases where $\frac{d}{dc_\theta}$ is not strictly less than 0 are precisely when (i) $w = 0$ and $c_\delta = 1$ or (ii) $w = 1$ and $c_\phi = 1$.

Since the gradient for the remaining values of w, c_ϕ, c_δ is constantly negative across

$c_\theta \in [0, 1]$, Eq. 4.35 must be monotonically decreasing across the interval for these values.

Combining the cases of zero gradient, with the root found at $c_\theta = 0$, gives the special cases for Eq. 4.32 needed to be considered as: (i) $w = 1$ and $c_\phi = 1$, (ii) $c_\theta = 0$, (iii) $w = 0$ and $c_\delta = 1$.

Case (i) $w = 1$ and $c_\phi = 1$. As $c_\theta = 1$, which is clearly maximal, we take $\frac{dc_\theta}{dw} = 0$ at this point.

Case (ii) $c_\theta = 0 \implies$ either $c_\phi = 0$ or $w = 0$. When $c_\phi = 0$ we have $c_\theta = 0$ for all w and so there is no turning point and no optimal value for w . When $w = 0$ we recall from Appendix A2 that as $c_\theta = 0$ which cannot be a maximum, the gradient must be strictly positive and, therefore, not a turning point (except in the special cases of $c_\phi = 0$ which was just discussed).

Case (iii) $w = 0$ and $c_\delta = 1$. This is a sub-case of case (ii) and hence was discussed above.

General case (turning point exists)

We now show that there is precisely one root for Eq. 4.32 with $w \in (0, 1]$, $c_\phi \in (0, 1]$, $c_\delta \in [0, 1]$, $c_\theta \in (0, 1)$.

From Appendix A1 we calculate that

$$\begin{aligned}
 a' &= 2(1 - 2w)c_\phi c_\delta \\
 b' &= 2w - 2(1 - w)(1 - c_\delta^2) \\
 c' &= -2(1 - 2w)c_\phi c_\delta \\
 d' &= -2wc_\phi^2
 \end{aligned} \tag{4.38}$$

Allowing us to rewrite the numerator of Eq. 4.32 as

$$2(1 - 2w)c_\phi c_\delta c_\theta^3 + (2w - 2(1 - w)(1 - c_\delta^2))c_\theta^2 - 2(1 - 2w)c_\phi c_\delta c_\theta - 2wc_\phi^2 \tag{4.39}$$

Considering the limit as $w \rightarrow 0^+$, noting that for this $c_\theta > 0$, we get

$$2c_\phi c_\delta c_\theta (c_\theta^2 - 1) + 2(c_\delta^2 - 1)c_\theta^2 \quad (4.40)$$

which is strictly negative. We know from case (ii) above, that the denominator at $w = 0$ is strictly positive and hence Eq. 4.32 must be strictly positive (due to the negation symbol in Eq. 4.32).

We now let $w \rightarrow 1^-$. From Appendix A2 we have $c_\theta \rightarrow c_\phi$ and the numerator of Eq. 4.32 becomes

$$2c_\phi^2 c_\delta (1 - c_\phi^2) \quad (4.41)$$

which is strictly positive, except for the specific cases of $c_\phi = 1$ or $c_\delta = 0$, in which the function tends to 0, implying the existence of a local maxima for c_θ at $w = 1$. The denominator in this case tends to $2c_\theta$, which is strictly positive and, hence, Eq. 4.32 is strictly non-positive as $w \rightarrow 1^-$.

We now invoke the intermediate value theorem, which states that as we have passed from a positive to a non-positive value in $[0, 1]$ there must exist at least one root in $[0, 1]$ for Eq. 4.32. If we return to Eq. 4.13 from the main text we note that this can be considered as a polynomial in w of maximum degree 2, and hence, can have *at most* one turning point as w varies.

Combining this with what we have just shown, proves the existence of one local maximum value in $[0, 1]$ for Eq. 4.13 in the main text.

4.6.4 Appendix A4 - Navigational efficiency of the BCRW model with $c_\delta < 1$ is relatively unaffected by the number of steps

In this appendix we include further plots illustrating how the navigational efficiency of the BCRW model with $c_\delta < 1$ is relatively unaffected by the number of steps in the random walk, in contrast to the case where $c_\delta < 1$ (as demonstrated in plots (a-c) in Fig. 4.1, Fig. 4.2 & Fig. 4.3)

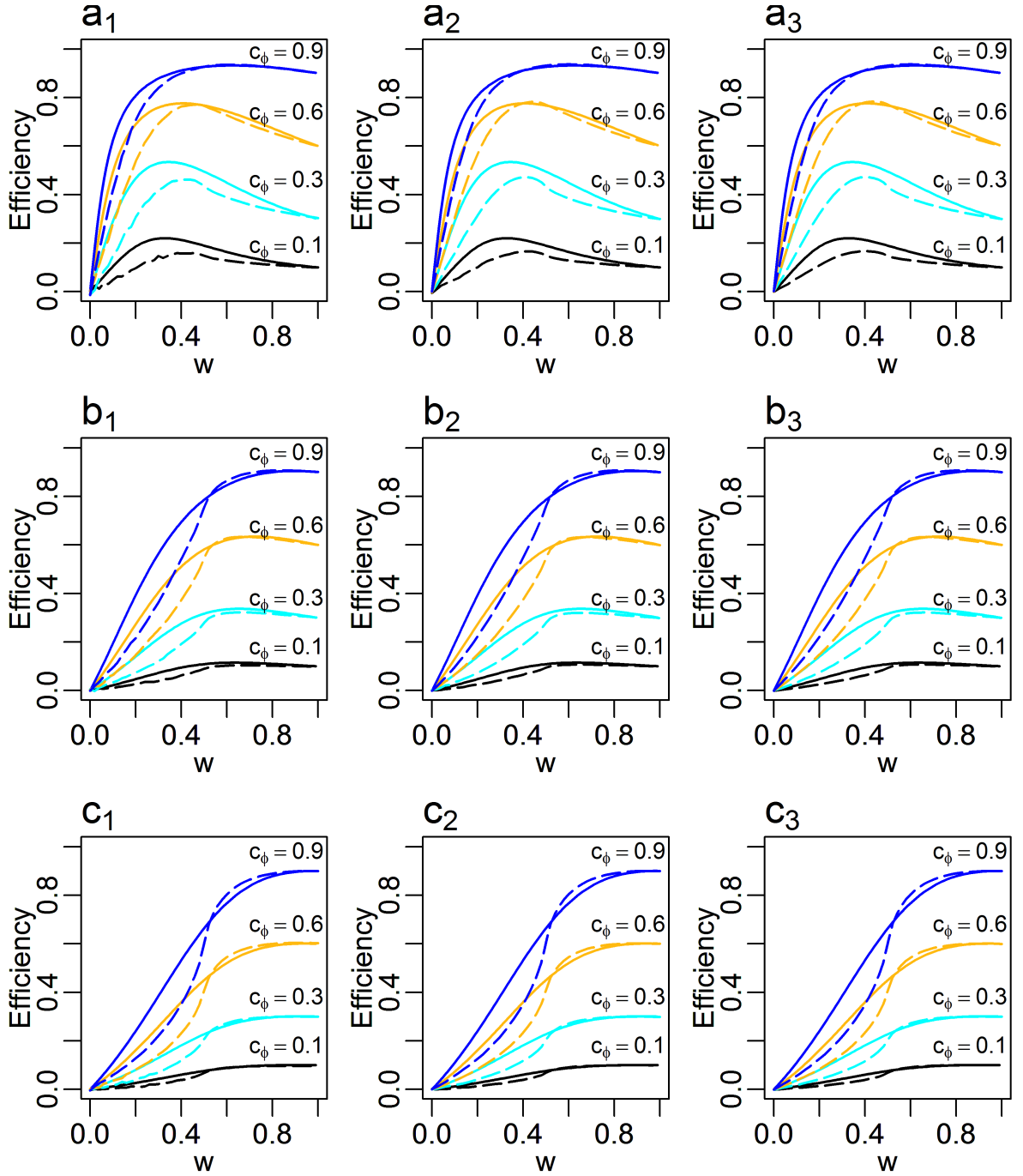


Figure 4.8: Plots of navigational efficiency, c_θ , against weighting factor, w , with non-zero persistence error: (a) $c_\delta = 0.9$, (b) $c_\delta = 0.5$ (c) $c_\delta = 0.1$, considered over different time scales: (a_1, b_1, c_1) 100 steps, (a_2, b_2, c_2) 1000 steps, (a_3, b_3, c_3) 10,000 steps, and for a range of navigation error levels, $c_\phi = 0.1$ (black), $c_\phi = 0.3$ (cyan), $c_\phi = 0.6$ (gold) & $c_\phi = 0.9$ (blue). In all plots the solid lines represent the 10 theoretical model predictions and the dashed lines represent the average results from simulations of 1000 individual random walkers; w ranges from 0 to 1 at 0.01 intervals.

5 Walking behaviour in the ground beetle *Poecilus cupreus*: individual variation, intermittency, and dispersal potential

This chapter is based on joint work with C. Benefer (Plymouth University), R. Blackshaw (Blackshaw Research and Consultancy) and E.A. Codling (University of Essex). All experiments were conceived, designed and performed by CB & RB.

In this chapter we see how RW theory can be used to analyse and characterise animal movement data. The ground beetle (*Poecilus cupreus*), an important carabid predator in agricultural land, were tracked at fine-scale by the use of a locomotion compensator to quantify key characteristics of the observed movement, such as dispersal ability. Our results showed that overall net displacement increased much more rapidly than predicted by a simple correlated random walk model, with near ballistic behaviour observed in some cases. Individuals displayed a latent ability to head on a constant bearing for a protracted length of time, despite showing no clear evidence of a global orientation bias at the population level. Intermittent bouts of movement and non-movement were observed, with both the frequency and duration of bouts of movement varying at the inter- and intra-individual level. Analysis of observed beetle movement suggests that individual beetles have the potential to rapidly disperse over a much wider area than predicted by simple movement models parameterised at the population level. This highlights the importance of considering the role of individual variation when analysing movement data and predicting dispersal distances.

5.1 Background

Dispersal is a key ecological process affecting population, species and community dynamics over small and large spatial scales. There is increasing interest in how individual variation in movement behaviour contributes to dispersal and subsequent population

distributions, since the movement of individuals can be very different to the ensemble average movement across a population (Petrovskii et al, 2011; Chapman et al, 2011). When using models to predict dispersal potential it is therefore important to consider variation in individual dispersal propensity rather than simply pooling data to provide population-level parameter estimates and hence (effectively) making assumptions that all individuals behave in the same way (Hawkes 2009). For species of ecological and economic importance, such as pest insects and their natural predators, it is essential to understand how dispersal behaviour leads to observed population distributions in order that effective management strategies can be implemented at appropriate scales (Petrovskii et al, 2014).

Ground beetles (*Coleoptera: Carabidae*) are widely recognised to be important components of terrestrial ecosystems, playing a major role in the food web as both predators of a wide range of invertebrates and as prey to a number of bird and mammal species, some of which are of conservation concern (Holland et al, 2006; Pocock & Jennings, 2007). They are also considered to be of bio-indicative value since they are sensitive to cultivation impacts, and particularly to intensification of agricultural practices (Rainio & Niemelä, 2003). For these reasons, and because of their importance in the natural control of invertebrate pests (Kromp, 1999) and weed populations (for seed feeding species; (Bohan et al, 2011)) in agricultural land, the biology and ecology of species within this family have been extensively studied.

Critical to their function in controlling pest populations within fields is their dispersal ability. Movement is mainly via walking, though flight may be used under some circumstances, e.g. longer distance dispersal (Lövei & Sunderland, 1996), and many species are highly mobile. Field margins act as refuges for natural enemy species and movement occurs into cropped fields from these semi-natural areas (Thomas et al, 1997), as such, 'beetle banks' - raised earth banks between fields sown with grass species - have been specifically created in farmland across the UK and Europe as overwintering habitats for beneficial invertebrates (Thomas et al, 1991; MacLeod et al, 2004). Knowledge of dispersal into fields from such areas and the effects of biological characteristics of individual

species and how this leads to their observed distribution in agricultural landscapes is key to understanding the maintenance of metapopulations and the dynamics of predator-prey interactions (Petrovskii et al, 2014; Bastola & Davis, 2018). This is particularly relevant in the context of climate change and habitat fragmentation, for which it is important to be able to predict effects of changes to the environment on species of economic and ecological importance.

Previous studies investigating ground beetle dispersal have used mark-release-recapture techniques (Rijnsdorp 1980; Thomas et al, 1997, 1998), though using this approach means that estimation of movement distance is limited to the maximum distance at which pitfall traps are set as discussed in section 2.3. Others have used harmonic radar to track individuals (Wallin & Ekblom, 1994; Lövei et al, 1997), which is similar in principle to mark-release-recapture since individuals are tagged and then located at a later time point. However, neither of these approaches gives fine-scale detail of walking movements since observation frequencies are low and often the majority of individuals released are not recovered.

To try to overcome these limitations, individual-based simulation models have been used, incorporating spatial and landscape parameters for forest carabids (Jopp & Reuter, 2005) and common agricultural (*Pterostichus*) species (Firle et al, 1998; Benjamin et al, 2008), or based on population level estimates of random walk movement parameters for a range of insects including ground beetles (Byers, 2001). Although such models may try to take into account factors that are likely to affect distribution and abundance in the field, they are frequently based on data collected from field studies like those described above, which do not explicitly consider inter- and intra-individual variation in walking behaviours and how this affects dispersal distances. This is particularly relevant when considering pest species and their natural enemies, since it is important to know the extent of dispersal in differing situations i.e. under alternate cultivation practices. Studies using high resolution movement data in a homogeneous featureless environment have been recorded for mealworm beetles (*Tenebrio molitor*) (Reynolds et al, 2013), where a power law distribution in the beetles' step-lengths was found. In the

same study, (Reynolds et al, 2013) also reported highly linear movements in *Poecilus* beetles, although did not undertake a full analysis for this species. *T. molitor* beetles were also studied experimentally by (Bearup et al, 2016), who found their movements and dispersal within a circular arena could be described by a simple diffusive model of a SRW/ Brownian motion.

Recent advances in tracking technology mean that fine-scale position data can now be more easily collected from real animal movement paths in both the field and laboratory. In this study we used a laboratory based technique, a locomotion compensator, to measure fine-scale walking movements of *P. cupreus*, one of the most common carabid species in European agricultural land (Kromp 1999; Luff 2002). It is a diurnal, macropterous species which is active in spring-summer and is found in relatively dry warm habitats such as open grassland and agricultural fields (Luff 1998), and its abundance and dominance in these habitats makes it an ideal species for investigating movement behaviour within- and between- individuals. Although the locomotion compensator is not a new technique (Kramer, 1976), to our knowledge it has not been used in this way before.

It should be noted that the artificial setup of the experiment results in limitations as to the conclusions which can be reliably drawn from these results. Whilst such problems regarding the artificiality and low generality of the setup are a recognised flaw in model systems (Carpenter, 1996) and lead to the common ‘replication versus realism’ debate (Srivastava et al, 2004; Schindler, 1998) there are inherent benefits of such model systems, such as repeatability and ease of experimentation (Levins, 1984; , Srivastava et al, 2004). In this experimental setup the use of the TrackSphere locomotion compensator allows for data to be collected with relative ease and accuracy, giving data with high frequency and greater accuracy than would be expected from simple video analysis or from capture-recapture techniques. Similarly, the setup removes any impedimentary effect a tracker attached to the beetle would have.

In the field insects’ movement and behaviour can be affected by a range of stimuli from social interactions, landscape heterogeneity and fragmentation of landscape, weather conditions as well as from seasonal and diurnal behavioural patterns and prey densities

(Firle et al, 1998; Mazzi & Dorn, 2012; Dahmen et al, 2018). Here we chose to focus on measuring the dispersal potential of *P. cupreus* as well as discerning whether there were significant differences in general movement patterns in an unobstructed environment. We quantify the observed movement using standard path analysis measures (mean-displacement, path straightness, distributions of instantaneous speeds/step-lengths and turning angles, and the number and duration of movement and non-movement bouts) and explore the level of inter- and intra-individual variation. We subsequently demonstrate how simple random walk movement models, parameterised at the population level from the observed data, do not adequately explain the observed dispersal behaviour.

5.2 Methods

5.2.1 Sample Collection

Adult *P. cupreus* (Fig. 5.1A) were captured daily using pitfall traps from a permanent grazed grassland in Dartington, Devon, UK (OS grid reference SX 78366 62988) between 8th and 20th July 2012. The beetles were maintained at 16°C in tanks containing soil, leaf litter and dead wood in mixed populations with other ground beetle species and fed on cat food every few days until needed for the experiment, whereby identified individuals (using (Luff 2002)) were transferred to separate 20ml universal tubes containing a small piece of damp tissue paper.

5.2.2 Tracking Beetle Walking Behaviour

A locomotion compensator (Tracksphere LC 300, Syntech, Hilversum, The Netherlands; Fig. 5.1A; Syntech, 2004) was used to track and measure the movement paths (measured in mm) for each beetle, which were tested three times each between 1st and 8th August 2012. Between trials individuals were maintained at 16°C. The locomotion compensator consists of a sphere (300mm diameter), onto which a beetle is placed, with a camera located directly above that measures the beetle's displacements. The sphere rotates opposite to these displacements by means of two electric motors, and two encoders contacting the sphere transmit the rotational movements to a computer as incremental

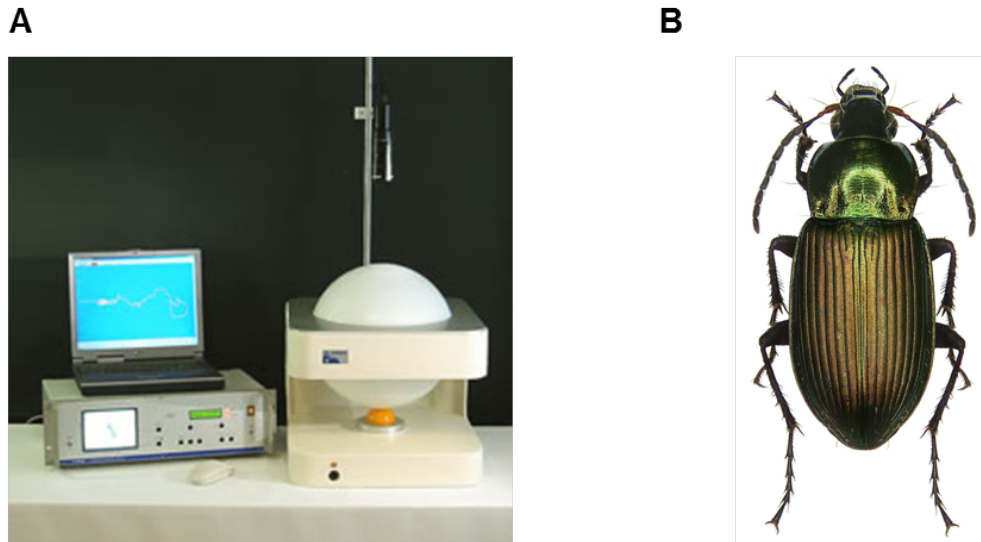


Figure 5.1: (A) TrackSphere LC 300 locomotion compensator (Syntech, 2004) used to track beetle movement. (B) Image of an adult *Poecilus cupreus* beetle (taken from Schmidt, 2008).

(x, y) coordinates, which are recorded 10 times per second. Experiments were carried out between 16.8 and 24.2°C, recorded at the beginning of each trial, and were illuminated by a fluorescent light located directly behind the sphere. A white cardboard screen was placed around the sphere to prevent external influences affecting beetle behaviour and the sphere was wiped clean with 70% ethanol after each trial. Individual beetles were allowed to acclimatise on the sphere for one minute before recording began for ten minutes. However, due to the sphere failing to properly compensate for the movements of eight beetles for the full ten minute period, the final analysis was performed on data recorded over a five minute span starting from 10 seconds into the track and finishing 5 minutes later (this period of data collection was available for all experimental trials). Trials in which beetles did not move at all during this period were removed from the dataset completely, giving data from 22 individual beetles. In summary, walking movement data ((x, y) coordinates recorded 10 times per second) over a five minute period were obtained for 22 individual beetles, repeated three times each (66 observations in total) (Fig. 5.2A & 5.2B).

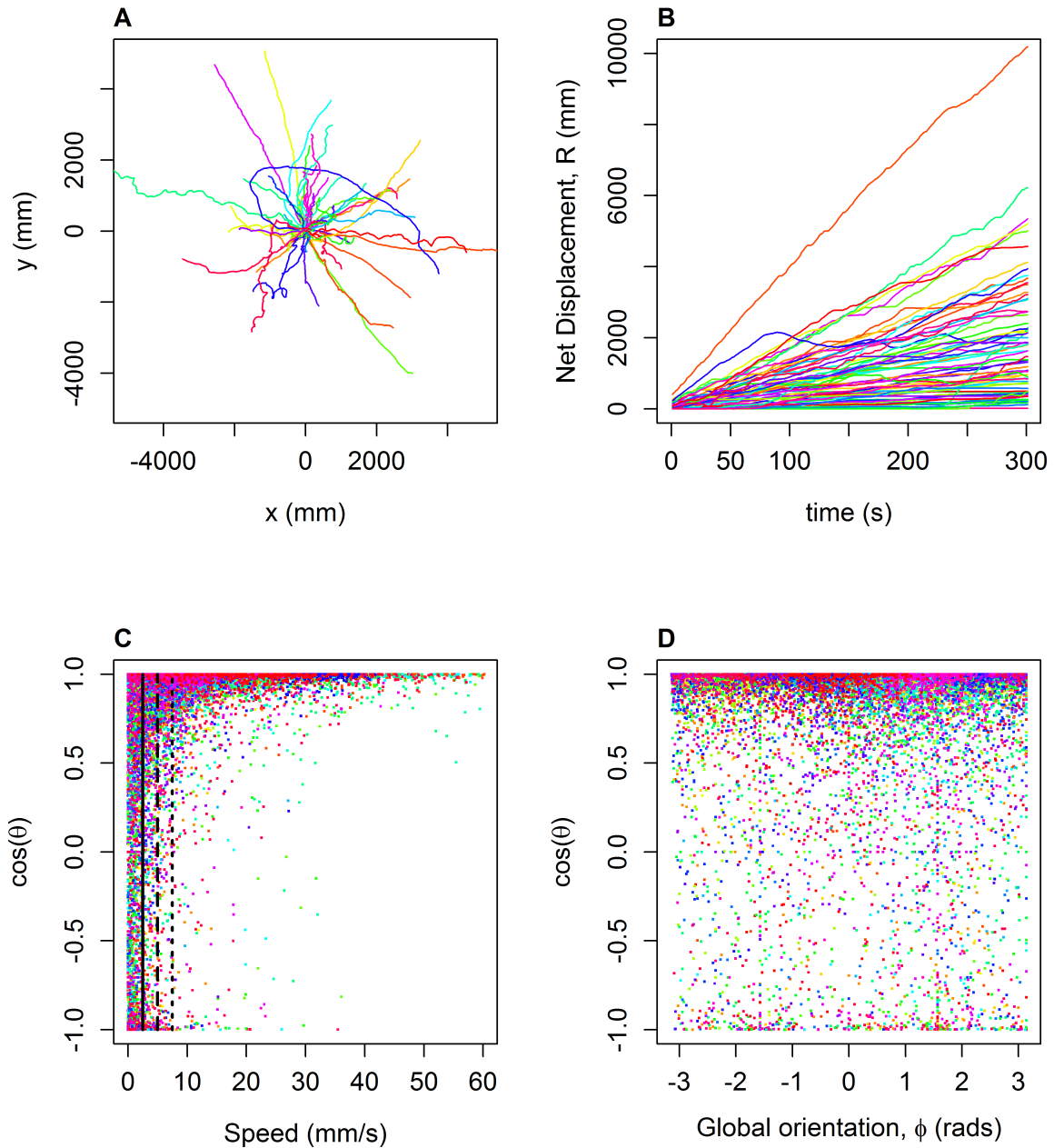


Figure 5.2: (A) Individual beetle movement paths, one colour per beetle. (B) Displacement over time for each individual beetle, using the same colours to depict beetles as in (A). (C) Cosine of the turning angle (the angle between successive steps) against the instantaneous speed at that step. The plot demonstrates that at high speeds the cosine of the turning angle is close to 1, indicating a small turn, whereas, at slower speeds the value of the cosine turning angle varies greatly, giving an almost uniform distribution across all turning angles. The vertical lines represent possible values for the speed threshold value (5mm/s, 10mm/s and 15mm/s) which were used to distinguish between purposeful movement and stationarity. Colours represent different beetles (as in (A) and (B)) with each beetle having the same colour across all three trials. (D) Global orientation of movement at each step (and the cosine of the corresponding turning angle (the angle between successive global orientations)). Colours represent different beetles (as in (A) and (B)). For all figures the sampling size used was 1Hz.

5.3 Data Analysis

5.3.1 Initial Processing of Movement Path data

The raw movement data, recorded at a frequency of 10Hz using the locomotion compensator, was found to have some artificial ‘pixelisation’ of the movement paths, leading to artificially high turning angles being recorded. To overcome this problem, the raw data were sub-sampled at a sampling rate of 1Hz to smooth the movement paths and avoid pixelisation effects (i.e. only every 10th location recorded in the raw data was included in the analysis). The choice of 1Hz as the subsampling rate was motivated by the frequency of how often beetles were seen to take steps on the locomotion compensator, but was nevertheless essentially an arbitrary choice. Hence other sampling rates of 2Hz, 0.5Hz and 0.2Hz (i.e. respectively only every 5th, 20th or 50th raw data point included) were also considered. Using these alternative sampling rates did not qualitatively change the results (Appendix B3; Tables 5.7-5.16).

To classify bouts of ‘purposeful movement’ (movement associated with relocation in space) and ‘stationarity’ (non-movement; periods where the beetle either turns on the spot or stops moving entirely, leading to zero or limited relocation in space), a minimum instantaneous speed threshold was used as an objective way to classify each step of the movement paths: observed instantaneous speeds lower than the minimum threshold are classified as stationarity; observed instantaneous speeds above the minimum threshold are classified as movement. A range of minimum speed threshold values were considered: 5mm/s, 10mm/s and 15mm/s, as well as no minimum speed threshold at all. The minimum speed threshold of 5mm/s was used for the main analysis presented as this allowed for the retention of the largest number of data points while allowing objective classification of bouts. The use of different minimum speed thresholds did not lead to qualitatively different results (Appendix B3; Tables 5.7-5.16).

Using the minimum speed threshold for each step of the (1Hz sampled) movement data leads to movement and non-movement bouts of very short length, due to noise in the recording and processing of the data. To account for this the (1Hz sampled) movement

data was smoothed, and bouts of movement and stationarity identified, through the use of a cumulative sum algorithm similar to (Knell & Codling, 2012) (see Appendix B1). Bouts that had not ended by the end of the experiment were considered to have been artificially truncated and hence were not included in the analysis presented in the main paper, since their true duration was indeterminable. However, results were qualitatively similar if these truncated bouts were included, under the assumption that they terminated at the end point of the experiment (see Appendix B4).

5.3.2 Path Analysis Measures

Standard path analysis measures adopted from random walk theory (Kareiva & Shigesada, 1983; Kramer & McLaughlin, 2001; Goodwin & Fahrig, 2002; Codling et al, 2008; Benhamou, 2006) were quantified for each of the observed movement paths. In particular, for each step of each (1Hz sampled) movement path we determined the turning angle between the directions of successive movement steps (Fig. 5.2C and 5.2D), the global direction of movement at each step (Fig. 5.2D), and step length / speed (Fig. 5.2C; step length and the instantaneous measured speed are exactly equivalent as we used a fixed sampling frequency of 1Hz). The observed speeds were then used to determine bouts of movement and stationarity as described in the previous section. Summary statistics for each movement path were determined: total net displacement (mm; Fig. 5.2B), mean cosine of turning angles, straightness (total track length/total net displacement; a measure of tortuosity), mean speed (mm/s; determined for bouts of movement only), number of bout transitions (movement to non-movement and vice versa), average bout duration (s), variance in bout duration (s^2), and proportion of time spent moving (%). Temperature was included as a covariate in the initial analyses but was found not to be significant and so was excluded from subsequent analysis.

5.3.3 Statistical analysis

5.3.3.1 Intra- & inter- individual variation

To determine if there were significant intra-individual differences in the basic summary path statistics, a repeated measures ANOVA was used to compare observed results across the three trials. Inter-individual variation across the study population was tested by a one-way ANOVA (or Kruskal-Wallis test for those summary statistics which violated the homogeneity of variance assumption) on the mean of each summary statistic across the three trials. These analyses were carried out using JASP v.0.8.0.0 (JASP Team, 2018) and R (R Core Team, 2018).

To measure the consistency of behaviour among individuals, the repeatability, r , (also known as the intra class coefficient, ICC (Lessels & Boag, 1987)) was calculated, where

$$\text{ICC} = \frac{V_{\text{ind}}}{V_{\text{ind}} + V_{\epsilon}} \quad (5.1)$$

with V_{ind} the variance among individuals and V_{ϵ} the residual (error) variance (Nakagawa & Schielzeth, 2010; Dingemanse & Dochtermann 2013; Houslay & Wilson 2017). Therefore, ICC tells us the relative strength of the variance between individuals compared to the total variance, with the total variance considered as the sum of the variance among individuals, V_{ind} , and the total variance within individuals V_{ϵ} – whilst this variance is technically a measure of the residuals, it is commonly referred to as within-individual variation (Brommer 2013; Dingemanse & Dochtermann 2013; Brommer et al 2014; Dosmann et al, 2015). These variances were found using Linear Mixed Effect Models using Restricted Maximum-Likelihood parameter estimation following the method described in Nakagawa & Schielzeth (2010) by use of the *rptR* package (Stoffel et al, 2017) in *R* (R Development Core Team, 2019).

5.3.3.2 Correlation in movement parameters

Between individuals

To see if there were a correlation between any of the parameters at the between-individual level, (e.g. does a beetle which has higher displacement on average also spend more time moving than the average?) a bivariate (two-trait) mixed model was used (Houslay & Wilson, 2017), with the individual beetle as the random intercept, the experiment number (centred) as the repeat number, and the parameters (centred and scaled) as the random effects, as per Houslay & Wilson (2017).

The model was then implemented by the *MCMCglmm* package (Hadfield 2010) in *R* (R Development Core Team, 2019). In order to ensure auto-correlation was not an effect, a large number of iterations were run 500,000 with a ‘burn-in’ period of 15,000 and a thinning of 100. Results were deemed to be significant if the confidence intervals (95%) did not span 0, as is standard with Bayesian CI’s (Houslay & Wilson 2017).

The correlation between two parameters, $r_{\text{ind}_\alpha, \text{ind}_\beta}$, is then found by calculating their between individual covariance, $COV_{\text{ind}_\alpha, \text{ind}_\beta}$, and dividing by the square root of the product of the between individual variances of the two parameters, $V_{\text{ind}_\alpha}, V_{\text{ind}_\beta}$ (Dingemanse & Dochterman 2013; Dosmann & Mateo, 2014; Dosmann et al, 2015).

$$r_{\text{ind}_\alpha, \text{ind}_\beta} = \frac{COV_{\text{ind}_\alpha, \text{ind}_\beta}}{\sqrt{V_{\text{ind}_\alpha} V_{\text{ind}_\beta}}} \quad (5.2)$$

Within individuals

For any parameter whose residual variance V_ϵ (equivalent to the variability within each individual across the three trial runs) was seen to be high, we might wish to answer the question whether a correlation exists within individual’s trial runs for each pair of parameters e.g. did trials with a higher displacement also feature fewer bouts?

We use the same bivariate mixed effect model used to find the between individual correlation (described above) to find any such correlation between two parameters, $r_{\epsilon_\alpha, \epsilon_\beta}$, using a similar calculation as in Eq. 5.2 except we now consider the covariance of the parameters at the within-individual level, $COV_{\epsilon_\alpha, \epsilon_\beta}$, divided by the square root of

the product of the variances of each parameter at the within-individual level $V_{\epsilon_\alpha}, V_{\epsilon_\beta}$ (Dingemanse & Dochterman 2013; Dosmann et al, 2014).

$$r_{\epsilon_\alpha, \epsilon_\beta} = \frac{COV_{\epsilon_\alpha, \epsilon_\beta}}{\sqrt{V_{\epsilon_\alpha} V_{\epsilon_\beta}}} \quad (5.3)$$

One could ask why a simple correlation test (Spearman’s, Pearson’s, etc.) for each individual trial or for the mean of each statistic across the three trials would not suffice as a test of the relationship between parameters. However, such a method has shown to be over generous with the significance level of any resulting correlations (Hadfield et al, 2010; Dingemanse et al 2012; Houslay & Wilson, 2017).

5.3.3.3 Analysis of population level movement dynamics

Global orientation of movement directions (corresponding to bouts of movement only) were considered at both the population and individual level, to ascertain whether there was a global or an individual preference in direction. As global orientations form circular data, the Watson Test was used to test if the distribution of orientations could be described by the circular uniform distribution (see section 3.6). The Rayleigh test then determined whether the distribution corresponded to a unimodal wrapped distribution with specific resultant vector, where a resultant vector close to 1 would indicate a strong preference in movement direction, while a resultant vector close to 0 would indicate no preference in movement direction (Mardia & Jupp, 2000; Jammalamadaka & SenGupta, 2011).

The observed turning angles (corresponding to bouts of movement only) were fitted to two standard circular probability distributions: the von Mises (which is a close approximation to the normal distribution on a circle) and the wrapped Cauchy (which is a heavy-tailed circular distribution). These distributions were fitted using the *CircStats* package in *R*. The Kuiper and the Watson- U^2 tests were used to check the validity of both models, with the Akaike Information Criterion (AIC) used to indicate the closer fitting distribution. Evidence of unimodal turning angle distributions centred around 0 would indicate persistence in the beetles’ movements.

Four distributions were considered for fitting the observed distribution of step lengths (instantaneous speeds; corresponding to bouts of movement only), with the same distributions also considered for the movement and non-movement bout durations: power-law, exponential, Weibull and log-normal. Distributions were fitted using the *fitdistrplus* package in *R*, except for the power-law that was fitted using the *power.law.fit* function in the *iGraph* package in *R*. We fit the power-law in two ways. Firstly, in order to ensure the power-law fitted all the data, we used a restricted power-law where the x_{\min} value was set at the smallest non-zero value of the data rather than the value for x_{\min} calculated by *power.law.fit* function (Virkar & Clauset, 2014). Secondly, we also consider a power-law fit to only the tail of the data, as this is one of the features described in the literature that is indicative of Lévy walk behaviour (Sims et al, 2007; Edwards et al, 2007; Reynolds et al, 2013; Ahmed et al, 2018). The tail of the data was calculated by using the best fit x_{\min} value calculated by the *power.law.fit* function, and then the potential distributions were fitted only to the data points which were greater than this minimum value. As the fitting algorithm for the power-law utilised a maximum likelihood estimation (MLE) method to maximise the p -value for the Kolmogorov–Smirnov (K-S) test, a G-test was also used to consider the fit of the distributions (Edwards et al, 2007).

Data for turning angles and step lengths (speeds) were fitted at the population level (10045 data points from 66 movement paths) and at the individual path level (between 37 and 298 data points for each movement path).

5.3.3.4 Comparison of paths as a CRW or BRW

To further investigate whether the characteristics of the beetle movement paths could be best classified as either a correlated random walk (CRW; i.e. movement is persistent but not globally directed) or a biased random walk (BRW; i.e. movement is globally directed), we measured the Δ statistic from (Marsh & Jones, 1988):

$$\Delta = \frac{1}{n^2} \left[\left(\sum \cos \phi_i \right)^2 + \left(\sum \sin \phi_i \right)^2 \right] - \frac{1}{(n-1)^2} \left[\left(\sum \cos \theta_i \right)^2 + \left(\sum \sin \theta_i \right)^2 \right] \quad (5.4)$$

where, ϕ_i is the global orientation and θ_i is the turning angle, at time i . The Δ statistic gives a relative measure of how well the observed data fits each of the two types of random walk movement model by returning a positive value for a BRW and a negative value for a CRW (see details in Appendix B5).

The Δ statistic was calculated for each individual movement path separately and also for all turning and global orientation angles aggregated at the population level. Data for bout durations were fitted only at the population level due to the limited number of data points from each individual path (326 data points from 66 movement paths).

An additional method was also used to determine evidence of either CRW or BRW behaviour. This involved sub-sampling the observed movement data across a range of steps and determining how the estimated mean cosine of turning angles changes with the sub-sampling step used (Bovet & Benhamou, 1988; Codling & Hill, 2005; Benhamou, 2006). For a CRW the observed mean cosine of turning angles is expected to decrease to 0 as correlation between increasingly distant steps diminishes. However, for a BRW, the observed mean cosine is expected to increase towards 1 as the movement path appears increasingly more linear due to the global directional bias present.

5.4 Results

5.4.1 Basic Path Analysis Measures

Fig. 5.2C illustrates how the observed movement paths mainly consisted of bouts of high speed and highly persistent movement (where the mean cosine of turning angles is close to 1), interspersed with bouts of low speed (0-10mm/s) in which the distribution of turning angles is more uniform. These periods of low speed were determined to be periods of stationarity. A possible explanation of the recorded large turns during these periods of stationarity is that the beetles paused during movement to engage in periods of reorientation or to examine the local environment, before returning to move in near straight line movement. This would be similar to movement observed in dung beetle movement and subsequent movement models (Byrne et al, 2003; Baird et al, 2012).

The beetles' net displacement ranged from 14 to 9785mm (Fig. 5.3A) with the

measure of straightness of each individual path varying from 0.98 (near straight-line movement) to 0.21 (tortuous) (Appendix B2 - Fig. 5.7). The average of the mean cosine values was found to be 0.7795 with a standard deviation of 0.1462, indicating a small range of values for the mean cosine across all trials, although, the spread of values across individuals appears to vary significantly, as can be seen in Fig. 5.3C. On average the beetles as a population spent 55.5% of the experiment moving, recording an average speed when moving in the range of 5.65mm/s to 36.3mm/s with the population average being 12.47mm/s (Fig. 5.3B; Appendix B2 - Fig. 5.7). The number of transitions from bouts of movement to stationarity (and vice-versa) in a single trial varied from 0 to 12 across the population, with individuals exhibiting a wide range in the number of transitions across their individual 3 trials (Fig. 5.3D), correspondingly the average bout length varied from 17s, for the individual trial which displayed 12 completed bouts, to 293s for the individual trial which displayed only one complete bout during the experiment.

5.4.2 Intra- and Inter-Individual Variation

There were significant differences ($p < 0.05$) in intra-individual behaviour across the three trials for displacement ($F(1.49, 31.292) = 4.032$, $p = 0.038$; Fig. 5.3A), mean cosine of turning angles ($F(2, 42) = 4.43$, $p = 0.018$; Fig. 5.3C), proportion of time spent moving ($F(2, 42) = 4.365$, $p = 0.019$) and average speed when moving ($F(2, 42) = 7.143$, $p = 0.002$; Fig. 5.3B). See Appendix B2 - Table 5.5 & Fig. 5.7; for complete results of the ANOVA test for intra-individual variation.

There were also significant inter-individual differences ($p < 0.05$) between the 22 observed beetles for mean cosine of turning angles (Kruskal-Wallis $\chi^2 = 33.53$, $p = 0.041$; Fig. 5.3C), number of bout transitions ($F(21, 44) = 1.883$, $p = 0.038$; Fig. 5.3D) With displacement (Kruskal-Wallis $\chi^2 = 30.925$, $p = 0.075$; Fig. 5.3A) and average bout duration (Kruskal-Wallis $\chi^2 = 31.091$, $p = 0.072$) also indicating significant differences, though not as strongly as mean cosine and number of bout transitions. (See Appendix B2 - Table 5.6; for complete results of the MANOVA test for inter-individual variation). This suggests a wide range of movement behaviours are possible, even across a relatively

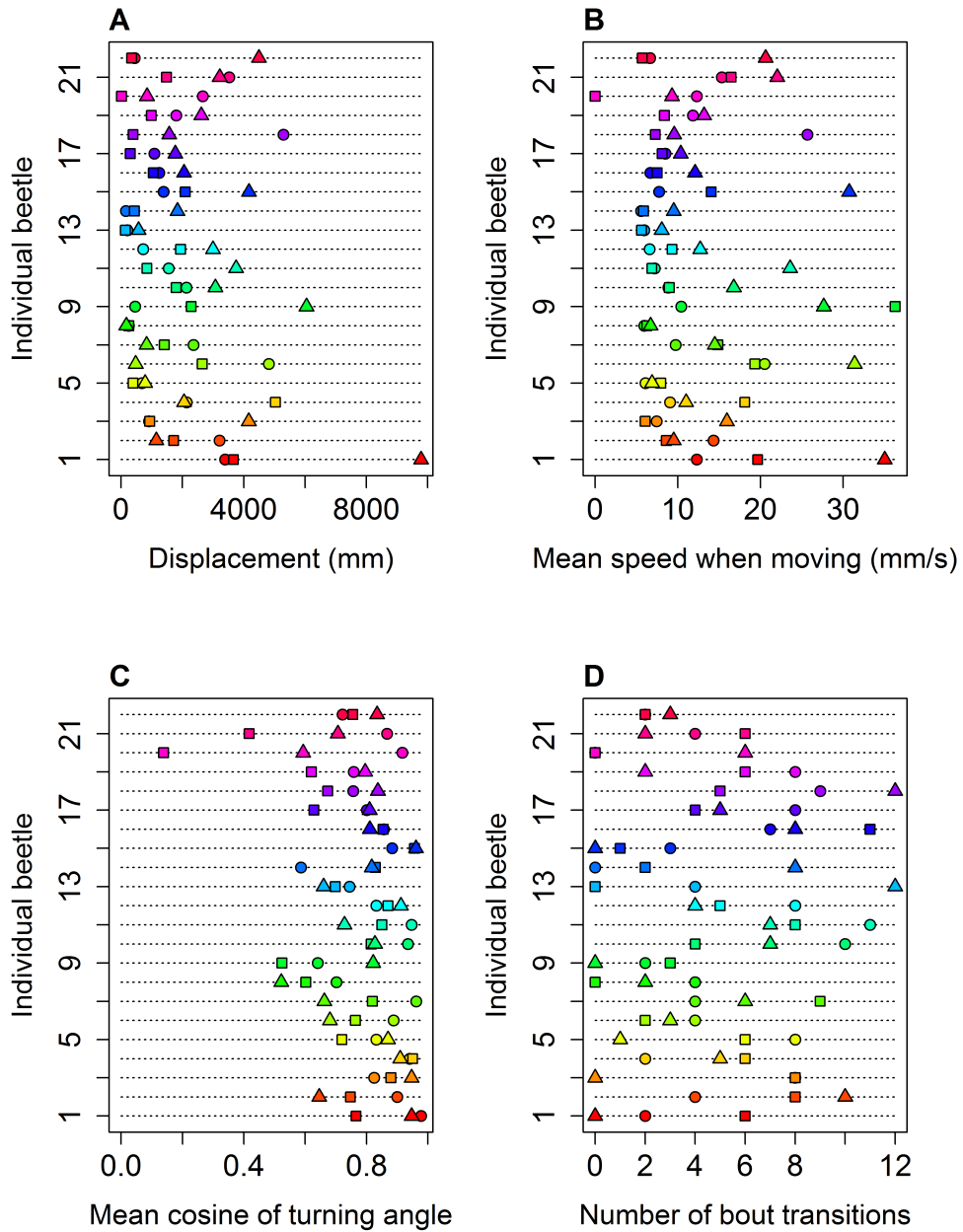


Figure 5.3: (A-D) (A) Total displacement, (B) mean cosine of turning angle, (C) mean speed when moving, and (D) number of bout transitions of each beetle for each trial (figures displaying variability across the other parameters are found in Appendix B2 - Fig. 5.7). In all plots, circle points correspond to Trial 1, square to Trial 2 and triangle to Trial 3.

small sample of a natural population of beetles and indicates a lack of consistency in individual movement behaviour across the three trials.

Repeatability

Considering the repeatability, ICC value, significant results were found for number of bouts, time spent moving (%) and average speed when moving ($p < 0.05$). All of these gave a repeatability of over 0.2, with the highest being average speed when moving, $ICC = 0.282$, implying that the beetles displayed individual consistency across the three trials. Whereas displacement, straightness, mean cosine of turning turn angles and average bout duration had non-significant values ($p > 0.05$) indicating that there was no evidence of individual repeatability for these parameters. When considering the 95% confidence intervals, we note that all the parameters admitted a large range, with the difference from the upper and lower CIs giving values between 0.32 – 0.513 for all parameters. It should be noted that whilst in Bayesian analyses CI's which do not cross zero are often assumed to indicate significance, in cases where the statistic in question is constrained to be non-negative, then a lower bound of 0 is often indicative of low confidence in a non-zero. Hence, as all parameters here have CI's which are bounded below by 0, with the exception of average speed. This indicates that there is no significant consistency in behaviour for the beetles across these parameters.

However, the results do demonstrate that between 12.7-36.2% of the variance in the parameters is caused by differences between individuals (Houslay & Wilson, 2017) indicating that the majority of the variation in the parameters is due to the differences within-individuals (Table 5.1).

Correlation in parameters between individuals

At the between individual level all combinations of parameters have confidence intervals which span 0 and we can conclude that there is no evidence of statistically significant correlation (Table 5.2A).

	Repeatability		
	ICC-stat	CI (95%)	p-value
Number of Bouts	0.227*	[0, 0.478]	0.0515
Displacement	0.151	[0, 0.382]	0.146
Straightness	0.127	[0, 0.399]	0.192
Mean Cosine	0.200	[0, 0.444]	0.077
Av. Bout Duration	0.211	[0, 0.466]	0.0665
Time Spent Moving (%)	0.234*	[0, 0.486]	0.0467
Average Speed	0.362*	[0.013, 0.526]	0.0206

Table 5.1: Values of the ICC for the calculated parameters, along with the 95% CIs. Values marked with an asterisk (*) indicate significant results ($p < 0.05$)

Correlation in parameters between individuals

At the within-individual level, a strong positive correlation ($p < 0.01$) between displacement, straightness and time spent moving was observed, as well as between displacement and average speed, as might be expected from standard movement. A strong negative correlation ($p < 0.01$) between the average bout duration and the number of bout transitions was anticipated: the longer a bout, the fewer there can be in a given time period. However, a significant positive correlation ($p < 0.01$) between the average speed when moving and the time spent moving was also found, indicating that the longer the time the beetles spent moving, the faster on average they moved, an interesting and unanticipated result (Table 5.2B).

<i>(A) Between</i>		Number of Bouts	Displacement	Straightness	Mean Cosine	Av. Bout Duration	Time Spent Moving (%)	Av. Speed
Number of Bouts			-0.006	0.301	0.332	-0.129	0.141	-0.291
Displacement		(-0.848, 0.812)		0.229	0.102	0.08	0.287	0.487
Straightness		(-0.555, 0.991)	(-0.673, 0.977)		0.095	-0.089	0.164	0.171
Mean Cosine		(-0.446, 0.987)	(-0.780, 0.837)	(-0.791, 0.848)		-0.072	0.206	-0.03
Av. Bout Duration T		(-0.851, 0.755)	(-0.723, 0.908)	(-0.876, 0.761)	(-0.857, 0.767)		0.101	-0.139
Time Spent Moving (%)		(-0.676, 0.900)	(-0.646, 0.967)	(-0.729, 0.924)	(-0.697, 0.958)	(-0.698, 0.892)		0.258
Av. Speed		(-0.940, 0.449)	(-0.450, 0.993)	(-0.659, 0.910)	(-0.879, 0.711)	(-0.893, 0.587)	(-0.534, 0.943)	
<i>(B) Within</i>		Number of Bouts	Displacement	Straightness	Mean Cosine	Av. Bout Duration	Time Spent Moving (%)	Av. Speed
Number of Bouts			-0.195	0.195	-0.031	-0.657*	0.004	-0.116
Displacement		(-0.445, 0.074)		0.564*	0.535*	0.189	0.747*	0.722*
Straightness		(-0.065, 0.463)	(0.384, 0.745)*		0.644*	-0.24	0.579*	0.241
Mean Cosine		(-0.318, 0.258)	(0.340, 0.743)*	(0.468, 0.801)*		-0.006	0.666*	0.228
Av. Bout Duration T		(-0.819, -0.496)*	(-0.093, 0.461)	(-0.487, 0.033)	(-0.290, 0.271)		0.011	0.176
Time Spent Moving (%)		(-0.272, 0.289)	(0.614, 0.860)*	(0.388, 0.753)*	(0.508, 0.823)*	(-0.274, 0.290)		0.425*
Av. Speed		(-0.418, 0.170)	(0.582, 0.856)*	(-0.022, 0.508)	(-0.061, 0.501)	(-0.102, 0.466)	(0.186, 0.670)*	

Table 5.2: Correlations between parameters calculated at both the (A) *between* and (B) *within* individuals level using the mixed effects model described in 5.3.3.2. Values in the upper triangle are the correlation coefficients and lower triangle values are the corresponding 95% CIs. Values marked with an asterisk (*) denote those which are significant as the CIs do not straddle 0.

5.4.3 Global Movement Direction

If beetle movement is consistently globally directed at the population level, possibly due to an external navigation cue, this would be evident in the distribution of the global direction of movement at each step. Fig. 5.2D shows a near uniform distribution in the global orientation angle, relative to the associated turning angle (the angle between successive global orientation angles) for the pooled data across all beetles and trials. This suggests that, at the population level, there is no consistent reorientation towards a specific global movement direction.

A Rayleigh test undertaken at the population level revealed a slight bias towards a global movement direction of $\bar{\mu} = 59^\circ$, although the resultant vector was low ($\bar{R} = 0.194$) suggesting this was only a weak effect. Further inspection highlighted that this weak global directional bias was directly correlated to the initial movement direction of the beetles at the start of recording, (presumably related to the initial orientation of the beetle as they were released onto the tracking sphere), and the global bias towards this specific orientation had disappeared by the end of each trial (Appendix B5). Hence, we conclude that there is no evidence for a consistent global bias towards a particular movement direction at the population level, as a result of an external source or from the experimental setup (see Fig. 5.2A).

At the individual level, beetles were observed to have highly consistent oriented movements, (resultant vector, \bar{R} , ranging from 0.1942 to 0.9724, and mean = 0.6616, s.d. = 0.2128) with the Watson test rejecting the possibility of a uniform distribution of global movement directions when considered separately for each individual. This leads to the interesting and counter-intuitive finding that, although there is no evidence for a consistent global bias towards a particular movement direction at the population level, movement at the individual level is highly directed with beetles moving consistently in (individual-specific) global directions over a sustained period.

5.4.4 Turning Angles

When considering the distribution of turning angles at the population level across all beetles and trials, both the wrapped Cauchy (MLE parameters: $\rho = 0.859$, $\mu = 0.005$) and von Mises distributions (MLE parameters: $\kappa = 6.431$, $\mu = 0.001$) were rejected by the Watson test ($U_{wc}^2 = 2.42$, $p < 0.01$; $U_{vM}^2 = 51.94$, $p < 0.01$) and the Kuiper test ($V_{wc} = 6.79$, $p < 0.01$; $V_{vM} = 21.06$, $p < 0.01$) (Appendix B3 - Tables 5.7 & 5.8). However, the AIC favours the wrapped Cauchy over the von Mises distribution ($AIC_{wc} = 7032$, $AIC_{vM} = 10668$), and visual inspection of the distributions (Fig. 5.4A) indicates that the wrapped Cauchy is clearly the better fit to the data. Tests at other sampling rates and speed thresholds revealed no significant differences from these results (Appendix B3 - Tables 5.7 & 5.8).

At the level of each individual beetle and trial, a wrapped Cauchy distribution was seen to be the best fitting distribution for 58 of the 66 trials. The resultant vectors for each of the individual trials were generally high, indicating highly persistent behaviour (\bar{R} ranging from 0.3972 to 0.9134 with mean = 0.7795, sd = 0.1473).

5.4.5 Step-lengths (Instantaneous Speeds)

When considering the distribution of the instantaneous speeds at the population level, both the Kolmogorov-Smirnov (K-S) test and G-test rejected all four distributions ($p < 0.01$) when fitted to the tail of the data, although the AIC value indicated that the Weibull distribution (MLE parameters; $\gamma = 0.992$, $\alpha = 9.668$) was the closest fit (Appendix B3 - Tables 5.9-5.11). When considering the full data set and using a restricted power-law with $x_{\min} = 5$, the K-S test and G-test still rejected all the distributions ($p < 0.01$), but the AIC value now favoured the log-normal distribution (Fig. 5.4B) with MLE parameters $\mu = 1.69$, $\sigma^2 = 1.28$ ($AIC_{\log\text{-norm}} = 60228$, $AIC_{\text{Weib}} = 60915$, $AIC_{\text{exp}} = 61302$, $AIC_{\text{power}} = 66472$). Choosing different values for the sampling rate and speed threshold did not qualitatively change these conclusions (Appendix B3 - Tables 5.9-5.11). Therefore, whilst no clear conclusion about the specific distribution of the speeds could be drawn from these results, there is an indication that the distribution

involves an exponential component, with no strong indication of power-law behaviour.

At the individual level, the log-normal and the Weibull distributions were favoured in 65 of the 66 trials when considering the full data set, and 61 of the 66 when looking only at the tail of the data.

5.4.6 Intermittency (movement and non-movement bouts)

Both the Weibull (MLE parameters; $\gamma = 0.97$, $\alpha = 45.73$) and log-normal (MLE parameters; $\mu = 3.30$, $\sigma^2 = 1.04$) distributions were accepted by the G-test for the distribution of the bouts of movement with the AIC value distinguishing between them by favouring the log-normal distribution ($G_{\text{weib}} = 26.562$, $p = 0.115$; $G_{\text{log-norm}} = 21.854$, $p = 0.292$; $\text{AIC}_{\text{weib}} = 2977$, $\text{AIC}_{\text{log-norm}} = 2902$). For the bouts of stationarity, the G-test and K-S test reject all the distributions ($p < 0.01$); although, again the log-normal distribution (MLE parameters; $\mu = 3.00$, $\sigma^2 = 0.94$) is favoured when calculating the AIC ($\text{AIC}_{\text{log-norm}} = 1373$, $\text{AIC}_{\text{exp}} = 1420$, $\text{AIC}_{\text{weib}} = 1422$) and visual inspection implies a reasonable fit here (Fig. 5.4C-D; Appendix B3 - Tables 5.15 & 5.16).

Subsequent analysis of the bout durations when considering different sampling rates indicates no clear best fit distribution, although the log-normal distribution is favoured in the majority of cases (Appendix B3 - Tables 5.15 & 5.16). As predicted by the lognormal distribution an inverse relation was found between lengths of following bouts, with a long bout often followed by a short bout, and bouts close to the median bout length mostly followed by bouts of comparable length (Appendix B3 - Fig. 5.8).

5.4.7 CRW v BRW Behaviour

Calculating the Marsh-Jones Δ statistic (Marsh & Jones 1988) at the individual level indicates that that the observed data does not fit with the expected result from either a CRW or BRW, with 60 paths giving an indeterminate result, five paths identified as most like a CRW and only one most like a BRW (Appendix B5 - Table 5.19). Similarly, when the population is considered as a whole, the statistic does not coincide with the expected result from either a BRW or a CRW, however, in this case the value ($\Delta = -0.3346$)

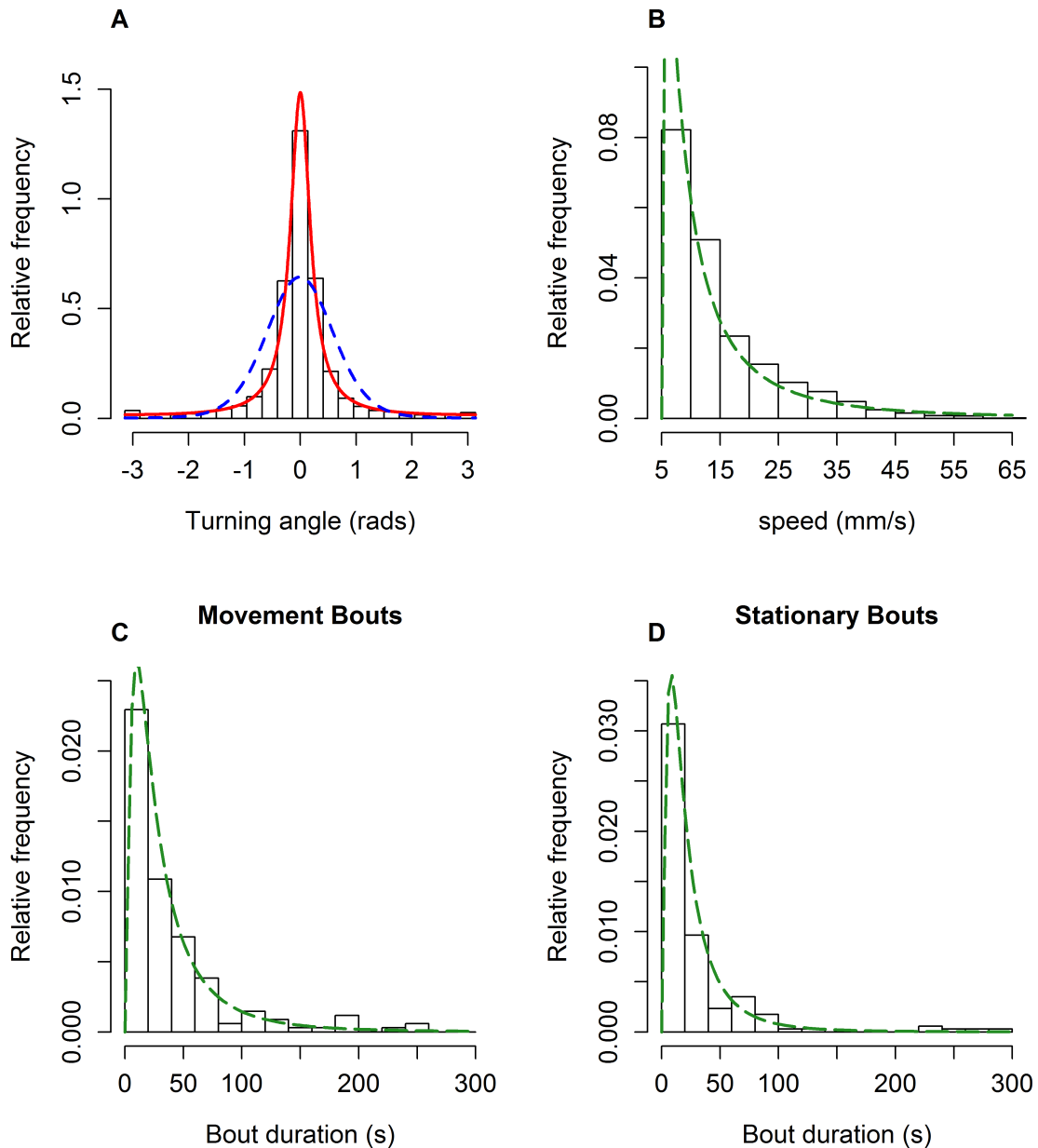


Figure 5.4: (A) Histogram of the turning angles. The red line shows the best fit wrapped Cauchy (WC) distribution with $\mu = 0.005$, $\rho = 0.859$ and the blue line shows the best fit von Mises (vM) distribution with $\mu = 0.001$ and $\kappa = 6.431$. The Watson test rejects WC ($U^2 = 2.42$, $p < 0.01$) as does the Kuiper test ($V = 6.79$, $p < 0.01$), similarly the Watson test rejects vM ($U^2 = 51.94$, $p < 0.01$) as does the Kuiper test ($V = 21.06$, $p < 0.01$). The AIC was used to determine the closer fitting distribution between the WC and vM, with the WC found as the most likely option ($AIC_{wc} = 7032$, $AIC_{vM} = 10668$). (B) Histogram for distribution of the instantaneous speeds. The green dashed line shows log-normal distribution which, though rejected by the G^2 -Test (stat = 595, $p < 0.01$) and K-S test (stat = 0.0692, $p < 0.01$), returned the lowest AIC value ($AIC_{1-n} = 60228$). (C) & (D) Histograms showing the distribution of the length of bouts of movement and stationarity. The golden line shows the best fitting log-normal distribution which had the lowest AIC value of any considered distribution in both the distributions of the bouts of movement and bouts of stationarity. In all cases, the sampling rate was 1Hz and speed cut-off threshold was 5mm/s

is strongly negative and much closer to the expected CRW value, indicating that, at the population level, the movement is more like a CRW movement process. This is consistent with the results from section 5.4.3, where movement appeared directed at the individual level (similar to a BRW) but not at the population level, and section 5.4.4, where movement was generally highly persistent across all paths, typical of a CRW.

However, when comparing the observed net displacement of beetles with that of a CRW parameterised by population level estimates of the speed and turning angle mean resultant length (Fig. 5.5A), it is clear that the beetles disperse considerably faster than expected. At the population average level (Figure 5A), there is an initial period of super-ballistic behaviour, with the beetles initially spreading at an increasing rate, and then movement starts to follow a linear increase in net displacement over time as predicted by a purely ballistic movement process. Interestingly, this type of diffusive behaviour has been noted before with *Tribolium confusum* beetles (Morales & Ellner, 2002), where a CRW model seemingly fit the movement data well despite the resulting model-predicted net displacement greatly underestimating the actual observed displacement.

Fig. 5.5B shows results from artificial sub-sampling of each observed beetle movement path to determine how the observed mean cosine, aggregated at the population level, changes with increasing (temporal) distance between sampling steps. Results are compared to the predicted change in mean cosine for a BRW and CRW under the same sub-sampling process, which were parameterised from the population-level mean speed, mean cosine of global movement directions (BRW), and mean cosine of turning angles (CRW). It is clear from Fig. 5.5B that beetle movement is far more persistent over time than is predicted from a CRW parameterised by the observed data. However, it is also clear that the observed beetle movement does not exactly match a BRW (or ballistic movement) either, and is in fact somewhere in-between a BRW and CRW. Similar results are obtained when considering each individual beetle separately (Fig. 5.5C), with all beetles showing behaviour that is more persistent than expected from a pure CRW. These results are consistent with those from section 5.4.3: beetles have highly persistent movement at the individual level but there is no clear evidence of a global orientation

bias in movement direction that is consistent across the population.

5.5 Discussion

Movement data of 22 *P. cupreus* beetles were collected over three replicate trials on a locomotion compensator. Analysis of observed trajectories highlighted high levels of inter- and intra-individual variation in movement path characteristics (Fig. 5.1 & 5.2), with a correlation between time spent moving and instantaneous speed, suggestive of possible ‘flight’ behaviour (Table 5.2). Observed turning angles were best fitted by the wrapped Cauchy distribution with step lengths (instantaneous speeds) best described by a log-normal distribution with no evidence of power-law behaviour (Fig. 5.4A-B). Beetle movements were observed to be highly persistent at the individual level, with beetles able to maintain forward movement towards a chosen direction over a sustained period. However, no evidence of a global preferred direction of movement was found at the population level. This could be an artefact of the experimental setup where such an unfamiliar setting caused the beetles to engage in ‘flight’ behaviour where movement was in a constant direction away from the starting location. Assuming the beetles were not placed facing exactly the same direction at the start of the experiment, then this along with the beetles’ inherent ability to travel in a straight line could explain the lack of global direction.

Intermittency in movement was observed, with the lengths of the bouts of movement and stationarity both best described by log-normal distributions (Fig. 5.4C-D). Movement bouts were found to highly vary between individuals at both the inter- and intra-individual level, with some trials consisting of bouts of constant movement and others involving highly intermittent stop-start behaviour. The intermittency in movement behaviour, along with the observation that bouts of short length are often followed by bouts of similar length (Appendix B3 - Fig. 5.8), has been characterised as foraging or searching behaviour in aphids (Mashanova et al, 2010) and has been reported for a number of species including crickets, copepods and ghost crabs (Kramer & McLaughlin, 2001).

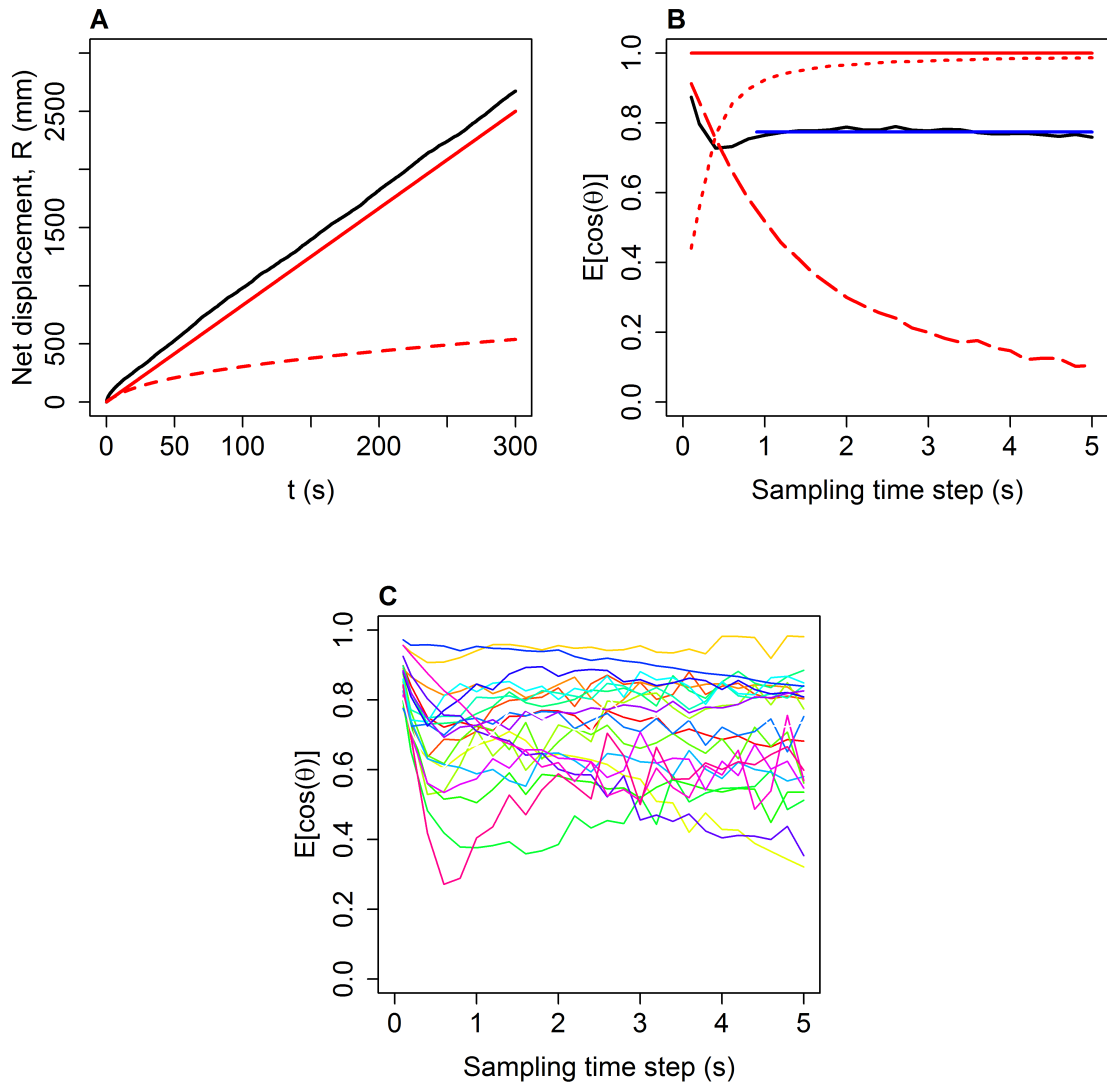


Figure 5.5: (A) Net displacement of beetles over time. The thick black line shows the mean net displacement of the beetle population with sampling rate 1Hz and no speed threshold; the red dashed line is the expected result for a CRW with turning angles taken from a zero centred wrapped Cauchy distribution with concentration parameter $\rho = 0.819$, and step length drawn from the exponential distribution with mean, $1/\lambda = 8.33$ (Appendix B5 - 5.8 & 5.11); the red solid line is ballistic movement. (B) Mean cosine calculated from the beetle population (black solid line) against different imposed sampling rates. The blue line shows the mean value for the population data for sampling size ≥ 1 . The red solid line represents pure ballistic motion, the red dashed line is the expected result for a pure BRW and the red dotted is the expected result for a CRW. The concentration parameter for BRW was determined by calculating the difference of global direction at each step for each individual trial compared to the overall mean cosine for that respective trial. The concentration parameter for the CRW was taken as the MLE parameter found for the best fitting wrapped Cauchy distribution as described in the main text (see section 5.4.4). The sampling rate is 1 Hz and the speed threshold is 5mm/s. (C) Same as in (B), except this shows the value of the mean cosine for the first trial of each of the 22 beetles

The ability for individual beetles to disperse over much larger distances than predicted by a simple CRW movement model, while showing no evidence of a global preferred direction at the population level, is an interesting finding. The beetles in this study showed an innate ability to travel on a near constant bearing with high persistence (Fig. 5.2A; Fig. 5.5B) a phenomena found in other insects such as dung beetles (Byrne et al, 2013) but has been shown to not be present in other animals such as humans (Souman et al, 2009). It is known that small errors in attempted straight line movement compound over time (Biegler, 2000; Cheung et al, 2007), therefore, if an individual can continue on a constant bearing for a protracted time period without any obvious external cues, the method by which these small errors are negated is interesting and may be due to some unknown internal cue. Similar underestimates of total displacement have also been reported when considering parameterised CRW models for *T. confusum* beetles (Morales & Ellner, 2002) and three *Eleodes sp.* (Crist et al, 1992). A possible explanation for these discrepancies is that the parameterised models do not consider the use of internal mechanisms or external cues that enable deviations in heading to be corrected so that forward movement is maintained. However, it is far from clear in this context what such mechanisms might be since there were no known visual navigation cues in the immediate walled environment of the locomotion compensator that could have been utilised.

P. cupreus has been observed to use chemical cues to navigate, orienting towards prey such as *Heteromurus nitidus*, a ground dwelling springtail (Mundy et al, 2000), though it is unlikely that this was the case within the confines of this experiment. Highly persistent movements have been observed in other beetle species, such as dung beetles, (e.g. *Scarabaeus sp.* and *Scarabaeini sp.*), which are known for their ability to maintain a constant orientation whilst walking backwards pushing their dung ball (Byrne et al, 2003; Baird et al, 2012). Dung beetles are thought to maintain forward movement in a chosen direction by using the polarisation of light source(s) and not visual cues (Dacke et al, 2004; Baird et al, 2012), and have been observed to successfully adjust course to continue the initial straight-line direction when trajectories are forcibly adjusted or obstacles placed in their path (Byrne et al, 2003; Baird et al, 2012). Although there were

no direct visual cues in our experimental arena, there was a fixed light source on the ceiling of the laboratory and it is possible that *P. cupreus* are using the polarisation of the light source relative to their initial starting direction to maintain their forward movement. This could be simply tested by running a similar experimental setup incorporating a light polariser, which would allow for the polarisation of light to be directly manipulated. If by changing the direction of polarisation during the experiment the beetles were seen to alter their direction of movement, then this would be indicative of navigation using polarisation. This method has been used to demonstrate the use of light polarisation in dung beetle navigation (Dacke et al, 2004; Baird et al, 2012)

Other insect species, such as bumblebees and other arthropods, (Chittka et al, 1999; and references therein) are thought to possess an internal magnetic compass that allows forward navigation in the absence of other cues. Bumblebees also use odour cues to direct movement within a featureless environment (Chittka et al, 1999) and are able to discriminate between hydrocarbon scent marks excreted from the tarsi left by themselves and conspecifics on flowers (Pearce et al, 2017); a similar mechanism in *P. cupreus* might allow them to track their own footprints on the locomotion compensator, although we have no direct evidence that this is the case

Whilst the experimental setup allowed for the collection of data both at a high frequency and high level of accuracy, giving answers to the questions regarding the dispersal potential and variability in movement behaviour of *P. cupreus*, the experimental setup itself causes the conclusions and applications of our findings to be limited. Due to the featureless conditions, caution must be taken in generalising these results as they are not indicative of movement in natural environments, in which encounters with obstacles or changing conditions would be present. However, a similar tracking device was used in Dahmen et al, 2018 to compare the movement of desert ants (*Cataglyphis sp.*) under experimental conditions to those observed in an open test field. They recorded movement in a test arena both outside with natural light and inside a laboratory with a polarised light source, comparing the observed movement to that recorded by using a cushioned tracking sphere under similar conditions. The findings reported no significant differences

between the movement recorded using the tracking sphere to that in the open test field. Whilst this may be the case for this specific species of ant, as we did not engage in similar direct comparisons of movement in natural settings to that on the TrackSphere, it is not necessarily clear that movement recorded on such a device can act as a sensible approximation for real world movement.

A specific area in which an understanding of the movement of *P. cupreus* would be beneficial is in agriculture and integrated pest management (IPM) strategies (Burn et al, 1987; Metcalf & Luckmann, 1994). *P. cupreus* are known to have a beneficial effect for crop yield as they can aid in controlling pests and weeds in valuable crops such as oil seed rape (Langmaack et al, 2001; Šlachta & Vokoun, 2011; Bohan et al, 2011), cereals and sugar beets (Kromp, 1999). Consequently, it is important that insect movement data is accurately interpreted to provide reliable parameters for population dynamics, density and dispersal when attempting to accurately implement IPM strategies (Petrovskii et al, 2014; Bastola & Davis, 2018).

In order to promote biological control of crop pests in agricultural landscapes, a thorough understanding of the movement behaviour and subsequent spatio-temporal distribution of the beneficial inhabitant predator species, such as *P. cupreus*, is required. Although the homogeneity of the experimental setup has been highlighted as a flaw in scaling up our findings to movement in the real world, the agricultural landscapes *P. cupreus* often inhabit, due to their beneficial pest nature, are by their cultivated nature more homogeneous relative to non-agricultural landscapes. Therefore, our recorded movement behaviour could be beneficial to studies which attempt to understand the invasive potential of *P. cupreus* in crop management.

Banks et al (2019) looked at the expected affect ladybirds and *P. cupreus* had on controlling aphid invasions of agricultural fields, with the aim of providing a pest management structure to efficiently eradicate aphid populations. Their model concluded that using a population of ladybirds was the most effective compared to a mixture of the two predators. However, the model explicitly relied on predicted movement rates of *P. cupreus* which had been aggregated at the population level. Therefore, it could be

interesting to see how our findings of the dispersal potential and movement behaviour affects the outcome of the study. Though as mentioned care would be needed in drawing conclusive results due to the artificiality of the model system

5.6 Conclusions

- The movement of *P. cupreus* beetles was observed to exhibit high levels of inter- and intra-individual variation in movement path characteristics.
- Movement was observed to be highly persistent at the individual level, with beetles able to maintain forward movement towards a chosen direction over a sustained period despite being placed in a featureless, homogeneous environment.
- No evidence of a global preferred direction was found at the population level and when recorded movement was compared to a simple CRW movement model, parameterised using the population level path characteristics, the beetles were seen to exhibit the potential to rapidly disperse over a much wider area than predicted.
- Our results highlight the importance of considering the role of individual variation when analysing movement data and predicting dispersal distances.
- *P. cupreus* is a beneficial biological control used in pest management strategies helping to increase yields and alleviate the reliance of chemical pest controls on agricultural crops (Burn et al, 1987; Metcalf & Luckmann, 1994). Specifically, *P. cupreus* benefits high yield crops such as rape seed (Langmaack et al, 2001; Šlachta & Vokoun, 2011; Bohan. et al, 2011), and therefore, a precise understanding of the dispersal ability of *P. cupreus* is important for correctly implementing IPM strategies (Petrovskii et al, 2014)

5.7 Appendices

5.7.1 Appendix B1 - Bout classification

The method to determine the transition between movement and stationary bouts is an adjusted version of the algorithm described in (Knell & Codling, 2012)

Smoothing algorithm

1. *Cumulative sum.*

Determine the cumulative sum

$$C_\tau = \sum_{t=2}^{\tau} S_t, \text{ with } C_1 = S_1, \text{ for } \tau = 2, \dots, T.$$

where C_τ denotes the cumulative sum of S_τ at time step τ and is calculated as:

$$S_t = \begin{cases} S_{t-1} + v_t, & \text{if } v_t > \text{speed threshold value} \\ S_{t+1} - v_t, & \text{if } v_t \leq \text{speed threshold value} \end{cases} \quad (5.5)$$

where v_t is the instantaneous speed calculated at time t .

2. *Time series.* Construct the time series C_τ vs. τ .
3. *Termination criterion.* Does a turning point exist within the generated time series?
 - Yes: proceed to 4
 - No: one cannot effectively analyse this movement path; terminate procedure.
4. *Max-min algorithm.* Determine turning points of the time series using the max-min algorithm (see Appendix 2 in (Knell & Codling, 2012) for full algorithm). Essentially, here the algorithm aims to find turning points (local maxima or minima) in the time series C_τ vs. τ . To do this a moving window of size ϵ is applied to the time series and for the case when $C_{\tau+\epsilon} < C_\tau$ a change is determined to have occurred if for the current maximum value of the cumulative sum at time τ , $C_{\tau_{\max}}$, we have $\max\{C_{\tau+1}, C_{\tau+2}, \dots, C_{\tau+\epsilon}\} < C_{\tau_{\max}}$ otherwise $C_{\tau_{\max}}$ is set at this max value and the method continues starting now at $\tau + 1$ (and similar for $C_{\tau+\epsilon} > C_\tau$ finding a

local minimum). Therefore, in essence the value ϵ represents the minimum size of a possible bout and is calculated by the algorithm to give the optimal value for identifying true transition behaviour.

5. 5 *Conclusion.* Classify turning points as either transitions from movement to stationary behaviour or vice-versa.

An example of the results of using this algorithm is demonstrated in Fig 5.6. The figure shows the variation in instantaneous speed over time for a single trial of an example beetle. The red horizontal line represents the speed threshold value of 5mm/s, which was used throughout the main analysis (other values were considered but did not qualitatively change the results; see Appendix B2). The lower plot demonstrates how the smoothing algorithm designated bouts of movement (state 1) and stationarity (state 0).

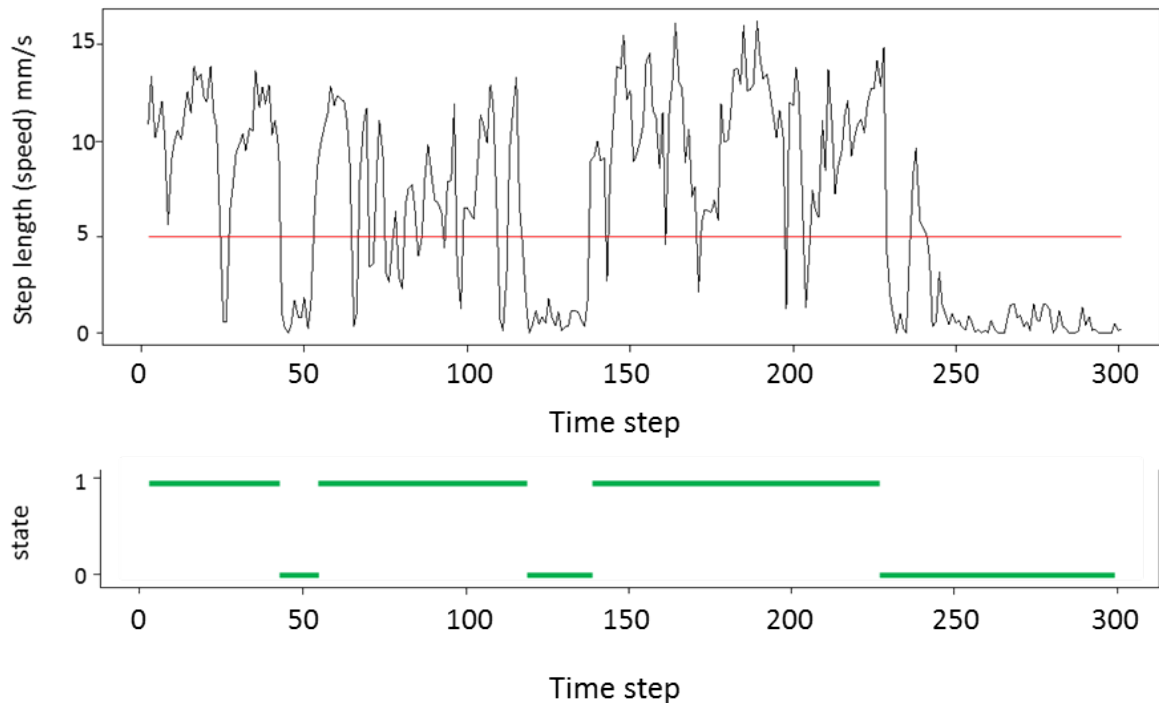


Figure 5.6: Demonstration of the bout classification algorithm

This algorithm requires calculating a value for the minimum possible length of a bout,

Type of bout	Restricted Power-law		Exponential	Weibull		Log-normal	
	x_{\min}	α	λ (rate)	γ (shape)	α (scale)	μ (mean)	σ^2 (s.d.)
All	1	1.33	0.028	0.97	35.41	3.07	0.94
Moving	1	1.28	0.016	0.96	47.55	3.39	1.06
Stationary	1	1.31	0.020	0.97	32.97	3.10	0.99

Table 5.3: Parameter values for the best fit distributions when the median ϵ value was used in the smoothing algorithm. Results shown are for same sampling rate of 1Hz and threshold value of 5mm/s as was used throughout the analysis in the main text

ϵ , per beetle per experimental trial, which was found to range from 3 to 17. As this value was not fixed for all experimental trials, results were also calculated when using a fixed ϵ across all trials (calculated as the median value of all ϵ , which in the case for the sampling rate being 1Hz and the speed threshold taking value 5mm/s gave, $\epsilon = 7$). However, this was not seen to significantly affect the outcome of the analysis (Table 5.3 & 5.4).

Bout type	Restricted Power Law			Exponential			Weibull			Log-normal										
	G^2 -Test	K-S Test		G^2 -Test	p	K-S Test		G^2 -Test	p	K-S Test		G^2 -Test	p							
		stat	p			stat	p			stat	p			stat	p					
All	119.70	0	0.419	0	3444	33.016	0.005	0.207	0	2991	31.000	0.009	0.177	0	2988	27.314	0.026	0.117	0	2932
Moving	73.15	0	0.366	0	1828	17.358	0.298	0.148	0	1568	18.054	0.260	0.158	0	1571	10.334	0.798	0.092	0.112	1553
Stationary	138.04	0	0.467	0	1599	51.802	0	0.284	0	1419	43.382	0	0.200	0	1409	37.514	0.001	0.142	0.002	1401

Table 5.4: Results of the statistical tests for each best fitting distribution when the median ϵ value was used in the smoothing algorithm. Results shown are for the same sampling rate of 1Hz and threshold value of 5mm/s as was used throughout the analysis in the main text. These results show that the favoured distribution was the log-normal for the distribution of movement bouts, stationary bouts and combined movement and stationary bouts. Comparing these with the findings with a varying epsilon (see section 5.4.6 and Appendix B3) shows no qualitative difference.

5.7.2 Appendix B2 - Comparison of Summary Statistics

The summary statistics discussed in section 5.3.2 (and not included in Fig. 5.3) of the main text are displayed here highlighting the variation across individuals as well as between individuals. The two tables (Table 5.5 & 5.6) show the full results of the ANOVA and MANOVA tests for significance in the variation of these statistics. All tests are for a sampling rate of 1Hz and speed threshold value of 5mm/s.

	Sphericity Correction	Sum of Squares	df	Mean Square	F	p
Displacement*	None	1.860e+7 *	2*	9.301e+6	4.032	0.025
	Greenhouse-Geisser	1.860e+7 *	1.49*	1.248e+7	4.032	0.038
Straightness	None	0.114	2	0.057	1.823	0.174
Mean Cosine	None	0.132	2	0.066	4.43	0.018
No. of Bouts	None	2.758	2	1.379	0.152	0.86
Mean Bout Duration	None	6669	2	3334	0.446	0.643
Variance in Bout Duration*	None	5.869e+7*	2*	2.934e+7	0.387	0.681
	Greenhouse-Geisser	5.869e+7 *	1.527*	3.843e+7	0.387	0.626
Time spent moving (%)	None	7290	2	3645.2	4.365	0.019
Mean speed (when moving)	None	473.7	2	236.83	7.143	0.002

Table 5.5: Repeated measures ANOVA test for variance in intra-beetle data per parameter. Test indicates that there significant differences in the behaviour across the three runs for Displacement ($F(1.49, 31.292) = 4.032$, $p = 0.038$), mean cosine of turning angles ($F(2, 42) = 4.43$, $p = 0.018$), time spent moving (%) ($F(2, 42) = 4.365$, $p = 0.019$) and the average speed when moving ($F(2, 42) = 7.143$, $p = 0.002$).

(*) Indicates Mauchly's test of sphericity indicates that the assumption of sphericity is violated ($p < 0.05$); therefore Greenhouse-Geisser corrected F-value should be used.

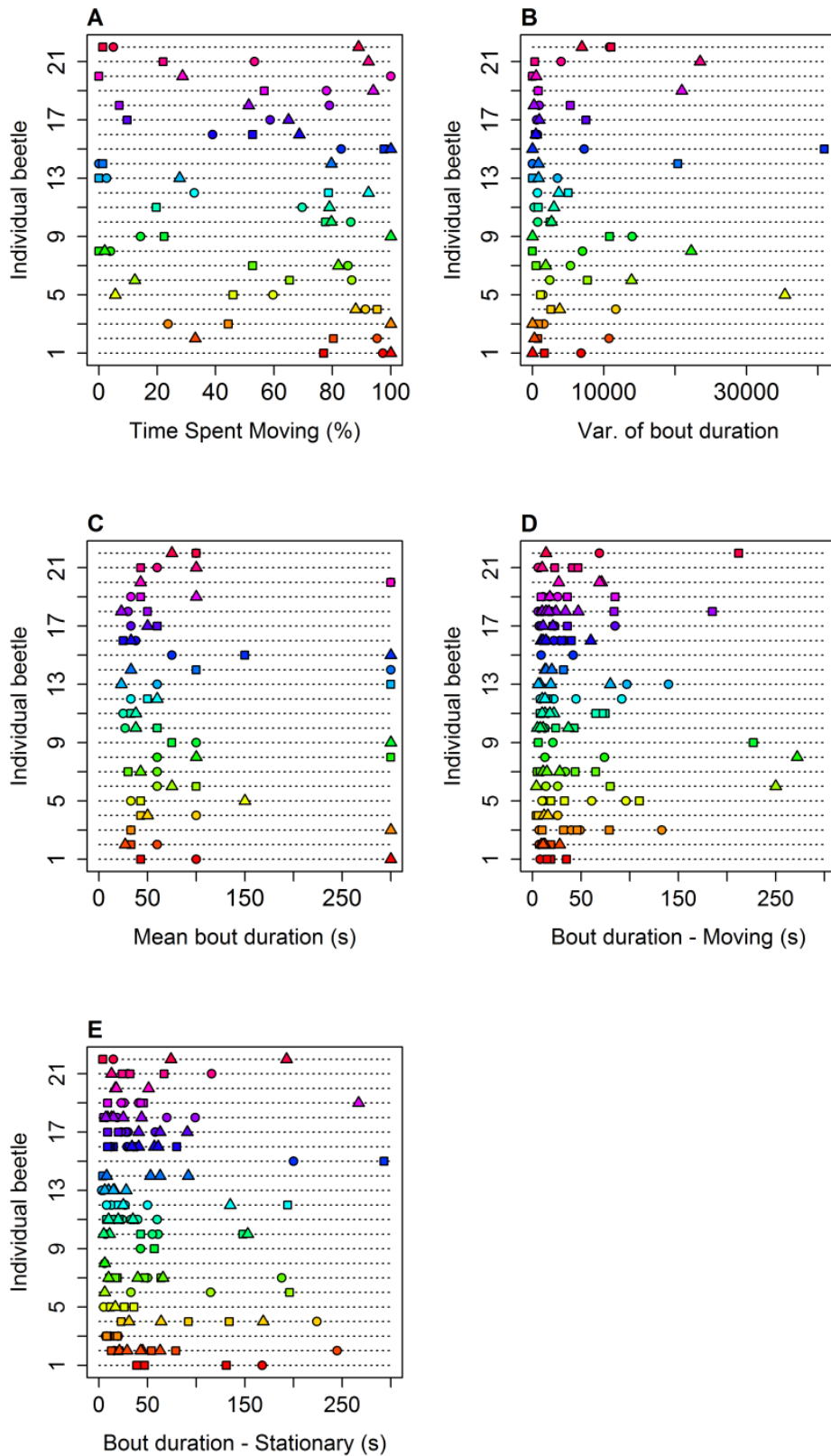


Figure 5.7: (A-C) variability in the statistical parameters described in the main text section 2.3.2 for each individual trial run per beetle; (A) Time spent moving, (B) Variance in Bout Duration and (C) average length of bouts. (D - E) lengths of bouts of movement and stationary respectively. In all plots, circle points correspond to trial 1, squares to trial 2 and triangles to trial 3.

	ANOVA				Levene's Test				Kruskal-Wallis		
	Sum of Squares	df	Mean Square	F	p	F	df1	df2	p	χ^2	p
Displacement**	8.456e+7	21	4.026e+6	1.534	0.115	3.323	21	44	<.001	30.925	0.07491
Straightness	0.98	21	0.047	1.437	0.154	2.169	21	44	0.015	27.331	0.1602
Mean cosine**	0.654	21	0.031	1.81	0.049	2.337	21	44	0.009	33.53	0.04066
No. of Bouts	345.8	21	16.465	1.883	0.038	1.54	21	44	0.113	31.091	0.07215
Mean Bout Duration**	188686	21	8985	1.234	0.272	6.018	21	44	<.001	31.091	0.07215
Variance in Bout Duration**	1.181e+9	21	5.625e+7	0.764	0.744	6.683	21	44	<.001	19.529	0.5512
Time Spent Moving (%)**	38724	21	1844	1.915	0.035	2.652	21	44	0.003	30.53	0.08185
Mean speed (when moving)**	1938	21	92.3	2.176	0.015	3.699	21	44	<.001	35.687	0.0237

Table 5.6: One-way ANOVA and Kruskal-Wallis (KW) test for inter-beetle variances. Here significant differences were found for displacement (KW $\chi^2 = 30.925$, $p = 0.075$), mean cosine of turning angles (KW $\chi^2 = 33.53$, $p = 0.041$), No. of bout transitions ($F(21, 44) = 1.883$, $p = 0.038$) and mean bout duration (KW $\chi^2 = 31.091$, $p = 0.072$). (**) Indicate instants where Levene's test of homogeneity of variance was violated and so Kruskal-Wallis test should be used (p<0.01)

5.7.3 Appendix B3 - Complete data analysis for all sampling rates and speed thresholds

Results detailed here include fitting distributions to the turning angles (Tables 5.7 & 5.8), instantaneous speeds (Tables 5.9-5.14) and bout durations (Tables 5.15-5.16) for all combinations of the sampling rates (2Hz, 1Hz, 0.5Hz and 0.2Hz) and speed threshold (15mm/s, 10mm/s 5mm/s and no threshold value). In the case of the turning angles (Tables 5.7-5.8), neither the Kuiper nor the Watson tests accepted either the wrapped Cauchy or the wrapped normal distributions. However, when comparing between the two, the AIC preferred the wrapped Cauchy distribution in all cases, and visual comparison confirmed that the wrapped Cauchy was a closer fit to the data.

Comparing the instantaneous speeds at differing sampling rates and speed thresholds, the results reveal that there was no clear likely best-fit distribution, as the preference for a particular distribution varied based on the speed threshold value regardless of the sampling rate; with a propensity for exponential and Weibull distributions when the speed threshold is high and a log-normal distribution for lower values of the threshold. Tables 5.9-5.11. present the results of fitting distributions to the tail of the data, that is the data which was greater than the optimal x_{\min} value of the best-fit power law distribution, which was used to infer the presence of a heavy-tailed distribution. As was mentioned in the main text (Section 5.4.5), the findings indicate that at any sampling rate and threshold value the power-law was not favoured over the other distributions.

In comparing the bout durations, distributions were considered for the length of moving bouts only, stationary bouts only and both moving and stationary combined. Tables 5.15-5.16 indicate that both the log-normal or Weibull distributions were accepted for certain combinations of the sampling rate and speed threshold, although, the AIC generally favoured the log-normal distribution over the Weibull. Data was not considered for no threshold value as this resulted in no stationary bouts (section 5.3.1 of the main text). Similarly, when the threshold value was too high (15mm/s) or the sampling rate too low (0.2Hz) the number of bouts measured was too small to give meaningful or accurate results and so have been omitted. Although, discerning an appropriate

distribution for the frequency of the bouts was not clear, an inverse relationship between the lengths of consecutive bouts was observed (Fig. 5.8A). That is, longer bouts were followed by shorter ones and vice versa, and medium length bouts were followed by bouts of similar length. Although (Fig. 5.8B-C), demonstrates that this is an expected result given the distribution found which best describes the bout lengths.

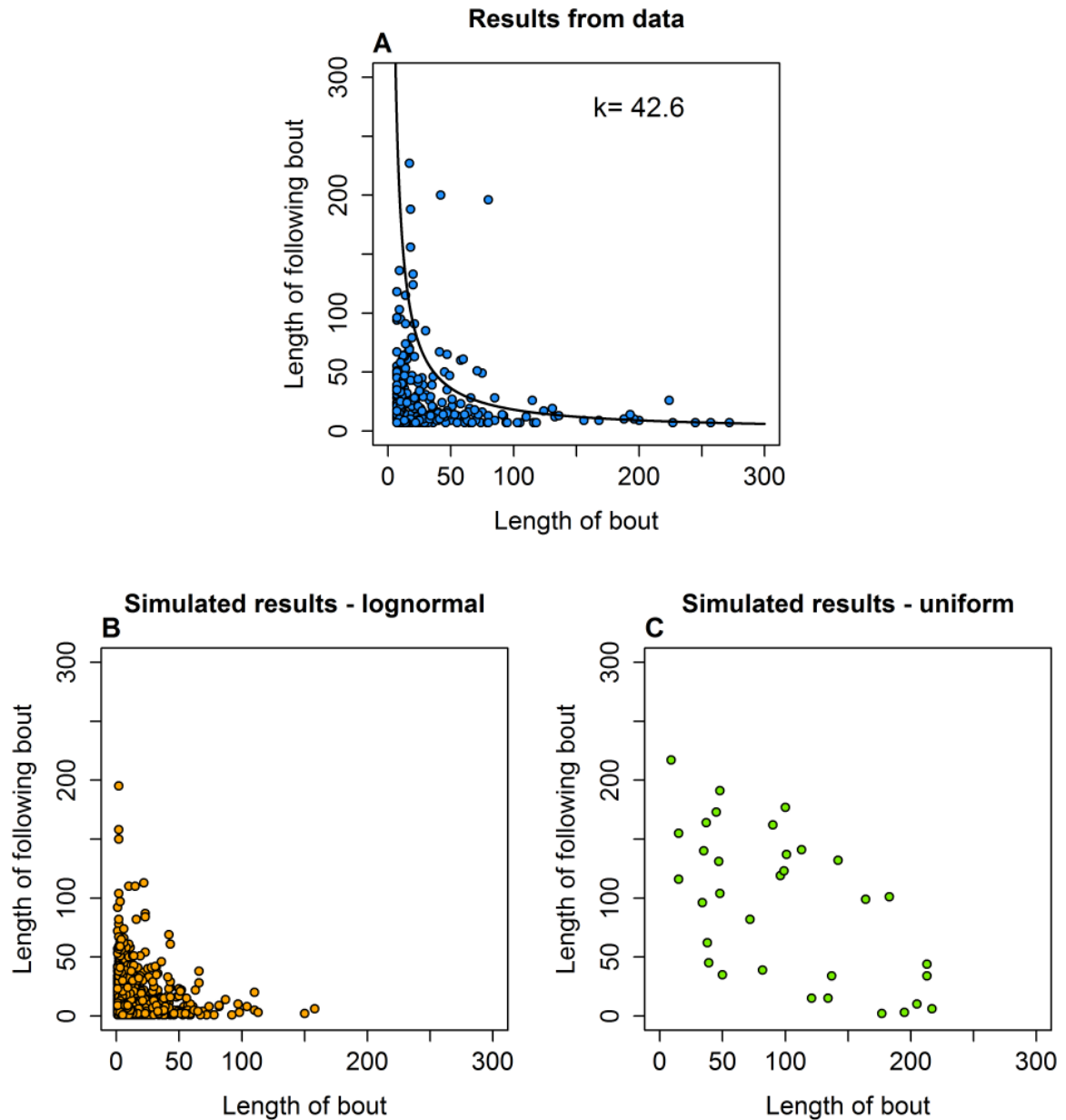


Figure 5.8: Comparing the lengths of following bouts. (A) displays the length of a completed bout compared to the length of the following completed bout, taken from the beetle data. The curve plotted in black shows the line of form k^2/x , where k is a constant shown in top right hand corner of the plot, which accounts for 90% of the plot points being located between the curve and the axes. Comparing this inverse relationship with the expected results from simulated models where the lengths of bouts were drawn from the best fitting log-normal distribution (B) and a uniform distribution (C) shows the similarity between the actual results and predicted log-normal results. This demonstrates that this inverse relationship between bout lengths is most likely due to the lognormal distribution of the lengths of bouts. Data was calculated with a sampling size of 1Hz and speed threshold of 5mm/s.

Sampling rate (HZ)	Speed cut-off (mm/s)	Number of points	Wrapped Cauchy						von Mises				
			Watson test			Kuiper test			Watson test		Kuiper test		AIC
			statistic (U^2)	p-value	statistic (V)	p-value	statistic (U^2)	p-value	statistic (V)	p-value			
2	none	39534	37.045	<0.01	29.148	<0.01	71744.16	342.2524	<0.01	54.7352	<0.01	95325.86	
	5	20155	2.8369	<0.01	7.0981	<0.01	20356.18	125.6914	<0.01	32.6401	<0.01	29315.92	
	10	12223	3.2087	<0.01	7.4731	<0.01	7318.787	71.0998	<0.01	24.7016	<0.01	12412.84	
	15	7028	2.1223	<0.01	6.0109	<0.01	3007.066	37.4251	<0.01	18.1023	<0.01	5641.406	
1	none	19734	8.8988	<0.01	14.7254	<0.01	32661.86	164.3228	<0.01	38.0826	<0.01	44129.71	
	5	10011	2.4193	<0.01	6.7936	<0.01	7031.784	51.9381	<0.01	21.0598	<0.01	10668.31	
	10	5900	1.9623	<0.01	6.1516	<0.01	2181.849	29.1009	<0.01	15.7044	<0.01	4249.526	
	15	3356	1.1261	<0.01	4.7802	<0.01	966.559	16.2974	<0.01	11.9061	<0.01	2129.47	
0.5	none	9834	1.9588	<0.01	7.6059	<0.01	16403.39	61.9318	<0.01	23.4196	<0.01	20787.61	
	5	5040	1.2417	<0.01	4.7511	<0.01	4275.96	18.824	<0.01	12.9362	<0.01	5454.31	
	10	2900	0.9912	<0.01	4.4125	<0.01	1580.272	9.9763	<0.01	9.4965	<0.01	2181.111	
	15	1580	0.6161	<0.01	3.5536	<0.01	724.7004	5.1869	<0.01	6.8364	<0.01	1036.83	
0.2	none	3894	0.3281	<0.01	2.8823	<0.01	7747.179	14.2082	<0.01	11.559	<0.01	8803.505	
	5	2024	0.4467	<0.01	3.068	<0.01	2501.256	5.3992	<0.01	7.018	<0.01	2772.177	
	10	1131	0.2489	0.01 < p < 0.025	2.6106	<0.01	1114.658	3.0138	<0.01	5.3566	<0.01	1252.11	
	15	604	0.1187	>0.10	2.0013	<0.01	535.0097	1.5012	<0.01	3.9792	<0.01	584.0033	

Table 5.7: Statistical test results for the turning angle distributions at all considered sampling rates and speed threshold values.

Sampling rate (Hz)	Speed cut-off (mm/s)	Wrapped Cauchy		von Mises	
		μ	ρ	μ	κ
2	none	-0.001	0.814	-0.0108	2.1842
	5	0.0026	0.8413	0.0041	4.5583
	10	0.0049	0.8653	0.0055	6.7311
	15	0.0028	0.8745	0.0037	8.192
1	none	0	0.8192	-0.0108	2.1842
	5	0.0045	0.8586	0.0011	6.4313
	10	0.0053	0.8768	0.0085	8.8482
	15	0.0026	0.8814	0.0024	9.5947
0.5	none	-0.0001	0.8049	0.0019	2.7213
	5	0.0066	0.8466	0.0094	6.3378
	10	0.0105	0.8649	0.0135	8.5942
	15	-0.0034	0.8694	0.0031	9.4126
0.2	none	0.0061	0.7553	0.0175	2.4435
	5	0.0004	0.8154	0.0189	4.9129
	10	0.0042	0.8365	0.0207	6.2121
	15	-0.0085	0.8454	0.0006	7.0781

Table 5.8: MLE for the parameters of the Wrapped Cauchy and von Mises distributions when considering the turning angle distribution for all considered sampling rates and speed threshold values.

Sampling rate (Hz)	Speed cut-off (mm/s)	Number of points	Power-law (MLE)			Exponential			Weibull			Log-normal			
			x_{\min}	K-S Statistic	p-value	AIC	K-S Statistic	p-value	AIC	K-S Statistic	p-value	AIC	K-S Statistic	p-value	AIC
2	none	1473	34.4	0.0517	0	9565	0.0326	0.087	9481	0.0334	0.075	9481	0.0762	0	9835
	5	1506	33.2	0.056	0	9788	0.0321	0.09	9690	0.0327	0.08	9691	0.0767	0	10059
	10	1422	33.8	0.0691	0	9250	0.0344	0.07	9139	0.0348	0.064	9141	0.0783	0	9467
	15	1537	33	0.0718	0	10073	0.0306	0.112	9909	0.0318	0.089	9909	0.0724	0	10297
1	none	6047	10.7	0.0715	0	40149	0.0406	0	39710	0.0275	0	39698	0.0594	0	40699
	5	5499	10.7	0.1027	0	37477	0.0416	0	36196	0.0245	0.003	36178	0.0694	0	37319
	10	620	33.7	0.0576	0.032	3827	0.0332	0.503	3784	0.0344	0.454	3785	0.0713	0.004	3898
	15	608	33.9	0.0647	0.012	3758	0.0343	0.473	3707	0.0351	0.443	3708	0.0731	0.003	3829
0.5	none	2884	10.1	0.0698	0	19110	0.0464	0	18630	0.0339	0.003	18626	0.0601	0	19161
	5	2711	10.6	0.099	0	18176	0.0472	0	17546	0.0359	0.002	17543	0.0633	0	18039
	10	265	33.7	0.0547	0.402	1550	0.0445	0.672	1532	0.0444	0.674	1534	0.0834	0.05	1588
	15	286	33.1	0.0608	0.237	1688	0.0394	0.766	1663	0.0399	0.752	1665	0.0773	0.066	1739
0.2	none	1201	10.6	0.0744	0	7591	0.039	0.052	7558	0.0346	0.114	7560	0.0633	0	7761
	5	596	15.3	0.1058	0	3940	0.0525	0.075	3813	0.0438	0.202	3811	0.0833	0.001	4009
	10	232	24.9	0.1269	0.001	1445	0.0868	0.061	1401	0.0635	0.307	1394	0.1132	0.005	1458
	15	225	25.2	0.1414	0	1408	0.0885	0.059	1353	0.066	0.282	1347	0.1182	0.004	1412

Table 5.9: Statistical test results for the instantaneous speed distribution at every considered sampling rate and speed threshold value, for the tail of the data only (calculated from the x_{\min} value given by the power-law distribution).

Sampling rate (Hz)	Speed cut-off (mm/s)	Number of points	Power-law (MLE)		Exponential		Weibull		Log-normal	
			G^2 -Stat	p-value	G^2 -Stat	p-value	G^2 -Stat	p-value	G^2 -Stat	p-value
2	none	1473	97.566	0	54.64	0	53.615	0	190.7	0
	5	1506	112.64	0	58.968	0	58.061	0	201.06	0
	10	1422	117.29	0	53.266	0	52.863	0	181.8	0
	15	1537	152.07	0	60.955	0	59.907	0	199.73	0
1	none	6047	474.71	0	127.95	0	105.87	0	467.07	0
	5	5499	788.32	0	139.6	0	115.05	0	505.81	0
	10	620	43.795	0	35.258	0.013	36.2	0.009973	71.707	0
	15	608	51.591	0	40.38	0.002916	40.75	0.002605	76.507	0
0.5	none	2884	217.46	0	80.254	0	68.17	0	216.77	0
	5	2711	348.12	0	69.982	0	59.646	0	205.26	0
	10	265	12.721	0.5486	18.402	0.4958	18.35	0.4992	30.416	0.04674
	15	286	14.722	0.3974	13.115	0.8326	13.27	0.8244	27.999	0.08345
0.2	none	1201	73.223	0	38.13	0.005713	35.757	0.0113	66.537	0
	5	596	79.829	0	26.142	0.1263	26.044	0.129	70.962	0
	10	232	37.324	0	24.979	0.1612	22.017	0.2834	39.791	0.003486
	15	225	40.923	0	23.062	0.2346	19.279	0.4391	37.747	0.006391

Table 5.10: Similar to Table 5.9, results of the G-Test for the distribution of instantaneous speed. Results are for the tail of the data only.

Sampling rate (Hz)	Speed cut -off (mm/s)	Number of points	Power-law (MLE)		Exponential λ (rate)	Weibull		Log-normal	
			α	x_{\min}		γ (shape)	α (scale)	μ (mean)	σ^2 (s.d.)
2	None	1473	5.56	34.39	0.109	1.02	9.27	1.65	1.31
	5	1506	4.86	33.2	0.109	1.02	9.24	1.64	1.32
	10	1422	4.37	33.76	0.109	1.02	9.21	1.64	1.31
	15	1537	3.68	32.95	0.108	1.03	9.35	1.66	1.3
1	None	6047	2.69	10.73	0.102	0.96	9.65	1.66	1.33
	5	5499	2.19	10.68	0.101	0.95	9.68	1.65	1.38
	10	620	4.84	33.68	0.129	1.03	7.85	1.49	1.26
	15	608	4.21	33.86	0.129	1.02	7.8	1.48	1.29
0.5	None	2884	2.79	10.11	0.108	0.96	9.15	1.61	1.34
	5	2711	2.22	10.63	0.107	0.97	9.23	1.62	1.34
	10	265	5.42	33.73	0.151	1	6.6	1.29	1.32
	15	286	4.49	33.11	0.149	1.01	6.74	1.32	1.34
0.2	None	1201	2.82	10.55	0.117	0.99	8.5	1.55	1.3
	5	596	2.81	15.33	0.111	1.06	9.2	1.65	1.34
	10	232	3.67	24.91	0.133	1.19	7.94	1.56	1.16
	15	225	3.04	25.24	0.135	1.17	7.8	1.53	1.19

Table 5.11: Parameter values calculated for the instantaneous speed distribution for the tail of the data only.

Sampling rate (Hz)	Speed cut-off (mm/s)	Number of points	Power-law (restricted) (x_{\min} = speed cut-off)			Exponential			Weibull			Log-normal		
			K-S Statistic	p-value	AIC	K-S Statistic	p-value	AIC	K-S Statistic	p-value	AIC	K-S Statistic	p-value	AIC
2	none	39600	0.1795	0	255834	0.1471	0	229424	0.1359	0	228179	0.2205	0	225598
	5	20188	0.249	0	136383	0.0274	0	125141	0.0253	0	124411	0.0691	0	122780
	10	12244	0.1349	0	81086	0.0417	0	75167	0.0209	0	74862	0.0579	0	74333
	15	7039	0.107	0	49828	0.0245	0	44916	0.0217	0.003	44465	0.078	0	44466
1	none	19800	0.1811	0	128277	0.1202	0	116833	0.1158	0	116233	0.2046	0	114963
	5	10045	0.2418	0	66472	0.0266	0	61302	0.0253	0	60915	0.0692	0	60228
	10	5919	0.2188	0	38818	0.0405	0	35861	0.0281	0	35646	0.0605	0	35445
	15	3365	0.1137	0	23603	0.0328	0.001	21154	0.0276	0.012	20844	0.0857	0	20891
0.5	none	9900	0.1865	0	64725	0.0998	0	59457	0.0938	0	59113	0.195	0	58505
	5	5074	0.2341	0	32856	0.0283	0.001	30309	0.0281	0.001	30078	0.0652	0	29705
	10	2918	0.2122	0	18727	0.046	0	17380	0.0343	0.002	17265	0.0586	0	17158
	15	1591	0.2552	0	11093	0.0492	0.001	9944	0.0316	0.083	9770	0.0979	0	9816
0.2	none	3960	0.1928	0	26104	0.0759	0	24162	0.0806	0	23990	0.1737	0	23783
	5	2058	0.2453	0	13063	0.0254	0.141	12053	0.0288	0.065	11933	0.0699	0	11765
	10	1149	0.2035	0	7087	0.0426	0.031	6630	0.0327	0.17	6581	0.07	0	6543
	15	613	0.2444	0	4057	0.051	0.083	3675	0.0396	0.291	3610	0.0804	0.001	3618

Table 5.12: Statistical test results for the speed distribution at every sampling rate and speed threshold value, without removing the tail of the data (the x_{\min} value was fixed at the speed cut off threshold value)

Sampling rate (Hz)	Speed cut-off (mm/s)	Number of points	Power-law (restricted) (xmin= speed cut-off)		Exponential		Weibull		Log-normal	
			G^2 -Stat	p-value	G^2 -Stat	p-value	G^2 -Stat	p-value	G^2 -Stat	p-value
2	none	39600	14849	0	327.23	0	296	0	1232.1	0
	5	20188	6158.5	0	191.51	0	172.68	0	1258.7	0
	10	12244	4145.9	0	213.83	0	160.31	0	1005.9	0
	15	7039	250.82	0	111.24	0	97.322	0	803.59	0
1	none	19800	7586.6	0	208.37	0	271.91	0	570.9	0
	5	10045	3545.2	0	122.2	0	117.36	0	594.79	0
	10	5919	2148.3	0	129.82	0	106.78	0	437.15	0
	15	3365	103.15	0	73.686	0	48.433	0	372.1	0
0.5	none	9900	3818	0	69.769	0	147.03	0	250.02	0
	5	5074	1813.6	0	66.227	0	65.857	0	252.52	0
	10	2918	981.76	0	75.85	0	64.231	0	212.87	0
	15	1591	898.04	0	46.329	0	30.643	0.006218	180.75	0
0.2	none	3960	1587.8	0	36.44	0	81.035	0	125.79	0
	5	2058	749.94	0	39.072	0	40.523	0	98.501	0
	10	1149	384.16	0	28.243	0.01321	22.594	0.06721	60.804	0
	15	613	315.25	0	24.079	0.04483	25.19	0.03274	56.18	0

Table 5.13: Similar to Table 5.12, with additional results of the G-Test. Results are for the whole data set without removing the tail of the data.

Sampling rate (Hz)	Speed cut -off (mm/s)	Number of points	Power-law (restricted)		Exponential	Weibull		Log-normal	
			α	x_{\min}		λ (rate)	γ (shape)	α (scale)	μ (mean)
2	None	39600	1.502	0	0.118	0.526	5.817	0.445	3.256
	5	20188	1.497	5	0.098	0.988	10.12	1.736	1.277
	10	12244	1.499	10	0.098	0.943	9.979	1.686	1.350
	15	7039	1.470	15	0.089	1.029	11.31	1.851	1.291
1	None	19800	1.509	0	0.121	0.579	6.10	0.620	2.99
	5	10045	1.508	5	0.103	0.992	9.668	1.690	1.28
	10	5919	1.503	10	0.102	0.965	9.687	1.667	1.329
	15	3365	1.475	15	0.094	1.066	10.87	1.826	1.268
0.5	None	9900	1.516	0	0.123	0.638	6.424	0.794	2.732
	5	5074	1.512	5	0.109	0.999	9.200	1.644	1.270
	10	2918	1.517	10	0.108	0.966	9.158	1.609	1.340
	15	1591	1.484	15	0.098	1.100	10.516	1.804	1.267
0.2	None	3960	1.524	0	0.126	0.714	6.731	0.973	2.418
	5	2058	1.530	5	0.116	1.022	8.665	1.597	1.251
	10	1149	1.538	10	0.118	0.973	8.406	1.529	1.320
	15	613	1.509	15	0.110	1.091	9.369	1.689	1.233

Table 5.14: Parameter values calculated for the speed distribution for the whole data set, without removing the tail of the data.

All Bouts		Power-law (restricted)						Exponential						Weibull						Log-normal					
Sampling rate (Hz)	Speed cut -off (mm/s)	x_{\min}	G^2 -Test		K-S Test		AIC	G^2 -Test		K-S Test		AIC	G^2 -Test		K-S Test		AIC	G^2 -Test		K-S Test		AIC			
			stat	p	stat	p		stat	p	stat	p		stat	p	stat	p	stat	p	stat	p	stat	p			
2	5	0.5	147.17	0	0.393	0	5593	42.001	0.002	0.163	0	4997	30.068	0.051	0.12	0	4986	33.128	0.006	0.095	0	4852			
	10	0.5	79.225	0	0.435	0	5515	38.11	0.006	0.159	0	4892	26.862	0.108	0.154	0	4883	13.855	0.792	0.099	0	4701			
1	5	1	117.38	0	0.390	0	3364	29.517	0.058	0.107	0.002	2976	26.562	0.115	0.11	0.001	2977	21.854	0.292	0.072	0.078	2902			
	10	1	92.14	0	0.438	0	3542	37.948	0.006	0.163	0	3111	38.141	0.006	0.162	0	3113	32.479	0.028	0.114	0	2986			
0.5	5	2	96.196	0	0.398	0	1865	23.963	0.198	0.143	0.001	1612	25.352	0.149	0.108	0.025	1609	20.298	0.377	0.078	0.195	1566			
	10	2	78.96	0	0.377	0	1696	31.515	0.035	0.14	0.002	1477	31.099	0.039	0.112	0.022	1474	20.441	0.369	0.06	0.536	1436			

Moving Bouts		Power-law (restricted)						Exponential						Weibull						Log-normal					
Sampling rate (Hz)	Speed cut -off (mm/s)	x_{\min}	G^2 -Test		K-S Test		AIC	G^2 -Test		K-S Test		AIC	G^2 -Test		K-S Test		AIC	G^2 -Test		K-S Test		AIC			
			stat	p	stat	p		stat	p	stat	p		stat	p	stat	p	stat	p	stat	p	stat	p			
2	5	0.5	141.56	0	0.385	0	2928	37.486	0.007	0.102	0.011	2582	30.537	0.045	0.086	0.05	2582	24.226	0.188	0.08	0.078	2541			
	10	0.5	79.666	0	0.432	0	2738	27.555	0.092	0.139	0	2363	32.858	0.025	0.126	0.001	2365	15.397	0.697	0.085	0.054	2292			
1	5	1	113.15	0	0.368	0	1760	26.489	0.117	0.083	0.216	1550	24.436	0.18	0.091	0.14	1552	16.895	0.597	0.049	0.837	1525			
	10	1	93.094	0	0.453	0	1726	32.261	0.029	0.196	0	1490	41.208	0.002	0.159	0	1488	33.806	0.019	0.094	0.09	1432			
0.5	5	2	94.111	0	0.408	0	974	22.783	0.247	0.142	0.041	840	24.251	0.187	0.122	0.117	839	18.24	0.561	0.076	0.642	822			
	10	2	80.961	0	0.380	0	804	28.548	0.073	0.156	0.027	695	27.964	0.084	0.102	0.314	693	18.412	0.48	0.068	0.811	673			

Stationary Bouts		Power-law (restricted)						Exponential						Weibull						Log-normal					
Sampling rate (Hz)	Speed cut -off (mm/s)	x_{\min}	G^2 -Test		K-S Test		AIC	G^2 -Test		K-S Test		AIC	G^2 -Test		K-S Test		AIC	G^2 -Test		K-S Test		AIC			
			stat	p	stat	p		stat	p	stat	p		stat	p	stat	p	stat	p	stat	p	stat	p			
2	5	0.5	27.703	0.01	0.414	0	2668	100.72	0	0.147	0	2407	60.513	0	0.157	0	2396	44.569	0	0.103	0.011	2300			
	10	0.5	55.006	0	0.439	0	2782	107.35	0	0.211	0	2519	58.785	0	0.171	0	2501	43.453	0.001	0.117	0.002	2406			
1	5	1	58.884	0	0.417	0	1607	38.405	0.005	0.132	0.009	1420	34.773	0.015	0.141	0.004	1422	29.876	0.053	0.11	0.045	1373			
	10	1	83.4	0	0.424	0	1820	73.289	0	0.177	0	1618	64.136	0	0.156	0	1618	55.506	0	0.131	0.004	1553			
0.5	5	2	96.775	0	0.408	0	895	29.755	0.055	0.162	0.015	772	31.026	0.04	0.121	0.132	771	19.605	0.419	0.106	0.252	745			
	10	2	77.426	0	0.385	0	895	26.728	0.111	0.131	0.09	779	28.235	0.079	0.126	0.11	779	20.212	0.382	0.09	0.457	761			

Table 5.15: Statistical test results for the bout distributions. 4 distributions were considered. Sampling size of 0.2Hz was not included as there were too few bouts to give reliable results, and similar for speed threshold value of 15mm/s. The case for no speed threshold was also not considered as the data returned few stationary bouts. Results are for the data as a whole with the fixed x_{\min} value at the minimum non-zero value of the data.

<i>All Bouts</i>		Power-law (restricted)		Exponential		Weibull		Log-normal	
Sampling rate (Hz)	Speed cut-off (mm/s)	α	x_{\min}	λ (rate)	γ (shape)	α (scale)	μ (mean)	σ^2 (s.d.)	
2	5	0.5	1.30	0.019	0.89	50.23	3.36	1.06	
	10	0.5	1.30	0.020	0.91	46.00	3.31	0.97	
1	5	1	1.32	0.025	0.96	39.30	3.15	1.00	
	10	1	1.34	0.034	1.00	29.77	2.92	0.88	
0.5	5	2	1.35	0.038	1.13	27.46	2.87	0.86	
	10	2	1.37	0.044	1.13	23.79	2.72	0.87	

<i>Moving Bouts</i>		Power-law (restricted)		Exponential		Weibull		Log-normal	
Sampling rate (Hz)	Speed cut-off (mm/s)	α	x_{\min}	λ (rate)	γ (shape)	α (scale)	μ (mean)	σ^2	
2	5	0.5	1.28	0.016	0.94	59.52	3.54	1.08	
	10	0.5	1.30	0.024	1.04	42.15	3.28	0.89	
1	5	1	1.30	0.022	0.97	45.73	3.30	1.04	
	10	1	1.35	0.039	1.12	27.07	2.87	0.82	
0.5	5	2	1.34	0.035	1.14	30.48	2.97	0.88	
	10	2	1.39	0.053	1.20	20.27	2.59	0.81	

<i>Stationary Bouts</i>		Power-law (restricted)		Exponential		Weibull		Log-normal	
Sampling rate (Hz)	Speed cut-off (mm/s)	α	x_{\min}	λ (rate)	γ (shape)	α (scale)	μ (mean)	σ^2	
2	5	0.5	1.31	0.022	0.86	41.65	3.19	1.00	
	10	0.5	1.30	0.018	0.84	49.76	3.35	1.04	
1	5	1	1.33	0.030	0.97	33.13	3.00	0.94	
	10	1	1.34	0.030	0.94	32.46	2.98	0.93	
0.5	5	2	1.36	0.043	1.14	24.46	2.77	0.81	
	10	2	1.35	0.038	1.11	27.39	2.85	0.90	

Table 5.16: MLE for the parameters of the four distributions considered for the distribution of the bout lengths.

5.7.4 Appendix B4 - Analysis of data when including truncated bouts

As discussed in the main text (Section 5.3.1), bouts which had not ended by the end of the experiment were not included in the final analysis as their true length was indeterminable. Tables 5.17-5.18 show the results of the statistical analysis used in the main text when these bouts were included (that is the final bout was deemed to have finished when the experiment had ended) at a sampling rate of 1HZ and speed threshold value of 5mm/s. In general, the inclusion of these truncated bouts resulted in the statistical tests rejecting the fitted distributions, with a higher frequency, with the G-test rejecting all distributions for all types of bouts and the K-S test rejecting the distributions for all bout types except for the exponential in the case of stationary bouts, the Weibull in the case of moving bouts and the log-normal for both moving and stationary bouts ($p > 0.1$). However, the log-normal distribution was favoured by the AIC likelihood for all bout types, which is the same for the findings when the truncated bouts were excluded (Appendix B3 - Tables 5.15-5.16).

Type of bout	Restricted Power-law		Exponential	Weibull		Log-normal	
	x_{\min}	α	λ (rate)	γ (shape)	α (scale)	μ (mean)	σ^2 (s.d.)
All	1	1.30	0.019	0.90	48.69	3.32	1.08
Moving	1	1.29	0.018	0.94	54.10	3.44	1.09
Stationary	1	1.31	0.021	0.87	43.41	3.21	1.07

Table 5.17: MLE for the parameters of the four distributions considered for the bout distributions when including truncated bouts. Results are for the data as a whole with the fixed x_{\min} value at the minimum non-zero value of the data. Results displayed are for sampling size 1Hz and speed threshold 5mm/s, which were the values used throughout the analysis in the main text.

Bout type	Restricted Power law					Exponential					Weibull					Log-normal				
	G^2 -Test		K-S Test		AIC	G^2 -Test		K-S Test		AIC	G^2 -Test		K-S Test		AIC	G^2 -Test		K-S Test		AIC
	stat	p	stat	p		stat	p	stat	p		stat	p	stat	p		stat	p	stat	p	
All	87.764	0	0.419	0	1726	54.884	0	0.130	0	1574	45.813	0	0.117	0	1537	40.48	0.004	0.065	0.075	1506
Moving	96.500	0	0.568	0	1609	56.667	0	0.104	0.031	1037	50.194	0	0.088	0.174	1017	39.878	0.005	0.042	0.879	993
Stationary	135.39	0	0.764	0	1809	91.156	0	0.085	0.121	1543	74.918	0	0.093	0.072	1545	54.538	0	0.094	0.164	1500

Table 5.18: Test results for the bout distributions when truncated bouts were included. 4 distributions were considered. Results are for the data as a whole with the fixed x_{\min} value at the minimum non-zero value of the data. Results displayed are for sampling size 1Hz and speed threshold 5mm/s, which were the values used throughout the analysis in the main text. The results indicate that the log-normal distribution was the favoured distribution for all types of bouts in simultitude with the analysis when the truncated bouts were not included (see section 5.4.6 and Appendix B3 - Tables 5.15-5.16).

5.7.5 Appendix B5 - Categorisation of movement paths as a BRW or a CRW

Here we discuss the methods used to categorise the movement of the beetles as either a CRW or a BRW at both the individual and population level.

It was noted in the main text that at the population level a slight preference in global direction was found (section 5.4.3). However, when looking at the individual level this apparent preferential angle can be explained by comparing the initial orientation of the beetles along with their final positions.

Fig. 5.9A shows the direction of each individual trial run at the beginning of the experiment, represented as a unit vector in the given direction (the direction was calculated by calculating the mean orientation across the first 10 moving steps of the trial). Fig. 5.9B shows the final location of the beetle for each trial run represented as a unit vector in the direction of the final position. These figures demonstrate that whilst the initial distribution of orientation angles appears to have a concentration of orientation angles be concentrated towards the top-right quadrant and away from the bottom-left, the final positions of the beetles have become more uniform in distribution. The implication here is that the beetles began heading in a similar direction, perhaps due to the initial orientation of their placement on the tracking sphere, and due to their observed innate persistent ability continued to head towards this initial bearing. Had the initial bearing been caused by some external source one would expect this dispersal to narrow over time as all the beetles eventually navigated towards the external source, however, over time the beetles dispersed over a greater space reflected in the location of the final data points, leading to the conclusion that there is no evidence of a global bias in direction. Hence, we conclude that at the population level, there is no consistent long-term global preferred direction of movement, and the slight preference in global orientation found when analysing all steps of the movement paths is due to the initial distribution of movement directions.

A direct method of ascertaining determining if a movement path is better described likely formed by either a CRW or BRW is to calculate the Marsh-Jones Δ -statistic

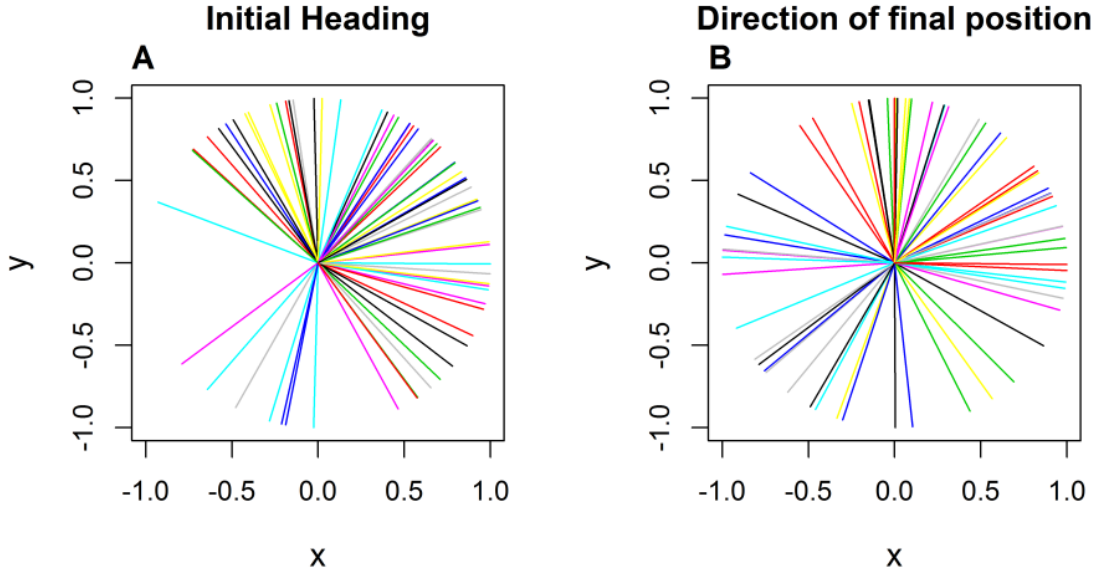


Figure 5.9: (A) Orientation of all the individual trials (shown as a unit vector in the direction of the angle of orientation) at the start of the experiment (orientation was taken as the mean of the first 10 steps of movement). In contrast (B) shows the final location of the beetle at the end of the experiment (shown as a unit vector in the direction of the final location). Each individual colour represents an individual beetle, as in Figures in the main text.

(Marsh & Jones, 1988) (section 5.3.3.4 - Eq. 5.4); given by:

$$\Delta = \frac{1}{n^2} \left[\left(\sum \cos \phi_i \right)^2 + \left(\sum \sin \phi_i \right)^2 \right] - \frac{1}{(n-1)^2} \left[\left(\sum \cos \theta_i \right)^2 + \left(\sum \sin \theta_i \right)^2 \right] \quad (5.6)$$

where, ϕ_i is the global orientation and θ_i is the turning angle, at time i .

The expected values of the Δ statistic are calculated by extensive simulations and thus depend upon the number of individuals and the number of time steps. Turning angles are calculated as the angle between the direction of successive steps and the global orientation of a given time step is calculated as the angle between the direction at that time step and the positive y-axis. The resultant vectors for the distribution of the orientation and turning angles are calculated directly from the observed data, with the orientation distributions transformed to give a zero-centred distribution. The expected values of the Δ statistic are calculated by extensive simulations using the equivalent number of data points as found in the observed data, therefore, the value of the statistic

depends upon both the number of individuals and the number of time steps. The global orientation and turning angles for these simulations are drawn from distributions with resultant vectors calculated directly from the global orientations and turning angles of the observed data, and thus depend upon the number of individuals and the number of time steps.

The analysis of the results of calculating the Δ -statistic is given in the main text, section 5.4.3. Table 5.1.9 shows how the Δ statistic classified each individual trial, with 5 trials corresponding to a CRW and only one as a BRW. The remaining trials could not be determined as being either type of random walk.

Beetle	Trial	Δ observed	Predicted Δ (BRW)	Predicted Δ (CRW)
1	1	-0.0151	(-0.0079, 0.0626)	(-1.0111, -0.4215)
2	1	-0.0145	(0.1441, 0.2113)	(-0.7498, -0.6336)
3	1	-0.0779	(0.2214, 0.2385)	(-0.6161, -0.5434)
4	1	-0.1473	(0.1567, 0.2196)	(-0.87, -0.6652)
5	1	0.0433	(0.1669, 0.225)	(-0.644, -0.5636)
6	1	0.0753	(0.1048, 0.1836)	(-0.719, -0.619)
7	1	-0.0954	(0.0751, 0.1594)	(-0.9646, -0.5823)
8	1	-0.2887	(0.0875, 0.1624)	(-0.4506, -0.4046)
9*	1*	-0.4143*	(-0.0077, 0.0266)*	(-0.4263, -0.3827)*
10	1	-0.111	(0.1157, 0.193)	(-0.9065, -0.6538)
11	1	-0.0984	(0.1011, 0.1816)	(-0.9191, -0.6444)
12	1	-0.5412	(0.0486, 0.123)	(-0.6497, -0.5705)
13	1	-0.1998	(0.2153, 0.2386)	(-0.6238, -0.5488)
14*	1*	-0.2871*	(-0.0073, 0.024)*	(-0.2995, -0.2678)*
15	1	-0.3388	(0.205, 0.2378)	(-0.7348, -0.6249)
16	1	0.0768	(0.0845, 0.1659)	(-0.7536, -0.6344)
17	1	-0.3343	(0.1587, 0.2194)	(-0.6182, -0.544)
18	1	-0.0491	(0.2226, 0.2374)	(-0.5038, -0.4521)

Beetle	Trial	Δ observed	Predicted Δ (BRW)	Predicted Δ (CRW)
19	1	-0.1062	(0.2252, 0.2376)	(-0.5697, -0.5057)
20	1	-0.1286	(0.166, 0.2251)	(-0.8259, -0.664)
21	1	-0.1229	(0.2069, 0.2389)	(-0.7173, -0.6145)
22	1	-0.0939	(0.2208, 0.2378)	(-0.5412, -0.4822)
1	2	-0.1798	(0.1929, 0.2347)	(-0.5347, -0.4768)
2	2	0.0821	(0.2045, 0.2381)	(-0.5134, -0.4588)
3	2	-0.135	(0.2067, 0.2394)	(-0.7297, -0.623)
4†	2†	0.0217†	(0.0147, 0.0929)†	(-0.9175, -0.6462)†
5*	2*	-0.4462*	(-0.0029, 0.0405)*	(-0.4584, -0.4112)*
6	2	0.0636	(0.2094, 0.2395)	(-0.5196, -0.4638)
7	2	-0.1473	(0.2065, 0.2389)	(-0.5373, -0.4801)
8	2	-0.0093	(0.1448, 0.2095)	(-0.2616, -0.2335)
9	2	-0.0559	(0.0417, 0.1143)	(-0.1471, -0.1266)
10	2	0.044	(0.1911, 0.2355)	(-0.5892, -0.5214)
11	2	-0.1272	(0.2225, 0.2392)	(-0.664, -0.5824)
12	2	0.0366	(0.145, 0.2131)	(-0.6917, -0.599)
13	2	-0.2612	(0.0413, 0.1136)	(-0.3539, -0.3173)
14	2	-0.2799	(0.1629, 0.2209)	(-0.5701, -0.5053)
15*	2*	-0.6147*	(0.1713, 0.225)*	(-0.9516, -0.6057)*
16	2	-0.2787	(0.223, 0.2394)	(-0.733, -0.6218)
17	2	0.0369	(0.2183, 0.2394)	(-0.514, -0.4595)
18	2	-0.0736	(0.2257, 0.2379)	(-0.5378, -0.4809)
19	2	-0.0409	(0.1654, 0.2226)	(-0.3359, -0.3026)
20	2	0.1448	(0.155, 0.2182)	(-0.5614, -0.4984)
21	2	-0.06	(0.052, 0.1266)	(-0.1694, -0.1479)
22	2	-0.2325	(0.1278, 0.1987)	(-0.4582, -0.4124)
1	3	0.0031	(0.0236, 0.1048)	(-0.9285, -0.6358)

Beetle	Trial	Δ observed	Predicted Δ (BRW)	Predicted Δ (CRW)
2	3	-0.19	(0.0999, 0.1751)	(-0.3687, -0.332)
3	3	-0.0977	(0.1002, 0.1805)	(-0.9257, -0.638)
4	3	-0.4701	(0.1812, 0.2301)	(-0.7996, -0.6538)
5	3	-0.0781	(0.1881, 0.2342)	(-0.7211, -0.6184)
6	3	-0.2405	(0.1994, 0.2364)	(-0.8602, -0.6691)
7	3	-0.3289	(0.0534, 0.1279)	(-0.44, -0.3964)
8	3	-0.2201	(0.0247, 0.0903)	(-0.2874, -0.2571)
9	3	-0.1472	(0.2258, 0.2381)	(-0.6678, -0.5791)
10	3	-0.2246	(0.2163, 0.2396)	(-0.6483, -0.5675)
11	3	0.0318	(0.2214, 0.2394)	(-0.4081, -0.3677)
12	3	-0.0704	(0.1298, 0.2031)	(-0.8328, -0.6674)
13	3	-0.1881	(0.149, 0.2128)	(-0.4508, -0.4059)
14	3	-0.0104	(0.2004, 0.2375)	(-0.6207, -0.5484)
15*	3*	-0.7675*	(0.0905, 0.1657)*	(-0.9685, -0.5703)*
16	3	-0.2012	(0.2077, 0.2386)	(-0.5973, -0.5288)
17	3	-0.2774	(0.1496, 0.2133)	(-0.5446, -0.486)
18	3	-0.035	(0.1863, 0.2336)	(-0.6828, -0.5931)
19	3	-0.0879	(0.2185, 0.2394)	(-0.641, -0.5612)
20	3	-0.2363	(0.0296, 0.0989)	(-0.3149, -0.283)
21	3	-0.3461	(0.0783, 0.1555)	(-0.4961, -0.4437)
22	3	-0.1682	(0.2258, 0.2385)	(-0.6897, -0.5979)

Table 5.19: The Δ statistic calculated from the observed movement paths. The intervals for the expected values of the BRW and CRW were calculated via extensive simulation of random walks generated using the same number of steps as observed in the experiment, and represent the 95% significance level for each respective RW type. Therefore any observed Δ falling outside these intervals can be rejected at the 5% significance level. Those marked with (*) have observed Δ corresponding to a CRW and those with a (†) correspond to a BRW.

6 Potential misinterpretation of directional data: apparent emergence of a heavy-tailed distribution from an underlying mixed distribution

In this chapter we demonstrate how a probability distribution formed by mixing two wrapped normal distributions can give the appearance of a single circular heavy tailed distribution. We show that this is dependent upon the values of the concentration parameters of the underlying wrapped normal distributions along with the value of the mixing parameter and demonstrate the parameter space for when this occurs. As inferring distributions is an important process in animal movement analysis, we conclude that the presence of a heavy tailed distribution in angular data can, on occasion, be a product of the data coming from two distinct distributions, possibly indicating multiple movement behaviours across a movement path.

6.1 Introduction

The analysis and applications of circular statistics to directional data plays a significant role in the study of many biological processes from plant phenology (Morellato et al, 2010) to the general movement patterns of animals and cells (Rivest et al, 2016; Landler et al, 2018). Ascertaining the distribution which most closely describes circular data is important as characteristics of circular distributions, such as heavy tails, have significant effects on the qualitative and quantitative results of descriptive and predictive models.

The most common distributions used to describe angular data are the wrapped normal (WN), von Mises (vM) (or circular normal) and the wrapped Cauchy (WC) (McClintock et al, 2012; McClintock & Michelot, 2018). These are defined by a probability density function (PDF) on the unit circle, and in the case of the WN and WC distributions, can be formed by ‘wrapping’ the equivalent one dimensional distributions on the real line around the unit circle (Stephens, 1963; Jammalamadaka & SenGupta, 2001;

Mardia & Jupp, 2009). Although the von Mises and wrapped normal distributions have differing PDFs, the two approximate each other very closely and produce similar qualitative results (Stephens, 1963; Collett & Lewis, 1981; Jammalamadaka & SenGupta, 2001; Mardia & Jupp, 2009; Codling et al, 2010). The WC distribution qualitatively differs from the WN and vM as it has a taller peak around the mean value and heavier tails which decay more slowly. Hence, many analyses classify angular data as being either heavy tailed (and therefore similar to wrapped Cauchy) or near normal (and thus either a von Mises or wrapped normal). For clarity the notion of ‘heavy-tailed’ in wrapped distributions refers to distributions whose analogous non-wrapped distributions are considered as being ‘heavy-tailed’.

In particular, when modelling movement by random walk (RW) or step-turn processes it is often necessary to understand the distribution of turning angles and movement directions (Kareiva & Shigesada, 1983; Bartumeus, 2008; Codling et al, 2008; Parton & Blackwell, 2017). Methods to determine the distribution which best describes observed directional data typically involves finding MLE parameters for the model distributions and choosing between them by the use of a likelihood or distance measure (Nilsen et al, 2013; Li & Bolker, 2017). Evidence that a WC distribution is the ‘best-fit’ for the distribution of turning angles or global orientations in a movement path has been found across a wide range of animals from insects and beetles, such as pea aphids *Acyrtosiphon pisum* (Nilsen et al, 2013) and the Baltimore checkerspot butterfly *Euphydryas phaeton* (Brown & Crone, 2016) to larger animals such as common brushtail possums *Trichosurus Vulpecula* (Postlethwaite & Dennis, 2013), cow elk, *Cervus elaphus*, (Morales et al, 2004), free-range cattle *Nothofagus Antarctica* (Seoane, 2015), Florida panthers, *Puma concolor coryi*, (van de Kerk et al, 2015; Li & Bolker, 2017), California sea lions *Zalophus californianus* (Breed et al, 2012), Giant tortoises *Testudinidae* (Blake et al, 2013), American lobster *Homarus americanus* (Bowlby et al, 2007) and seals *Erignathus barbatus* and *Monachus schauinslandi* (McClintock et al, 2015). The studies mentioned above range from high frequency data having locations given every second to large scale movement with data sent every 24hr, illustrating that heavy tailed distributions occur

across a range of scales.

A basic search on Google Scholar reveals that whilst both types of distribution have been frequently used and reported in recent animal movement data analyses, there has been a marked increase in the prevalence of the WC distribution over the last 10-15 years. A key word search of “animal movement” and “wrapped Cauchy” returns only 22 articles published before 2008, compared to the equivalent for either “von Mises” or “wrapped normal” returning 81, a four-fold difference. However, since 2008 this ratio has halved with 200 articles mentioning WC and 398 for WN demonstrating a marked increase in the prevalence of the WC distribution.

In comparison the WN or vM distribution has been reported across a similarly wide range of animals, from *E. coli* bacterium (Taylor-King et al, 2015), Fender’s blue butterfly *Icaricia icarioides* fender (Schultz & Crone, 2001) and bog fritillary butterfly *Procllossiana Eunomia* (Schtickzelle et al, 2007) to larger animals such as red-cockaded woodpecker *Picoides borealis* (McKellar et al, 2014), lesser black-backed gull *L. fuscus* (Taylor-King et al, 2015), king penguin *Aptenodytes patagonicus* (Pistorius et al, 2017), reindeer *Rangifer tarandus* (Langrock et al, 2014) and southern elephant seal *Mirounga leonine* (Michelot et al, 2017).

One biological interpretation of the presence of a heavy tailed distribution is that the individual mainly travels on a near constant bearing, with the majority of turns occurring within small deviations from 0 whereas medium to large turns happen only occasionally but with a similar frequency. This would indicate the animal has a tendency for sudden large changes in direction of movement, rather than a gradual change in orientation over a course of a series of larger turns which would be expected from a normal or Gaussian distribution. Various RW movement models have shown that observably different qualitative and quantitative results are produced depending upon whether a WC or vM (heavy-tailed or not) distribution has been used (Bartumeus et al, 2008; Codling et al, 2010), demonstrating the importance of accurately determining the underlying distributions.

If the way in which data is collected, analysed or processed can affect how well a

candidate distribution fits the observed data then this needs to be well understood and acknowledged. For example it has been shown that errors in GPS data locations can give rise to spurious large 180° turns, which would enhance the heavy-tailed nature of recorded turning angles (Jerde & Visscher, 2005; Hurford, 2009). Other reported issues with data collection which artificially increased the number of large turns include the effect of recording data in a restricted area, where edge effects can cause sudden large turns as the animal encounters a wall. Young et al (2013) found that flour beetles, *Tribolium confusum* took smaller steps with larger turn angles closer to the border of the experimental setup, which resulted in a flatter heavy-tailed distribution. Similar results relating the experimental setup to artificially heavier tails in angular data has been recorded in other species such as parasitic wasps, *Encarsia formosa* (Drose et al, 2000).

When considering movement behaviour it is known that animals can exhibit different movement modes when travelling (Schtickzelle et al, 2007; Gurarie et al, 2016; Cagnacci et al, 2016), perhaps due to switching from a foraging/exploration phase to an encamped/feeding phase which can lead to periods of small turns followed by periods of larger turns (McClintock et al, 2015; Torres et al, 2017). Similarly, changes in the terrain or climate could alter the movement behaviour (Patterson et al, 2009; Dahmen et al, 2017; Pérez-Barbería et al, 2015). The qualitative behaviour of each movement phase will be best described by a specific model and set of parameters and if these strategies are not known a priori the movement data could be analysed under the assumption of a single movement strategy resulting in the mixing of the data from the individual behavioural states. The simplest example of such multiple movement behaviour is a two state movement model where one phase is described by large variability in turning angles between steps relating to highly tortuous movement perhaps indicative of foraging or encamped behaviour, and another phase with more directed, straighter movement where the deviation in turning angles from the mean is smaller, akin to purposeful goal based movement or flight behaviour (Patterson et al, 2010; Jonsen et al, 2013; Langrock et al, 2012; Parton & Blackwell, 2017; McClintock & Michelot, 2018; Nams, 2014).

Here we demonstrate that a single heavy-tailed wrapped Cauchy distribution can appear to fit directional data mixed from two different underlying wrapped normal distributions. We derive analytical expressions used to calculate the parameter space for which this occurs. Our results show that, in general, when the two WN distributions forming the mixed distribution have a large difference in their respective concentration parameters (≥ 0.5) a WC is the best fitting single distribution, indicating that a mixed distribution can enhance the appearance of a heavy tail in the distribution of turning angles when interpreted as a single distribution.

6.2 Background: Circular Statistics and Distributions

6.2.1 Symmetric Wrapped Stable Distributions

A symmetric wrapped stable (SWS) distribution has the density function given by:

$$f_{\text{sws}}(\theta; \rho, \mu) = \frac{1}{2\pi} \left(1 + 2 \sum_{n=1}^{\infty} \rho^{n^a} \cos n(\theta - \mu) \right), \quad n \in \mathbb{N} \quad (6.1)$$

where $\rho \in [0, 1)$ is the concentration parameter, $\mu \in [-\pi, \pi)$ is the location parameter around which the distribution is symmetric and $a \in (0, 2]$, with $\theta \in [-\pi, \pi)$.

In the specific case for $a = 1$ the SWS distribution returns the WC distribution and for $a=2$ we get the WN distribution (Jammalamadaka & SenGupta, 2001).

It is well known that for any given WN distribution a vM can be found as an accurate approximation (Stephens, 1963; Collett & Leiwis, 1981; Jammalamadaka & SenGupta, 2001). Hence, both give qualitatively similar results when used in random walk (RW) models (Codling et al, 2010). Therefore, we consider only a WN distribution as it allows for easier algebraic manipulation.

If we let the SWS be centred around 0, ($\mu = 0$), then $\rho^{n^a} = \alpha_n$, where α_n is the n th cosine moment of f_{sws} . Note that in this case we need only consider the cosine moments the sine moments are all 0 (Mardia & Jupp, 2009; Jammalamadaka & SenGupta, 2001).

6.2.2 Mixed wrapped distributions

One can also consider distributions formed by mixing two circular distributions, f_{md} , where random variables are drawn from one of the two distributions according to a certain probability, ω .

$$f_{\text{md}}(\theta; \omega) = \omega f_1(\theta) + (1 - \omega) f_2(\theta)$$

where f_1 and f_2 are SWS distributions and $\omega \in [0, 1]$ is defined as the mixing parameter of the two initial distributions. Note that the trivial cases for $\omega = 0, 1$ are equivalent to $f_{\text{md}} = f_2$ and $f_{\text{md}} = f_1$ respectively.

Lemma 1. *Let $f_{\text{md}}(\theta; \omega)$ be a distribution formed by mixing two SWS distributions centred around zero ($\mu = 0$), then f_{md} itself is a wrapped distribution with cosine moments, $\alpha_n^{\{\text{md}\}}$, given by*

$$\alpha_n^{\{\text{md}\}} = \omega \alpha_n^{\{1\}} + (1 - \omega) \alpha_n^{\{2\}} \quad (6.2)$$

where $\alpha_n^{\{1\}}, \alpha_n^{\{2\}}$ are the n th cosine trigonometric moments of f_1 and f_2 respectively.

Proof. Lemma 1 follows directly from the definition of f_{md} and f_{sws} .

As both f_1 and f_2 are SWS distributions with $\mu = 0$, we have

$$\begin{aligned} f_{\text{md}}(\theta) &= \omega \frac{1}{2\pi} \left(1 + 2 \sum_{n=1}^{\infty} \alpha_n^{\{1\}} \cos(n\theta) \right) + (1 - \omega) \frac{1}{2\pi} \left(1 + 2 \sum_{n=1}^{\infty} \alpha_n^{\{2\}} \cos(n\theta) \right) \\ &= \frac{1}{2\pi} \left(1 + 2 \sum_{n=1}^{\infty} [\omega \alpha_n^{\{1\}} + (1 - \omega) \alpha_n^{\{2\}}] \cos(n\theta) \right) \end{aligned}$$

This is analogous the form of a general SWS given in Eq. 6.1 centred around 0 with trigonometric moments $\omega \alpha_n^{\{1\}} + (1 - \omega) \alpha_n^{\{2\}}$ as required. Note, as f_{md} is a wrapped distribution, symmetric around $\mu = 0$ the trigonometric sine moments are all 0 and hence the trigonometric moments of f_{md} are purely the cosine moments. \square

6.2.3 Determining between best-fit circular distributions

When calculating a measure of the distance between two given PDFs, one can consider many statistical measures (Gibbs & Su, 2002). However one of the simplest is to consider

the sum of the squares of the differences between the distributions across their domain; equivalent to finding the L^2 -distance. Hence, we will consider the distance, $d(\cdot, \cdot)$ between two continuous probability functions, f and g , over the finite domain X as

$$d(f, g) = \int_{x \in X} [f(x) - g(x)]^2 dx$$

We use the L^2 distance throughout this study as it allows for simple algebraic manipulation, however Appendix C1 and Figs 6.3-6.5 detail the results of using other metrics, found using simulations and show they are qualitatively similar to those found using the L^2 distance (Fig. 6.1). Therefore, when comparing between multiple PDFs we infer the closest fitting distribution as the one which minimises the L^2 distance.

6.3 Fitting individual wrapped distributions to a mixed distribution

6.3.1 Statement of main claim

Here we consider a mixed distribution formed from two WN distributions and demonstrate the parameter space for which it is best described by either a single WN or single WC distribution. By considering the L^2 distance we derive expressions for calculating the best-fitting WN and WC distributions as functions of the parameters of the mixed distribution and determine the parameter space for whether a WN or WC best describes the mixed distribution, by selecting the distribution with the smallest value L^2 distance.

Proposition 1. *Let Θ be a mixed SWS distribution formed by mixing two wrapped normal distributions, defined as*

$$\Theta(\theta; \mu_0, \rho_1, \rho_2, \omega) = \omega f_{wn}(\theta; \mu_0, \rho_1) + (1 - \omega) f_{wn}(\theta; \mu_0, \rho_2) \quad (6.3)$$

for $\theta \in [-\pi, \pi)$, with $\mu_0 \in [-\pi, \pi)$, $\rho_1, \rho_2 \in [0, 1)$ and $\omega \in [0, 1]$. Define

$$\Delta_{wn}(\rho, \mu) = d(f_{wn}(\theta; \rho, \mu), \Theta(\theta; \mu_0, \rho_1, \rho_2, \omega))$$

$$\Delta_{wc}(\rho, \mu) = d(f_{wc}(\theta; \rho, \mu), \Theta(\theta; \mu_0, \rho_1, \rho_2, \omega))$$

Let ρ_{wn}, μ_{wn} minimise Δ_{wn} and ρ_{wc}, μ_{wc} minimise Δ_{wc} . Then there always exists a parameter space for ρ_1, ρ_2, ω such that:

$$\Delta_{wc}(\rho_{wc}, \mu_{wc}) < \Delta_{wn}(\rho_{wn}, \mu_{wn}) \quad (6.4)$$

As Δ_{wn} and Δ_{wc} give the values of the L^2 distance for each distribution compared to Θ , the smaller value of Δ_{wn} and Δ_{wc} indicates the closer fitting distribution.

Note, as both distributions forming the mixed distribution, Θ , are from the same family of distributions (Eq. 6.3) without loss of generality we can consider the distribution with concentration parameter ρ_1 to be the distribution which has the smaller probability of being chosen and, therefore, by symmetry we need only consider $\omega \in [0, 1/2]$.

We only consider the distributions within the mixed distribution Θ to be WN rather than WC as the latter leads to the mixed distribution always being classified as a single WC and our main concern is determining when a heavy tailed distribution fits data from non-heavy tailed distributions (see Appendix C2 and Figs. 6.6-6.7 for a complete discussion of this along with the results of having a WC and a WN as the initial mixed distributions). To demonstrate this proposition we give an analytical method for calculating the specific parameter values which minimise Δ_{wn} and Δ_{wc} for fixed ρ_1, ρ_2, ω . By directly comparing these minimised values we show the parameter space for which the WC distribution (or WN) is the closest fitting distribution when the L^2 distance metric is used.

6.3.2 Demonstration of main claim

First we note that if we assume $\mu = 0$ for the two underlying initial WN distributions, then clearly Θ is centred around 0 and we must have $\mu_{wn} = \mu_{wc} = 0$ (?).

Using Lemma 6.1 we can write Θ from Prop. 6.1 as

$$\Theta = \frac{1}{2\pi} \left(1 + 2 \sum_{n=1}^{\infty} \alpha_n^{\{\Theta\}} \cos(n\theta) \right)$$

with

$$\alpha_n^{\{\Theta\}} = \omega \alpha_n^{\{1\}} + (1 - \omega) \alpha_n^{\{2\}}$$

where $\alpha_n^{\{1\}}$ and $\alpha_n^{\{2\}}$ are the n th cosine moments of the WN distributions with concentration parameters ρ_1 and ρ_2 respectively.

Recalling that $\alpha_n^{\text{wn}} = \rho_{\text{wn}}^{n^2}$, we have

$$\alpha_n^{\{\Theta\}} = \omega \rho_1^{n^2} + (1 - \omega) \rho_2^{n^2}$$

We now show that when considering the L^2 distance between two zero centred SWS distributions it suffices to calculate the sum of the squares of the differences between their respective cosine moments.

Lemma 2. *Let $f_1(\theta)$ and $f_2(\theta)$ be SWS distributions centred around 0 with cosine moments $\alpha_n^{\{1\}}$ and $\alpha_n^{\{2\}}$ respectively, then*

$$d(f_1, f_2) = \frac{1}{\pi} \sum_{n=1}^{\infty} (\alpha_n^{\{1\}} - \alpha_n^{\{2\}})^2$$

Proof. As $f_1(\theta)$ and $f_2(\theta)$ are zero-centred SWS distributions, the square of the difference between the distributions at any given value of $\theta \in [-\pi, \pi)$ is given by

$$\begin{aligned} [f_1(\theta) - f_2(\theta)]^2 &= \left[\frac{1}{2\pi} \left(1 + 2 \sum_{n=1}^{\infty} \alpha_n^{\{1\}} \cos(n\theta) \right) - \frac{1}{2\pi} \left(1 + 2 \sum_{n=1}^{\infty} \alpha_n^{\{2\}} \cos(n\theta) \right) \right]^2 \\ &= \left[\frac{1}{\pi} \sum_{n=1}^{\infty} (\alpha_n^{\{1\}} - \alpha_n^{\{2\}}) \cos(n\theta) \right]^2 \end{aligned}$$

integrating over $[-\pi, \pi)$ with respect to θ gives

$$\int_{-\pi}^{\pi} [f_1(\theta) - f_2(\theta)]^2 d\theta = \int_{-\pi}^{\pi} \left[\frac{1}{\pi} \sum_{n=1}^{\infty} (\alpha_n^{\{1\}} - \alpha_n^{\{2\}}) \cos(n\theta) \right]^2 d\theta$$

Expanding the right hand side gives

$$= \frac{1}{\pi^2} \int_{-\pi}^{\pi} \left[\sum_{n=1}^{\infty} (\alpha_n^{\{1\}} - \alpha_n^{\{2\}})^2 \cos^2(n\theta) + 2 \sum_{i=1}^{\infty} \sum_{j=i+1}^{\infty} (\alpha_i^{\{1\}} - \alpha_i^{\{2\}}) (\alpha_j^{\{1\}} - \alpha_j^{\{2\}}) \cos(i\theta) \cos(j\theta) \right] d\theta$$

By Fubini-Tonelli Theorem we have

$$= \frac{1}{\pi^2} \left[\sum_{n=1}^{\infty} (\alpha_n^{\{1\}} - \alpha_n^{\{2\}})^2 \int_{-\pi}^{\pi} \cos^2(n\theta) d\theta + 2 \sum_{i=1}^{\infty} \sum_{j=i+1}^{\infty} (\alpha_i^{\{1\}} - \alpha_i^{\{2\}}) (\alpha_j^{\{1\}} - \alpha_j^{\{2\}}) \int_{-\pi}^{\pi} \cos(i\theta) \cos(j\theta) d\theta \right]$$

noting that the integral in the first term yields π and the integral in the second gives 0, this expression reduces to

$$\frac{1}{\pi} \sum_{n=1}^{\infty} (\alpha_n^{\{1\}} - \alpha_n^{\{2\}})^2$$

For a more complete derivation including the intermediary steps see Supplementary Material Appendix C □

Therefore, we can re-write Δ_{wc} and Δ_{wn} as

$$\Delta_{wc}(\rho, 0) = \frac{1}{\pi} \sum_{n=1}^{\infty} (\alpha_n^{\{wc\}} - \alpha_n^{\{\Theta\}})^2 = \frac{1}{\pi} \sum_{n=1}^{\infty} \left[\rho^n - (\omega \rho_1^{n^2} + (1 - \omega) \rho_2^{n^2}) \right]^2 \quad (6.5)$$

$$\Delta_{wn}(\rho, 0) = \frac{1}{\pi} \sum_{n=1}^{\infty} (\alpha_n^{\{wn\}} - \alpha_n^{\{\Theta\}})^2 = \frac{1}{\pi} \sum_{n=1}^{\infty} \left[\rho^{n^2} - (\omega \rho_1^{n^2} + (1 - \omega) \rho_2^{n^2}) \right]^2 \quad (6.6)$$

As ρ_{wc} and ρ_{wn} are the values which minimise Δ_{wc} and Δ_{wn} respectively, they can be found by differentiating Eq. 6.5 & 6.6 with respect to ρ and equating for 0.

Hence, we require

$$0 = \frac{d}{d\rho} \Delta_{wc} = \frac{1}{\pi} \sum_{n=1}^{\infty} 2n \rho^{n-1} \left[\rho^n - (\omega \rho_1^{n^2} + (1 - \omega) \rho_2^{n^2}) \right] \quad (6.7)$$

$$0 = \frac{d}{d\rho} \Delta_{wn} = \frac{1}{\pi} \sum_{n=1}^{\infty} 2n^2 \rho^{n^2-1} \left[\rho^{n^2} - (\omega \rho_1^{n^2} + (1 - \omega) \rho_2^{n^2}) \right] \quad (6.8)$$

The precise values of ρ which satisfy Eq. 6.7 & 6.8 will therefore be the values for ρ_{wc} and ρ_{wn} respectively, and can be found via numerical methods. Substituting ρ_{wc} and ρ_{wn} back into the expressions for Δ_{wc} and Δ_{wn} in Eq. 6.5 & 6.6 yield the respective minimum values. We can now determine the parameter space of ρ_1, ρ_2, ω for which a WC distribution is favoured over a WN distribution when compared to Θ by considering when $\Delta_{wc}(\rho_{wc}, \mu_{wc}) < \Delta_{wn}(\rho_{wn}, \mu_{wn})$. Therefore, calculating

$$D_{\Delta} = \Delta_{wc}(\rho_{wc}, 0) - \Delta_{wn}(\rho_{wn}, 0)$$

will give us an indication, not only of which distribution is favoured (negative in the case of a WC and positive for a WN), but also the relative ‘strength’; that is the larger the absolute value, the larger the difference in the total variation distance between the distributions, and thus the closer the preferred distribution is to the mixed distribution relative to the other.

6.4 Results

Fig. 6.1 shows the results of plotting D_{Δ} across the parameter space of ρ_1, ρ_2, ω with the areas in yellow (areas bounded by the dashed line) representing combinations for which the WN distribution is considered closer to the mixed distribution Θ and blue areas showing where a WC is considered closer; the darker the colour the stronger the preference.

In the simplest case where the mixed distribution is formed by mixing the two underlying distributions equally ($\omega = 0.5$; Fig 6.1K) the plot is symmetric about the lead diagonal (corresponding to $\rho_1 = \rho_2$) as expected, with the WN favoured whenever $|\rho_1 - \rho_2|$ is small, shown by the concentration of yellow near to the main diagonal. The areas for which the WC is favoured occur predominantly when the difference between ρ_1, ρ_2 is large ($|\rho_1 - \rho_2| \geq 0.5$). However, in the case when both concentration parameters are greater than 0.5, the area for which a WC is favoured is much smaller occurring now only if $5\rho_1 - \rho_2 \geq 4$ (or $5\rho_2 - \rho_1 \geq 4$).

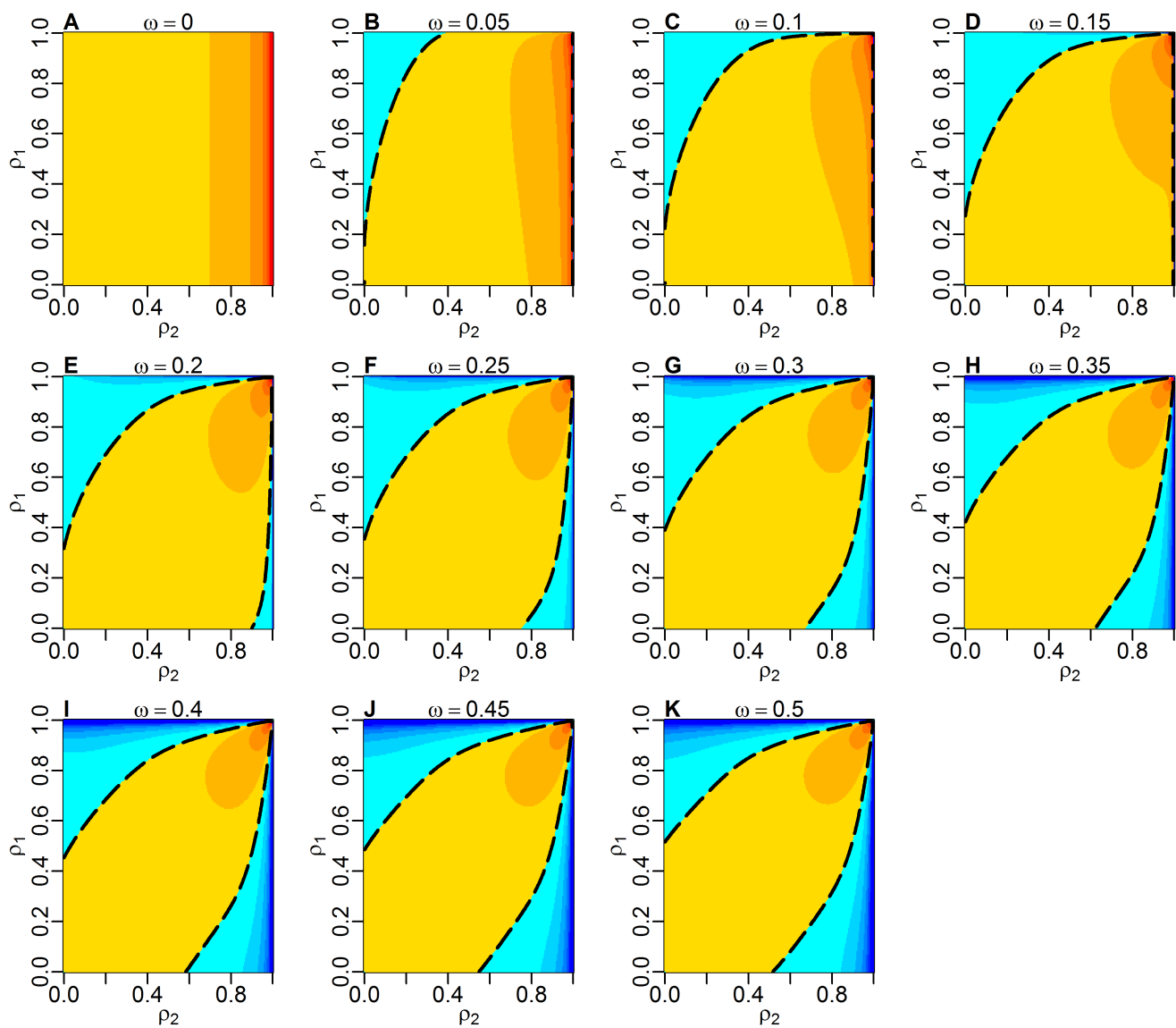


Figure 6.1: Plots demonstrating the parameter space for where a single wrapped Cauchy or wrapped normal is the favoured distribution for $\rho_1, \rho_2 \in [0, 1]$ calculated at 0.001 intervals with the mixing ratio $\omega \in [0, 0.5]$ at 0.05 intervals (due to symmetry the results for $\omega > 0.5$ are not displayed - see section 6.3.1). Areas in blue represent parameter combinations for which the wrapped Cauchy was favoured whereas areas of yellow/orange show combinations for which the wrapped normal was favoured. The darker the hue, the larger the difference between the distributions, indicating the favoured distribution was closer to the mixed distribution. The dashed black line indicates where the transition from preferred distribution occurs.

In general the plots remain almost unchanged across $0.35 \leq \omega \leq 0.5$ (Figs 6.1H-J). In particular, the areas of the plots above the lead diagonal (corresponding to $\rho_1 > \rho_2$) remain remarkably unchanged for $0.1 \leq \omega \leq 0.5$. However, as $\omega \rightarrow 0$ the area favouring the WC (blue) begins to vanish (demonstrated in Fig. 6.1B with $\omega = 0.05$) and disappears entirely when $\omega = 0$ (Fig 6.1A) due to the the definition of the mixed distribution, Θ (Eq. 6.3) ($\omega = 0$ is equivalent to $\Theta = f_2$ and since f_2 was chosen to be WN it will never be best classified as WC).

Considering now the areas of the plots below the lead diagonal (corresponding to $\rho_2 > \rho_1$), as ω decreases below 0.3 (Fig. 6.1A-G) the area favouring the WC shrinks and only exists for large values of ρ_2 (> 0.8). And for $\omega \leq 0.15$, corresponding to distributions where the majority of angles are drawn from the distribution with parameter ρ_2 , the plots indicate that there is no combination of parameters for which the WC will be favoured when $\rho_2 > \rho_1$ (Figs 6.1A-C).

6.5 Example: analysis of elephant movement

As an example of data which is well-fitted by a single WC and after a simple analysis appears to be better fitted by a mixed distribution, we use tracking data from bull African elephants *Loxodonta africana* previously published in Wall et al, (2014b). Here, location data were recorded for two elephants, we consider the data for the elephant id: *Habiba* which had locations recorded every 15 minutes for a period of over 4 days giving 1522 data points (data from Movebank data repository; Wall et al, 2014b). Visual inspection of the movement path (Fig. 6.2A) appears to show segments of high tortuosity where the movement path includes large variations in turning angles, along with periods of more straight-line behaviour with mainly small deviations in direction and fewer larger turns. Simply pooling the turning angles across the entire path gives the distribution shown in Fig. 6.2B. Using the standard practice of best fitting a WN and WC distribution using the packages in *R* (in this case *CircStats*) reveals that a WN (green, $\rho_{\text{wn}} = 0.3844, d_{\text{wn}} = 0.599$) is a poor fit, whereas a WC (blue, $\rho_{\text{wc}} = 0.4563, d_{\text{wc}} = 0.00506$) is a close fit, indicated by the respective L^2 values (Fig

6.2C). If instead, we assume turns are drawn from two distinct distributions, we can consider the observed data to be a mixed distribution (as in Eq. 6.3). Further assuming that the underlying distributions are WN, the best fitting mixed distribution can be found by simply comparing the density distribution of the observed data (calculated using the circular package in *R* (R Team, 2018) with all possible mixed distributions formed with parameters ρ_1, ρ_2, ω at 0.01 intervals, selecting the specific combination of parameters which minimises the L^2 distance. In this case we find that the best fitting mixed distribution is one with $\rho_1 = 0.24, \rho_2 = 0.84, \omega = 0.68$ giving $d_{\text{mix}} = 0.0004$ (Fig 6.2D). In calculating the continuous density curve for the discrete observed data, the histogram bandwidth used was the automatic selection from *R* as would be the case for a simple initial analysis, however, fixing this width at other values did not change the qualitative results.

When comparing this mixed distribution with the best fitting WC we see that both are close matches (Fig 6.2C & 6.2D), however, as the visual inspection of the movement path indicated more than one movement behaviour then one could conclude the mixed distribution is the better for describing the movement as it implies that the turning angles across the elephant's path came from two distinct distributions, with 32% of angles drawn from a highly peaked distribution and 68% from a flatter, more uniform distribution.

The possible presence of a mixed distribution could indicate two distinct movement behaviours over the path, with one behaviour admitting turning angles drawn from a distribution tightly peaked around 0 and the other behaviour with angles taken from a flatter distribution. However, it should be noted that one cannot use this analysis as a method of predicting such multiple state behaviour, as it provides no information of the movement state any given part of the path is likely to be in, neither does it provide a 'switching' parameter which determines the likelihood of switching between states; as is expected in behavioural state analyses although ω acts as a proxy for this (Johnson et al, 2008; Patterson et al, 2009; Parton & Blackwell, 2017; McClintock & Michelot, 2018). Similarly, it does not consider any other covariates or parameters of the movement path

typically used in CRW movement models, such as step-length or bout distribution, nor any correlation between these parameters (i.e. having smaller step lengths when the variation in turning angle is large and vice-versa).

A method of analysis which does consider switching parameters and other covariates to predict behavioural states is the *momentuHMM* package in *R* which was introduced in McClintock & Michelot (2018) and used to analyse the companion elephant dataset from Wall et al (2014a)). The results found by applying this analysis to these data gives the best-fitting mixed distribution formed from WN distributions to be one with concentration parameters $\rho_1 = 0.11, \rho_2 = 0.80$ and a mixing parameter of $\omega = 0.56$ (The package requires using von Mises rather than WN distributions, however, as has been discussed these distributions are known to be similar).

Whilst the results found considering a mixed distribution and those found using the *momentuHMM* package are qualitatively similar, they are not equivalent since the HMM method of McClintock & Michelot (2018) specifically attempts to identify periods of distinct behaviour taking into account various aspects of the movement path, whereas, our results simply looked for the distribution which best described the distribution of turning angles. The observation that the outcomes are similar indicates that this analysis on the distribution of turning angles can give credible results for the underlying distribution and demonstrates that multiple movement behaviours can lead to artificial heavy tails in turning angle distributions. Also, in the specific case where HMM techniques wish to be used to analyse movement behaviour, using the naive approach to get an initial parameter selection for the concentration and switching parameters could be beneficial due to HMMs sensitivity to the set of initial conditions.

6.6 Discussion

Accurately identifying parameters of movement models is clearly crucial when analysing, predicting and understanding animal behaviour. Identifying the most accurate distribution in turning angles is important as differing distributions can result in noticeably different predictive outcomes (Bartumeus, 2008; Codling et al, 2010). In movement data

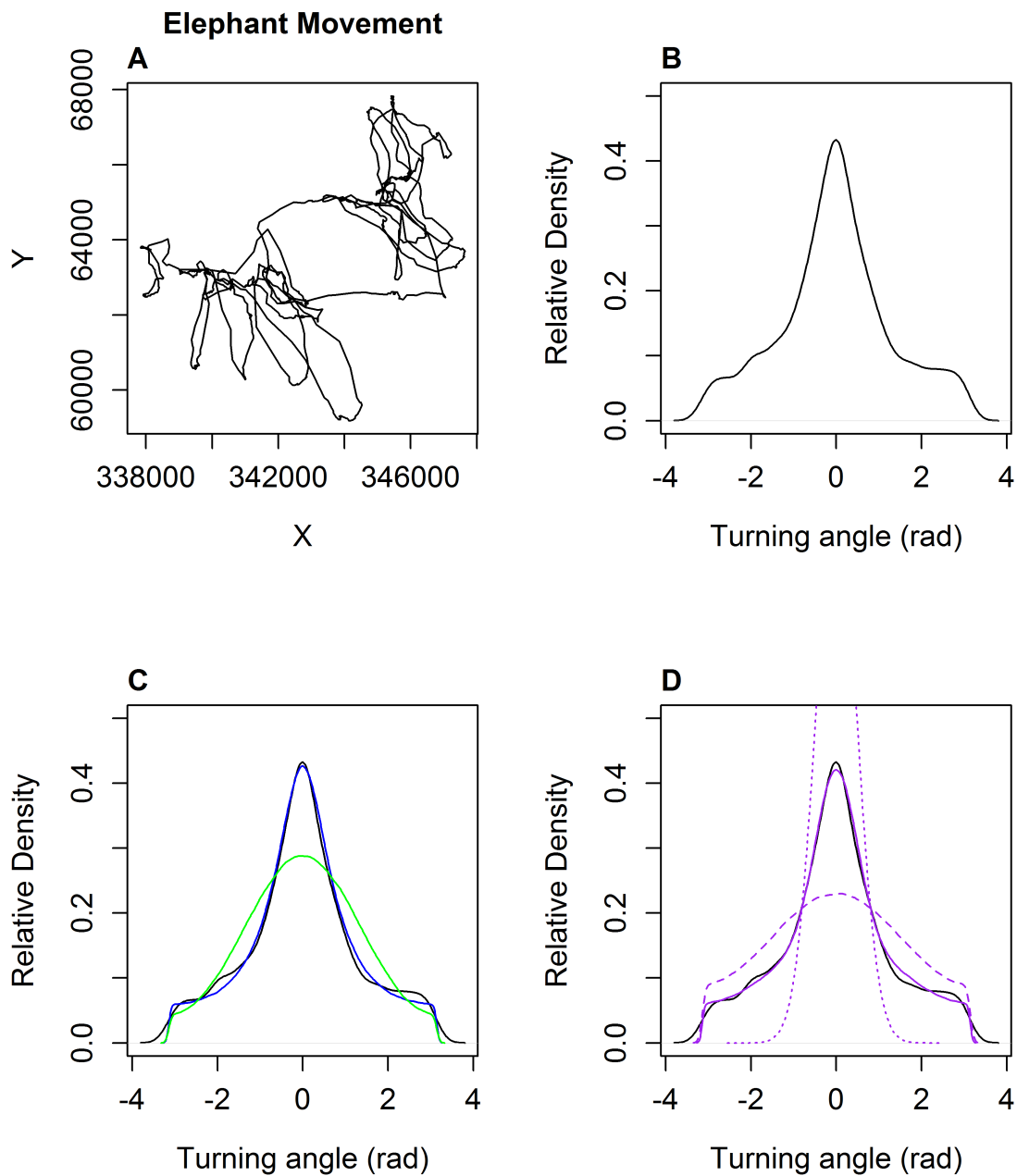


Figure 6.2: Movement data analysis of African elephant (ID: *Habiba*) from Wall et al (2014a). (A) shows the movement path recorded at 15 minute time intervals across a 4 day period (1522 data points); (B) is the corresponding turning angle distribution. (C) shows the best fitting wrapped Cauchy distribution (blue; $\rho_{wc} = 0.4563$) and best fitting wrapped normal (green; $\rho_{wn} = 0.3844$), visual inspection indicates that the wrapped Cauchy is the closer fitting distribution and the total variance distance measure confirms this. (D) shows the best fitting mixed distribution (purple solid) determined by numerical simulations with parameters $\rho_1 = 0.22, \rho_2 = 0.89, \omega = 0.68$. Purple dashed line corresponds to a wrapped normal with concentration parameter ρ_1 and the purple dotted line corresponds to a wrapped normal with concentration parameter ρ_2 . Comparing the actual data distribution (black; B) with the best fitting wrapped distribution (blue; C) and the mixed distribution (purple; D) shows both are good fits however, the total variance distance determines between them favouring the mixed distribution ($TV_{mix} = 1.201$ for mixed dist; $TV_{wc} = 1.720$ for wrapped Cauchy)

analyses it is often assumed that angles are drawn from a single underlying distribution, here we have demonstrated the parameter space for when a mixed distribution can be best described by a single distribution with either a normal type, WN, or a heavy tailed distribution, WC; two distributions commonly associated with the analysis of directional movement.

Our results indicate that a mixed distribution formed from two WN distributions will, in general, be best fitted by a WC distribution when the difference between the concentration parameters of the underlying initial WN distributions is large ($|\rho_1 - \rho_2| \geq 0.5$). This has been reported when analysing and classifying animal movement behaviour into two movement states, such as “foraging” and “exploratory” (Langrock et al, 2014; McClintock et al, 2018) The characteristic distributions found in such movement include a flat almost uniform distribution attributed to the “foraging” stage, and would be equivalent to a low concentration parameter in a SWS distribution, along with another much more peaked distribution for the “exploratory” phase, given by a distribution with a concentration parameter close to 1. Evidence of such results after model fitting have been observed in a range of animals including American lobster, *Homarus americanus*, (Bowly et al, 2007), African elephants (McClintock & Michelot, 2018), *Cataglyphis* desert ants (Dahmen et al, 2017) and elk, *C. elaphus*, (Parton & Blackwell, 2017). Specifically, Langrock et al (2014), found that reindeer in a 2 state model exhibited angular distributions described by a von Mises distribution with $\kappa = 0.246$ (approximately equivalent to a WN with $\rho = 0.1218$) for the “foraging” behaviour and $\kappa = 3.517$ (approximately equivalent to a WN with $\rho = 0.8389$) for the “exploratory” behaviour.

That this relatively straight forward approach of analysing movement data revealed results consistent with those using more complex methods is interesting as it relies solely on the angular data. However, as it gives no information as to which distribution any particular part of the movement path belongs, it cannot be used as an indicator of periods of behaviour. Discovering when a period of movement comes from a particular state with prescribed model and parameter set is an active area of research, and as such there has been much work on behavioural change point analysis (BCPA) utilising

a range of methods from hidden Markov models (HMMs) (Michelot et al, 2016; Jonsen et al, 2016; McClintock & Michelot, 2018) and Markov chain Monte Carlo processes (McClintock et al, 2012; Parton & Blackwell, 2017), to wavelet analysis (Polansky et al, 2010) and time series CUSUM techniques (Knell & Codling, 2012) (see Gurarie et al (2016), for a more complete list). Currently the analysis described here may be used to predict the values of the initial distributions required in HMM techniques (Michelot et al, 2016; Jonsen et al, 2016; McClintock & Michelot, 2018), but could also be extended to predict breaks in behaviour by including additional ‘smoothing’ techniques in order to ascertain when a change from using one distribution to another has occurred, most likely utilising a time-series break point analysis such as that used in Knell & Codling (2012). For this to be the case, many improvements would be needed in the method for finding the ρ_1, ρ_2, w parameters, for example a more efficient search algorithm, such as Nelder-Mead (Nelder & Mead, 1965) could be used rather than the slow parameter sweep method used here in section 6.5.

There are many other potential avenues for enhancing and extending the work shown here, for example, this method could be extended to mixing more than two normal distributions by simply including more ρ_i and mixing ratio terms in the summation for the mixed distribution and editing the subsequent calculations appropriately. However, interpreting the results obviously increases in difficulty due to the increasing dimension of the required parameter space. It should be noted that Jammalamadaka & Kozubowski (2017) have shown that a WC distribution can in fact be recovered precisely when one considers mixing an infinite number of WN distributions and therefore taking the mixture distribution as a continuous function across all possible concentration parameter values in $[0, 1]$ for the initial WN distributions.

Whilst we chose to focus on two particular distributions, other wrapped distributions such as wrapped Gompertz and the wrapped exponential have also been used to describe animal movement (Roy & Adnan, 2012; Ravindran & Ghosh, 2011) and could be included in a more complete analysis. Similarly, families of distributions on the unit circle exist such as the Jones-Pewsey (Jones & Pewsey, 2005), Kato-Jones (Kato & Jones, 2013) and

wrapped t (Pewsey et al, 2007) all of which contain the wrapped normal and Cauchy distributions as special cases and could have been considered. However, these are all multi-parameter distributions and as such can prove computationally harder to fit to actual data. Since our main aim here is to illustrate a possible mechanism for how heavy tailed distributions, such as the wrapped Cauchy, may (incorrectly) emerge in observed directional data, a full and complete classification of mixed circular distributions along with their combinations is beyond the scope of this work.

6.7 Conclusions

- We have shown that a distribution formed by mixing two wrapped normal distributions can have the appearance of a single heavy tailed distribution, especially when the underlying wrapped normal distributions have a large difference in their concentration parameters.
- This indicates that when analysing circular data, care must be taken if the simplest approach of best-fitting a single distribution is used as this can give unreliable results and miss important details of the underlying process which produced the data.
- It was shown that in certain circumstances the two underlying distributions in the mixed distribution can be attached to specific behaviours in animal movement and therefore, the presence of a heavy tailed distribution can (on occasion) be an indicator that there may be more complex behaviour occurring across a movement path.
- This multiple behaviour was demonstrated by using data from an Elephant's movement path (Wall et al, 2014a), which showed that by a simple analysis of the turning angles in a movement path, a mixed distribution of two distinct normal-type distributions best-fit the data, compared to a single distribution. This agreed with the findings of more advanced statistical methods, which attributed each distribution to a specific movement behaviour.

- That a simple analysis based purely on the distribution of turning angles corresponded with the findings of more advanced statistical analyses, indicates that this finding could potentially lead to a method for deciphering movement behaviours from animal paths, or help to improve upon those complex methods already in place.

6.8 Appendices

6.8.1 Appendix C1 - Alternative methods of calculating the distance between two PDFs

Here we consider how using alternative methods of calculating the distance between two PDFs compares to the use of the L^2 distance which was used throughout the main text (Section 6.2.3). We demonstrate that the results are qualitatively similar to those found by using the L^2 distance and therefore conclude that the choice of the L^2 distance does not affect the results found.

The distances used to compare with the results from the main text were the Kullback-Leibler (similar to the Jensen-Shannon), the Wasserstein and the Bhattacharyya (equivalent to the Hellinger distance); there are many other distance metrics which could be considered (see Gibbs & Su (2002) and *philentropy* package (Drost, 2018) in *R*, for a more in depth list).

In order to compare results across the different distance metrics, the parameter space for which a mixed distribution was best fit by either a WC or WN was calculated by numerical simulations rather than by a derived analytical expression as was found in the main text. For each of the three extra distance metrics, this parameter space was found by the following process:

- For each individual distance metric, a mixed distribution, formed with parameters ρ_1, ρ_2, ω , was considered.
- The best fitting WN distribution was then found by comparing the PDF of the mixed distribution with the PDFs of WN distributions with concentration parameters, ρ_{wn} , ranging from 0 to 1 at 0.001 intervals and the distances between them calculated using the *distance* function in the *philentropy* package in *R*. The concentration parameter which minimised the distance was then chosen as the best fitting WN distribution.
- This was repeated with a WC in place of the WN to find the best fitting WC

distribution.

- The distance between the best fitting WN and the mixed distribution, d_{wn} , was compared with the distance between the best fitting WC and mixed distribution, d_{wc} , with the smaller value giving the best fitting single distribution.
- The value,

$$\tilde{D} = d_{\text{wc}} - d_{\text{wn}}$$

was then calculated, with negative values indicating areas where the WC was favoured and positive values indicating where the WN was favoured.

- This was repeated across all combinations of the mixed distribution parameters ρ_1, ρ_2, ω

The results of plotting \tilde{D} using the Bhattacharyya, Kullback-Leibler and Wasserstein distances against the parameters of the mixed distribution are shown in Figs 6.3-6.5 respectively. Areas of blue indicate where the WC was found to be the best fitting distribution and yellow indicate areas where the WN was the better fitting. Here, values for the concentration parameters of the mixed distribution, ρ_1, ρ_2 , were calculated from 0 to 1 at 0.01 intervals with the mixing parameter, ω , taking values from 0 to 0.5 at 0.05 intervals.

Comparing Fig. 6.3-6.5 we can see that they are similar although with a few clear discrepancies, indicating that there is little difference between using any of these three distance metrics. Comparing these to Fig. 6.1 from the main text shows that the results are qualitatively similar and quantitatively similar, allowing us to conclude that the specific distance metric used in the computation of the distance between PDFs does not affect the results and hence, our use of the L^2 distance in the main text does not affect the results found.

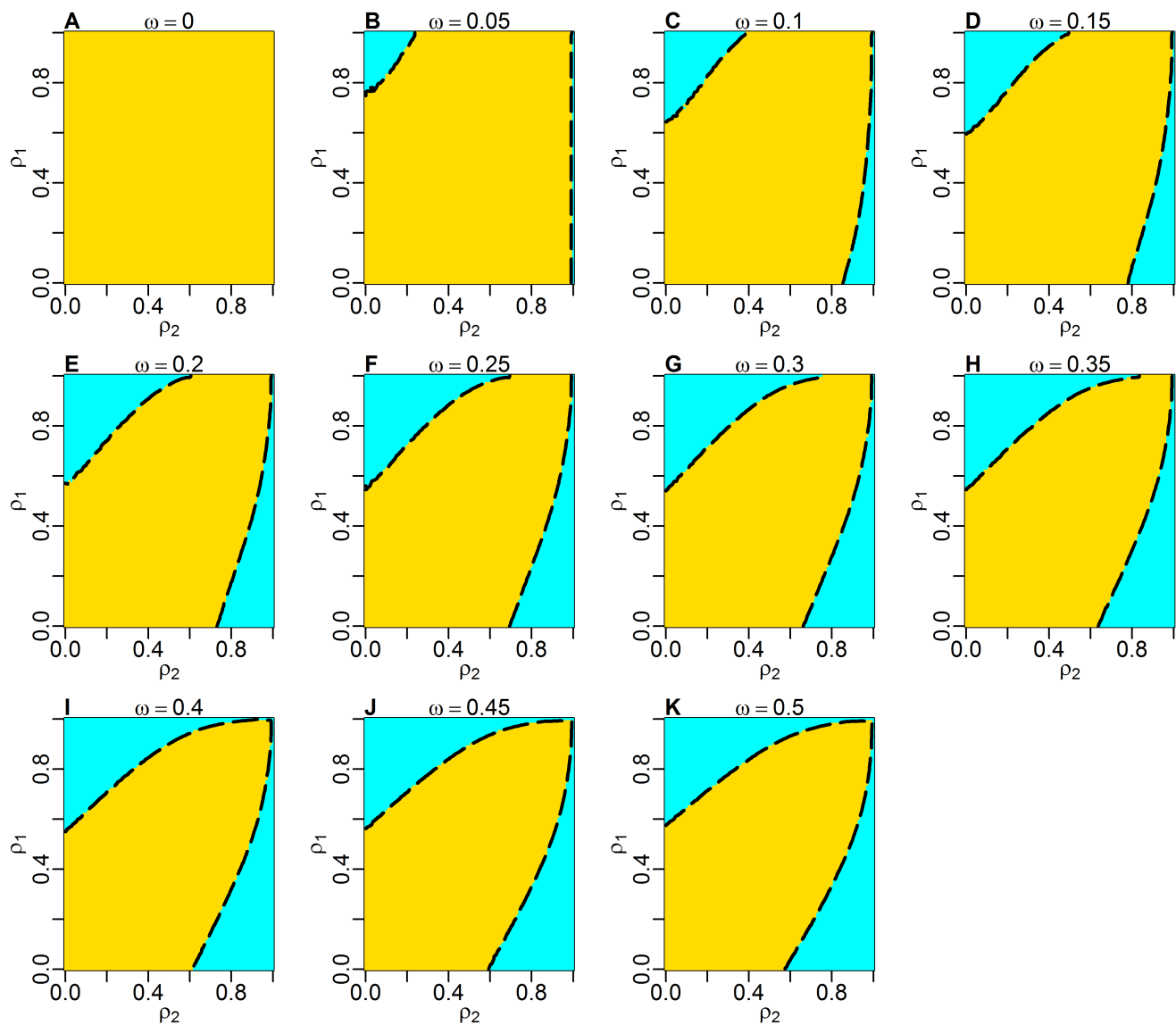


Figure 6.3: Indicating the parameter space for whether a wrapped normal (yellow) or wrapped Cauchy (blue) was considered the closer fitting distribution when compared to a mixed distribution formed of two wrapped normal's with concentration parameters ρ_1 (y-axis) and ρ_2 (x-axis) using the *Bhattacharyya metric*

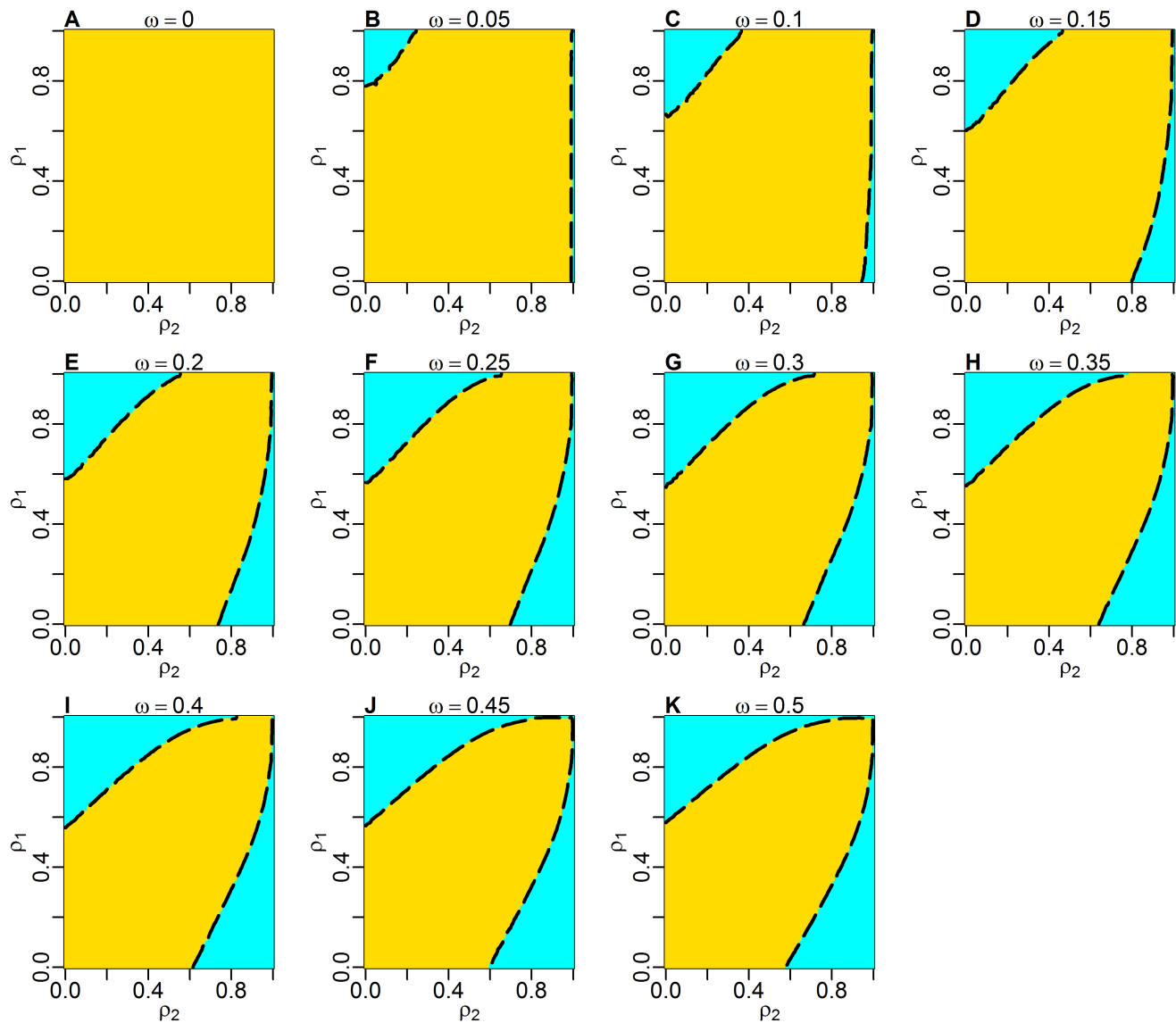


Figure 6.4: Indicating the parameter space for whether a wrapped normal (yellow) or wrapped Cauchy (blue) was considered the closer fitting distribution when compared to a mixed distribution formed of two wrapped normal's with concentration parameters ρ_1 (y-axis) and ρ_2 (x-axis) using the *Kullback-Leibler metric*

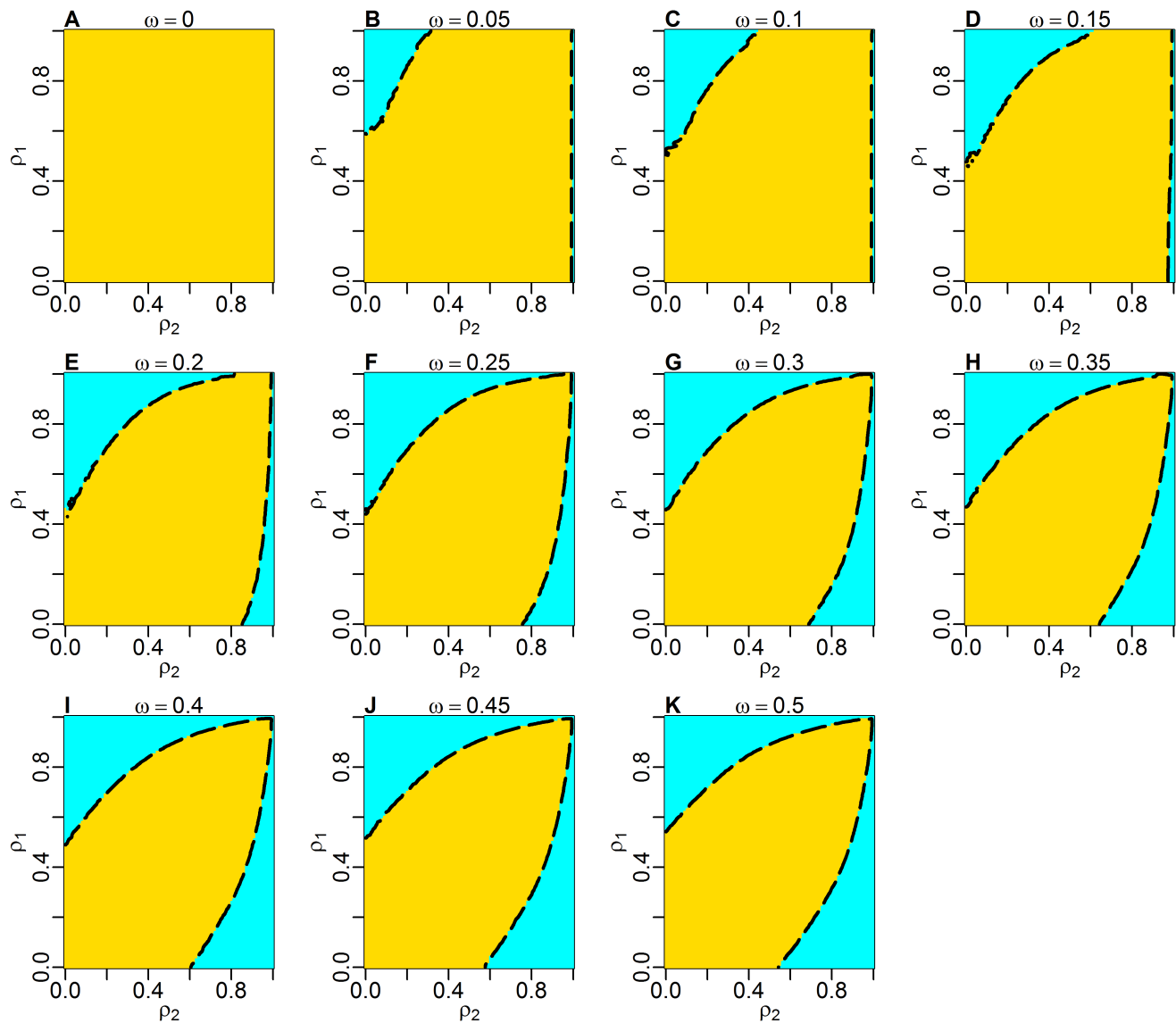


Figure 6.5: Indicating the parameter space for whether a wrapped normal (yellow) or wrapped Cauchy (blue) was considered the closer fitting distribution when compared to a mixed distribution formed of two wrapped normal's with concentration parameters ρ_1 (y-axis) and ρ_2 (x-axis) using the *Wasserstein metric*

6.8.2 Appendix C2 - Considering mixed distributions formed from (i) two wrapped Cauchy distributions; (ii) a wrapped Cauchy and a wrapped normal distribution

(i) Considering a mixed distribution formed from two wrapped Cauchy distributions

Here we consider how forming the mixed distribution given in Prop. 1 in the main text, from two WC distributions effects the results.

If we consider the mixed distribution given in Prop. 1 to be formed of two wrapped Cauchy distributions, we have

$$\tilde{\Theta}(\theta; \mu_0, \rho_1, \rho_2, \omega) = \omega f_{wc}(\theta; \mu_0, \rho_1) + (1 - \omega) f_{wc}(\theta; \mu_0, \rho_2) \quad (6.9)$$

for $-\pi < \theta \leq \pi$, with $\mu_0 \in [-\pi, \pi)$ and $\rho_1, \rho_2 \in [0, 1]$. Following the exact arguments from the main paper except now with $\alpha_p^{\{1\}} = \rho_1^n$ and $\alpha_p^{\{2\}} = \rho_2^n$, (see section 6.2.1) we get the amended expressions for S_{wc}, S_{wn}

$$\tilde{S}_{wc}(\rho, 0) = \sum_{n=1}^{\infty} [\rho^n - (\omega \rho_1^n + (1 - \omega) \rho_2^n)]^2 \quad (6.10)$$

$$\tilde{S}_{wn}(\rho, 0) = \sum_{n=1}^{\infty} [\rho^{n^2} - (\omega \rho_1^n + (1 - \omega) \rho_2^n)]^2 \quad (6.11)$$

and hence,

$$0 = \tilde{S}'_{wc} = \frac{d}{d\rho} S_{wc} = \sum_{n=1}^{\infty} 2p\rho^{n-1} [\rho^n - (\omega \rho_1^n + (1 - \omega) \rho_2^n)] \quad (6.12)$$

$$0 = \tilde{S}'_{wn} = \frac{d}{d\rho} S_{wn} = \sum_{n=1}^{\infty} 2p^2 \rho^{n^2-1} [\rho^{n^2} - (\omega \rho_1^n + (1 - \omega) \rho_2^n)] \quad (6.13)$$

Denoting the roots for Eq. 6.12 & 6.13 as $\tilde{\rho}_{wc}, \tilde{\rho}_{wn}$ and substituting these into Eq. 6.10 & 6.11 respectively gives the values of the distance between $\tilde{\Theta}$ and the best fitting wrapped Cauchy and wrapped normal distribution respectively.

As in the main text, we can calculate the value of

$$\tilde{D}_{\tilde{\mathcal{S}}} = \tilde{S}_{wc}(\rho_{wc}, 0) - \tilde{S}_{wn}(\rho_{wn}, 0) \quad (6.14)$$

across the parameter space for ρ_1, ρ_2, ω and plot the results (Fig. 6.6).

Similar to Fig. 6.1 in the main text, areas in blue represent a negative value for Eq. 6.14, corresponding to the WC distribution being the closer fit to the mixed distribution, $\tilde{\Theta}$, and places in yellow corresponding to the WN distribution being closer. The lighter the colour the smaller the magnitude of \tilde{D} . Fig. 6.6 shows only areas of blue and therefore, the WC was always the preferred distribution regardless of the parameter values.

These results show that in considering a mixed distribution consisting of two WC distributions, the single distribution which best describes this mixed distribution will always be a WC.

(ii) Considering a mixed distribution formed from one wrapped normal and one wrapped Cauchy distributions

We can also consider the case for the mixed distribution being formed of one wrapped Cauchy and one wrapped normal. Following the same method as described above and in the main text (Section 6.3.2) we can calculate the parameter space for which a WC will be the favoured distribution. The results for these cases are shown in (Fig. 6.7), and as expected lie in between the initial case with the mixed distribution formed from two wrapped normal distributions (Fig. 6.1) and the case with the mixed distribution formed from two wrapped Cauchy distributions (Fig. 6.6).

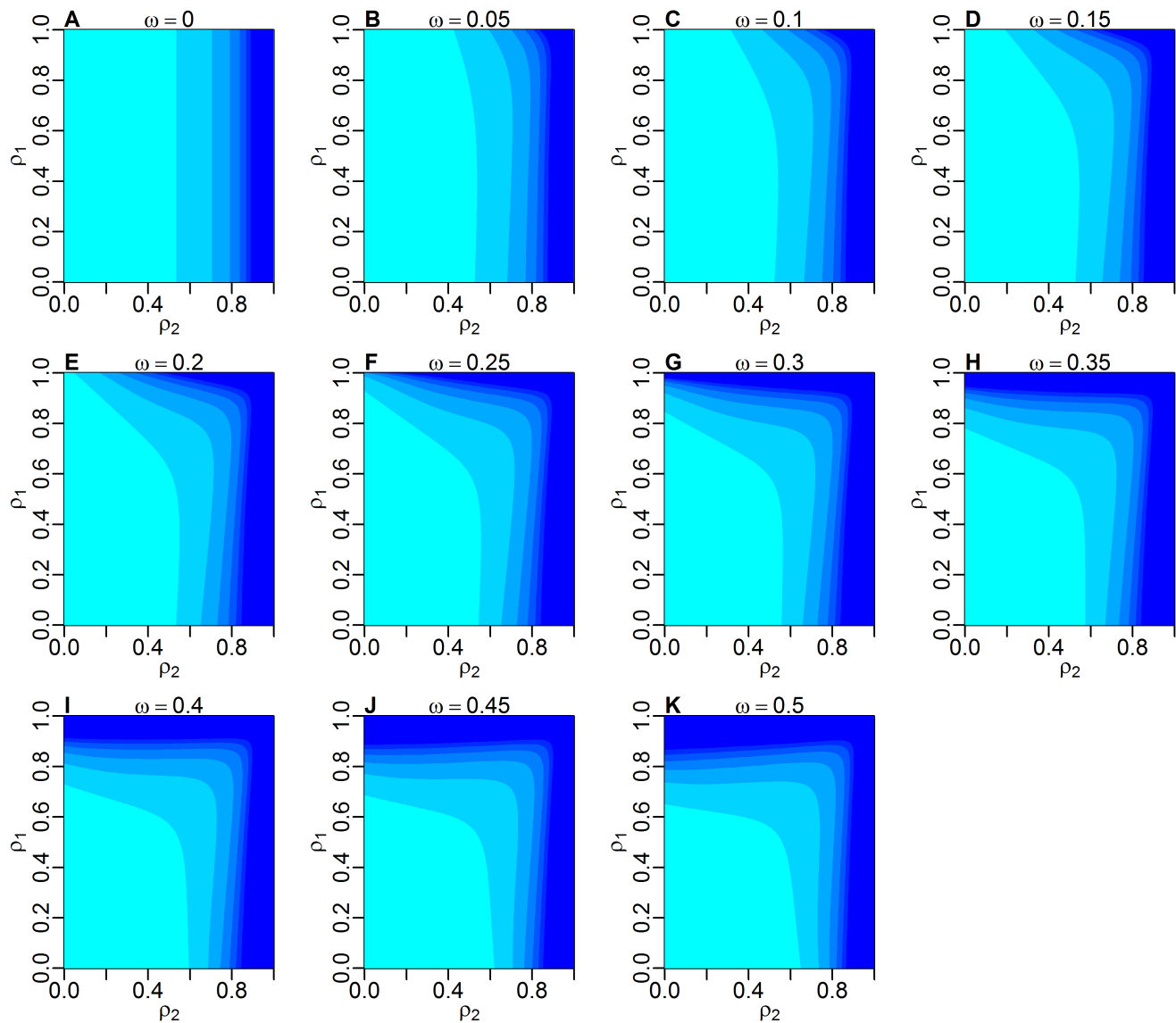


Figure 6.6: Similar to Fig. 6.1 except the mixed distribution is formed from two WC distributions. Plots were calculated for $\rho_1, \rho_2 \in [0, 1]$ at 0.001 intervals with the mixing ratio $\omega \in [0, 0.5]$ at 0.05 intervals (due to symmetry the results for $\omega > 0.5$ are not displayed - see section 6.3.1) Areas in blue represent parameter values for which a single WC was the favoured distribution and areas of yellow would indicate values for which a WN was the favoured distribution, however, the results indicate that the WN is never the favoured distribution in this case.

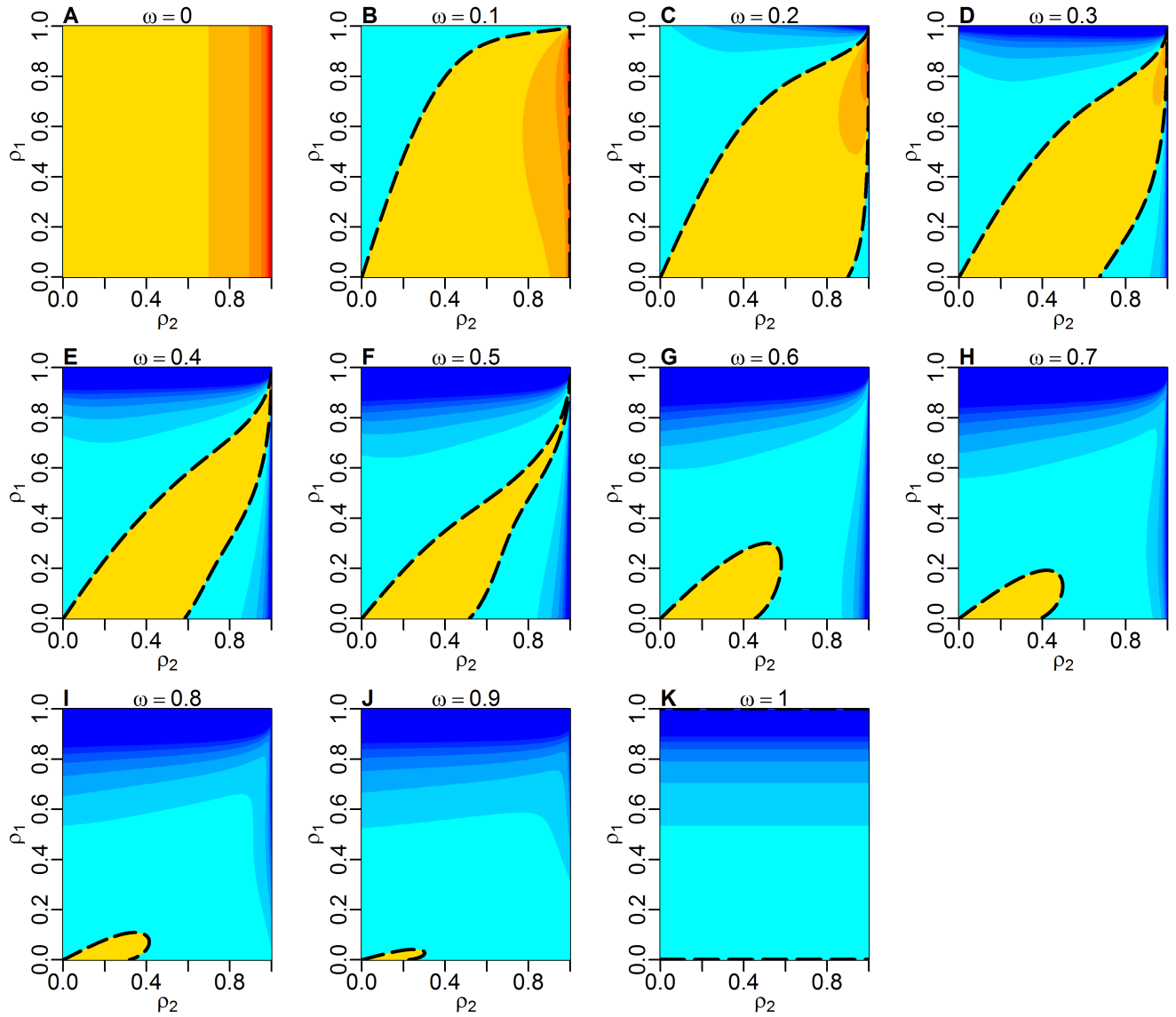


Figure 6.7: Similar to Fig. 6.1 & 6.6 except the mixed distribution is formed from one WN and one WC distribution. Plots were calculated for $\rho_1, \rho_2 \in [0, 1]$ at 0.001 intervals with the mixing ratio $\omega \in [0, 1]$ at 0.1 intervals (unlike Figs. 6.1 & 6.6 the results for $\omega > 0.5$ are displayed as the mixed distribution is formed from distributions from different families - see section 6.3.1) Areas in blue represent parameter values for which a single WC was the favoured distribution and areas of yellow would indicate values for which a WN was the favoured distribution, however, the results indicate that the WN is never the favoured distribution in this case.

6.8.3 Appendix C – Detailed Proof of Lemma 2 from the Main Text

Lemma 3. Let $f_1(\theta)$ and $f_2(\theta)$ be SWS distributions centred around 0 with cosine moments α_n^1 and α_n^2 respectively, then

$$d(f_1, f_2) = \frac{1}{\pi} \sum_{n=1}^{\infty} (\alpha_n^1 - \alpha_n^2)^2 \quad (6.15)$$

Proof. As $f_1(\theta)$ and $f_2(\theta)$ are zero-centred SWS distributions, the square of the difference between the distributions at any given value of $\theta \in [-\pi, \pi)$ is given by

$$\begin{aligned} [f_1(\theta) - f_2(\theta)]^2 &= \left[\frac{1}{2\pi} \left(1 + 2 \sum_{n=1}^{\infty} \alpha_n^{\{1\}} \cos(n\theta) \right) - \frac{1}{2\pi} \left(1 + 2 \sum_{n=1}^{\infty} \alpha_n^{\{2\}} \cos(n\theta) \right) \right]^2 \\ &= \left[\frac{1}{\pi} \sum_{n=1}^{\infty} (\alpha_n^{\{1\}} - \alpha_n^{\{2\}}) \cos(n\theta) \right]^2 \end{aligned}$$

integrating over $[-\pi, \pi)$ with respect to θ gives

$$\begin{aligned} \int_{-\pi}^{\pi} [f_1(\theta) - f_2(\theta)]^2 d\theta &= \int_{-\pi}^{\pi} \frac{1}{\pi} \left[\sum_{n=1}^{\infty} \alpha_n^1 - \alpha_n^2 \cos(n\theta) \right]^2 d\theta \\ &= \frac{1}{\pi^2} \int_{-\pi}^{\pi} \left[\sum_{n=1}^{\infty} (\alpha_n^{\{1\}} - \alpha_n^{\{2\}})^2 \cos^2(n\theta) \right. \\ &\quad \left. + 2 \sum_{i=1}^{\infty} \sum_{j=i+1}^{\infty} (\alpha_i^{\{1\}} - \alpha_i^{\{2\}}) (\alpha_j^{\{1\}} - \alpha_j^{\{2\}}) \cos(i\theta) \cos(j\theta) \right] d\theta \end{aligned}$$

Here we note that as $(\alpha_n^1 - \alpha_n^2)^2 \cos^2(n\theta)$ is non-negative for all n then by Fubini-Tonelli we can interchange the integral and summation in the first term. To show we can similarly interchange the integral and summations in the second term we will show that the expression is absolutely finite.

Considering the expression in the second term in an absolute form, we have

$$\begin{aligned}
& \sum_{i=1}^{\infty} \sum_{j=i+1}^{\infty} \left| \left(\alpha_i^{\{1\}} - \alpha_i^{\{2\}} \right) \left(\alpha_j^{\{1\}} - \alpha_j^{\{2\}} \right) \cos(i\theta) \cos(j\theta) \right| \\
& \leq \sum_{i=1}^{\infty} \sum_{j=i+1}^{\infty} \left| \left(\alpha_i^{\{1\}} - \alpha_i^{\{2\}} \right) \left(\alpha_j^{\{1\}} - \alpha_j^{\{2\}} \right) \right| \\
& = \sum_{i=1}^{\infty} \sum_{j=i+1}^{\infty} \left| \left(\alpha_i^{\{1\}} - \alpha_i^{\{2\}} \right) \right| \left| \left(\alpha_j^{\{1\}} - \alpha_j^{\{2\}} \right) \right| \\
& = \sum_{i=1}^{\infty} \left| \left(\alpha_i^{\{1\}} - \alpha_i^{\{2\}} \right) \right| \sum_{j=i+1}^{\infty} \left| \left(\alpha_j^{\{1\}} - \alpha_j^{\{2\}} \right) \right| \\
& \leq \sum_{i=1}^{\infty} \left| \left(\alpha_i^{\{1\}} - \alpha_i^{\{2\}} \right) \right| \sum_{j=1}^{\infty} \left| \left(\alpha_j^{\{1\}} - \alpha_j^{\{2\}} \right) \right|
\end{aligned}$$

here we note that as the series of $\alpha_j^{\{1\}}$ corresponds to the trigonometric moments of distribution $f_1(\theta)$ and similar for $\alpha_j^{\{2\}}$ and $f_2(\theta)$ with both distributions being stable and finite across their domains then the sum of the trigonometric moments must be finite (see Eq. 6.1 in Main Text), and hence, the absolute difference between the sums of the trigonometric moments of two distributions must also be finite. Therefore we have that

$$\sum_{j=1}^{\infty} \left| \left(\alpha_j^{\{1\}} - \alpha_j^{\{2\}} \right) \right| < K$$

Where K is some finite real value. Therefore we now have

$$\begin{aligned}
\sum_{i=1}^{\infty} \left| \left(\alpha_i^{\{1\}} - \alpha_i^{\{2\}} \right) \right| \sum_{j=1}^{\infty} \left| \left(\alpha_j^{\{1\}} - \alpha_j^{\{2\}} \right) \right| & \leq \sum_{i=1}^{\infty} K \left| \left(\alpha_i^{\{1\}} - \alpha_i^{\{2\}} \right) \right| \\
& = K \sum_{i=1}^{\infty} \left| \left(\alpha_i^{\{1\}} - \alpha_i^{\{2\}} \right) \right|
\end{aligned}$$

Using the same argument as before we must have that $\sum_{i=1}^{\infty} \left| \left(\alpha_i^{\{1\}} - \alpha_i^{\{2\}} \right) \right| < K$ and hence

$$K \sum_{i=1}^{\infty} \left| \left(\alpha_i^{\{1\}} - \alpha_i^{\{2\}} \right) \right| \leq K \cdot K = K^2 < \infty$$

Therefore as $\left| \left(\alpha_i^{\{1\}} - \alpha_i^{\{2\}} \right) \left(\alpha_j^{\{1\}} - \alpha_j^{\{2\}} \right) \cos(i\theta) \cos(j\theta) \right|$ is finite across the entire summation we can interchange the summations and integrals by Fubini-Tonelli. Giving Eq. 6.16

now as

$$\begin{aligned}
&= \frac{1}{\pi^2} \left[\sum_{n=1}^{\infty} (\alpha_n^{\{1\}} - \alpha_n^{\{2\}})^2 \int_{-\pi}^{\pi} \cos^2(n\theta) \, d\theta \right. \\
&\quad \left. + 2 \sum_{i=1}^{\infty} \sum_{j=i+1}^{\infty} (\alpha_i^{\{1\}} - \alpha_i^{\{2\}}) (\alpha_j^{\{1\}} - \alpha_j^{\{2\}}) \int_{-\pi}^{\pi} \cos(i\theta) \cos(j\theta) \, d\theta \right] \\
&= \frac{1}{\pi^2} \left[\sum_{n=1}^{\infty} (\alpha_n^1 - \alpha_n^2)^2 \left(\frac{\sin(2n\pi)}{2n} + \pi \right) \right. \\
&\quad \left. + 2 \sum_{i=1}^{\infty} \sum_{j=i+1}^{\infty} (\alpha_i^1 - \alpha_i^2) (\alpha_j^1 - \alpha_j^2) \left(\frac{2i \sin(i\pi) \cos(j\pi) - 2j \cos(i\pi) \sin(j\pi)}{i^2 - j^2} \right) \right]
\end{aligned}$$

Noting that as n, i and j are positive integers all the sin terms in the above expression are 0 and hence, this reduces to

$$\frac{1}{\pi} \sum_{n=1}^{\infty} (\alpha_n^{\{1\}} - \alpha_n^2)^2$$

as required

7 Intraspecific movement specialisations and their implications for ‘personality’ and movement ecology research

This is joint work with A King, A Short, G Johns and I Fürtbauer (Swansea University). Experimental setup and procurement of data was conducted by A Short, G Johns and A King.

In this chapter we consider how consistency in individual behaviour can affect population-level movement dynamics by observing the movement of a sample population of stickleback fish, *Gastro aculealus*, in response to changes in the number of objects present in an otherwise featureless experimental environment. We will show that individuality has a more significant impact in movement behaviour than the changes in environment although there was evidence to suggest individuals became more active as the environment became increasingly filled with objects. We demonstrate how a simple CRW model of individual movement can give reasonable approximations for the population level movement dynamics when a parameter controlling the proportion of time spent stationary is included.

7.1 Introduction

As has been highlighted in previous chapters understanding and predicting animal space use is central in ecological research (Nathan et al, 2008) as it leads to a better understanding of the effect of important ecological phenomena such as climate and landscape change (Kanagaraj et al, 2013), biological invasions and species management (Barton et al, 2015; Westley et al, 2018) as well as the control of pests and diseases (Fofana & Hurford, 2017; Dougherty et al, 2018; Petrovskii et al, 2014).

In previous chapters we have assumed movement is through homogeneous environments with one model sufficient to describe all individuals within a given population. In

the case for heterogeneous environments, it is common that the parameters of the model might vary due to the characteristics of the environment but the underlying model is assumed constant across individuals within the population, a simplification which is often used in modelling movement ecology (Fofana & Hurford, 2017; Moorcroft, 2012; Reynolds, 2014; Grunbaum, 1998). However, these assumptions do not hold in general as environments are rarely homogeneous and featureless, with animals frequently passing through changing landscapes, resulting in possible differing movement strategies dependent upon a given spatial location (Ben-Ari & Inbar, 2014; Hopkins, 2016; Lemasson et al, 2009). Similarly, assuming that every individual within a population utilises precisely the same movement strategy incorporating the same parameter values (e.g. when modelling using a step-turn process assuming fixed values for parameters describing step length distribution and turning angle distribution) is naive and has been shown to not reflect true animal movement in general (Herbert-Read et al, 2013; Herborn et al, 2010; King et al, 2013). Clearly, in trying to predict population level movement dynamics and attempting to understand the patterns found in ecological movement processes one must take into account the within- and between- individual variation (Morales & Ellner, 2002; Spiegel et al, 2017; Getz et al, 2018; Sih et al, 2018; Belgrand & Griffen, 2018; Dingemanse & Dochtermann 2013) as well as the effect of the spatial structure and features of the landscape (Sueur et al, 2011; Lima & Zollner, 1996; With et al, 1999).

Interpreting the effects of individual differences on movement at the population level has an established history, with much work in the last 15-20 years focusing on the role of animal ‘personality’. Personality refers to behaviour of individuals which is consistent across time and ecological contexts and has been used to help answer the question as to why individuals differ consistently in various behaviours (Winanady & Denoel, 2015; Biro & Stamps, 2008; Carter et al, 2013; Sih et al 2012; Sih et al 2004; Dall et al 2004; Sih & Bell 2008; Fürtbauer et al 2015). Traits which are attributed to personality cover behaviours such as boldness/shyness, activity and aggression (Carter et al 2013), and have clear impacts upon the movement behaviour of individuals. Personality has been empirically demonstrated as having a clear effect upon the spatial dynamics of

individual movement (Spiegel et al, 2017; Cote et al, 2010), despite this, the integration of individual personality and movement ecology has yet to be fully achieved (Spiegel et al, 2017; Nilsson et al, 2014). Therefore, understanding the spread of individuality across a population must be taken into account when analysing data from a sample population in order to correctly infer entire population level movement dynamics.

Personality can arise as a genetic effect or can be the result of developmental plasticity where phenotypic changes in juvenile stage of development, due to local environment, remain constant into adulthood (Del Giudice, 2015). Understanding the concept of personality in a mathematical manner is a non-trivial task as measuring the ‘amount’ of variation in behaviour which is caused by the influence of the local environment compared to that of a personality is non-trivial (Dochtermann et al, 2015). Similarly attempting to discern how personality is formed requires this variation to be further split by the influences of genetic effects as well as physical traits of the individual such as age, size and sex. There are however many benefits to such a mathematical description of personality as it allows questions around individual variation (such as repeatability and statistical significance) to be tested by established and powerful statistical techniques (Koski, 2011). Because of this, individual variation and therefore personality is often quantified in terms of ‘repeatability’ (Dingemanse et al, 2012; King et al, 2013, 2015; Fürtbauer et al, 2015; Sih et al, 2018). This quantitative framing of personality allows for statistical and mathematical approaches to analysing evidence of personality, as well helping to frame questions of personality in other biological fields such as evolutionary ecology and evolutionary theory, where the concept of repeatability has an established history (Dingemanse & Dochtermann, 2013; Penke et al, 2007). For this reason we will consider that personality can be considered by the individual variance found in any measurable quantity.

Here, we assess whether (i) changes in environmental features, and (ii) fish identity, explain variation in the movement of stickleback fish (*Gastro aculeatus*). 15 fish were observed in three different environments (two, three or five plastic plants), across two experimental runs. Video tracking software was used to generate coordinates for indi-



Figure 7.1: Adult *Gasterosteus aculeatus* (Offermans, 2004)

viduals, at a rate of 25Hz for a total of 10 minutes. This simple set-up provides sufficient control for repetitive observations, and brings ecological realism without confounding factors. We find that individual fish show highly repeatable movement and show that fish identity, not environment, explained the variation in fish movement. However, as more objects were included in the environment all fish were seen to decrease the amount of time spent stationary. A simple CRW movement model (informed by our data) which explicitly incorporates individuality by controlling the time spent stationary was created to illustrate how different patterns of space use emerged from our sample population.

7.2 Methods

7.2.1 Subjects and Housing

Three-spined sticklebacks (*Gasterosteus aculeatus*), wild-caught on Swansea University campus, Wales, were studied in autumn 2016 (Fig. 7.1). Subjects were kept in a holding tank (300 x 390 x 1220 mm) containing gravel substrate, plants, and driftwood for 2 weeks prior to the experiment at a consistent temperature of 16°C at 8L:16D photoperiod regime, and kept in individual 2.8L gravel-lined, aerated tanks during behavioural tests. Fish remained in these individual tanks for the experimental period when not being assayed. Water was changed every two days and all fish were fed 5 defrosted bloodworms (*Chironomid* larvae) each day.

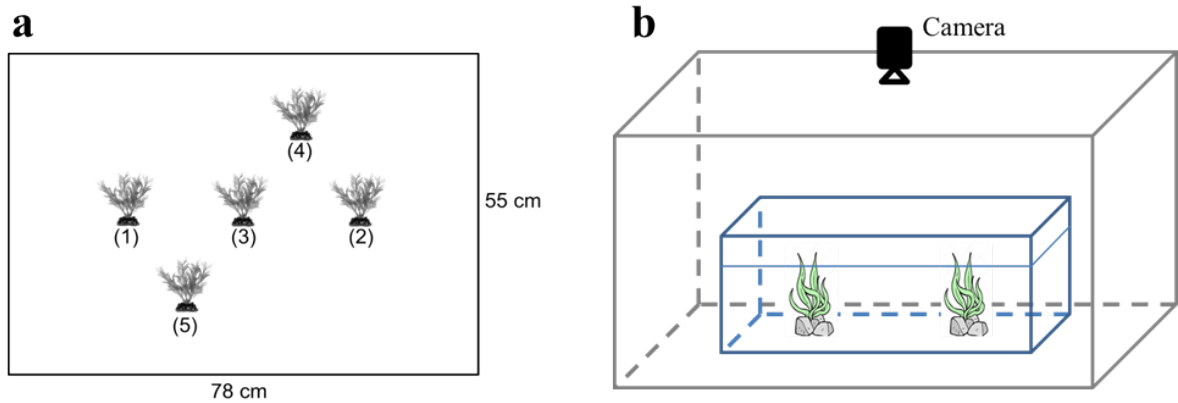


Figure 7.2: (a) Top-down schematic of the tank setup. The 'simple' environment contained two plastic plants (objects) – plants(1-2). The 'moderate' environment contained plants 1-3. The 'complex' environment contained plants 1-5 (b) Experimental arena setup. The tank contained 2, 3 or 5 plastic plants and was covered in a metal frame shrouded with white sheeting. the camera, Panasonic HDC-SD60 HD, was suspended at a height of 1.5m.

7.2.2 Behavioural Tests

Behavioural tests were conducted in a test tank that was surrounded by white sheeting (PhotoSEL BK13CW White Screen) held up by a custom built metal frame (within a metal frame: 1 x 1 x 1.5 m). Four photographer's lights (each with 4 x 25w 240v 6400K True Day light bulbs) lit the arenas from outside the white sheet, dispersing light evenly over the four arenas . The arena was filmed using a Panasonic HDC-SD60 HD video camera (Panasonic Corporation of North America, Seracucus, NJ, USA) mounted above the arena. $N = 15$ fish were observed in an opaque plastic tank, 78 cm length by 55 cm width by 16 cm height, lined with white gravel. The tank was filled with water to 12 cm and changed after each trial. Fish were observed for 15 minutes after being placed in the bottom left-hand corner. Fish were observed in 3 different experimental setups: (i) a 'simple' environment with 2 plastic plants (ii) a 'moderate' environment with 3 plastic plants, and (iii) a 'complex' environment with 5 plastic plants (Fig. 7.2). Fish were repeat tested one week later.

7.2.3 Movement Data

Video recordings were processed using IDTracker software (Perez-Escudero et al, 2014) to generate x, y coordinates, frame by frame (25 Hz recording). Data were then manually checked and a value of 5mm/s was chosen as a threshold to determine between purposeful and non-purposeful movement. A sub-sampling rate of 2.5 Hz was used to prevent false large turns which can occur due to the processing of the video recording (Delcourt et al, 2013). The movement threshold and sub-sampling rates are in essence arbitrary values however, they were chosen to retain as much information about the movement path, whilst minimising any causal effects such sub-sampling can have on characteristics of movement trajectories (Codling & Hill, 2005; Benhamou 2004, McClintock et al, 2014; Gurarie & Ovaskainen, 2011, Marcus-Rowcliffe et al, 2012; Benhamou, 2014). (See Appendix D1 for a complete discussion on the initial processing of the data) (Fig 7.3).

Movement was considered to be formed by a discrete step-turn process (see Introduction) and as such models are generated using step lengths (instantaneous speeds) and turning angles (Kareiva & Shigesada 1983; Lima & Zollner 1996; Codling et al, 2008; Lemasson et al, 2009; Sueur et al, 2011; Ben-Ari & Inbar 2014; Hopkins 2016) we therefore extracted, for each fish and for each trial: (i) step-length mean value (SL), (ii) mean cosine of turning angle (TA), along with an additional measure to quantify the intermittency in movement, (iii) proportion of time spent stationary (%).

Additional descriptive values attributed to movement which are calculated as measures over the movement path as a whole were; (iv) sinuosity (S), calculated as: $S = \sqrt{(-2 \log R/\bar{s})}$ (Benhamou, 2004), where R = mean resultant vector, \bar{s} = mean step length, and (v) Burst Frequency (the relative frequency of periods of movement with a speed above 3 s.d's of the mean step-length of the fish when moving (Kane et al, 2004)).

Measures calculated which directly corresponded to the spatial use of the experimental setup were (vi) Net Distance Moved (mm), (vii) Space Use (%) and (viii) Occupation Time (%), all of which are statistics commonly used in animal personality studies (distance travelled and space-use (Dzieweczynski & Crovo 2011; King et al, 2013; Mamuneas et al, 2015; Jolles et al, 2018)). Space Use was calculated by considering the amount

of the tank the fish visited at least once along its movement path as a percentage of the entire space. To calculate this, the tank was split into an n by n array. For the analysis n was chosen as 50, other values were considered with the results unaffected for n between 10-100 (see Appendix D2). Occupation Time (%) split the tank into three distinct areas: ‘Near’ the wall (Occupation Time - Wall), ‘near’ an object (Occupation Time - Object) and free water (Occupation Time - Free Water). Here ‘near’ was considered to be within 7cm, (other values were considered from 2cm to 15cm, but there were no observable differences; except for the extreme values where the overlapping of areas became an issue; Appendix D3).

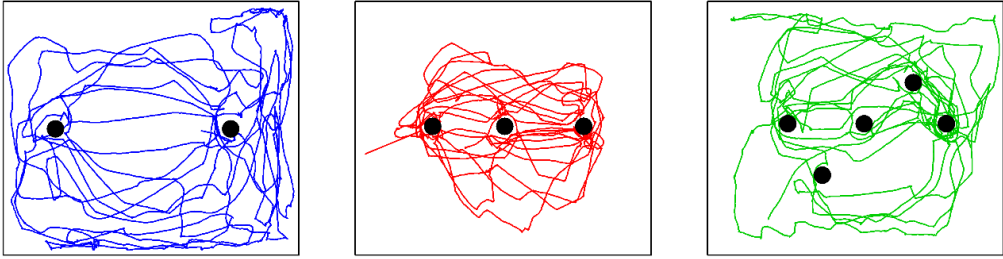
7.2.4 Statistical Analyses

Analysis of the movement paths looked to answer the following:

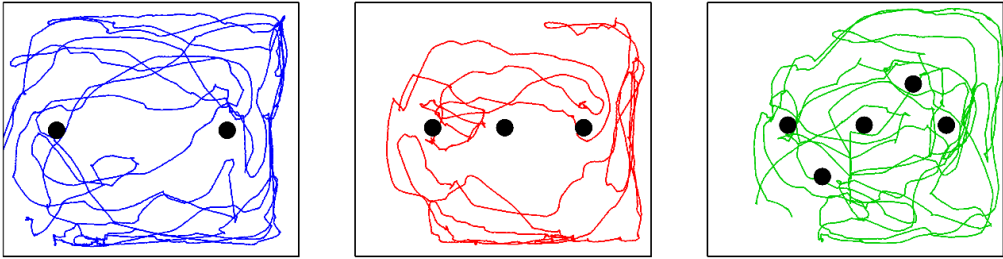
1. Did the population level movement behaviour change depending on how many objects were in the tank?
2. Did the environment affect the behaviour of fish at the individual level?
3. Did the environment affect the behaviour of the fish at the population level?
4. If the environment did not affect behaviour, were there differences in the behaviour of fish when compared to each other disregarding the environmental factors?
5. Was the behaviour of individuals consistent throughout the experiment?

Whilst we do not directly compare correlations between statistics here, auto-correlation between the movement parameters is expected (Boyce et al, 2010, Dray et al, 2010) and is a common problem with the analysis of discrete step-turn processes which can be introduced through the recording and sampling process (Nams, 2013). The standard approach for such auto-correlation relies on lag times (Cushman, 2010; Boyce et al, 2010; Teimouri et al, 2018) and has been introduced through the sub-sampling, therefore as we expect some auto-correlation between the movement parameters we will not over-interpret the

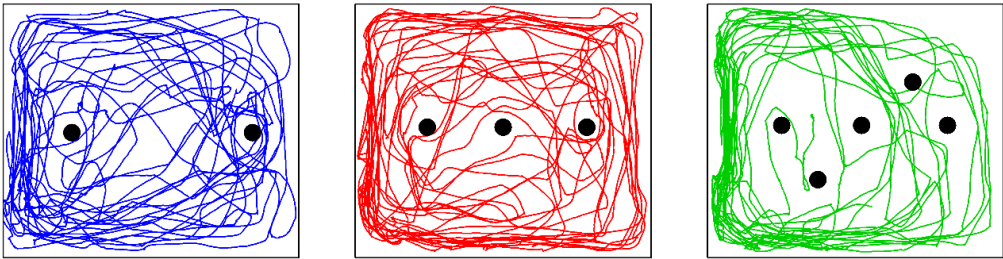
Fish A



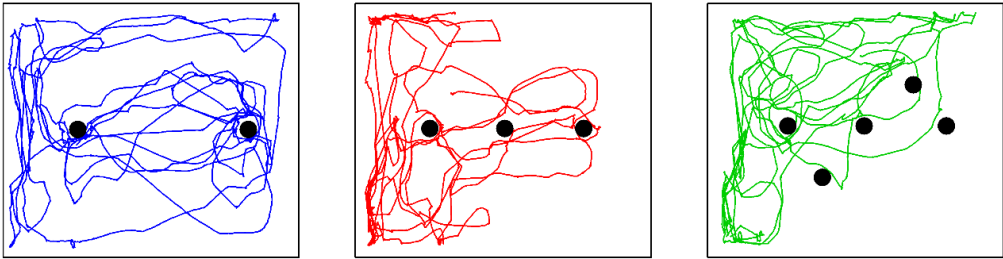
Fish B



Fish C



Fish D



Fish E

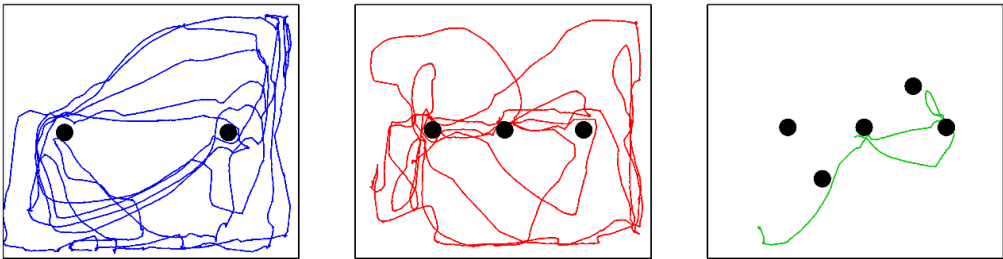


Figure 7.3: Examples of movement paths for 5 individual fish across the simple environment (black), moderate environment (red) and complex environment (green)

results. This is in contrast to Chapter 5 where the correlations were explicitly calculated and the auto-correlation effects were further accounted in the mixed-effects model.

To determine if there were significant differences in all the basic summary movement statistics, a repeated measures ANOVA was used to compare observed results across the three environments. As evidence for changes in behaviour would be expected to be most stark when comparing between the simple (2 objects) and complex (5 objects) environments, a Wilcoxon two-sample paired test was used to test for differences between pairs of environments. The Wilcoxon test being used here as it does not assume normally distributed data.

Variation between fish over each environment was tested by a one-way ANOVA (or Kruskal-Wallis test for those summary statistics which violated the homogeneity of variance assumption) on the mean of each summary statistic across the two trials per environment.

To test if the level of variance displayed by each individual fish across all of the trials (2 per environment giving 6 in total) was consistent across the population, Levene's test was used and a subsequent ANOVA tested for significance differences in the fishes mean values.

Repeatability of parameters (see section 5.3.3.1) was assessed by calculating intra-class correlation coefficients (ICC) and 95% confidence intervals (CIs) and was also used as an indicator for 'personality' traits (see Carter et al, 2013 for a discussion of this)

The motivations for the various tests are summarised in Table 7.1. These analyses were carried out using JASP v.0.8.0.0 (JASP Team, 2018) and R (R Development Core Team 2019).

7.2.5 Movement Model

A simple individual movement model incorporating inter-individual variation was constructed to illustrate how different patterns of space use can emerge as a consequence of incorporating individual variations. Predicting individual and group level dynamics of stickleback fish is important to help understand and solve ecological questions such as

Question to answer	Test	Motivation for test
1. Did the population level movement behaviour change depending on how many objects were in the tank?	ANOVA	Test for similarities in mean values.
2. Did the environment affect the behaviour of fish at the individual level?	Deviation from mean	Test to see if individuals changed behaviour as environment changed by measuring differences from their mean behaviour across all trials
3. Did the environment affect the behaviour of the fish at the population level?	MANOVA	Test for similarities in mean values of the population across the three environments
	Wilcoxon-paired	Compared the population means in pairs of environments (e.g. behaviour in simple and moderate environments may be similar but movement in complex could be different). This detail would not necessarily be picked up by the MANOVA.
4. If the environment did not affect behaviour, were there differences in the behaviour of fish when compared to each other disregarding the environmental factors?	ANOVA	Test for similarity of mean values.
	Levene's	Test for similarity in variances for each statistic between fish.
5. Was the behaviour of individuals consistent throughout the experiment?	ICC	Measure of repeatability and for indicating proportion of variance which can be assigned to differences within and between individuals

Table 7.1: Summary of statistical tests used in the analysis of the fish movement

shoaling behaviour (Hoare et al, 2000; Harcourt et al, 2009), social interaction (Jolles et al, 2015) and foraging activity (Giles, 1987). The complex group level movement dynamics can be explained by building up models from rules of individual movement. Therefore, an accurate model of individual movement can be used to describe group level movement dynamics as well as inform predicted individual movement patterns (Gautrais et al, 2012; Zienkiewicz et al, 2015).

Three simple models were initially considered and compared, with parameter values derived from the data. These were: (i) a simple random walk (SRW) (See Chapters 2 & 3), (ii) a correlated random walk (CRW) (see Chapters 2 & 3) with turning angles drawn from a wrapped Cauchy (WC) distribution with $\rho = 0.7$ (the best fitting distribution at the population level, found using the *circular* package in *R* (Agostinelli & Lund, 2017)), (iii) a CRW with turning angles from a WC distribution with $\rho = 0.85$ (average rho value of the best fitting wrapped distribution of the 5 most active fish - that is the 5 recordings where the fish were deemed stationary for the least amount of time, across any of the environments, for any fish and any run) and an additional parameter, ν , controlling the amount of time spent stationary (%). These models were chosen as; model (i) acts as a simple null model with essentially Brownian motion, model (ii) is the simple CRW model often used in individual animal movement (Kareiva & Shigesada, 1983) and model (iii) gives a more complicated model utilising the time spent stationary parameter as a proxy for individuality. The ρ value was not chosen as the parameter to determine individuality as, though it would affect most space-use statistics, it would not result in differences for Distance Moved. Whereas, varying time spent stationary would affect all of these statistics. A more advanced model would take into account varying both parameters, but here we wanted to consider only the simplest extension of the traditional CRW model. Step lengths were all drawn from a truncated exponential distribution, $TEXP(x)$ which has form

$$TEXP(x; \lambda, k) = \frac{\lambda^{-1} \exp(-x\lambda^{-1})}{1 - \exp(-k\lambda^{-1})}$$

where, λ , is known as the *rate* and, k , the *threshold value*. Values for these parameters

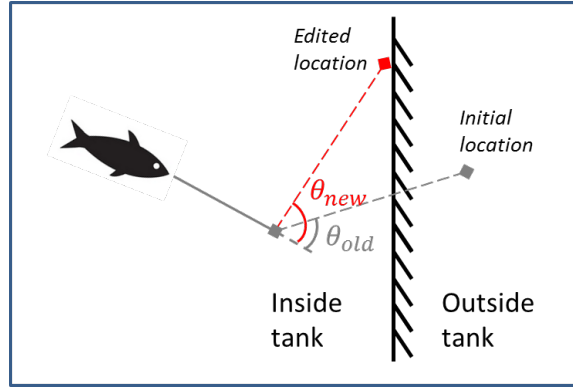


Figure 7.4: Method for calculating the new location in the movement model if a step took the fish out of the bounds of the tank, or into an object. The step-length was not changed but the new angle θ_{new} was chosen so that the value $|\theta_{old} - \theta_{new}|$ was minimised with the new location being inside the confines of the tank

were calculated directly from the data and were determined to be $\lambda = 1/40$ and threshold value of $k = 5$ (corresponding to the movement threshold value discussed in section 7.2.3). These were found using the *fitdistrplus* package in *R* (Delignette-Muller & Dutang, 2015).

For all models the rule governing the interaction of fish with the tank wall or the objects was that if the initial step took the simulation past the wall or into an object, the initial step length was kept and a new turning angle was calculated by finding the smallest magnitude change from the original angle which would result with the new location not being in a restricted area (Fig. 7.4). This was chosen for the model as the recorded movement indicated that fish had a propensity to follow the walls of the tank and the boundary of the objects (Fig 7.3).

To compare the accuracy of the models with the observed data, simulations were run for the same number of fish ($n = 15$) and the same number of time steps (138).

7.3 Results

7.3.1 Comparing Between Fish per Environment

Individual fish displayed significant differences from each other in all three environment (Simple (Sim) – 2 objects; Moderate (Mod) – 3 objects; Complex (Com) – 5 objects) for Distance Moved (Sim $F = 9.329, p < 0.001$; Mod $F = 5.712, p = 0.002$; Com $F = 5.763, p = 0.002$) and SL (Sim $F = 2.718, p = 0.036$; Mod $F = 8.343, p < 0.001$; Com

$F = 5.151, p = 0.002$). TA varied significantly for both the moderate ($F = 3.827, p = 0.009$) and complex environments ($F = 2.595, p = 0.043$) and the variance in Sinuosity was found to be significant only in the complex environment ($F = 4.400, p = 0.004$) along with Time Spent Stationary ($F = 5.151, p = 0.002$). Burst Frequency was found to vary significantly only in the simple environment ($F = 3.373, p = 0.015$). The results showed that the number of parameters with significant differences increased as the complexity of the environment increased, which could be evidence that the fish display more varied behaviour as the environment became more occupied with objects (see Appendix D4 for the complete ANOVA test results).

7.3.2 Comparing Fish across Environments

7.3.2.1 Population Level

Aggregating the data at the population level for each environment and performing a MANOVA to test for differences between mean values across all three environments indicated that there were significant changes in Time Spent Stationary ($F = 3.209, p = 0.048$) and Occupation Time - Object ($F = 6.934, p = 0.002$) (Appendix D5). Visual inspection of boxplots for the parameters (Fig 7.5) indicate that in general, there was little variation across environments with the exception of Occupation Time - Object. Interestingly, Time Spent Stationary does not clearly vary across the environments despite the result from the MANOVA (Fig 7.5B; Appendix D5), although this is further explained when considering the behaviour at the individual level (see section 7.3.2.2). Conversely, Occupation Time - Wall does appear to vary across environments although this was not picked up by the MANOVA (Fig 7.5H; Appendix D5).

To test for differences between pairs of environments the Wilcoxon two-sample paired signed rank test was used. Table 7.2 demonstrates that in general, similar to the MANOVA, there were not statistically significant differences between pairs of environments for any parameters, with the exception of Occupation Time - Free Water when comparing between the simple and moderate environments ($V = 332, p = 0.040$) and Occupation Time - Object between the simple and complex environment ($V = 76, p =$

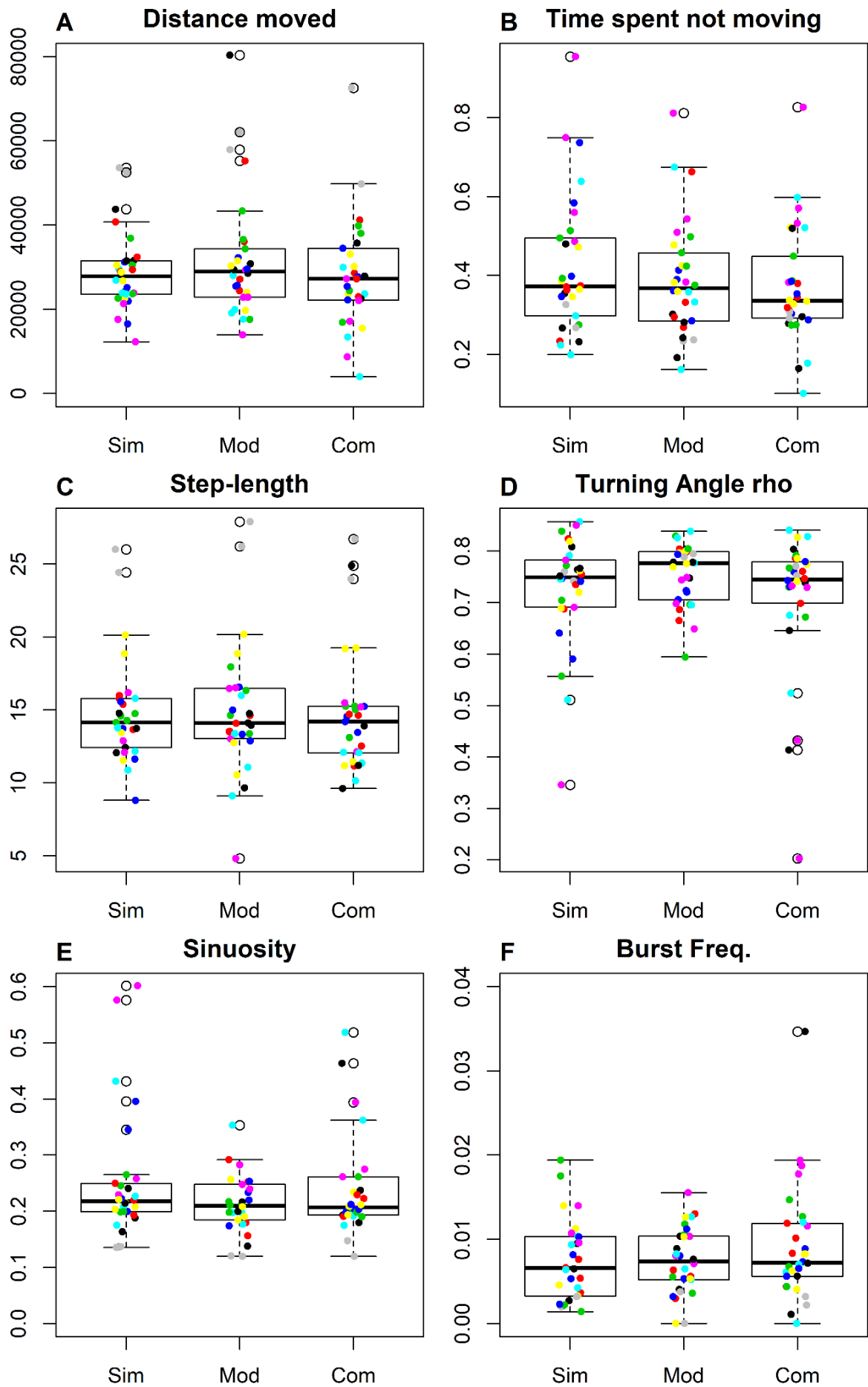
	Sim-Mod		Sim-Com		Mod-Com	
	Stat (V)	p-value	Stat (V)	p-value	Stat (V)	p-value
Distance Moved	178	0.271	254	0.670	273	0.416
Time spent stationary	447	<0.001*	437	<0.001*	352	0.013*
SL	190.5	0.567	182	0.449	225	0.882
TA	307	0.129	252	0.700	185	0.339
Sinuosity	304	0.146	254	0.670	163	0.158
Burst Freq.	239	0.903	183	0.318	191	0.405
Space Use	221	0.824	249.5	0.734	250.5	0.719
Occupation Time -Free Water (%)	332	0.040*	321	0.070	246	0.792
Occupation Time - Wall (%)	182	0.449	298	0.184	317	0.084
Occupation Time - Object (%)	141	0.061	76	0.001*	155	0.114

Table 7.2: Results of the Wilcoxon-paired test looking for similarities in the mean values between pairs of environments. Results marked with an asterisk (*) indicate significant ($p < 0.05$) differences between means

0.001). However, there was clear indication the median value for Time Spent Stationary did change, supporting the finding of the MANOVA.

7.3.2.2 Individual level

Testing for statistically significant results in how individuals varied their behaviour between environments is unreliable due to the small number of repeats (2 per environment), therefore a reliable direct comparison of measures such as variance, mean, median is not possible. However, a simple line plot connecting the mean value of each parameter across each environment, Fig. 7.6 appears to indicate that there is no general pattern in the change of the parameter as the environment changed e.g. if Distance Moved was to decrease as the environment got more complex we would expect to see a constant negative gradient across the majority of fish, however this does not appear to be the case. As this relies purely on visual inspection a simple residual calculation was used to identify if any trend existed in the change of the mean values. This calculated the sum of the



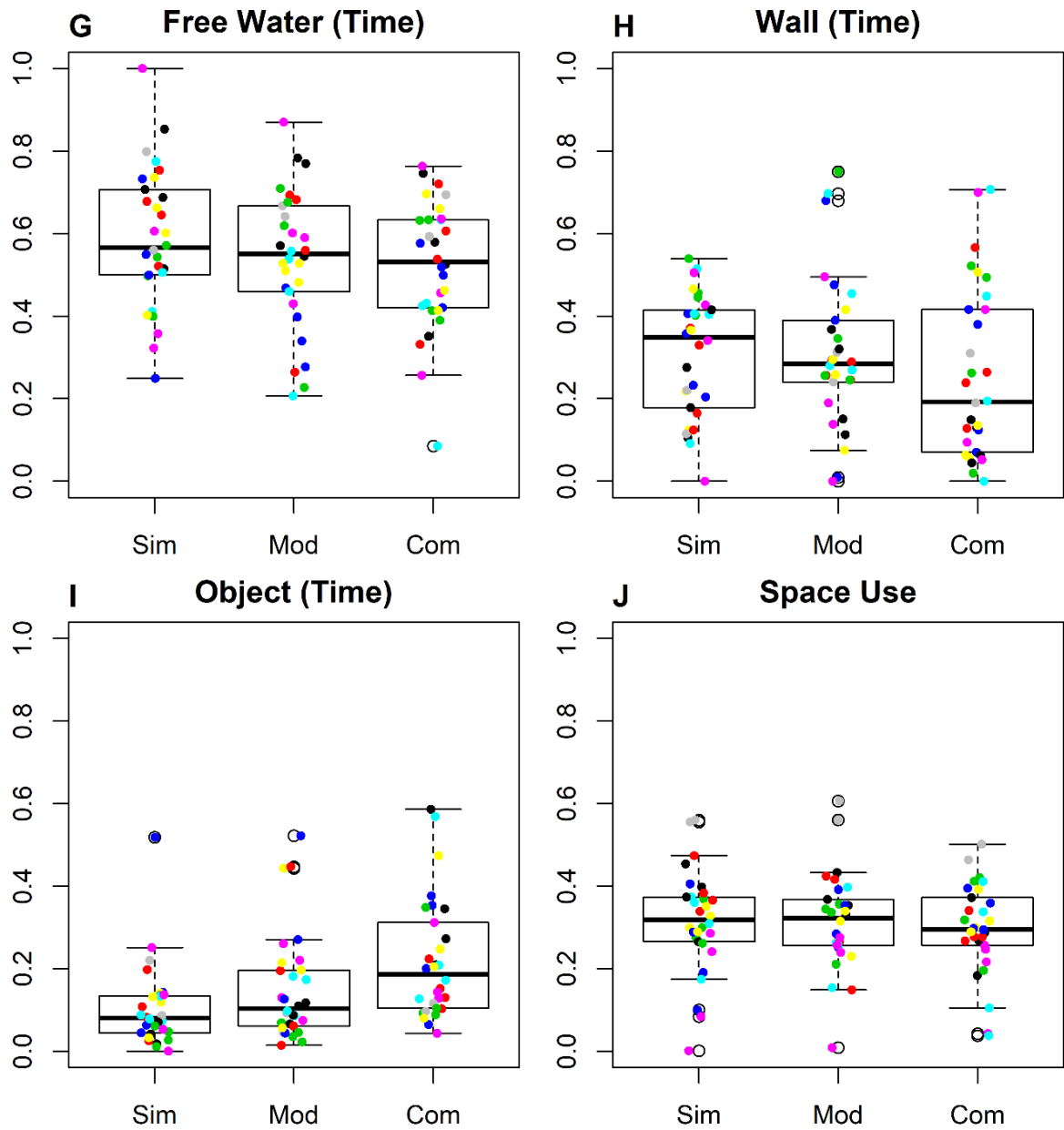
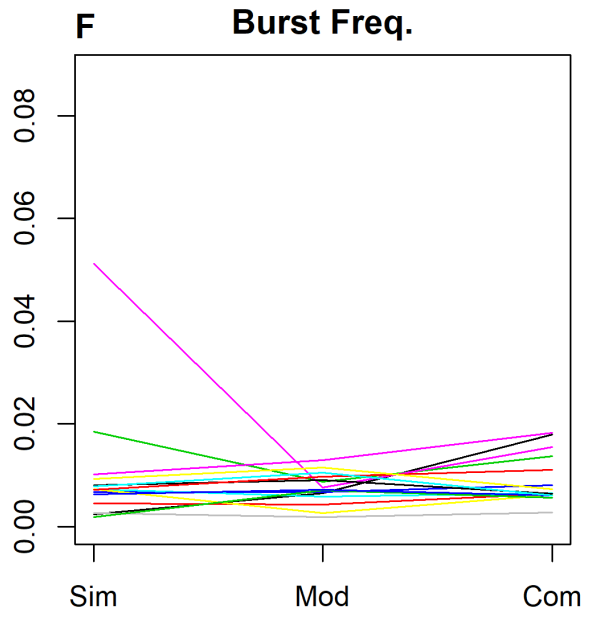
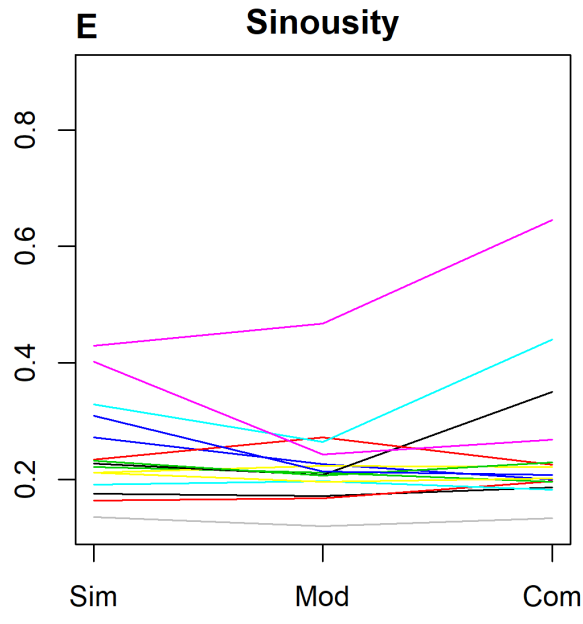
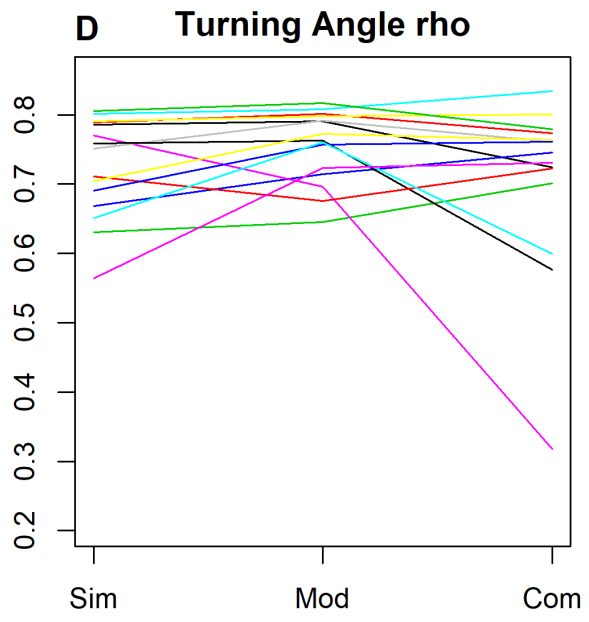
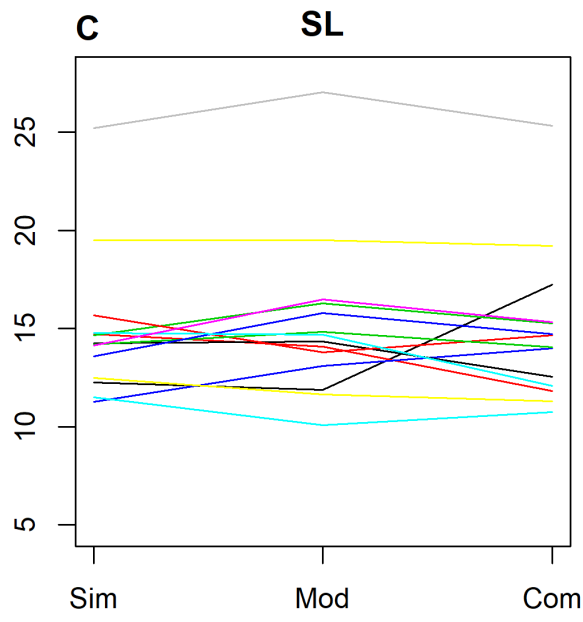
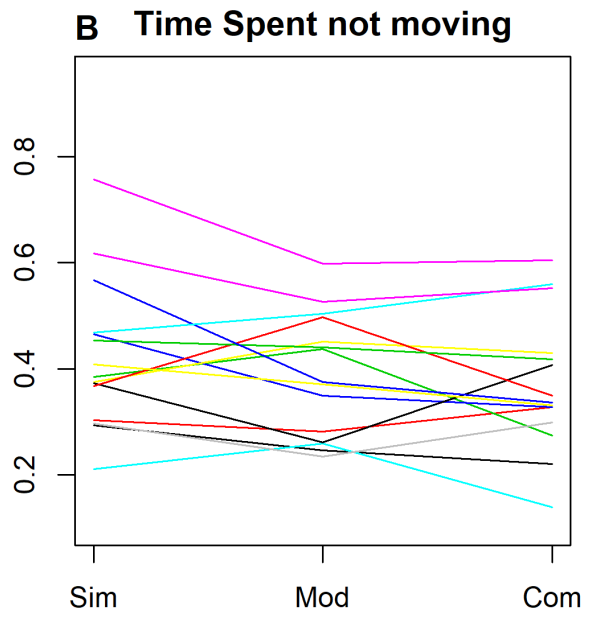
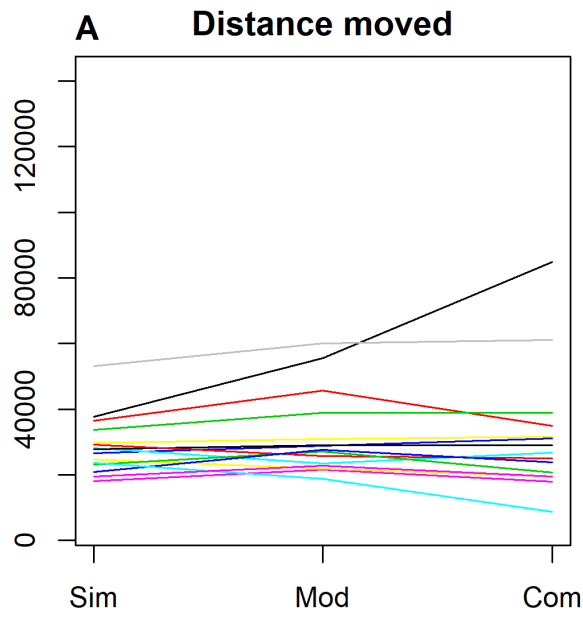


Figure 7.5: Boxplots of calculated statistics for every individual run compared across environments. Colours represent individual fish, with the same fish having the same colour across all runs and environments

distances of the two data points measured in each environment, from the mean of the parameter across all 6 measurements for each individual. This measure gives an idea of how much individuals varied their behaviour in each environment compared to their average behaviour over all environments and therefore gives a clearer indication of trends across the population. Figure 7.7 plots these values for all fish by environment per measured statistic. The plots indicate that Burst Frequency and Occupation Time - Free Water, Occupation Time - Wall and Occupation Time - Object did not change as the environment changed at the individual level. Both Distance Moved and Space Use (%) displayed a general increase from the Simple to the other two environments although this was not the case for all the fish, indicated by the plots straddling 0 for all environments. Sinuosity was seen to decrease, whereas SL and TA increased in general as the environment got more complex indicating that on the whole fish swam in straighter lines with longer steps, taking smaller turns as the environment became more complex. This initially seems counter-intuitive as one might expect that the fishes' movement would become more tortuous, featuring smaller steps and larger turns as the environment became more cluttered with objects, however, our findings could be explained by the high correlation between these measures; that is large steps often occur with smaller turning angles (see Appendix D1; Fig 7.13). Therefore in environments with more objects, the fish are forced to swim in areas with less free water so they cannot take as meandering a path and therefore, move with smaller turning angles. Most striking is the Time Spent Stationary which is clearly shown to decrease as the environment complexity increases, the plots are seen to hardly overlap indicating that for almost all fish there was a consistent negative change across the environments. This shows that as the number of objects in the environment increased, the amount of time fish spent moving also increased.

7.3.3 Comparing Fish disregarding environments

To look for evidence of consistent movement behaviour within individuals we consider the variance of the calculated statistics for each fish across all environments; 6 data points (2 runs per environment) per individual. Comparing the size of variation in the



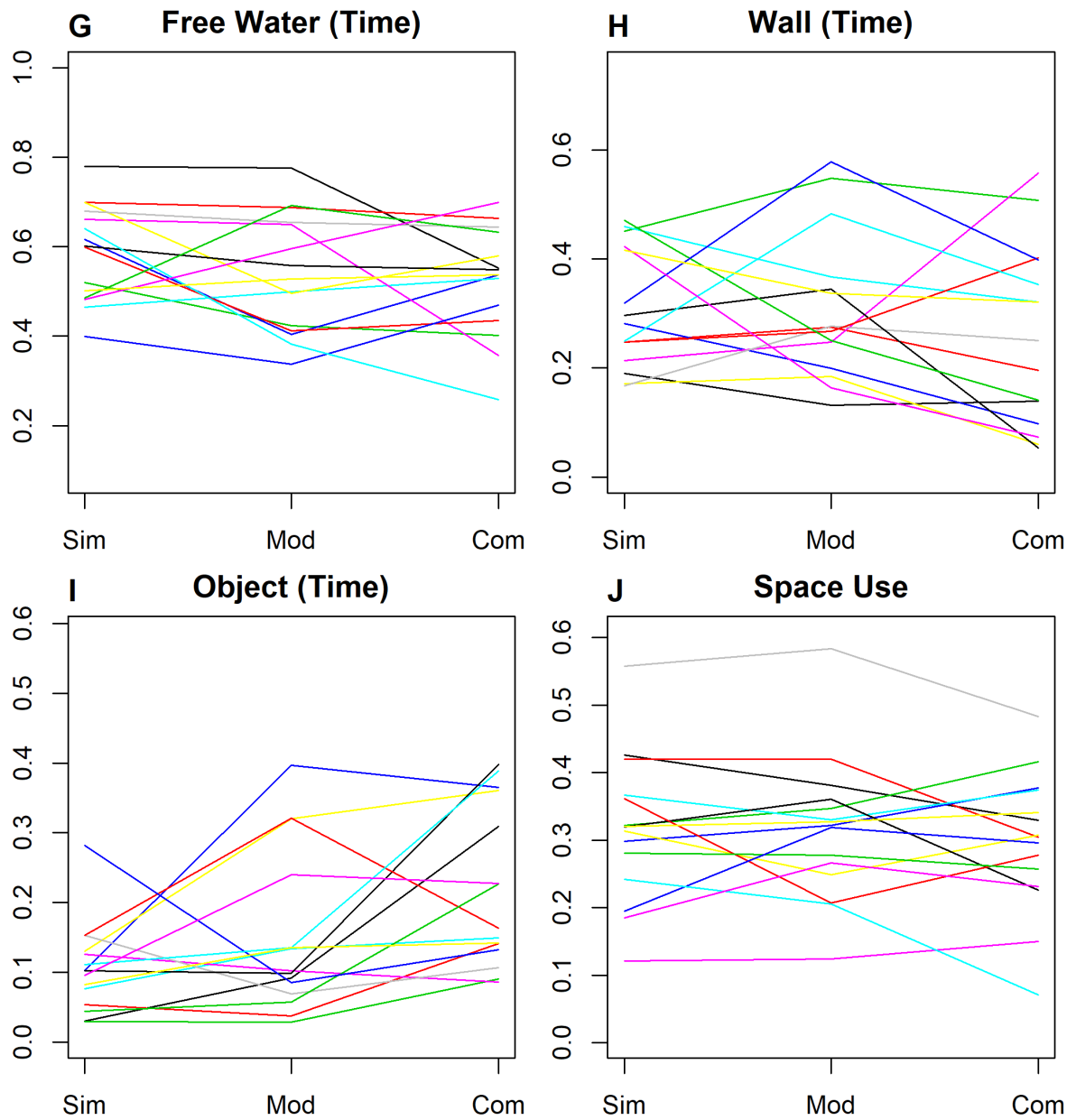
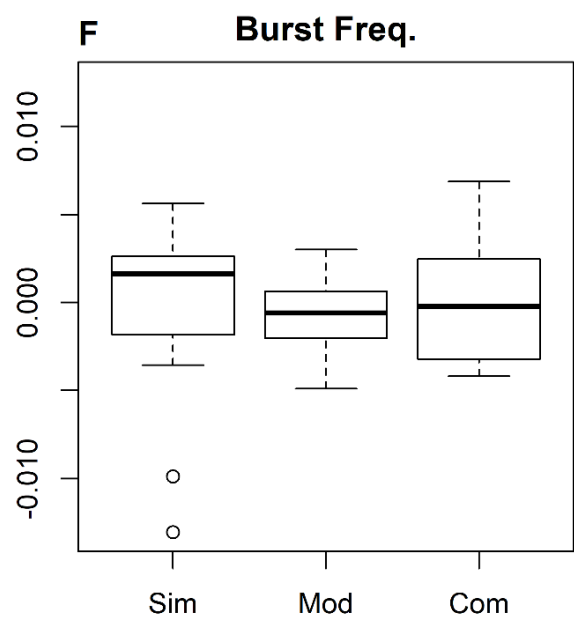
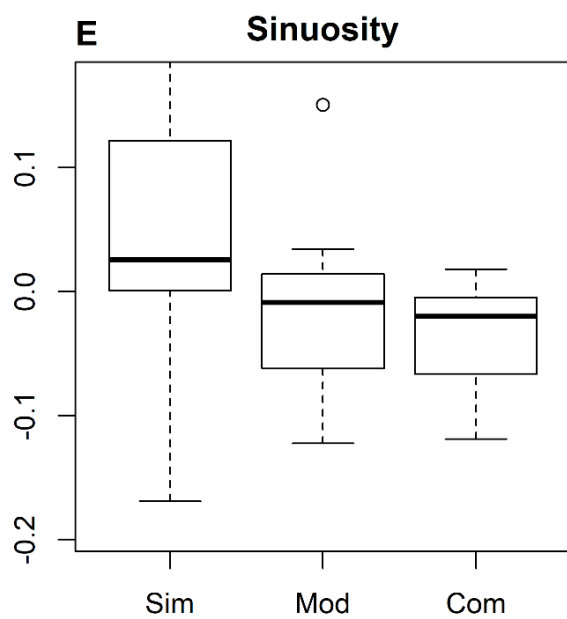
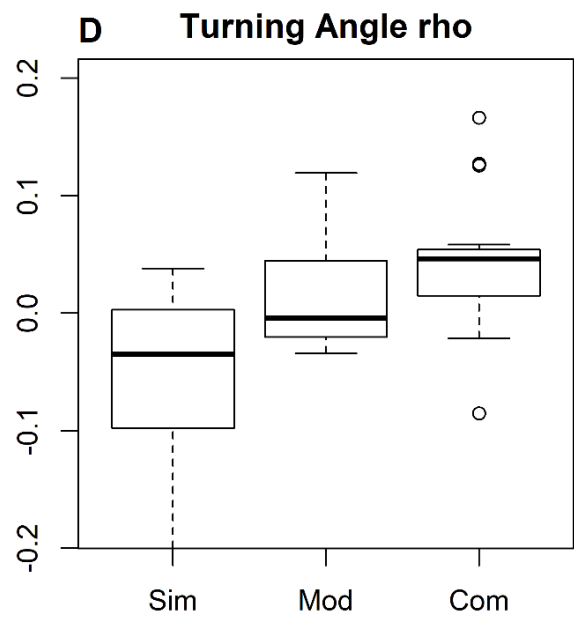
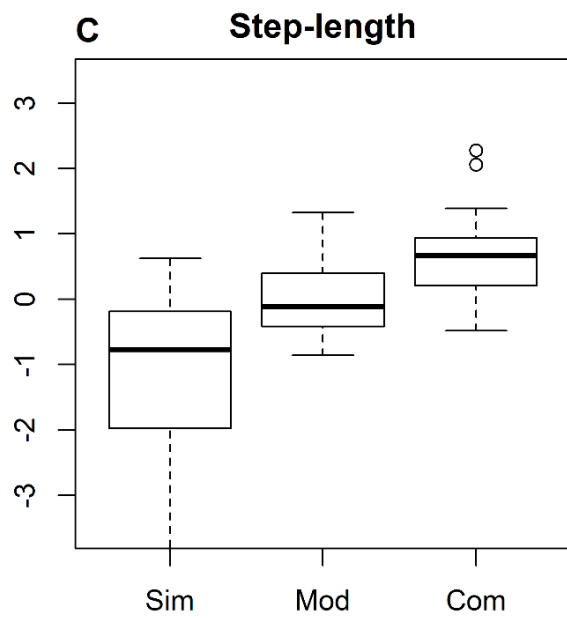
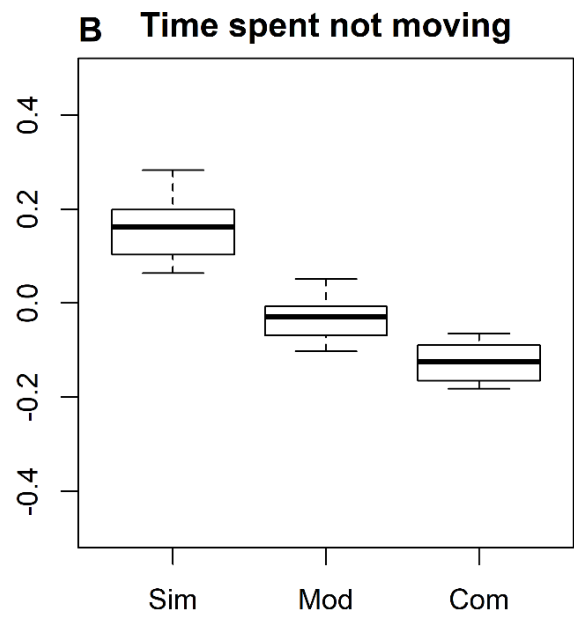
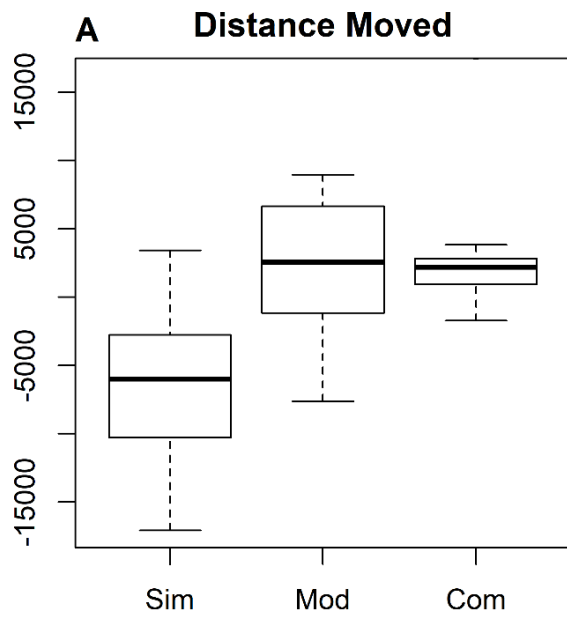


Figure 7.6: Line plots demonstrating how the calculated statistics varied for individual fish across environments. The mean value of the two runs per environment are plotted with each individual represented by a different colour



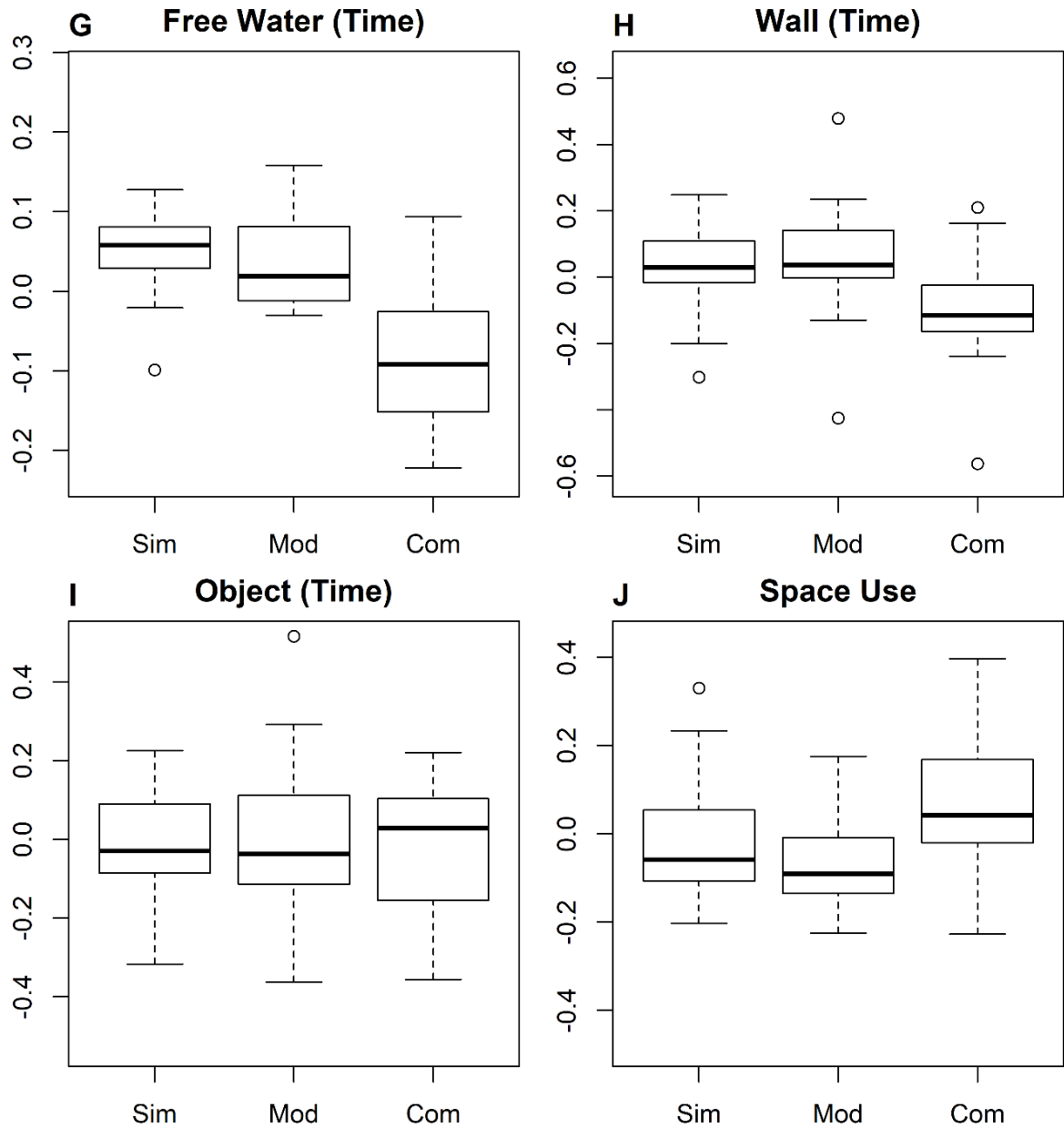


Figure 7.7: Boxplots indicating the difference between the mean value for an individual fish across all six individual trials and each individual trial. The 2 differences for each environment were summed for each individual with plots representing these values for the whole population (15 individuals)

	Distance Moved	Time spent stationary	Step-length	TA (rho)	Sinuosity
Stat (W)	2.4292	2.2065	0.80821	1.717	4.4776
p-value	0.007*	0.015*	0.641	0.07	<0.001*

	Burst Freq.	Space Use	Occupation Time - Free Water	Occupation Time - Wall	Occupation Time - Object
Stat (W)	1.1769	1.3878	1.3568	1.6311	0.74517
p-value	0.311	0.180	0.196	0.090	0.723

Table 7.3: Results of Levene’s Test comparing between fish disregarding the change in environment. Values marked with an asterisk (*) indicate significant results ($p < 0.05$)

statistics across all fish will give an indication if any statistic has a consistent level of variability across the environments. Figure 7.8 indicates a similar level of spread around the median value across the 6 data points for all fish, regardless of the median value. Levene’s Test indicated that there was significant similarity across all fish for all of the calculated statistics except for Distance Moved ($W = 2.4292, p = 0.007$), Time Spent Stationary ($W = 2.2065, p = 0.015$) and Sinuosity ($W = 4.4776, p < 0.001$) (Table 7.3). However, it is worth noting that if the extreme outliers are removed from the data (points which are greater than $Q3 + 1.5 \times IQR$ or less than $Q1 - 1.5 \times IQR$; where $Q1$, $Q3$ are the lower and upper quartiles respectively and IQR is the inter-quartile range of the population) then there is evidence that the variances across all fish for Distance Moved are similar ($W = 1.6326, p = 0.10$). Similarly, the plot for Sinuosity (Fig 7.8E) shows that Fish 6 is the clear outlier, giving a much larger spread than any of the other individuals, without this the spread amongst the remaining fish is much closer.

As Levene’s Test revealed that the variances were similar across all measures an ANOVA was then used in order to discern whether there was significant differences in the means of the measures between fish. Table 7.4 demonstrates that there were statistically significant differences between the fish across all the measures ($p < 0.01$), indicating that the fish displayed highly variable behaviour when compared between each other.

The results of calculating the ICC indicate that all the summary movement parameters and the space-use parameters have significant consistency ($p < 0.05$; Table 7.5)

Cases	Sum of Squares	df	Mean Square	F	p
Distance moved	1.391e+10	14	9.934e+8	5.987	<.001
<i>Residual</i>	1.244e+10	75	1.659e+8		
Time spent stationary %	1.171	14	0.084	6.243	<.001
<i>Residual</i>	1.004	75	0.013		
Step length	125.4	14	8.957	12.91	<.001
<i>Residual</i>	49.96	72	0.694		
Turning Angle	0.331	14	0.024	2.514	0.005
<i>Residual</i>	0.706	75	0.009		
Sinuosity	0.696	14	0.05	6.256	<.001
<i>Residual</i>	0.596	75	0.008		
Burst Frequency	0.002	14	1.711e-4	1.984	0.03
<i>Residual</i>	0.006	75	8.622e-5		
Space Use	0.786	14	0.056	10.18	<.001
<i>Residual</i>	0.413	75	0.006		
Occupation - Free Water	0.698	14	0.05	2.228	0.014
<i>Residual</i>	1.68	75	0.022		
Occupation - Wall	0.909	14	0.065	2.44	0.007
<i>Residual</i>	1.997	75	0.027		
Occupation - Object	0.402	14	0.029	1.823	0.05
<i>Residual</i>	1.181	75	0.016		

Table 7.4: Results of the ANOVA comparing between fish disregarding the change in environment.

Measure	ICC	95% CIs	p-value
Time spent stationary	0.54	(0.32, 0.77)	<0.001
Step length	0.73	(0.56, 0.88)	<0.001
Turning angle	0.20	(0.04, 0.48)	0.037
Sinuosity	0.50	(0.29, 0.74)	<0.001
Burst Freq	0.50	(0.00, 0.81)	0.030
Space-use	0.62	(0.42, 0.82)	<0.001
Distance travelled	0.83	(0.66, 0.94)	<0.001
Occupation time – Free Water	0.17	(0.02, 0.44)	0.014
Occupation time – Wall	0.19	(0.03, 0.47)	0.007
Occupation time – Object	0.16	(0.00, 0.43)	0.019

Table 7.5: Results of calculating the ICC for the calculated statistics, along with the 95% CIs and the associated p-value

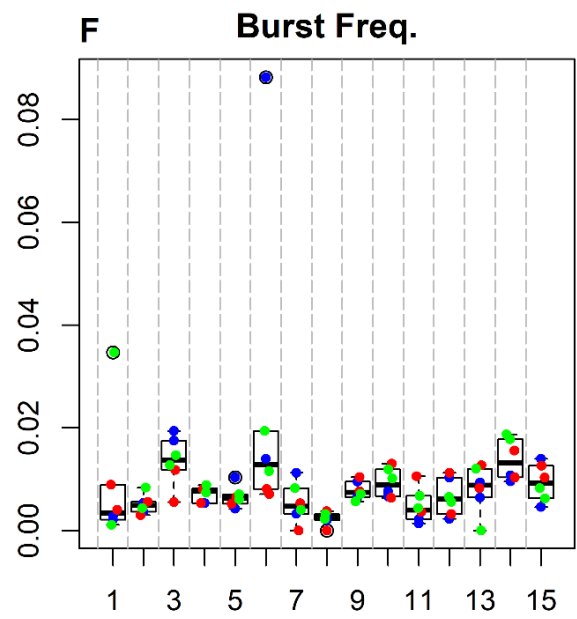
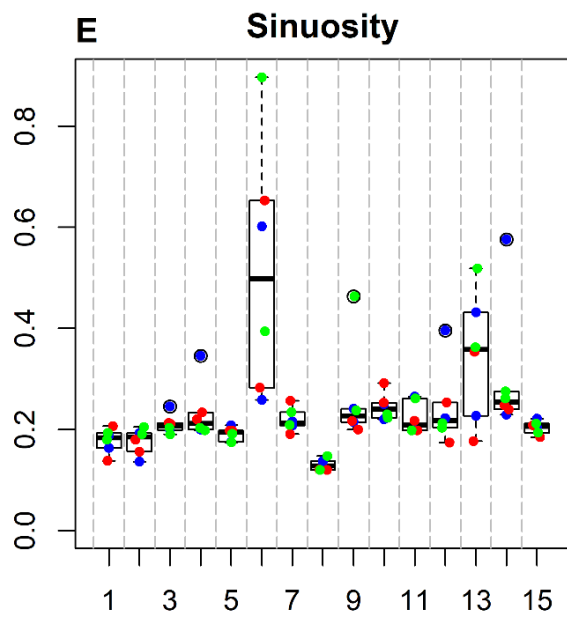
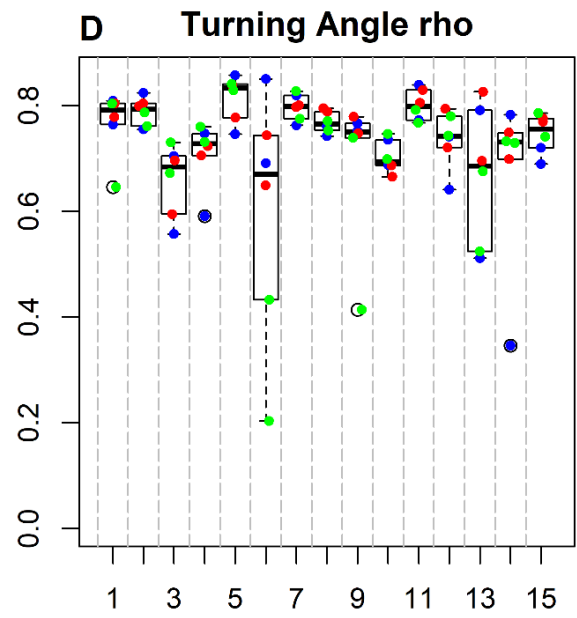
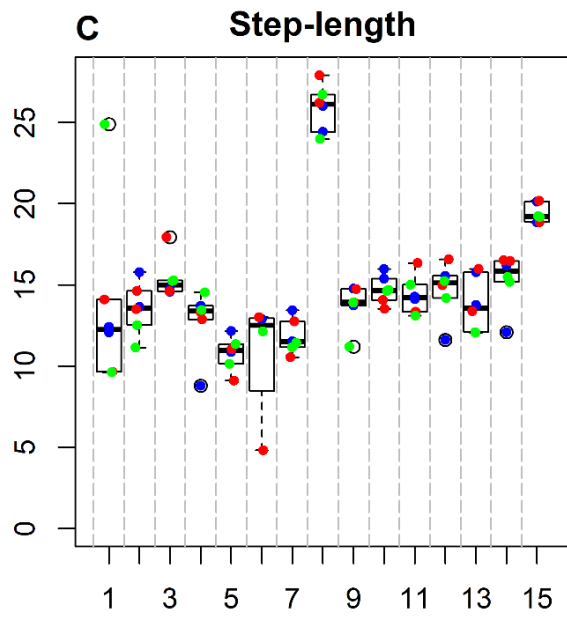
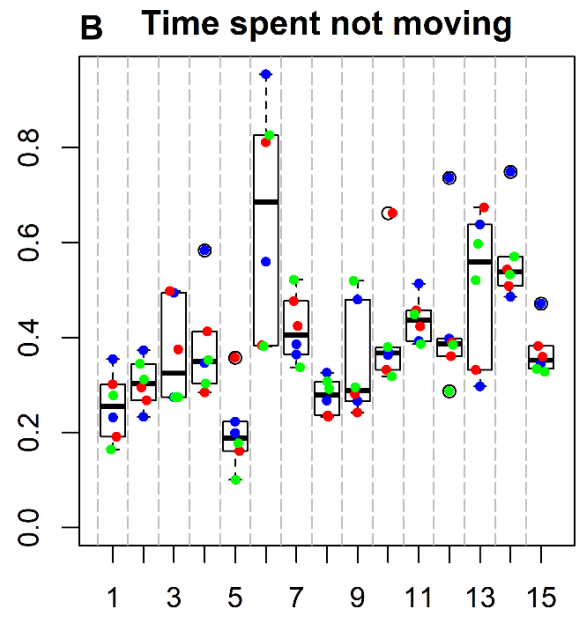
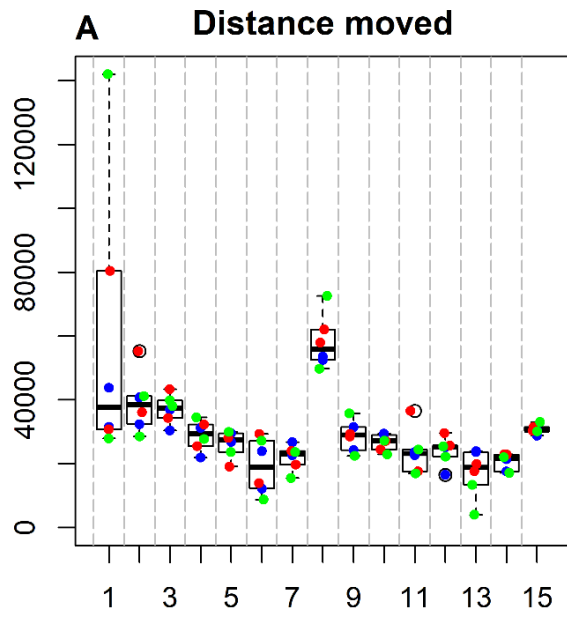
although the values at the 95% CI are quite wide for all parameters, indicating that whilst there is evidence for consistency it is not conclusive.

The ICC also revealed that a statistically significant proportion of the variation in all the parameters was attributed to variation among individuals. The variation in the key descriptive movement parameters of Time Spent Stationary (ICC = 0.54 [0.32 – 0.77], $p < 0.001$), SL (ICC = 0.73 [0.56 – 0.88], $p < 0.001$) and TA (ICC = 0.20 [0.04 – 0.48], $p = 0.0037$), indicate that the fish displayed intra-specific movement specialisations. That a significant proportion of the variation in fish activity (Distance Moved; ICC = 0.83 [0.66 – 0.94], $p < 0.001$) and exploration (space use; ICC = 0.62 [0.42 – 0.82], $p < 0.001$).

7.3.4 Movement Model

7.3.4.1 Model Selection

To compare between the three considered models (see section 7.2.5), the summary statistics of Distance Moved, Space Use (%), Occupation Time – Free Water, Occupation Time – Wall and Occupation Time – Object were compared in pairwise plots against the observed data. From these it was clear that Model (iii), a CRW with a parameter controlling Time Spent Stationary, most closely fit the observed data (see Appendix D6 for a more complete comparison). Whilst this is to be expected as model (iii) is the most complex, that the model reproduces the observed results for the space use statistics,



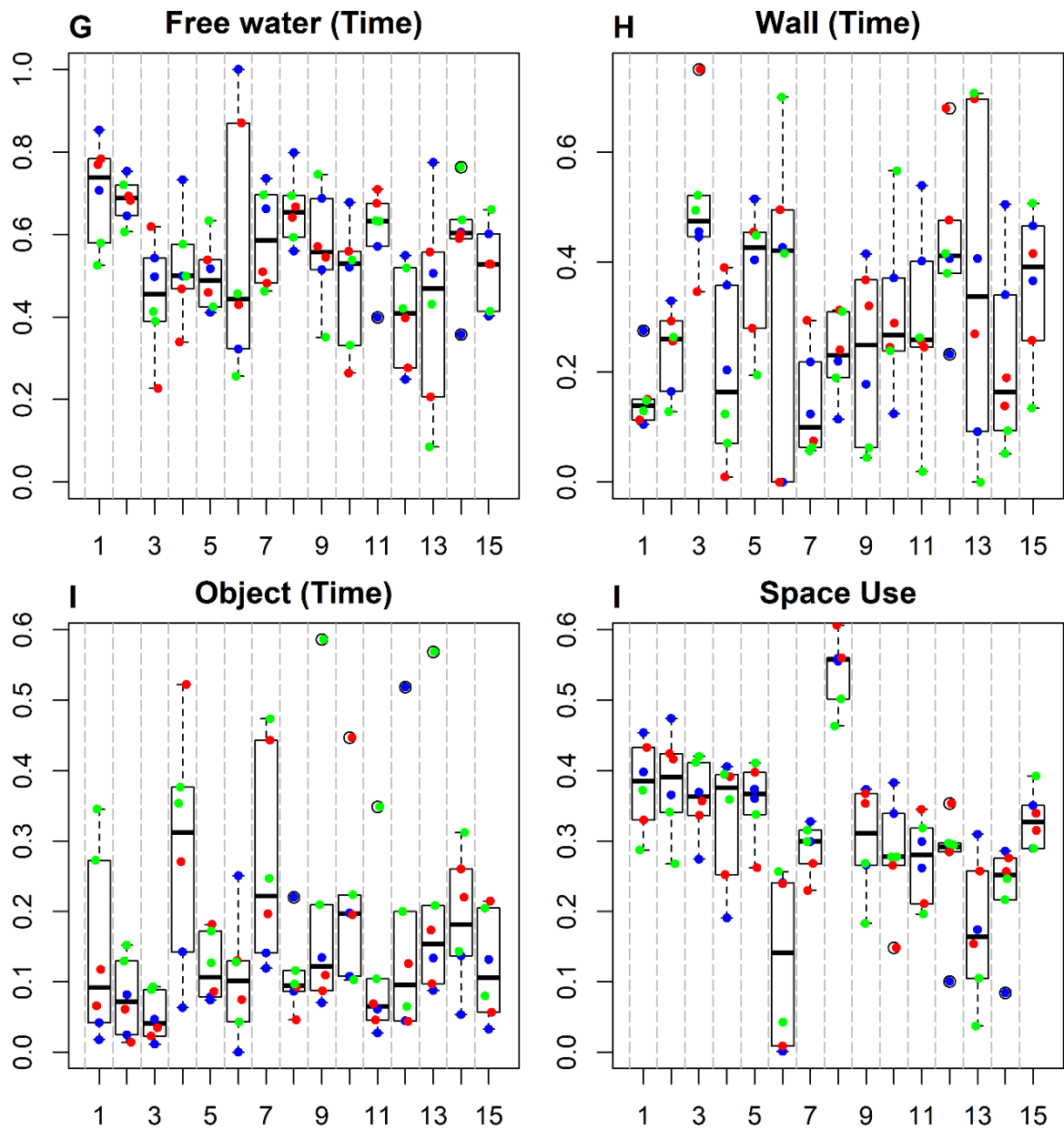


Figure 7.8: Box plots indicating the spread of the calculated statistics for each individual fish across all environments (red = Simple, blue = Moderate, green = Complex)

despite only being a simple extension on the CRW in model (ii), is interesting.

7.3.4.2 Comparison between observed data and model

Having determined the model which most closely fits the observed data, we consider the accuracy of such a model by directly comparing how the Distance Travelled, Space Use and Occupation Time values vary against the Time Spent Stationary for the model and the observed data.

Figure 7.9 shows the results when comparing the Distance Moved against Time Spent Stationary (%). Figure 7.9A plots the results from the simulated data with the filled grey triangles representing individual data points and the open red triangles representing the calculated average in Distance moved, y , for a specific value of Time Spent Stationary, x . This average was calculated as a type of moving average. Each plot point, (\bar{x}, \bar{y}) , was found by considering all data points with x coordinate within ϵ of \bar{x} . The corresponding y values were mean averaged to find the value for \bar{y} . Here ϵ was chosen as 0.05 (for example for $\bar{x} = 0.5$ all y values with corresponding x value between 0.45 and 0.55 were averaged to give \bar{y} , the coordinate for $\bar{x} = 0.5$). Other values were considered for epsilon, with too small values giving unreliable results as points on the x -axis (Time Spent Stationary) were often too spread out, and too large values resulting in overly smoothed results. However it should be noted that the results of differing epsilons gave similar results when comparing between simulated and observed data. The dashed lines represent this moving average value plus/minus the standard deviation of the data points within the $\pm\epsilon$ window. Fig 7.9B plots the Distance Travelled against Time Spent Stationary from the observed data, with the open black circles representing the same moving average as described previously. Visual comparison of the moving average values for both the simulated and observed data (Fig 7.9C) demonstrates a reasonable fit, however, there is a clear difference in the level of variation observed, highlighted by the associated dashed lines (corresponding to the s.d's) with the observed data having a much wider range of values, although the overall trend of the moving average is similar in both. The linearity in the model results is expected due to the setup of the model since the expected distance

travelled in the model can be calculated simply by, $D = \tau(1 - \nu) \mathbb{E}[l]$, where τ = number of time steps, ν = Time spent stationary (%), $\mathbb{E}[l]$ = expected step length. In model (iii) the step lengths were described by an exponential distribution with rate = $1/40$, so $\mathbb{E}[l] = 40$, and as τ was simply a constant, D will therefore decrease linearly as ν increases.

Figure 7.10 shows the results for the Occupation Time. Similar to Distance Moved, the moving average points show a good overall fit, however, the spread of values is not as accurate (demonstrated by the dashed lines). The values here for Occupation Time are for all environments combined as each individual environment was shown to give quantitatively similar results.

Figure 7.11 directly compares the Space Use for all environments combined (Space Use compared by each environment separately was seen to be similar with no noticeable difference), here both the moving average and spread were closely matched by the simulations.

In general the simulations seem to indicate that the simple model is a reasonable reconstruction of the movement, for the specific confines of the experimental setup.

7.4 Discussion

Understanding how animals move through and interact with their environment is a key aim in movement ecology. It has been shown in recent reports that in order to understand a species' utilisation of space, individual behaviour and variation must be included in models especially when attempting to scale up behaviour to population level (Dingemanse & Dochtermann 2013; Sih et al, 2018). Here individuality was incorporated into a movement model by simply allowing the time spent stationary to vary, and it was demonstrated that even this simple change resulted in a model with more accuracy than a basic CRW.

Here we have demonstrated that individuality rather than environment plays a more significant role in explaining the variation in movement of stickleback fish in our sample population. Simple statistics used to describe and characterise movement, such as dis-

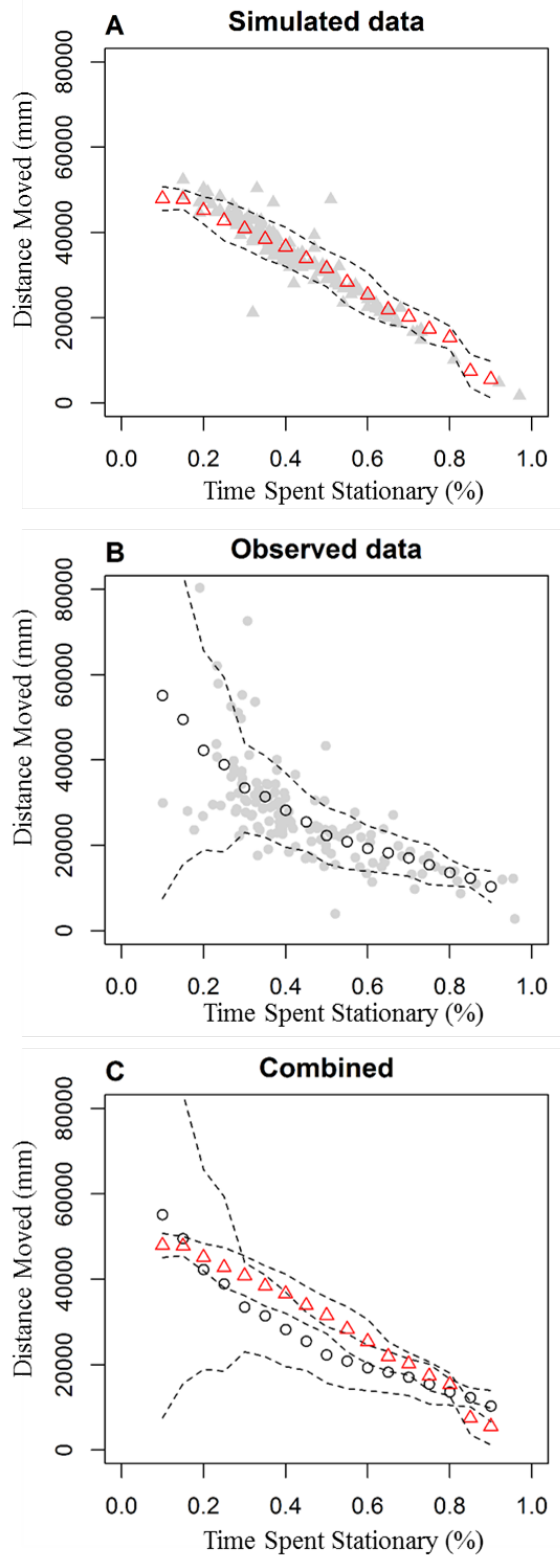


Figure 7.9: Distance Travelled against Time Spent Stationary (%) for the simulated model (A), the observed data (B) and comparing both of them grouping data from all environments (C). Grey points represent each individual result, with the open red triangles and open black circles giving the moving average as described in the text. Dashed lines represent the moving average plus/minus the standard deviation within epsilon of the x -values plot points.

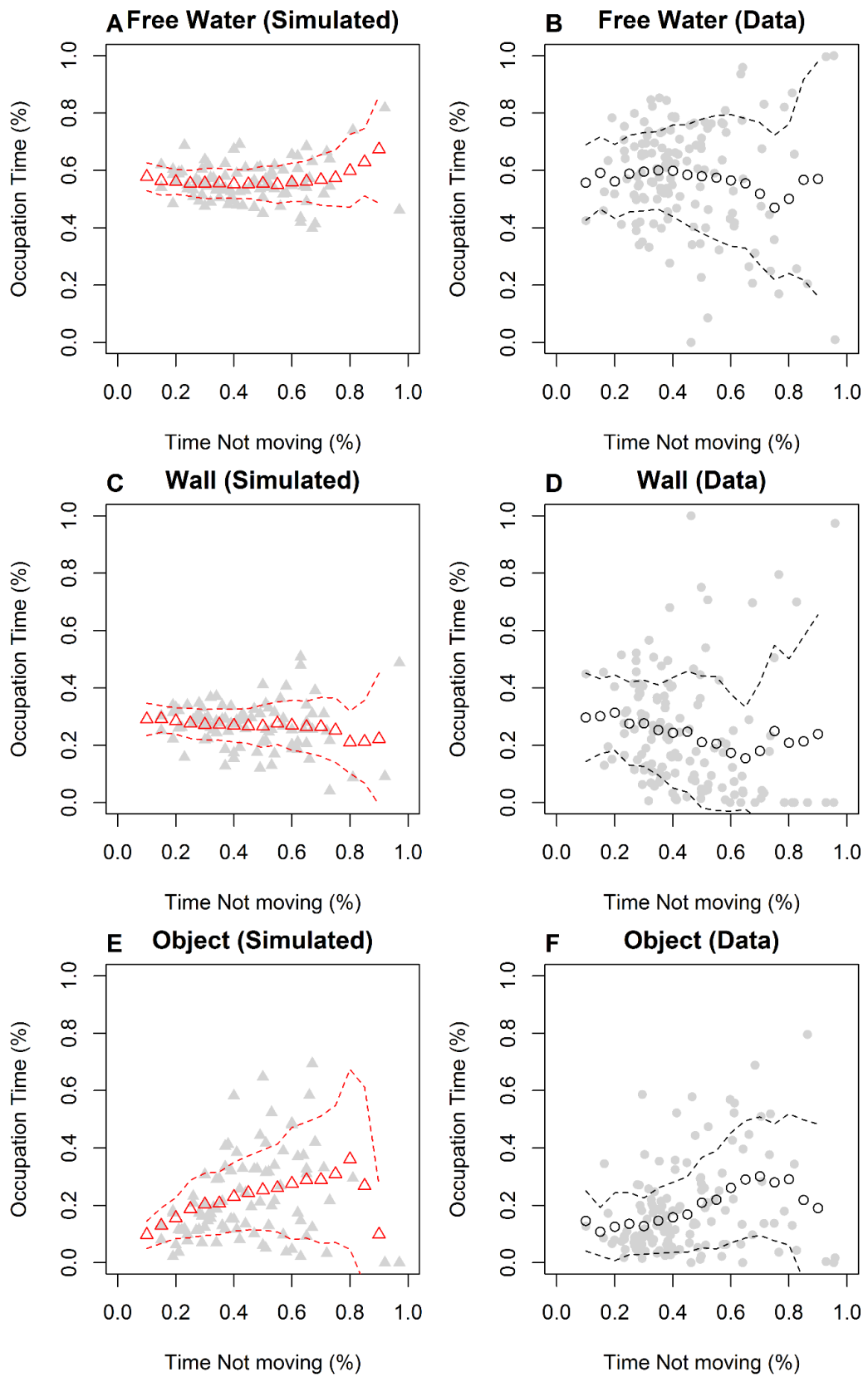


Figure 7.10: Comparing the Occupation Time (%) of the simulations (A-C) and the observed data (D-F) as functions of Time Spent Stationary (%).

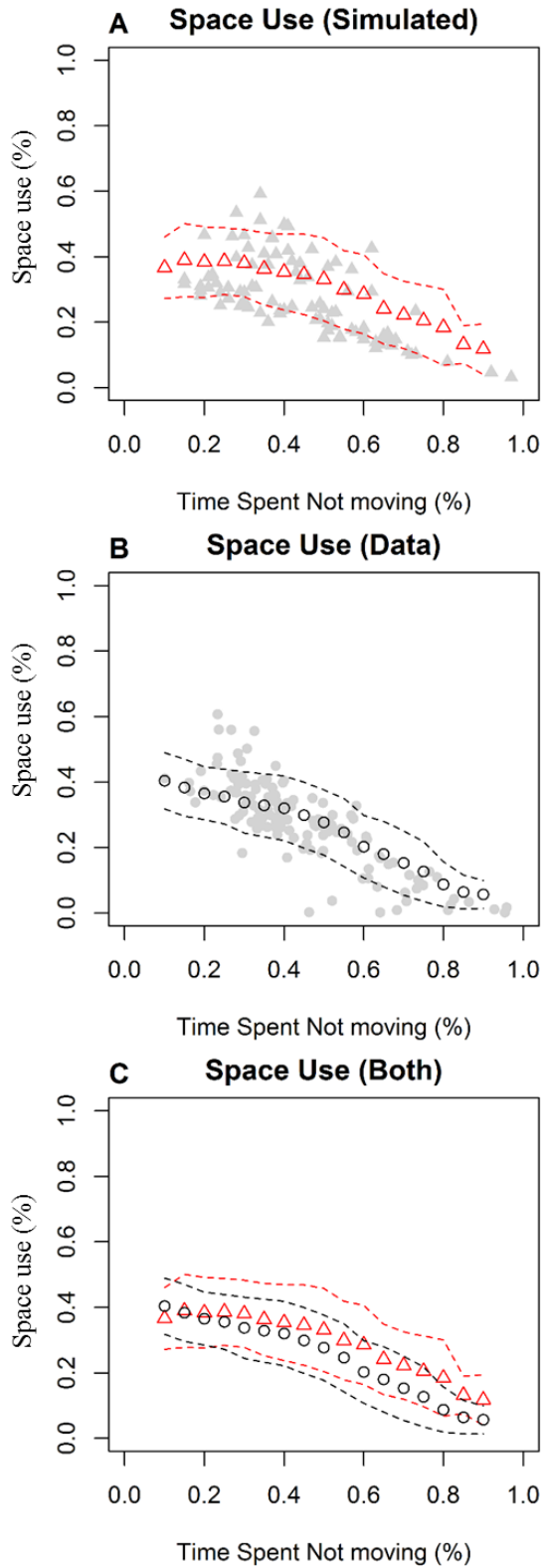


Figure 7.11: Space Use (%) against Time Spent Stationary (%) for the simulated model (A), the observed data (B) and a direct comparison (C). Data is grouped from all environments. Grey points represent each individual result, with the open red triangles and open black circles giving the moving average as described in the text. Dashed lines represent the moving average plus/minus the standard deviation within epsilon of the x -values plot points

tance moved, space use and sinuosity were seen to take a range of mean values across the population. However, the variance for each statistic was similar across all fish, possibly indicating that whilst fish have the ability to move in a variety of manners at the population level, each individual will only deviate from its average behaviour by a similar amount. Specifically, the finding that Space-Use and Distance Moved were also consistent and repeatable within individuals (shown by ICC results, Table 7.5) is consistent with other studies, which subsequently used this as evidence to suggest that sticklebacks display ‘personality’ traits of shyness and boldness (Harcourt et al, 2009; Nakayama et al, 2012; Dingemanse et al, 2012).

In general, the variance of each movement statistic was similar for each fish regardless of the number of objects in the environment. However, the Wilcoxon-paired test (Table 7.2) found that there was significant differences in the Time Spent Stationary, when comparing between environments. Our results indicated that as the number of objects in the tank increased the fish spent more time active, which agrees with the finding that in the simple environment, the majority of fish covered less distance on average compared to the moderate and complex (Fig. 7.7A). A naive explanation for this could be due to the fish having fewer novel objects to explore. However, as the time spent near an object (Occupation Time – Object) did not noticeably increase with the number of objects this suggests that this is not the case and therefore the reasoning for this increase in movement is unclear.

The observation that fish varied from movement covering a large percentage of the tank to less exploratory more localised movement has been noted in previous experiments with sticklebacks and other fish (Zienkiewicz et al, 2015; Furtbauer et al, 2015, Gautrais et al, 2009) and has been considered a further indicator of the personality traits of boldness and shyness (Huntingford 1976). Characterising and understanding these specific traits is an important question in fish ecology as they have demonstrable consequences in key ecological tasks, such as foraging (Nakayama et al, 2012) and shoaling preference (Harcourt et al, 2009).

Zienkiewicz (Zienkiewicz et al, 2015) noted that in a tank of similar dimensions to

the one used here, across a sample population of 20 zebrafish (*Danio rerio*), movement was seen to highly vary across individuals, from tightly winding paths to more ‘fluid trajectories’ which explored a large percentage of the tank. More specific characteristics of the movement were also found to be similar to our observations, with many fish displaying movement interspersed with times of stationarity and sudden bursts of movement. Interestingly, the movement model which Zienkiewicz found to be the most pertinent in replicating the movement was a continuous time ‘Persistent Turning Walker’ (adapted from the model of Gautrais; Gautrais et al, 2009; Gautrais et al, 2012) where constant speed was insufficient in describing the individual variability, similar to the findings in our simple model of the movement. However, in contrast to our model in which the time spent stationary was controlled, a parameter controlling sudden burst movement was included. Whilst the model of Zienkiewicz is more complex and detailed than the one demonstrated here it is notable that both models represented individual variability in movement purely by including some stochasticity in either sudden spontaneous increase in speed (Zienkiewicz et al (2015), or as in our model, sudden bouts of stationarity.

Persistence in movement direction has also been a feature in other movement models of fish (Gautrais et al, 2009; Mwaffo et al, 2014; Gautrais et al, 2012), and whilst the simple model used here was not produced as a reliable reconstruction of general stickleback movement, the inclusion of a parameter controlling the time spent stationary made the simple discrete CRW a straightforward ersatz movement model of individual sticklebacks. There are many ways in which the model could be adapted to become more realistic, including a term representing sudden burst of activity would take into account the fishes propensity for sudden movement (as mentioned above in Zienkiewicz et al, 2015). Similarly, as has been discussed previously there was a clear indication that the time spent stationary decreased across the population as the number of objects in the experimental arena increased, therefore adapting the current parameter to be a function of the number of objects should increase the accuracy. However, as the model was only intended to be a simple reconstruction of the movement for our specific experimental setup, making complicated adjustments would likely return only small improvements

without yielding any major insight into the movement behaviour of our population. Ideally any improvements should allow the model to be scaled up to environments of differing dimensions and features in order to explore and predict the expected behaviour in more natural and less contrived environments. This could then allow for predictions of important ecological questions such as foraging success (Day & McPhail, 1996; Webster & Hart, 2006), encounter rate (Kozak et al, 2013) and dispersal ability or shoal selection (Harcourt et al, 2009). In general the simple model compared qualitatively well to the observed data and its simplicity results in a model which is easier to understand and use than the more complicated alternatives found in other fish models (Mwaffo et al, 2015; Zienkiewicz et al, 2014; Gautrais et al, 2009).

Bringing together movement ecology and personality theory is important as it will lead to models of animal movement informed by observed data which can reliably and accurately reproduce movement at both individual and population level leading to a better and more complete understanding and predictability of movement across all spatial scales (King et al, 2018). Although it should be said that social interactions and their effects on individual movement behaviour must also be studied to better understand the impacts social connections can have on movement behaviours (Herbert-Read et al, 2013; King et al, 2015; Fürtbauer & Fry, 2018).

7.5 Conclusions

- We found that in 3 simple experimental environments containing differing number of objects/shelters, stickleback fish movements were highly consistent within individuals but varied significantly between individuals. This indicates that fish in our sample population had a range of possible mean behaviours. However, individuals could only vary behaviour from their norm by a similar amount.
- Changes in the environment did not explain variability in the sample population, with a significant proportion of the observed variation attributed to individuality.
- Fish were seen to increase their movement activity as the number of objects in the

environment increased.

- Our findings highlight the importance of including individual variation when attempting to analyse and understand population or group level behaviour. Future work should further develop how measures of individual variation in movement parameters can be used to understand and classify animal ‘personality’ and vice-versa.
- We demonstrate that a CRW incorporating a parameter controlling time spent stationary provides a straightforward model to recreate the observed measures concerning space use.
- More experimentation would need to be done to analyse the simple model’s veracity as in its current form it is unlikely to scale to differing size arenas including differing spatial characteristics, since it relies heavily on values for parameters fitted to the data from this particular experimental setup. However, as a simple measure to understand the variation within a sample population of fish it matches the observed data reasonably.

7.6 Appendices

7.6.1 Appendix D1– Initial processing of data and population level analyses

Initial processing of data

The raw movement data, filmed using a Panasonic HDC-SD60 HD video camera (Panasonic Corporation of North America, Secaucus, NJ, USA) and processed at a frequency of 25Hz using IDTracker software (Pérez-Escudero et al, 2014), was initially analysed by considering the distribution of turning angles in order to check for obvious issues caused by the recording and processing methods.

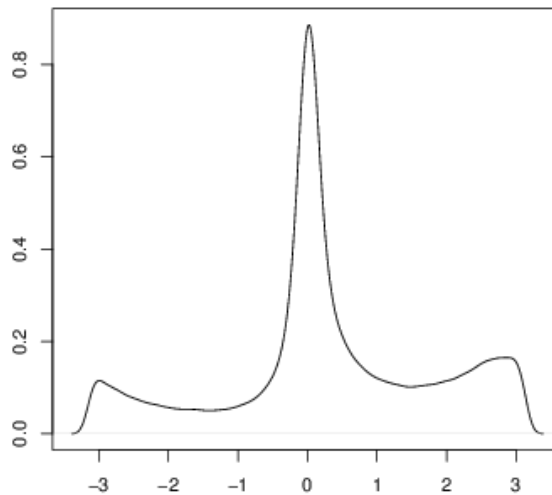


Figure 7.12: Distribution of turning angles for the raw data

The distribution displayed “swan-tails” at the extremes (Fig. 7.12) indicating a high frequency in near 180° turns. Whilst this could be a feature of the movement paths or a possible indication of multiple movement phases (Chapter 6; Parton & Blackwell, 2017) the raw data was checked for common problems associated with this type of movement data analysis.

Firstly, similar to the data processing in Chapter 5, as movement would be classified into periods of purposeful movement and stationarity a minimum instantaneous speed threshold was introduced (Chapter 5; Mashanova et al, 2010). Instantaneous speeds (distance travelled between consecutive time steps) above this threshold would

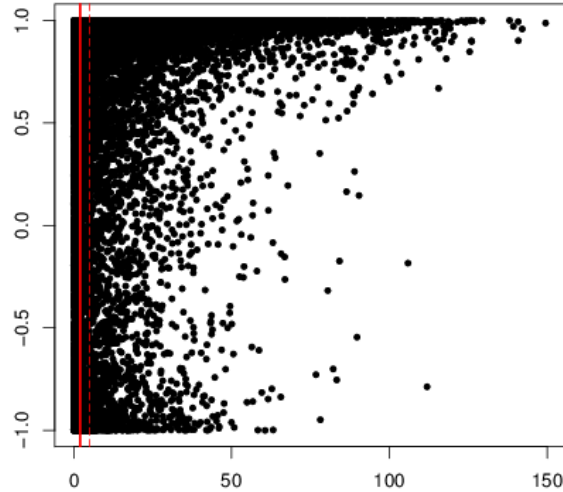


Figure 7.13: Step-length (x-axis) against the preceding cosine of the turning angle (y-axis). Red vertical lines represent possible speed thresholds to determine purposeful movement.

be classified as purposeful movement, whereas any speeds below would be considered as non-purposeful movement and would therefore be given a speed of 0. This would help separate movement attributed to true dislocation, from movement caused by attempting to remain stationary such as movement due to currents or eddies in the tank. A range of minimum speed threshold values were considered: 2mm/s, 5mm/s, 12.5mm/s , as well as no minimum speed threshold at all (Fig. 7.13). The minimum speed threshold of 5mm/s was used for the main analysis presented as this allowed for the retention of the largest number of data points while allowing objective classification of bouts. The use of different minimum speed thresholds did not lead to qualitatively different results.

Closer inspection of the processed movement paths revealed that paths were formed of jagged movement, despite the corresponding video showing no evidence of such piecewise movement (Fig 7.14). This is most likely due to the method used by the processing software (IDTracker software) and the way in which it determines the ‘centre’ of the moving fish when processing the videos. This gives slight variances in the precise central position of the fish, similarly, it was noted that due to occasional activity around the outside of the tank, there was occasional swaying visible during the recording itself. To combat this, a sampling rate was introduced to help prevent false large turns being recorded, which also ensured the fish had enough time to move between temporal points.

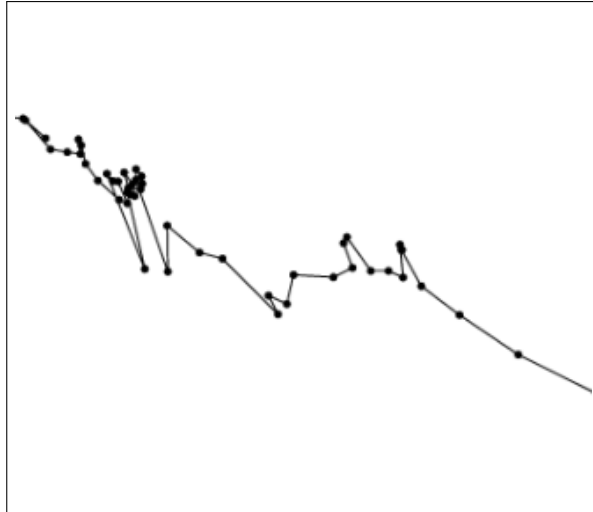


Figure 7.14: A zoomed in segment of an individual path. The points are the location found at the recorded level of 25Hz

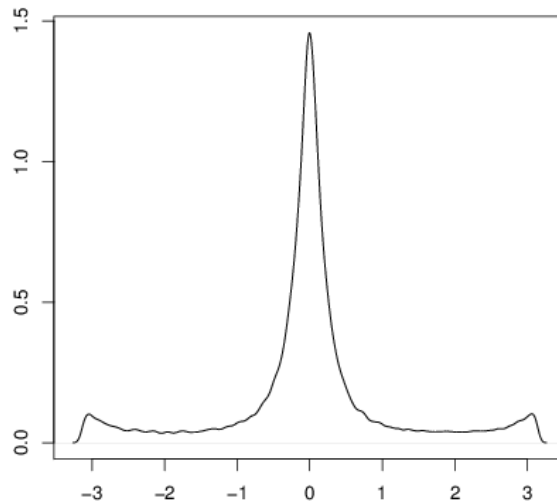


Figure 7.15: Distribution of turning angles after the data had been sampled at a rate of 2.5Hz and a speed threshold of 5mm/s had been introduced.

Various sampling rates were used; 25Hz, 10Hz, 2.5Hz and 1Hz. In order to not lose the fidelity of the turning angles, whilst still removing as many of the erroneous large turns as possible, as well as giving a large enough temporal window between time steps to give a reasonable spread of step-lengths, the 2.5Hz sampling rate was considered the most accurate (Delcourt et al, 2013), although it should be noted the alternative sampling rates did not qualitatively change the results.

The consequences of instigating a speed threshold as well as a sampling rate resulted in a turning angle distribution which had smaller swan wings and was symmetric about 0 (Fig. 7.15).

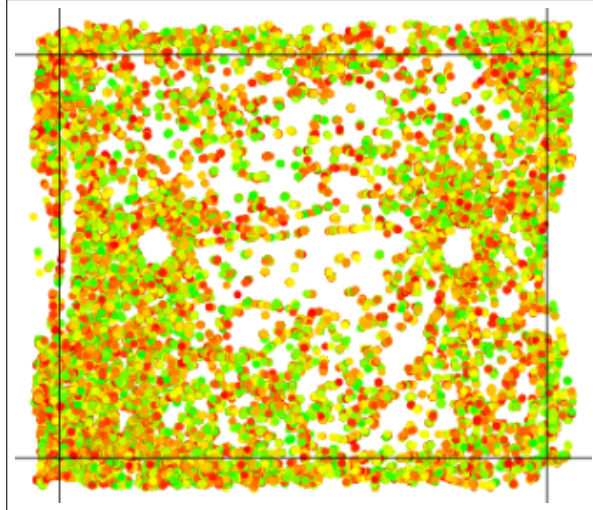


Figure 7.16: Demonstrating the locations of large turns with magnitude ($> \pi/2$). Green points are closer to $\pi/2$ with red turns closer to π . Points are for all fish across all trials in the simple environment only.

Finally, due to the confines of the experimental setup, the effect of the borders of the tank were investigated to ascertain as to whether the majority of the large turns were caused by the fish coming into contact or proximity with the walls of the tank. This was tested by plotting the locations of all large turns (those with magnitude greater than $\pi/2$). Fig. 7.16 demonstrates that these large turns were concentrated, not just at the walls but also near to the objects, with fewer taking place within open water, although there was a spread across the entirety of the experimental arena. Simply removing the turns which took place within close proximity to the wall (in this case turns which took place within 5cm of the wall), did not significantly alter the distribution of turning angles (Fig A6) however, as this caused more data to be removed from the analyses without altering the results these points were included in the final analysis. More advanced techniques for interpreting interactions with walls and barriers have been considered by Gautrais et al (2009) however here these were not included in order to keep the analysis as simple as possible.

Therefore, in the final analysis a speed threshold of 5mm/s and a sampling rate of 2.5Hz was chosen, without any additional effects caused by barrier interaction taken into account.

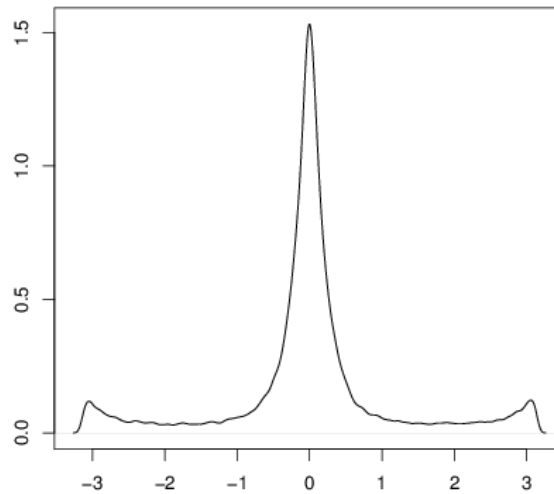


Figure 7.17: Distribution of turning angles with a sub-sampling rate of 2.5Hz, a speed threshold of 5mm/s and the removal of turns close to the border of the experimental tank.

Simple Population level analysis

As a simple preliminary comparison of the effect the different environments had on the movement of the fish when considered as a population, the distributions of turning angles and the instantaneous speeds (step-lengths) were compared. Figures 7.18 & 7.19 indicate that at the population level there was no discernible differences between these simple summary distributions.

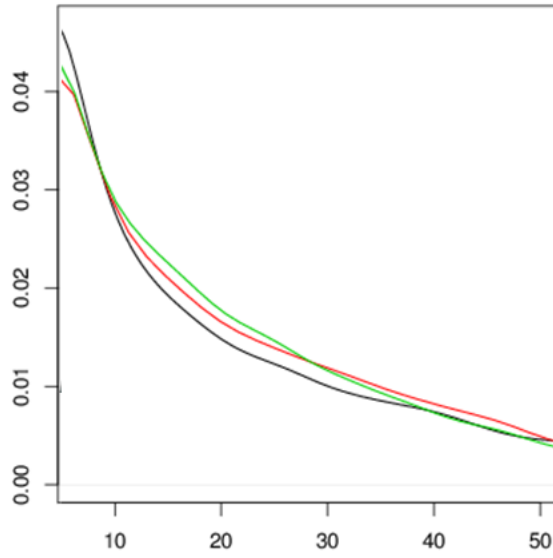


Figure 7.18: Distribution of step-lengths for the simple environment (2 objects) – black; moderate environment (3 objects) red; complex environment (5 objects) – green. Data were subsampled at a rate of 2.5Hz with speed threshold of 5mm/s

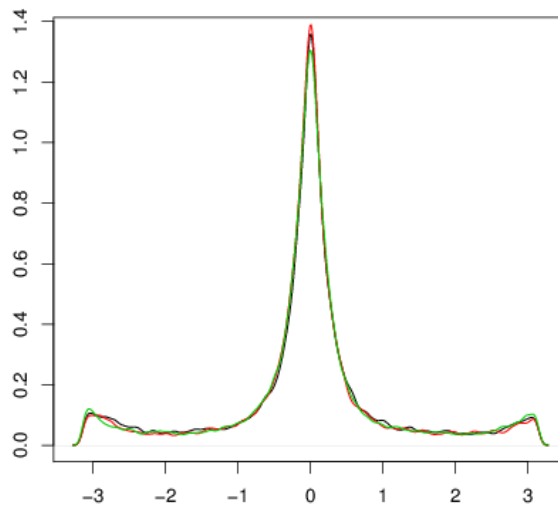


Figure 7.19: Distribution of turning angles for the simple environment (2 objects) – black; moderate environment (3 objects) – red; and complex environment (5 objects) – green. Data were subsampled at 2.5Hz with a speed threshold of 5mm/s

7.6.2 Appendix D2 - Effect of using a different array size for determining space use

In order to estimate the percentage of the arena which the fish visited throughout the experiment the tank was subdivided into an n by n array and the space use percentage was calculated by counting the number of subdivisions which the fish visited at least once divided by the total number of subdivisions. The results would depend upon the number of subdivisions made with too few leading to large areas which would give falsely high values for the space use measure, whereas too fine an array would result in many cells registering as not being visited giving similar and falsely low values for space use. Values considered for n ranged from 10 to 100 at intervals of 10. Fig 7.20 demonstrates that in general the value for n did not affect the value for Space Use relative to each other, although as expected small values of n gave high levels of space use and larger values returned smaller values. The value 50 was chosen as this represented the value of n for which the relative Space Use between fish was constant and it returned the value at which the curves in Fig 7.20 began to return a shallow gradient.

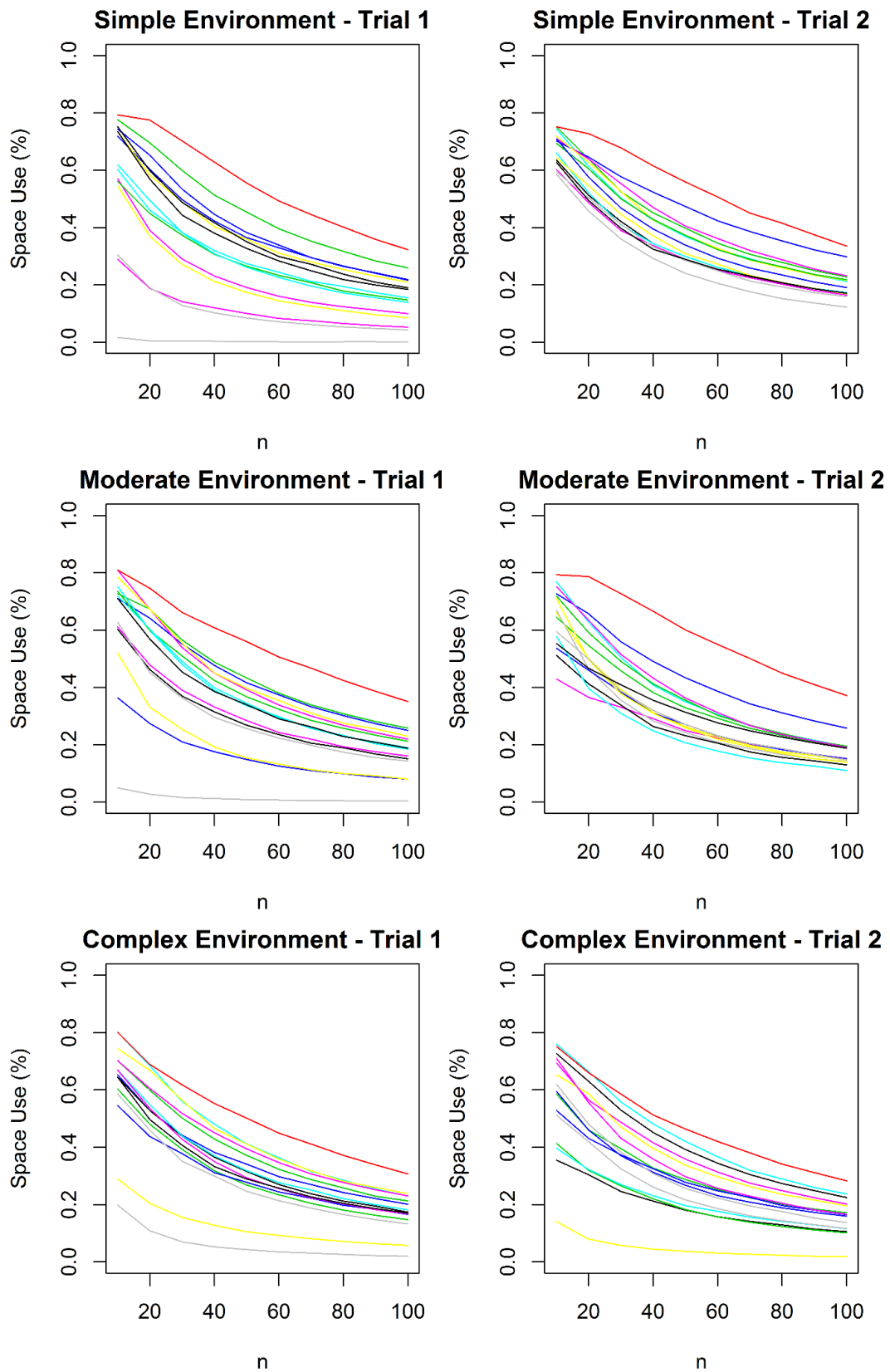


Figure 7.20: The effect of array size (n) against calculated Space Use (%). Results are shown for both the first trial (left column) and the second trial (right column) across each separate environment (rows). Each fish has the same colour in all plots.

7.6.3 Appendix D3 - Effect of using a different value for dividing tank into regions of Free Water, Near the Wall and Near an Object

When considering whether a fish was remaining within the proximity of either an object or the boundary of the tank (wall) a fixed distance was required to be chosen. This classified locations of fish into three distinct areas, Near to an Object, Near to a Wall – where ‘Near to’ was considered being with the fixed distance; all other areas were considered Free Water. In order to determine the most appropriate value for this distance a range of values were initially considered from 10mm to 150mm at 10mm intervals. Fig 7.21 shows how the percentage of time in each location changed as the distance value changed across each environment. In general the plots show a linear relationship between the distance and the % Time for all locations across all three environments, a relationship which becomes even clearer when considering the middle range of 40-100mm. Therefore, whilst the specific choice of value to be used throughout the analysis was somewhat arbitrary, 70mm was chosen as it lay within the middle of the viable range and is the approximate body length of an individual fish.

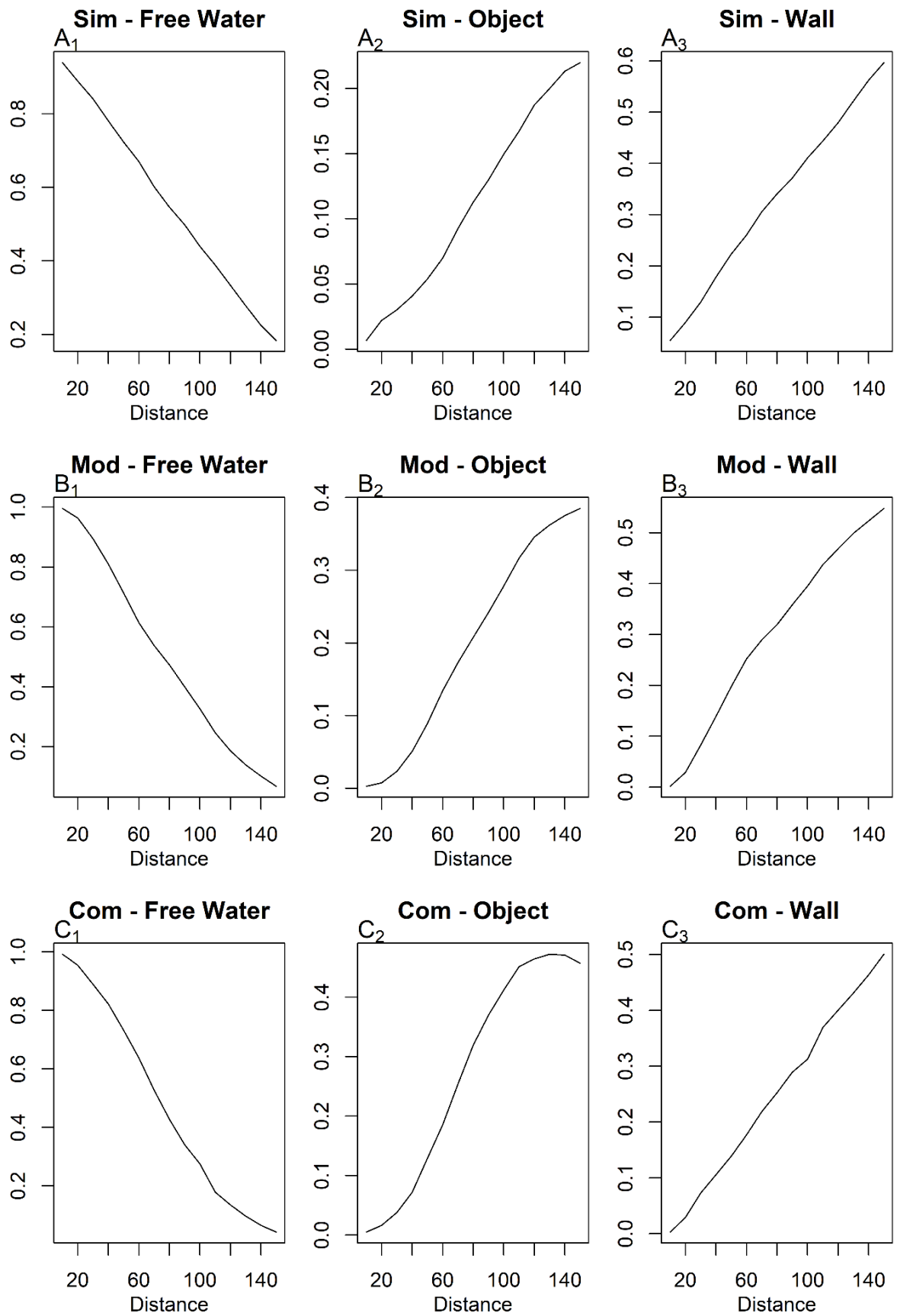


Figure 7.21: Demonstrating how distance for determining if fish were 'near' to a part of the environment (x-axis) effects the % of time spent in that section of the environment.

7.6.4 Appendix D4 - ANOVA Results between fish per environment

An ANOVA was used to test for similarity in the mean values of the calculated statistics between the 15 fish per environment (see section 7.2.4).

Tables 7.6-7.8 show the full results of the ANOVA tests for significance in the variation of the summary statistics discussed in the main text across each other three environments. All tests are for a sampling rate of 2.5Hz and speed threshold value of 5mm/s. Significant results (those with $p < 0.05$) are denoted with an asterisk (*) and imply statistics for which there were significant differences comparing between the 15 fish per environment.

Simple Environment

Cases	Sum of Squares	df	Mean Square	F	p
Distance Moved	2.200e+9	14	1.572e+8	7.246	<.001*
<i>Residual</i>	3.253e+8	15	2.169e+7		
Time spent stationary	0.553	14	0.04	1.752	0.146
<i>Residual</i>	0.338	15	0.023		
Step-length	38.39	14	2.742	2.718	0.036*
<i>Residual</i>	14.12	15	1.009		
TA (rho)	0.147	14	0.011	0.827	0.636
<i>Residual</i>	0.19	15	0.013		
Sinuosity	0.2	14	0.014	1.24	0.341
<i>Residual</i>	0.173	15	0.012		
Burst Frequency	0.004	14	2.897e-4	1.497	0.224
<i>Residual</i>	0.003	15	1.935e-4		
% Space used	0.326	14	0.023	2.893	0.025*
<i>Residual</i>	0.121	15	0.008		
% Time Free Water	0.328	14	0.023	0.725	0.724
<i>Residual</i>	0.485	15	0.032		
% Time Wall	0.336	14	0.024	1.205	0.361
<i>Residual</i>	0.298	15	0.02		
% Time Object	0.112	14	0.008	0.688	0.755
<i>Residual</i>	0.175	15	0.012		

Table 7.6: Results of the ANOVA comparing between individuals for the Simple environment

Moderate Environment

Cases	Sum of Squares	df	Mean Square	F	p
Distance Moved	4.435e+9	14	3.168e+8	2.57	0.04*
<i>Residual</i>	1.849e+9	15	1.233e+8		
Time spent stationary	0.374	14	0.027	1.598	0.189
<i>Residual</i>	0.25	15	0.017		
Step-length	59.827	14	4.273	8.343	<.001*
<i>Residual</i>	7.171	15	0.512		
TA (rho)	0.076	14	0.005	3.192	0.016*
<i>Residual</i>	0.026	15	0.002		
Sinuosity	0.165	14	0.012	1.895	0.116
<i>Residual</i>	0.094	15	0.006		
Burst Frequency	2.657e-4	14	1.898e-5	1.68	0.165
<i>Residual</i>	1.694e-4	15	1.130e-5		
% Space used	0.319	14	0.023	4.447	0.003*
<i>Residual</i>	0.077	15	0.005		
% Time Free Water	0.496	14	0.035	1.774	0.141
<i>Residual</i>	0.3	15	0.02		
% Time Wall	0.512	14	0.037	1.226	0.35
<i>Residual</i>	0.448	15	0.03		
% Time Object	0.365	14	0.026	3.166	0.017*
<i>Residual</i>	0.124	15	0.008		

Table 7.7: Results of the ANOVA comparing between individuals for the Moderate environment

Complex Environment

Cases	Sum of Squares	df	Mean Square	F	p
Distance Moved	4.435e+9	14	3.168e+8	2.57	0.04*
<i>Residual</i>	1.849e+9	15	1.233e+8		
Time spent stationary	0.374	14	0.027	1.598	0.189
<i>Residual</i>	0.25	15	0.017		
Step-length	59.827	14	4.273	8.343	<.001*
<i>Residual</i>	7.171	15	0.512		
TA (rho)	0.076	14	0.005	3.192	0.016*
<i>Residual</i>	0.026	15	0.002		
Sinuosity	0.165	14	0.012	1.895	0.116
<i>Residual</i>	0.094	15	0.006		
Burst Frequency	2.657e-4	14	1.898e-5	1.68	0.165
<i>Residual</i>	1.694e-4	15	1.130e-5		
% Space used	0.319	14	0.023	4.447	0.003*
<i>Residual</i>	0.077	15	0.005		
% Time Free Water	0.496	14	0.035	1.774	0.141
<i>Residual</i>	0.3	15	0.02		
% Time Wall	0.512	14	0.037	1.226	0.35
<i>Residual</i>	0.448	15	0.03		
% Time Object	0.365	14	0.026	3.166	0.017*
<i>Residual</i>	0.124	15	0.008		

Table 7.8: Results of the ANOVA comparing between individuals for the Complex environment

7.6.5 Appendix D5 - MANOVA Results

A MANOVA was used to test whether the mean values of the calculated statistics changed at the population level as the environment changed (see section 7.2.4).

Table 7.9 show the full results of the MANOVA tests for significance in the variation of the summary statistics when comparing the results for all fish at the population level across the three environments. All tests are for a sampling rate of 2.5Hz and speed threshold value of 5mm/s. Significant results (those with $p < 0.05$) are denoted with an asterisk (*) and imply statistics for which there were significant differences comparing between the environments.

	Sphericity		Sum of Squares	Df	Mean Square	F	p
	Correction						
Distance Moved	None		1.693e+8†	2†	8.467e+7†	0.762†	0.471†
	G-G		1.693e+8†	1.272†	1.331e+8†	0.762†	0.418†
<i>Residual</i>	None		6.442e+9	58	1.111e+8		
	G-G		6.442e+9	36.9	1.746e+8		
Time spent stationary	None		0.041	2	0.02	3.209	0.048*
<i>Residual</i>	None		0.366	58	0.006		
Step-length	None		0.956	2	0.478	0.738	0.483
<i>Residual</i>	None		36.263	58	0.648		
TA (rho)	None		0.035†	2†	0.018†	1.765†	0.18†
	G-G		0.035†	1.302†	0.027†	1.765†	0.192†
<i>Residual</i>	None		0.581	58	0.01		
	G-G		0.581	37.76	0.015		
Sinuosity	None		0.017†	2†	0.009†	1.848†	0.167†
	G-G		0.017†	1.54†	0.011†	1.848†	0.177†
<i>Residual</i>	None		0.274	58	0.005		
	G-G		0.274	44.667	0.006		
Burst freq.	None		1.045e-4†	2†	5.223e-5†	0.587†	0.559†
	G-G		1.045e-4†	1.247†	8.380e-5†	0.587†	0.484†
<i>Residual</i>	None		0.005	58	8.897e-5		
	G-G		0.005	36.149	1.428e-4		
Space Used	None		0.007	2	0.004	0.847	0.434
<i>Residual</i>	None		0.243	58	0.004		
% Time Free Water	None		0.07	2	0.035	1.663	0.198
<i>Residual</i>	None		1.219	58	0.021		
% Time Wall	None		0.051	2	0.026	0.923	0.403
<i>Residual</i>	None		1.606	58	0.028		
% Time Object	None		0.199	2	0.1	6.934	0.002*
<i>Residual</i>	None		0.833	58	0.014		

Table 7.9: Results of the MANOVA comparing within individuals as the environment changed. Values marked with (†) indicates the assumption of sphericity is violated found by Mauchly's test of sphericity ($p < 0.05$), hence the G-G (Greenhouse-Geisser) correction is implemented

7.6.6 Appendix D6 - Movement Model Comparison and Selection

To compare between the three simple models for individual fish movement considered in the main text (section 7.2.4), plots comparing the observed summary statistics to do with spatial characteristics of movement (Net Distance Moved, Space Use (%), Occupation Time in Free Water, Occupation Time near Object, Occupation Time near Wall) were compared with those found by running simulations for each of the models for an equivalent number of individuals (15), trials (2) and environments (3). Figs. 7.22-7.24 show the results and indicates that the third model, a CRW with a parameter controlling the Time Spent stationary, gave the closest results to the observed data.

Figure 7.25 gives examples of the movement created using the CRW movement model with ν the parameter for time spent stationary. Plots show example movement through the complex environment (5 objects) with 3 different values for time spent stationary (ν), $\nu = 0.8, 0.6, 0.3$ (Fig 7.25A-C respectively)

Model (i) - SRW

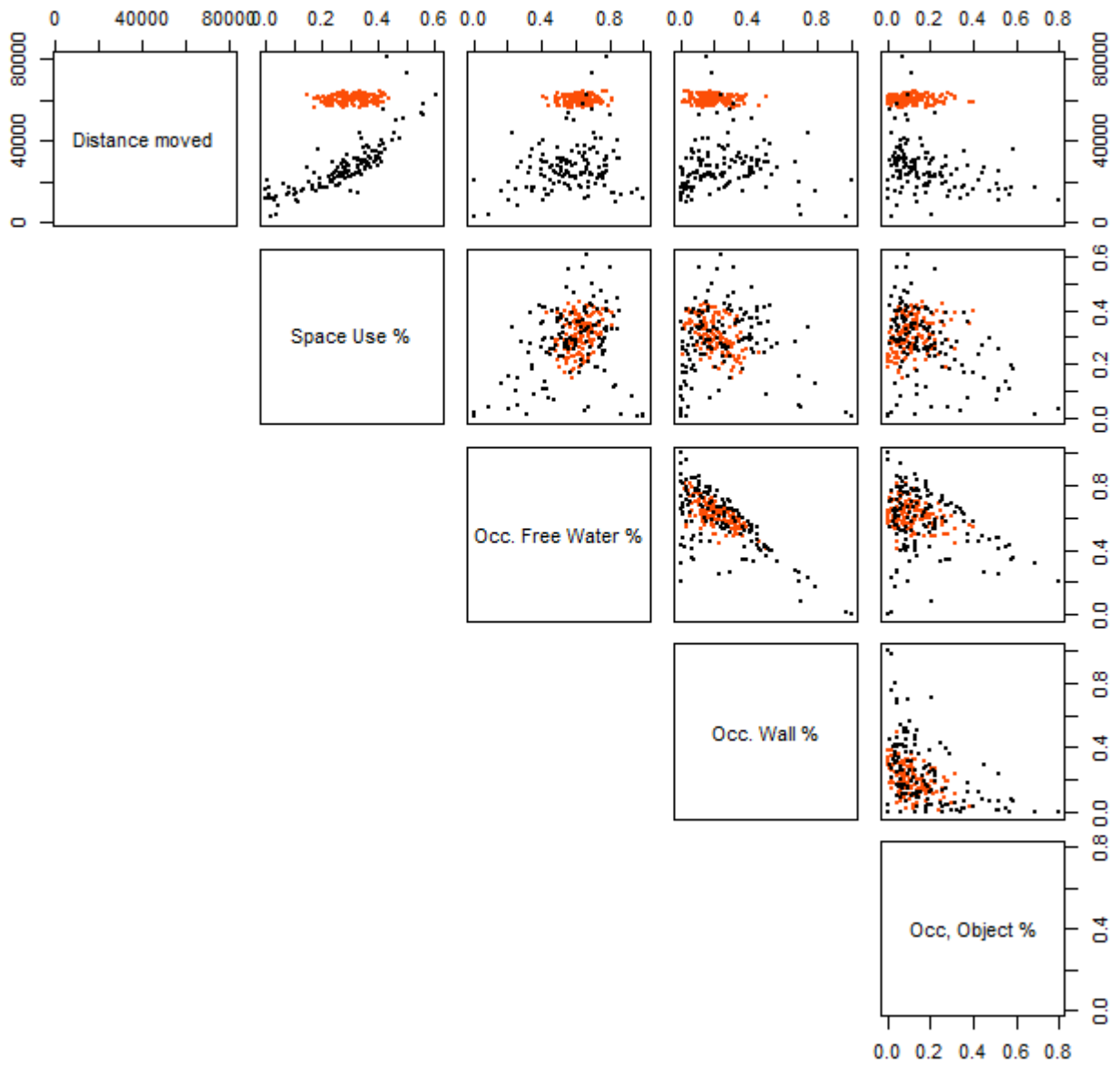


Figure 7.22: Scatter-plots of the calculated statistics of Distance Moved, Space Use & Occupation Time, comparing between the simulations for model (i) a SRW (orange) and the observed data (black)

Model (ii) - CRW

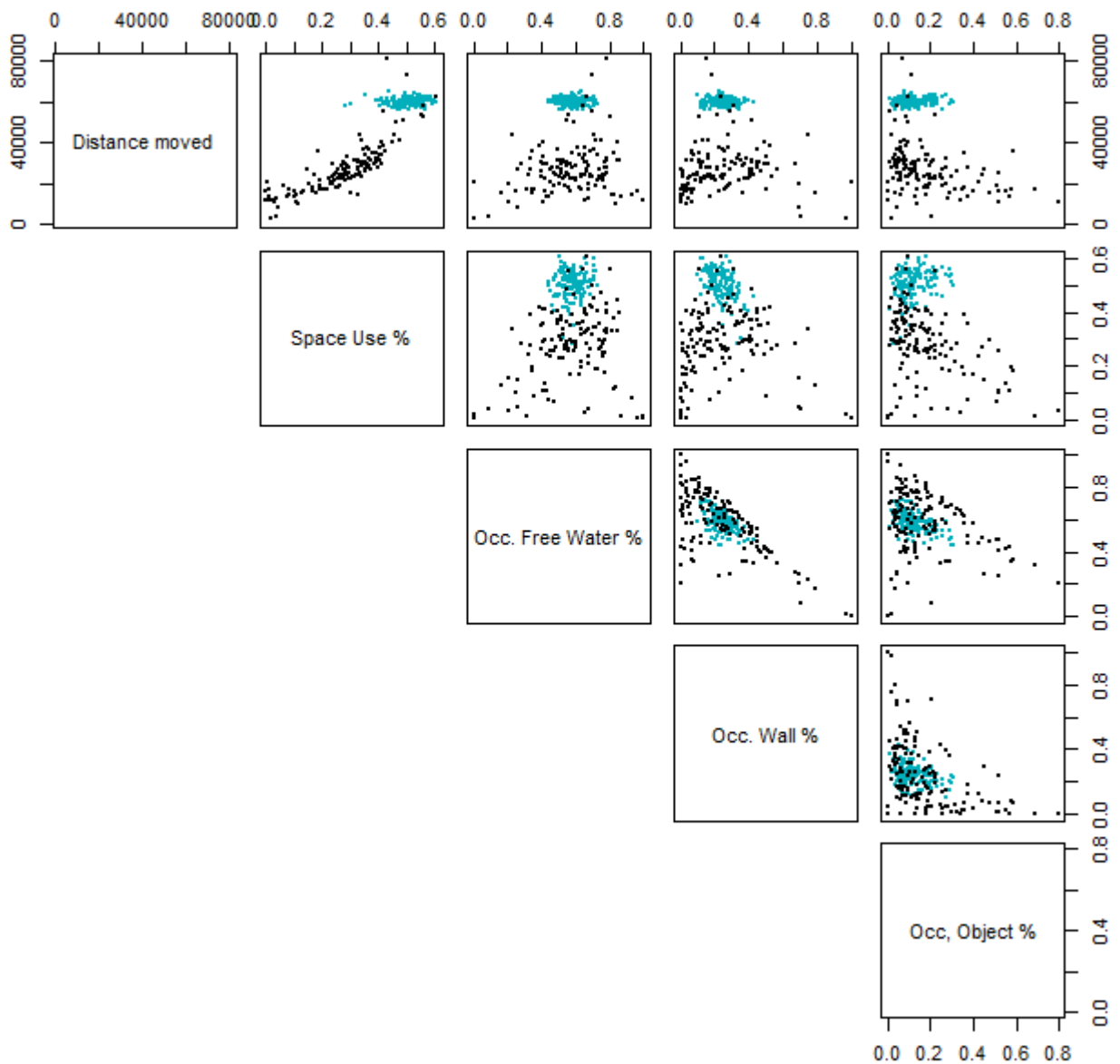


Figure 7.23: Scatter-plots of the calculated statistics of Distance Moved, Space Use & Occupation Time, comparing between the simulations for model (ii) a CRW (blue) and the observed data (black)

Model (iii) - CRW with non-moving parameter

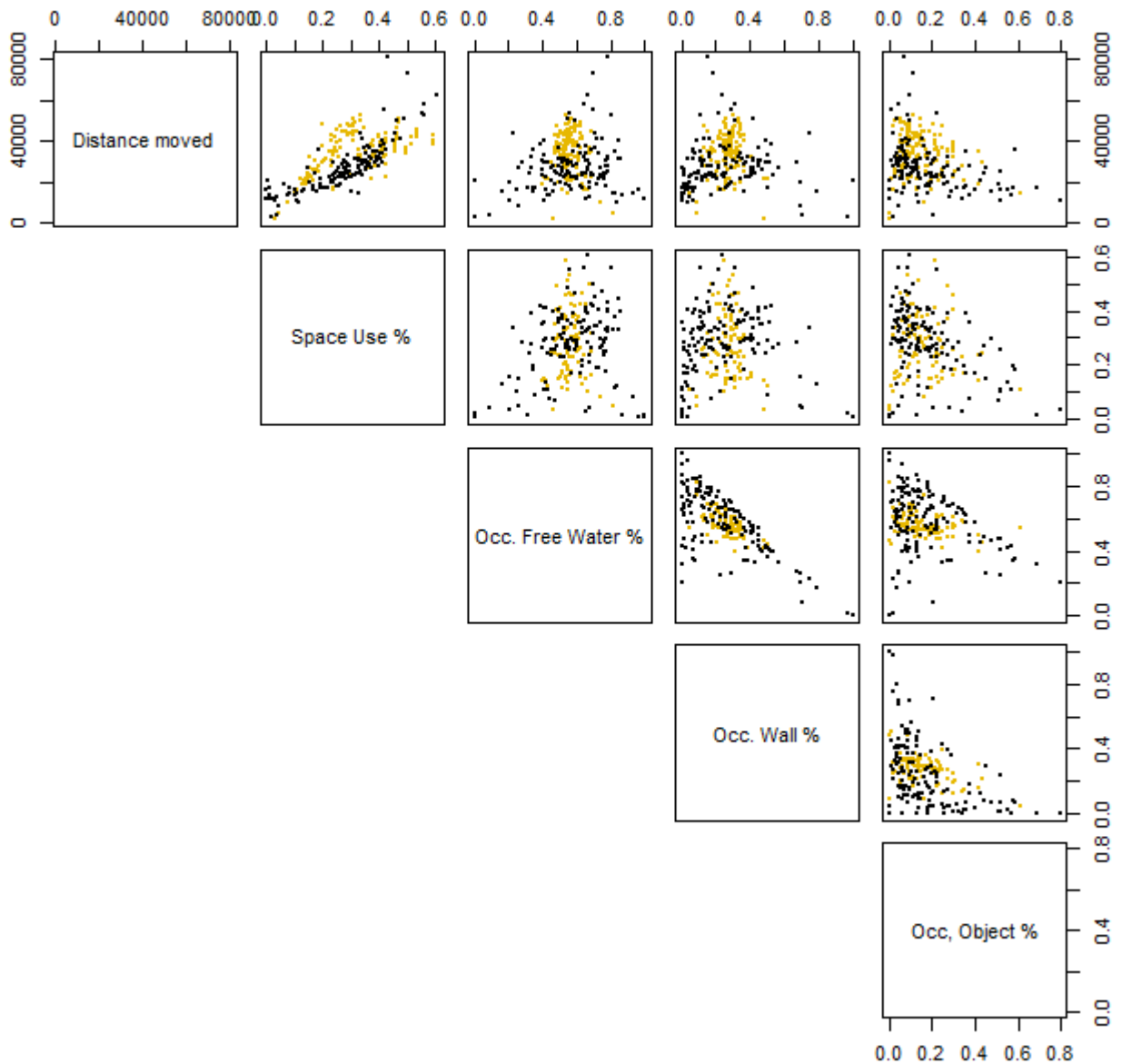


Figure 7.24: Scatter-plots of the calculated statistics of Distance Moved, Space Use & Occupation Time, comparing between the simulations for model (iii) a CRW with waiting times (gold) and the observed data (black)

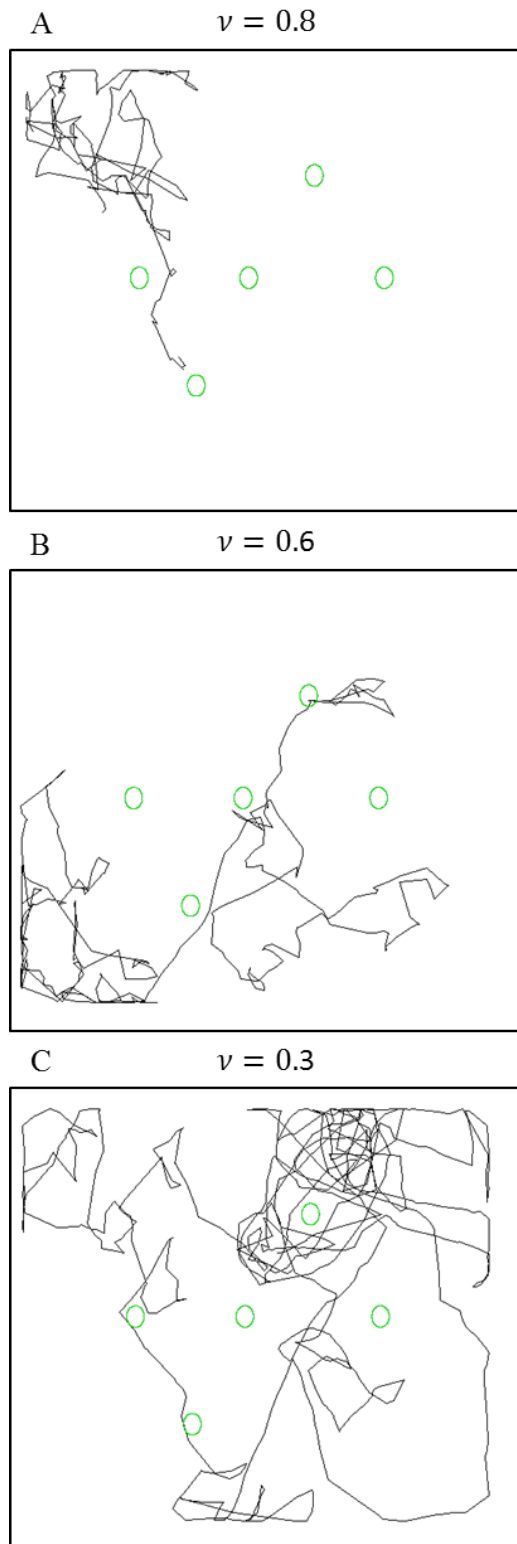


Figure 7.25: Example movement paths from a simulation of model (iii) a CRW with waiting times, over the complex environment (featuring 5 objects) for a range of values of Time Spent Stationary (ν)

8 Conclusion

In this thesis we have used both theoretical and data driven techniques to analyse and describe individual animal movement. We have demonstrated how theoretical approaches to modelling animal movement can help inform and understand the mechanics of movement. Such as how the efficiency in navigation is affected by the level of uncertainty in the knowledge of the location of a target (Chapter 4) and how the distribution of turning angles across a movement path can indicate the presence of different movement behaviours (Chapter 6).

We have used the framework of RW theory to investigate the dispersal potential of *P. cupreus* beetles (Chapter 5), demonstrating that individual variability must be taken into account when attempting to predict movement behaviour and that simply aggregating behaviour at the population level fails to predict the observed movement behaviours, such as the expected displacement (Fig 5.5A). Similarly, we have explored how a simple change in experimental setup can affect movement behaviour of stickleback fish and have indicated how movement parameters can relate to animal ‘personality’ (Chapter 7).

There are a number of ways in which the work here can be furthered, with many having been highlighted in the Discussion sections of Chapters 4-7. Here the most pertinent of these are briefly introduced and we highlight some of the other aspects in the field of movement ecology which should be explored in future research.

8.1 Extending the BCRW model in Chapter 4 to include group dynamics

One clear area in which the BCRW movement model described in Chapter 4 could be extended is consider group navigation. This would require introducing extra parameters describing how individuals interact with the group (Herbert-Read et al, 2011; Mann et al, 2013; Eriksson et al, 2010; Pettit et al, 2013). This has been explored by Codling & Bode (2014; 2016) who included an extra parameter which at each time step moved

the individual along the averaged direction of the group from the previous step. The results demonstrated that the most efficient navigational strategy was to give a high weighting to indirect cues (copying the movement of other group members or using forward persistence), rather than relying on direct navigational cues. However, this was done through simulations only and an analytical approach could give more information into why this finding is the case. It would also potentially lead to predictions of models were the rules for the group interaction differ. Similarly, Ose & Ohmann (2017) have demonstrated through extensive simulation that random noise in individual movement, facilitates improvements in the efficiency of group movement as well as helping to ensure compactness of the groups, an important factor in herd movement. Ose & Ohmann (2017) used a Voroni cell configuration in their group interaction term, however, if an analytical method for predicting the movement behaviour could be determined, then this unexpected finding of randomness being beneficial for efficient movement could be explained. Such analytical solutions would also allow for predictions of long term movement behaviour without needing to run large scale simulations. Both these problems would prove to be analytically difficult and utilising the method from Chapter 4 for the individual case would be non-trivial as that method made use of many approximations which will compound at the group level. Therefore another approach perhaps similar to that of Binhi (2017) who used SDEs to model individual movement within the group could be used.

8.2 Integrating animal ‘personality’ and movement ecology

Results from the analysis of the beetles’ and fish movement indicated that individuality has a clear impact on movement dynamics at both the individual and the population level. As ‘personality’ is often defined by consistency in individual behaviour across time and changing environment then understanding how ‘personality’ traits are linked with movement behaviour should have important ramifications in spatial ecology. ‘Personality’ has already been shown to affect foraging behaviour, sociability (reactions and interactions to others), exploration and migration (Nilsson et al, 2014).

In general the integration of personality has not explicitly been included in movement ecology studies (Nilsson et al, 2014; Spiegel et al, 2017; Patrick & Weimerskirch, 2014). This has recently been addressed by Spiegel et al (2017) who focused on expanding the framework of personality dependent dispersal behaviour to include methods from movement ecology into what they term *personality dependent spatial ecology*. This aims to link the spatial consequences of various personality traits with the effects these spatial dynamics have on space-use, therefore, linking personality into important movement ecological behaviour such as foraging strategy and efficiency. Expanding our simple experimental setup from Chapter 7 to include the paradigm of Spiegel et al (2017) could help integrate the two fields. Although there are many pitfalls which need to be considered in any future work. Spiegel et al (2017) discussed many of these, including the problem of identifying between changes in behaviour within movement data due to the change in environment compared to changes in behaviour due to individuality. Much work has been recently developed in identifying changes in behaviour in movement ecology, through behavioural change point analyses (BCPA) (Gurarie et al, 2016; Parton & Blackwell, 2017; Michelot & McClintock, 2018). Work to identify which common movement descriptors are effected by personality traits, would allow the variation of these parameters at both the within and between individual level to be included in the methods used in these analyses, giving more accurate classifications of movement behaviour, space-use and personality.

8.3 Understanding and analysing large data sets

As we have seen in Chapter 5 and 7 data can now be recorded at high frequencies and high densities. Section 2.7 noted that as tagging methods become cheaper, smaller, more accurate and more efficient the volume of movement data available for analysis has rapidly increased and out-grown many of the current analytical techniques used in movement ecology (Rodriguez et al, 2017; Munden et al, 2018)

An area in which handling such large-scale data has seen recent developments is that of human behaviour. This has been caused by the rise of personal data-logging tech-

nologies (Thums et al, 2018). Therefore, integrating the techniques used for analysing and understanding these big data sets could lead to more accurate and efficient computational techniques for movement ecology (Miller et al, 2019). Miller et al (2019) identifies the similarities in the aims of the fields, such as measuring and classifying interactions between individuals, analysing movement behaviours across a changing environment and/or time period, integrating covariates which are now readily measurable alongside simple time-position data (e.g. temperature, humidity, depth, pressure) as well as conditions of the individual themselves (e.g. heart rate, body temperature, breathing rate). They suggest approaches which could be integrated into movement ecology taken from the human movement literature, such as context-aware movement models which investigate how a changing environment effects individual movement (Dodge, 2014) and how interactions amongst individuals can be classified; building on the work of (Do & Gatica-Perez, 2013; Sapiezynski et al, 2017) who used Bluetooth or Wi-Fi sensors in mobile devices to infer the behaviour from interactions.

Similarly, Thums et al (2018) listed four main areas in which movement ecology would benefit from a closer relationship with human mobility research due to the latter's adoption of dig data techniques; these were "(1) identification of emergent properties in animal movement, (2) analysis of networks of animal movement and behaviour, (3) development of machine learning algorithms to understand and characterise patterns from "big" animal movement data and (4) advanced visualisation techniques for complex datasets of movement" (Thums et al, 2018).

8.4 Extending the work in Chapter 6 for use in data analysis

The work in Chapter 6 indicated that the mixing of two normal-type circular distributions could produce a highly peaked, heavy-tailed circular distribution and that it was therefore possible to discern multiple behaviours in a movement path based on the distribution of the turning angles. In the brief example using data from an African Elephant (Wall et al, 2014a) it was demonstrated that two distinct behaviours in turning angles could be found, along with the mixing parameter which described the relative

frequency of drawing angles form one distribution compared to the other. An extension here would be to then use these values to segregate the movement path into passages from each distribution and therefore allowing for the classification of movement into two behaviours.

Although as is mentioned in the example in Chapter 6 more advanced techniques which take into account the distribution of step-lengths as well as other covariates, already exist (Michelot & McClintock, 2018) and are therefore more powerful in their analysis than this method would be. However, these advanced methods often rely on using HMM techniques which are sensitive to initial conditions, therefore a more practical use of the findings from Chapter 6 would be to find an efficient method for estimating the concentration parameters of the two distributions for the turning angles and the mixing parameter. This could be achieved by introducing an efficient search algorithm such as Nelder-Mead (Nelder & Mead, 1965) rather than the slow parameter sweep method used in the example (section 6.4). These parameter values could then be used to classify the behaviour of the path in order to extract likely parameters for the step-lengths which could then be used in the HMM technique as the initial conditions in order to give an accurate final classification.

Other extensions for this chapter would be to expand to more than two distributions in the initial case, therefore corresponding to more behaviours across the movement path. In general, behavioural states of animals are limited to 2-3 in any given path and so, any work beyond mixing three distributions would seem unnecessary. Also the current techniques require numerical simulations and even simply increasing to three distributions we increase the number of parameters by two (an additional concentration parameter and mixing term) which will greatly affect any attempt to efficiently calculate such parameters from actual data. Hence an increase in the number of distributions without a more thorough method for discerning the best-fit distribution, would need to be limited.

9 References

- Aebischer, A., Nyffeler, P. and Arlettaz, R. (2010). Wide-range dispersal in juvenile Eagle Owls (*Bubo bubo*) across the European Alps calls for transnational conservation programmes. *Journal of Ornithology*, 151(1), 1.
- Agostinelli C. and Lund, U. (2017). R package 'circular': Circular Statistics (version 0.4-93). URL <https://r-forge.r-project.org/projects/circular>.
- Ahmed, D.A., Petrovskii, S.V. and Tilles, P.F.C. (2018). The “Lévy or Diffusion” Controversy: How Important Is the Movement Pattern in the Context of Trapping? *Mathematics*, 6(77).
- Auger-Méthé, M., St Clair, C. C., Lewis, M. A., and Derocher, A. E. (2011). Sampling rate and misidentification of Lévy and non-Lévy movement paths: comment. *Ecology*, 92(8), 1699-1701.
- Bachelier, L. (1900). Théorie de la spéculation. In *Annales scientifiques de l'École normale supérieure* (Vol. 17, pp. 21-86).
- Bailey, H. and Thompson, P. (2006). Quantitative analysis of bottlenose dolphin movement patterns and their relationship with foraging. *Journal of Animal Ecology*, 75: 456–465.
- Bailey, J.D., Benerfer, C., Blackshaw, R. and Codling, E.A. (2019). Walking behaviour in the ground beetle *Poecilus cupreus*: individual variation, intermittency, and dispersal potential. Unpublished data
- Bailey, J.D., Wallis, J. and Codling, E.A. (2018). Navigational efficiency in a biased and correlated random walk model of individual animal movement. *Ecology*, 99(1), 217–223.
- Baird, E., Byrne, M.J., Smolka, J., Warrant, E.J. and Dacke, M. (2012). The Dung Beetle Dance: An Orientation Behaviour? *PLOS ONE*, 7(1), e30211.

- Banks, J.E., Laubmeier, A.N. and Banks, H.T. (2019). Modelling the effects of field spatial scale and natural enemy colonization behaviour on pest suppression in diversified agroecosystems. *Agricultural and Forest Entomology*
- Bartoń, K. A., Phillips, B. L., Morales, J. M. and Travis, J. M. J. (2009). The evolution of an ‘intelligent’ dispersal strategy: biased, correlated random walks in patchy landscapes. *Oikos*, 118(2), 309–319.
- Barton, P.S., Lentini, P.E., Alacs, E., Bau, S., Buckley, Y.M., Burns, E.L., Driscoll, D.A., Guja, L.K., Kujala, H., Lahoz-Monfort, J.J. and Mortelliti, A. (2015). Guidelines for Using Movement Science to Inform Biodiversity Policy. *Environmental Management*, 56(4), 791-801.
- Bartumeus, F., Catalan, J., Viswanathan, G. M., Raposo, E. P., and da Luz, M. G. E. (2008). The influence of turning angles on the success of non-oriented animal searches. *Journal of Theoretical Biology*, 252(1), 43–55.
- Bastola, A. and Davis, J.A. (2018). Determining in-field dispersal of the redbanded stink bug (Hemiptera: Pentatomidae) in soybean fields using a protein based mark-capture method. *Crop Protection*, 112, 24–32.
- Bearup, D., Benefer, C. M., Petrovskii, S. V., and Blackshaw, R. P. (2016). Revisiting Brownian motion as a description of animal movement: a comparison to experimental movement data. *Methods in Ecology and Evolution*, 7(12), 1525-1537.
- Ben-Ari, M. and Inbar, M. (2014). Aphids link different sensory meanities to accurately interpret ambiguous cues. *Behavioral Ecology*, 25(3), 627-632.
- Bengtsson, G., Rydén, T., Öhrn, M. S. and Wiktorsson, M. (2002). Statistical analysis of the influence of conspecifics on the dispersal of a soil Collembola. *Theoretical Population Biology*, 61(2), 97-113.
- Benhamou, S. (2004). How to reliably estimate the tortuosity of an animal’s path: straightness, sinuosity, or fractal dimension? *Journal of Theoretical Biology*, 229(2), 209-220.

- Benhamou, S. (2006). Detecting an orientation component in animal paths when the preferred direction is individual dependent. *Ecology*, 87(2), 518-528
- Benhamou, S. (2014). Of scales and stationarity in animal movements. *Ecology Letters*, 17(3), 261-272.
- Benhamou, S., and Bovet, P. (1992). Distinguishing between elementary orientation mechanisms by means of path analysis. *Animal Behaviour*, 43(3), 371-377.
- Benjamin, R., Cédric, G. and Pablo, I. (2008). Modeling spatially explicit population dynamics of *Pterostichus melanarius* I11. (Coleoptera: Carabidae) in response to changes in the composition and configuration of agricultural landscapes. *Landscape and Urban Planning*, 84(3-4), 191–9.
- Berkes, F., Colding, J. and Folke, C. (Eds.). (2008). *Navigating social-ecological systems: building resilience for complexity and change*. Cambridge University Press.
- Berthold, P. (2001). *Bird migration: a general survey*. Oxford University Press on Demand.
- Biegler, R. (2000). Possible uses of path integration in animal navigation. *Animal Learning and Behavior*, 28(3), 257-277.
- Binhi, V.N. (2017). Restrictions on the dynamic growth of navigation accuracy in groups of animals. eprint arXiv:1702.00590
- Biro P.A. and Stamps, J.A. (2008). Are animal personality traits linked to life-history productivity? *Trends in Ecology and Evolution*. 23(7), 361-368.
- Blackwell, P. G., Niu, M., Lambert, M. S. and LaPoint, S. D. (2016). Exact Bayesian inference for animal movement in continuous time. *Methods in Ecology and Evolution*, 7(2), 184-195.
- Blake, S., Yackulic, C. B., Cabrera, F., Tapia, W., Gibbs, J. P., Kummeth, F., and Wikelski, M. (2013). Vegetation dynamics drive segregation by body size in Gala-

- pagos tortoises migrating across altitudinal gradients. *Journal of Animal Ecology*, 82(2), 310–321.
- Bode, N.W.F., Faria, J.J., Franks, D.W., Krause, J. and Wood, A.J. (2010). How perceived threat increases synchronization in collectively moving animal groups. *Proceedings of the Royal Society B*, 277(1697), 3065-3070.
- Bohan, D.A., Boursault, A., Brooks, D.R. and Petit, S. (2011). National-scale regulation of the weed seedbank by carabid predators. *Journal of Applied Ecology*, 48(4), 888–98.
- Bohrer, G., Brandes, D., Mandel, J. T., Bildstein, K. L., Miller, T. A., Lanzone, M., Katzner, T., Maisonneuve, C. and Tremblay, J. A. (2012). Estimating updraft velocity components over large spatial scales: contrasting migration strategies of golden eagles and turkey vultures. *Ecology Letters*, 15(2), 96-103.
- Boulinier, T., Kada, S., Ponchon, A., Dupraz, M., Dietrich, M., Gamble, A., Bourret, V., Duriez, O., Bazire, R., Tornos, J. and Tveraa, T. (2016). Migration, prospecting, dispersal? What host movement matters for infectious agent circulation?. *Integrative and Comparative Biology*, 56(2), 330-342.
- Bovet, P., and Benhamou, S. (1988). Spatial analysis of animals' movements using a correlated random walk model. *Journal of Theoretical Biology*, 131(4), 419-433.
- Bowlby, H. D., Hanson, J. M., and Hutchings, J. A. (2007). Resident and dispersal behavior among individuals within a population of american lobster *homarus americanus*. *Marine Ecology Progress Series*, 331, 207–218.
- Boyce, M. S., Pitt, J., Northrup, J. M., Morehouse, A. T., Knopff, K. H., Cristescu, B., and Stenhouse, G. B. (2010). Temporal autocorrelation functions for movement rates from global positioning system radiotelemetry data. *Philosophical Transactions of the Royal Society B: Biological Sciences*, 365(1550), 2213-2219

- Boyd, C., Punt, A.E., Weimerskirch, A. and Bertrand, S. (2014). Movement models provide insights into variation in the foraging effort of central place foragers. *Ecological Modelling*, 286, 13-25.
- Breder, Jr C. M. (1954). Equations Descriptive of Fish Schools and Other Animal Aggregations. *Ecology*, 35(3); 361-370.
- Breed, G. A., Costa, D. P., Jonsen, I. D., Robinson, P. W., and Mills-Flemming, J. (2012). State-space methods for more completely capturing behavioral dynamics from animal tracks. *Ecological Modelling*, 235, 49–58.
- Brommer, J. E. (2013). On between-individual and residual (co) variances in the study of animal personality: are you willing to take the “individual gambit”? *Behavioral Ecology and Sociobiology*, 67(6), 1027-1032.
- Brommer, J. E., Karell, P., Ahola, K. and Karstinen, T. (2014). Residual correlations, and not individual properties, determine a nest defense boldness syndrome. *Behavioral Ecology*, 25(4), 802-812.
- Brown, L. M. and Crone, E. E. (2016). Individual variation changes dispersal distance and area requirements of a checkerspot butterfly. *Ecology*, 97(1), 106–115.
- Brown, R. (1828). A brief account of microscopical observations made in the months of June, July and August, 1827, on the particles contained in the pollen of plants; and on the general existence of active molecules in organic and inorganic bodies, *Philosophical Magazine N. S.* 4 ,161-173.
- Burn, A.J., Coaker, T.H. and Jepson, P.C. (Eds). (1987). *Integrated pest management*. Academic Press; 1987.
- Byers, J.A. (2001). Correlated random walk equations of animal dispersal resolved by simulation. *Ecology*, 82(6), 1680-1690.
- Byrne, M., Dacke, M., Nordström, P., Scholtz, C. and Warrant, E. (2003). Visual cues used by ball-rolling dung beetles for orientation. *Journal of Comparative*

Physiology A, 189(6), 411-418.

- Cagnacci, F., Boitani, L., Powell, R. A. and Boyce, M. S. (2010). Animal ecology meets GPS-based radiotelemetry: a perfect storm of opportunities and challenges. *Philosophical Transactions of the Royal Society B: Biological Sciences*, 365, 2157-2162.
- Cagnacci, F., Focardi, S., Ghisla, A., van Moorter, B., Merrill, E. H., Gurarie, E., Heurich, M., Mysterud, A., Linnell, J., Panzacchi, M. and May, R. (2016). How many routes lead to migration? Comparison of methods to assess and characterize migratory movements. *Journal of Animal Ecology*, 85(1), 54–68.
- Carter, A.J., Feeney, W.E., Marshall, H.H., Cowlshaw, G. and Heinsohn, R. (2013). Animal personality: what are behavioural ecologists measuring? *Biological Reviews*, 88(2), 465-475.
- Carpenter, S.R. (1996). Microcosm experiments have limited relevance for community and ecosystem ecology. *Ecology*, 77(3), 677–680
- Carter, A.J., Marshall, H.H., Heinsohn, R. and Cowlshaw, G. (2013). Personality predicts decision making only when information is unreliable. *Animal Behaviour*, 86(3), 633-639.
- Castle, K. T., Weller, T. J., Cryan, P. M., Hein, C. D. and Schirmacher, M. R. (2015). Using sutures to attach miniature tracking tags to small bats for multimonth movement and behavioral studies. *Ecology and Evolution*, 5(14), 2980-2989.
- Chapman, B.B., Hulthén, K., Blomqvist, D.R., Hansson, L.-A., Nilsson, J.-Å., Brodersen, J., Anders Nilsson, P., Skov, C. and Brönmark, C. (2011). To boldly go: individual differences in boldness influence migratory tendency: Boldness influences migratory tendency. *Ecology Letters*, 14(9), 871–6.
- Cheung, A., Zhang, S. W., Stricker, C. and Srinivasan, M.V. (2007). Animal navigation: the difficulty of moving in a straight line. *Biological Cybernetics*, 97(1), 47-61.

- Cheung, A., Zhang, S. W., Stricker, C. and Srinivasan, M.V. (2008). Animal navigation: general characteristics of directed walks. *Biological Cybernetics* 99(3), 197-217.
- Chittka, L., Williams, N.M., Rasmussen, H., Thomson, J.D. (1999). Navigation without vision: bumblebee orientation in complete darkness. *Proceedings of the Royal Society of London. Series B: Biological Sciences*, 266(1414), 45-50.
- Codling, E.A., and Plank, M.J. (2011). Turn designation, sampling rate and the misidentification of power laws in movement path data using maximum likelihood estimates. *Theoretical Ecology*, 4(3), 397-406.
- Codling, E.A., and Bode, N.W.F. (2014). Copycat dynamics in leaderless animal group navigation. *Movement Ecology*, 2(1), 11.
- Codling, E.A., and Bode, N.W.F. (2016). Balancing direct and indirect sources of navigational information in a leaderless model of collective animal movement. *Journal of Theoretical Biology*, 39, 32-42.
- Codling, E.A., and Hill, N.A. (2005). Sampling rate effects on measurements of correlated and biased random walks. *Journal of Theoretical Biology*, 233(4), 573-588.
- Codling, E.A., Bearon, R.N. and Thorn, G.J. (2010). Diffusion about the mean drift location in a biased random walk. *Ecology*, 91(10), 3106-3113.
- Codling, E.A., Plank, M.J. and Benhamou, S. (2008). Random walk models in biology. *Journal of the Royal Society Interface*, 5(25), 813-834.
- Collett, D. and Lewis, T. (1981). Discriminating between the von mises and wrapped normal distributions. *Australian Journal of Statistics*, 23(1), 73-79.
- Cooke, S. J., Midwood, J. D., Thiem, J. D., Klimley, P., Lucas, M. C., Thorstad, E. B., Eiler, J., Holbrook, C. and Ebner, B.C. (2013). Tracking animals in freshwater with electronic tags: past, present and future. *Animal Biotelemetry*, 1(1), 5.
- Cote, J., Clobert, J., Brodin, T., Fogarty, S. and Sih, A. (2010). Personality-dependent dispersal: characterization, ontogeny and consequences for spatially structured

- populations. *Philosophical Transactions of the Royal Society B: Biological Sciences*, 365(1560), 4065-4076.
- Crist, T.O., Guertin, D.S., Wiens, J.A. and Milne, B.T. (1992). Animal Movement in Heterogeneous Landscapes: An Experiment with *Eleodes* Beetles in Shortgrass Prairie. *Functional Ecology*, 536-544.
- Cushman, S. A. (2010). Animal movement data: GPS telemetry, autocorrelation and the need for path-level analysis. In *Spatial complexity, informatics, and wildlife conservation* (pp. 131-149). Springer, Tokyo
- Dacke, M., Byrne, M.J., Scholtz, C.H. and Warrant, E.J. (2004). Lunar orientation in a beetle. *Proceedings of the Royal Society of London B: Biological Sciences*, 271(1537), 361–5.
- Dahmen, H., Wahl, V. L., Pfeffer, S. E., Mallot, H. A., and Wittlinger, M. (2017). Naturalistic path integration of *Cataglyphis* desert ants on an air-cushioned lightweight spherical treadmill. *Journal of Experimental Biology*, 220(4), 634–644.
- Dall, S.R., Houston, A.I. and McNamara, J.M. (2004). The behavioural ecology of personality: consistent individual differences from an adaptive perspective. *Ecology Letters*, 7(8), 734-747.
- Darwin, C. (2004). *On the origin of species*, 1859. Routledge.
- DasGupta, A. (2008). Metrics, Information Theory, Convergence, and Poisson Approximations. In DasGupta, A., editor, *Asymptotic Theory of Statistics and Probability*, Springer Texts in Statistics, pages 19–34. Springer New York, New York, NY.
- Datadryad.org. (2019). Dryad Digital Repository - Dryad. [online] Available at: <http://www.datadryad.org/> [Accessed 9 Apr. 2019].
- Day, T. and McPhail, J.D. (1996). The effect of behavioural and morphological plasticity on foraging efficiency in the threespine stickleback (*Gasterosteus* sp.) *Oecologia* 108(2), 380-388.

- de Jager, M., Weissing, F. J., Herman, P. M., Nolet, B. A. and van de Koppel, J. (2011). Lévy walks evolve through interaction between movement and environmental complexity. *Science*, 332(6037), 1551-1553.
- Delcourt, J., Denoël, M., Ylief, M. and Poncin, P. (2013). Video multitracking of fish behaviour: a synthesis and future perspectives. *Fish and Fisheries*, 14(2), 186-204.
- Del Giudice, M. (2015). Plasticity as a developing trait: exploring the implications. *Frontiers in Zoology*, 12(S1), S4.
- Delignette-Muller, M.L. and Dutang, C. (2015). *fitdistrplus: An R Package for Fitting Distributions*. *Journal of Statistical Software*, 64(4), 1-34.
- Dingemanse N.J. and Dochtermann, N.A. (2013). Quantifying individual variation in behaviour: mixed-effect modelling approaches. *Journal of Animal Ecology*, 82(1), 39-54.
- Dingemanse, N.J. and Wolf, M. (2013). Between-individual differences in behavioural plasticity within populations: causes and consequences. *Animal Behaviour*, 85(5), 1031-1039.
- Dingemanse, N.J., Barber, I., Wright, J. and Brommer, J.E. (2012). Quantitative genetics of behavioural reaction norms: genetic correlations between personality and behavioural plasticity vary across stickleback populations. *Journal of Evolutionary Biology*, 25(3), 485-496.
- Diosdado, J. A. V., Barker, Z. E., Hodges, H. R., Amory, J. R., Croft, D. P., Bell, N. J. and Codling, E. A. (2018). Space-use patterns highlight behavioural differences linked to lameness, parity, and days in milk in barn-housed dairy cows. *PLOS ONE*, 13(12), e0208424.
- Do, T. M. and Gatica-Perez, D. (2013). Human interaction discovery in smartphone proximity networks. *Personal and Ubiquitous Computing*, 17(3), 413-431.

- Dochtermann, N. A., Schwab, T., and Sih, A. (2015). The contribution of additive genetic variation to personality variation: heritability of personality. *Proceedings of the Royal Society B: Biological Sciences*, 282(1798), 20142201.
- Dodge, S., Bohrer, G., Bildstein, K., Davidson, S. C., Weinzierl, R., Bechard, M. J., D., Kays, R., Brandes, D., Han, J. and Wikelski, M. (2014). Environmental drivers of variability in the movement ecology of turkey vultures (*Cathartes aura*) in North and South America. *Philosophical Transactions of the Royal Society B: Biological Sciences*, 369(1643), 20130195.
- Dosmann, A. and Mateo, J. M. (2014). Food, sex and predators: animal personality persists with multidimensional plasticity across complex environments. *Animal Behaviour*, 90, 109-116.
- Dosmann, A. J., Brooks, K. C. and Mateo, J. M. (2015). Within-individual correlations reveal link between a behavioral syndrome, condition, and cortisol in free-ranging belding's ground squirrels. *Ethology*, 121(2), 125-134.
- Dougherty, E. R., Seidel, D. P., Carlson, C. J., Spiegel, O. and Getz, W. M. (2018), Going through the motions: incorporating movement analyses into disease research. *Ecology Letters*, 21(4), 588-604.
- Dray, S., Royer-Carenzi, M. and Calenge, C. (2010). The exploratory analysis of autocorrelation in animal-movement studies. *Ecological Research*, 25(3), 673-681.
- Drost, H.-G. (2018). philentropy: Similarity and Distance Quantification Between Probability Functions. R package version 0.1. 0.
- Duchesne, T., Fortin, D., and Rivest, L. P. (2015). Equivalence between step selection functions and biased correlated random walks for statistical inference on animal movement. *PLOS ONE*, 10(4), e0122947.
- Dujon, A. M., Lindstrom, R. T. and Hays, G. C. (2014). The accuracy of Fastloc-GPS locations and implications for animal tracking. *Methods in Ecology and Evolution*, 5(11), 1162-1169.

- Dybiec, B., Gudowska-Nowak, E., Barkai, E. and Dubkov, A. A. (2017). Lévy flights versus Lévy walks in bounded domains. *Physical Review E*, 95(5), 052102.
- Dziewieczynski, T.L. and Crovo, J.A. (2011) Shyness and boldness differences across contexts in juvenile three-spined stickleback *Gasterosteus aculeatus* from an anadromous population. *Journal of Fish Biology*, 79(3), 776-788.
- Edelhoff, H., Signer, J. and Balkenhol, N. (2016). Path segmentation for beginners: an overview of current methods for detecting changes in animal movement patterns. *Movement Ecology*, 4(1), 21.
- Edwards, A.M., Phillips, R.A., Watkins, N.W., Freeman, M.P., Murphy, E.J., Afanasyev, V., Buldyrev, S.V., da Luz, M.G., Raposo, E.P., Stanley, H.E. and Viswanathan, G.M. (2007). Revisiting Lévy flight search patterns of wandering albatrosses, bumblebees and deer. *Nature*, 449(7165), 1044–8.
- Efford, M. G. (2011). Estimation of population density by spatially explicit capture–recapture analysis of data from area searches. *Ecology*, 92(12), 2202-2207.
- Einstein, A. (1905). Über die von der molekularkinetischen Theorie der Wärme geforderte Bewegung von in ruhenden Flüssigkeiten suspendierten Teilchen. *Annalen der physik*, 322(8), 549-560.
- Englund, G. and Cooper, S. D. (2003). Scale effects and extrapolation in ecological experiments. *Advances in Ecological Research*, Academic Press, 33, 161-213.
- Eriksson, A., Nilsson Jacobi, M., Nyström, J. and Tunstrøm, K. (2010). Determining interaction rules in animal swarms. *Behavioral Ecology*, 21(5), 1106-1111.
- Fagan, W. F. and Calabrese, J. M. (2014). The correlated random walk and the rise of movement ecology. *The Bulletin of the Ecological Society of America*, 95(3), 204-206.
- Firle, S., Bommarco, R., Ekblom, B. and Natiello, M. (1998). The influence of movement and resting behavior on the range of three carabid beetles. *Ecology*, 79(6), 2113–22.

- Fleming, C. H., Sheldon, D., Gurarie, E., Fagan, W. F., LaPoint, S. and Calabrese, J. M. (2017). Kálmán filters for continuous-time movement models. *Ecological Informatics*, 40, 8-21.
- Fleming, C. H., Subaşı, Y. and Calabrese, J. M. (2015). Maximum-entropy description of animal movement. *Physical Review E*, 91(3), 032107.
- Fortin, D., Beyer, H. L., Boyce, M. S., Smith, D. W., Duchesne, T. and Mao, J. S. (2005). Wolves influence elk movements: behavior shapes a trophic cascade in Yellowstone National Park. *Ecology*, 86(5), 1320-1330.
- Fortin, D., Fryxell, J.M., O’Brodovich, L. and Frandsen, D. (2003). Foraging ecology of bison at the landscape and plant community levels: the applicability of energy maximization principles. *Oecologia*, 134(2), 219-227.
- Fortin, D., Morales, J.M. and Boyce, M.S. (2005). Elk winter foraging at fine scale in Yellowstone National Park. *Oecologia*, 145(2), 335–343.
- Fortin, M. J., and Dale, M. R. (2005). *Spatial analysis: a guide for ecologists*. Cambridge University Press.
- Frair, J. L., Merrill, E. H., Visscher, D. R., Fortin, D., Beyer, H. L. and Morales, J. M. (2005). Scales of movement by elk (*Cervus elaphus*) in response to heterogeneity in forage resources and predation risk. *Landscape Ecology*, 20(3), 273-287.
- Fritz, H., Said, S. and Weimerskirch, H. (2003). Scale-dependent hierarchical adjustments of movement patterns in a long-range foraging seabird. *Proceedings of the Royal Society of London. Series B: Biological Sciences*, 270(1520), 1143-1148.
- Fürtbauer, I. and Fry, A. (2018). Social conformity in solitary crabs, *Carcinus maenas*, is driven by individual differences in behavioural plasticity. *Animal Behaviour*, 135, 131-137.
- Fürtbauer, I., Pond, A., Heistermann, M. and King A.J. (2015) Personality, plasticity and predation: linking endocrine and behavioural reaction norms in stickleback

- fish. *Functional Ecology*, 29(7), 931-940.
- Gardiner, J.M., Whitney, N.M. and Hueter, R.E. (2015). Smells Like Home: The Role of Olfactory Cues in the Homing Behavior of Blacktip Sharks, *Carcharhinus limbatus*. *Integrative and Comparative Biology*, 55(3), 495-506.
- Gautrais, J., Ginelli, F., Fournier, R., Blanco, S., Soria, M., Chaté, H. and Theraulaz, G. (2012). Deciphering interactions in moving animal groups. *PLOS Computational Biology*, 8(9), e1002678.
- Gautrais, J., Jost, C., Soria, M., Campo, A., Motsch, S., Fournier, R., Blanco, S. and Theraulaz, G. (2009). Analyzing fish movement as a persistent turning walker. *Journal of Mathematical Biology*, 58(3), 429-445.
- Getz, W. M. and Saltz, D. (2008). A framework for generating and analyzing movement paths on ecological landscapes. *Proceedings of the National Academy of Sciences*, 105(49), 19066-19071.
- Getz, W.M., Marshall, C.R., Carlson, C.J., Giuggioli, L., Ryan, S.J., Romanach, S.S., Boettiger, C., Chamberlain, S.D., Larsen, L., D'Odorico, P. and O'Sullivan, D. (2018). Making ecological models adequate. *Ecology Letters* 21(2), 153-166.
- Gibbs, A. L. and Su, F. E. (2002). On Choosing and Bounding Probability Metrics. *International Statistical Review*, 70(3), 419-435.
- Giles, N. (1987). Predation risk and reduced foraging activity in fish: experiments with parasitized and non-parasitized three-spined sticklebacks, *Gasterosteus aculeatus* L. *Journal of Fish Biology*, 31(1), 37-44.
- Goodwin, B.J. and Fahrig, L. (2002). Effect of landscape structure on the movement behaviour of a specialized goldenrod beetle, *Trirhabda borealis*. *Canadian Journal of Zoology*, 80:24-35.
- Gourret, A., Alford, R. and Schwarzkopf, L. (2011). Very small, light dipole harmonic tags for tracking small animals. *Herpetological Review*, 42, 522-525.

- Gray, J. (1933). Studies in animal locomotion: I. The movement of fish with special reference to the eel. *Journal of Experimental Biology*, 10(1), 88-104.
- Grunbaum, D. (1998). Using spatially explicit models to characterize foraging performance in heterogeneous landscapes. *The American Naturalist*, 151(2), 97-115.
- Grünewälder, S., Broekhuis, F., Macdonald, D.W., Wilson, A.M., McNutt, J.W., Shawe-Taylor, J. and Hailes, S. (2012). Movement Activity Based Classification of Animal Behaviour with an Application to Data from Cheetah (*Acinonyx jubatus*). *PLOS ONE*, 7(11), e49120.
- Gurarie, E. (2008). Models and analysis of animal movements: From individual tracks to mass dispersal (Doctoral dissertation, University of Washington).
- Gurarie, E. and Ovaskainen, O. (2011). Characteristic spatial and temporal scales unify models of animal movement. *The American Naturalist*, 178(1), 113-123.
- Gurarie, E., Bracis, C., Delgado, M., Meckley, T. D., Kojola, I., and Wagner, C. M. (2016). What is the animal doing? Tools for exploring behavioural structure in animal movements. *Journal of Animal Ecology*, 85(1), 69–84.
- Hadfield, J. D. (2010). MCMC methods for multi-response generalized linear mixed models: the MCMCglmm R package. *Journal of Statistical Software*, 33(2), 1-22.
- Harcourt, J. L., Sweetman, G., Johnstone, R. A. and Manica, A. (2009). Personality counts: the effect of boldness on shoal choice in three-spined sticklebacks. *Animal Behaviour*, 77(6), 1501-1505
- Harris, R. J. and Touchette, H. (2009). Current fluctuations in stochastic systems with long-range memory. *Journal of Physics A: Mathematical and Theoretical*, 42(34), 342001.
- Hawkes C. (2009). Linking movement behaviour, dispersal and population processes: is individual variation a key? *Journal of Animal Ecology*, 78(5), 894–906.

- Hazen, E.L., Maxwell, S.M., Bailey, H., Bograd, S.J., Hamann, M., Gaspar, P., Godley, B.J. and Shillinger, G.L. (2012). Ontogeny in marine tagging and tracking science: technologies and data gaps. *Marine Ecology Progress Series*, 457, 221-240.
- Herbert-Read, J. E., Perna, A., Mann, R. P., Schaerf, T. M., Sumpter, D. J. and Ward, A. J. (2011). Inferring the rules of interaction of shoaling fish. *Proceedings of the National Academy of Sciences*, 108(46), 18726-18731.
- Herbert-Read, J.E., Krause, S., Morrell, L.J., Schaerf, T.M., Krause, J. and Ward, A.J.W. (2013). The role of individuality in collective group movement. *Proceedings of the Royal Society B: Biological Sciences*, 280(1752), p.20122564.
- Herborn K.A., Macleod R., Miles W.T.S., Schofield A.N.B., Alexander L. and Arnold K.E. (2010). Personality in captivity reflects personality in the wild. *Animal Behaviour*, 79(4), 835-843.
- Hill, J.M. and Renfrew, R.B. (2019). Migratory patterns and connectivity of two North American grassland bird species. *Ecology and Evolution*, 9(1), 680– 692.
- Hill, N.A., and Häder, D.-P. (1997). A biased random walk model for the trajectories of swimming micro-organisms. *Journal of Theoretical Biology*, 186(4), 503-526.
- Hoare, D. J., Krause, J., Peuhkuri, N. and Godin, J. G. (2000). Body size and shoaling in fish. *Journal of Fish Biology*, 57(6), 1351-1366.
- Holland, J.M., Hutchison, M.A.S., Smith, B. and Aebischer, N.J. (2006). A review of invertebrates and seed-bearing plants as food for farmland birds in Europe. *Annals of Applied Biology*, 148(1), 49–71.
- Holmes, P., Full, R. J., Koditschek, D. and Guckenheimer, J. (2006). The dynamics of legged locomotion: Models, analyses, and challenges. *SIAM review*, 48(2), 207-304.
- Holzmann, H., Munk, A., Suster, M. and Zucchini, W. (2006). Hidden markov models for circular and linear-circular time series. *Environmental and Ecological Statistics*, 13(3), 325–347.

- Hopkins M.E. (2016). Mantled howler monkey spatial foraging decisions reflect spatial and temporal knowledge of resource distributions. *Animal Cognition*, 19(2), 387-403.
- Houslay, T. M. and Wilson, A. J. (2017). Avoiding the misuse of BLUP in behavioural ecology. *Behavioral Ecology*, 28(4), 948-952.
- Hughes, G. M. (1952). The Co-Ordination of insect movements: I The walking movements of insects. *Journal of Experimental Biology*, 29(2), 267-285.
- Huntingford, F.A. (1976). The relationship between anti-predator behaviour and aggression among conspecifics in the three-spined stickleback, *Gasterosteus Aculeatus*. *Animal Behaviour*, 24(2), 245-260.
- Hurford, A. (2009). GPS Measurement Error Gives Rise to Spurious 180 Turning Angles and Strong Directional Biases in Animal Movement Data. *PLOS ONE*, 4(5), e5632.
- Iwajomo, S. B., Willemoes, M. , Ottosson, U. , Strandberg, R. and Thorup, K. (2018). Intra-African movements of the African cuckoo *Cuculus gularis* as revealed by satellite telemetry. *Journal of Avian Biology*, 49(1).
- Jammalamadaka, S. R. and Kozubowski, T. J. (2017). A general approach for obtaining wrapped circular distributions via mixtures. *Sankhya A*, 79(1), 133–157.
- Jammalamadaka, S. R. and Sengupta, A. (2001). *Topics in Circular Statistics*. World Scientific.
- Jansen V. A. A., Mashanova, A. and Petrovskii, S. (2012). Comment on “Lévy walks evolve through interaction between movement and environmental complexity”. *Science*, 335(6071), 918-918.
- JASP Team (2018). JASP (Version 0.9)[Computer software]
- Jeltsch, F., Bonte, D., Pe’er, G., Reineking, B., Leimgruber, P., Balkenhol, N., Schröder, B., Buchmann, C.M., Mueller, T., Blaum, N. and Zurell, D. (2013). Integrating

- movement ecology with biodiversity research—exploring new avenues to address spatiotemporal biodiversity dynamics. *Movement Ecology*, 1(1), 6.
- Jerde, C. L. and Visscher, D. R. (2005). GPS measurement error influences on movement model parameterization. *Ecological Applications*, 15(3), 806–810.
- Johnson, D. S., London, J. M., Lea, M.-A., and Durban, J. W. (2008). Continuous-time correlated random walk model for animal telemetry data. *Ecology*, 89(5), 1208–1215.
- Jolles, J. W., Fleetwood-Wilson, A., Nakayama, S., Stumpe, M. C., Johnstone, R. A. and Manica, A. (2015). The role of social attraction and its link with boldness in the collective movements of three-spined sticklebacks. *Animal Behaviour*, 99, 147-153.
- Jolles, J.W., Laskowski, K.L., Boogert, N.J. and Manica, A. (2018) Repeatable group differences in the collective behaviour of stickleback shoals across ecological contexts. *Proceedings of the Royal Society B: Biological Sciences*, 285(1872), 20172629.
- Jones, M. C. and Pewsey, A. (2005). A family of symmetric distributions on the circle. *Journal of the American Statistical Association*, 100(472), 1422-1428.
- Jonsen, I. (2016). Joint estimation over multiple individuals improves behavioural state inference from animal movement data. *Scientific Reports*, 6, 20625.
- Jonsen, I. D., Basson, M., Bestley, S., Bravington, M. V., Patterson, T. A., Pedersen, M. W., Thomson, R., Thygesen, U. H., and Wotherspoon, S. J. (2013). State-space models for bio-loggers: A methodological road map. *Deep Sea Research Part II: Topical Studies in Oceanography*, 88, 34–46.
- Jonsen, I.D., J. M. Flemming, and R. A. Myers. (2005). Robust state-space modelling of animal movement data. *Ecology*, 86(11), 2874-2880.
- Jopp, F. and Reuter, H. (2005). Dispersal of carabid beetles—emergence of distribution patterns. *Ecological Modelling*, 186(4), 389–405.

- Kanagaraj R., Wiegand T., Kramer-Schadt S. and Goyal S.P. (2013). Using individual-based movement models to assess inter-patch connectivity for large carnivores in fragmented landscapes. *Biological Conservation*, 167, 298-309.
- Kane, A.S., Salierno, J.D., Gipson, G.T., Molteno, T.C.A. and Hunter, C. (2004). A video-based movement analysis system to quantify behavioural stress responses of fish. *Water Research*, 38(18), 3993-4001.
- Kareiva, P.M. and Shigesada, N. (1983). Analyzing insect movement as a correlated random walk. *Oecologia*, 56:234–8.
- Kato, S. and Jones, M. C. (2013). An extended family of circular distributions related to wrapped Cauchy distributions via Brownian motion. *Bernoulli*, 19(1), 154–171.
- King, A.J., Fehlmann, G., Biro, D., Ward, A.J. and Fürtbauer, I. (2018). Re-wilding Collective Behaviour: An ecological perspective. *Trends in Ecology and Evolution*, 33(5), 347-357.
- King, A.J., Fürtbauer, I., Mamuneas, D., James, C. and Manica, A. (2013). Sex-Differences and Temporal Consistency in Stickleback Fish Boldness. *PLOS ONE*, 8(12), e81116.
- King, A.J., Williams, L.J and Mettke-Hofmann, C. (2015). The effects of social conformity on Gouldian finch personality. *Animal Behaviour*, 99, 25-31.
- King, R. (2012). A review of Bayesian state-space modelling of capture–recapture–recovery data. *Interface Focus*, 2(2), 190-204.
- Knell, A. S. and Codling, E. A. (2012). Classifying area-restricted search (ARS) using a partial sum approach. *Theoretical Ecology*, 5(3), 325–339.
- Koski, S. E. (2011). How to measure animal personality and why does it matter? Integrating the psychological and biological approaches to animal personality. In *From genes to animal behavior* (pp. 115-136). Springer, Tokyo.

- Kozak, G. M., Head, M. L., Lackey, A. C. and Boughman, J. W. (2013). Sequential mate choice and sexual isolation in threespine stickleback species. *Journal of Evolutionary Biology*, 26(1), 130-140.
- Kramer, D.L. and McLaughlin, R.L. (2001). The Behavioral Ecology of Intermittent Locomotion. *American Zoologist*, 41(2), 137-53.
- Kramer, E. (1976). The orientation of walking honeybees in odour fields with small concentration gradients. *Physiological Entomology*, 1(1), 27-37.
- Kromp, B. (1999). Carabid beetles in sustainable agriculture: a review on pest control efficacy, cultivation impacts and enhancement. In *Invertebrate biodiversity as bioindicators of sustainable landscapes* (pp. 187-228). Elsevier.
- Landler, L., Ruxton, G.D. and Malkemper, E.P. (2018). Circular data in biology: Advice for effectively implementing statistical procedures. *Behavioral Ecology and Sociobiology*, 72(8), 128.
- Langmaack, M., Land, S. and Büchs, W. (2001). Effects of different field management systems on the carabid coenosis in oil seed rape with special respect to ecology and nutritional status of predacious *Poecilus cupreus* L. (Col., Carabidae). *Journal of Applied Entomology*, 125(6), 313-20.
- Langrock, R., Hopcraft, J. G. C., Blackwell, P. G., Goodall, V., King, R., Niu, M., Patterson, T. A., Pedersen, M. W., Skarin, A., and Schick, R. S. (2014). Modelling group dynamic animal movement. *Methods in Ecology and Evolution*, 5(2), 190-199.
- Langrock, R., King, R., Matthiopoulos, J., Thomas, L., Fortin, D., and Morales, J. M. (2012). Flexible and practical modeling of animal telemetry data: hidden Markov models and extensions. *Ecology*, 93(11), 2336-2342.
- Lemasson, B.H., Anderson, J.J. and Goodwin, R.A. (2009). Collective motion in animal groups from a neurobiological perspective: The adaptive benefits of dynamic

- sensory loads and selective attention. *Journal of Theoretical Biology*, 261(4), 501-510.
- Levin S.A. (1986). Random Walk Models of Movement and Their Implications. In: Hallam T.G., Levin S.A. (Eds.) *Mathematical Ecology*. Biomathematics, vol 17. Springer, Berlin, Heidelberg
- Levins, R. (1984). The strategy of model building in population biology. In *Conceptual Issues in Evolutionary Biology* (Sober, E., ed.), pp. 18–27, Cambridge University Press.
- Li, M. and Bolker, B. M. (2017). Incorporating periodic variability in hidden Markov models for animal movement. *Movement Ecology*, 5(1), 1.
- Lima, S.L. and Zollner, P.A. (1996). Towards a behavioral ecology of ecological landscapes. *Trends in Ecology and Evolution*, 11(3), 131-135.
- Lövei, G.L. and Sunderland, K.D. (1996). Ecology and behavior of ground beetles (Coleoptera: Carabidae). *Annual Review of Entomology*, 41(1), 231–56.
- Lövei, G.L., Stringer, I.A.N., Devine, C.D. and Cartellieri, M. (1997). Harmonic radar - A method using inexpensive tags to study invertebrate movement on land. *New Zealand Journal of Ecology*, 21, 187–93.
- Luff, M.L. (1998). Provisional atlas of the ground beetles (Coleoptera: Carabidae) of Britain. Huntingdon: Biological Records Centre; 1998.
- Luff, M.L. (2002). Carabid assemblage organization and species composition. In: Holland, J.M. (Editor). *The agroecology of Carabid beetles*. Intercept, Andover, UK; 41–80.
- MacLeod, A., Wratten, S.D., Sotherton, N.W. and Thomas, M.B. (2004). ‘Beetle banks’ as refuges for beneficial arthropods in farmland: long-term changes in predator communities and habitat. *Agricultural and Forest Entomology*, 6(2), 147–54.

- Mamuneas, D., Spence, A.J., Manica, A. and King, A.J. (2015). Bolder stickleback fish make faster decisions, but they are not less accurate. *Behavioral Ecology*, 26(1), 91-96.
- Mann, R. P., Perna, A., Strömbom, D., Garnett, R., Herbert-Read, J. E., Sumpter, D. J. and Ward, A. J. (2013). Multi-scale inference of interaction rules in animal groups using Bayesian model selection. *PLOS Computational Biology*, 9(3), e1002961.
- Marcus Rowcliffe, J., Carbone, C., Kays, R., Kranstauber, B. and Jansen, P. A. (2012). Bias in estimating animal travel distance: the effect of sampling frequency. *Methods in Ecology and Evolution*, 3(4), 653-662.
- Mardia, K. V. and Jupp, P. E. (1999). *Circular Data*. In *Directional Statistics*, Wiley Series in Probability and Statistics. John Wiley and Sons, 2nd ed. edition.
- Mardia, K. V. and Sutton, T. W. (1975). On the modes of a mixture of two von Mises distributions. *Biometrika*, 62(3), 699–701.
- Mårell, A., Ball, J. P. and Hofgaard, A. (2002). Foraging and movement paths of female reindeer: insights from fractal analysis, correlated random walks, and Lévy flights. *Canadian Journal of Zoology*, 80(5), 854-865.
- Marsh, L.M., and R. E. Jones. (1988). The form and consequences of random walk movement models. *Journal of Theoretical Biology*, 133(1), 113-131.
- Mashanova, A., Oliver, T. H. and Jansen, V. A. (2009). Evidence for intermittency and a truncated power law from highly resolved aphid movement data. *Journal of the Royal Society Interface*, 7(42), 199-208.
- McClintock, B. T. and Michelot, T. (2018). *momentuhmm*: R package for generalized hidden markov models of animal movement. *Methods in Ecology and Evolution*, 9(6), 1518–1530.
- McClintock, B. T., Johnson, D. S., Hooten, M. B., Ver Hoef, J. M. and Morales, J. M. (2014). When to be discrete: the importance of time formulation in understanding

- animal movement. *Movement Ecology*, 2(1), 21.
- McClintock, B. T., King, R., Thomas, L., Matthiopoulos, J., McConnell, B. J., and Morales, J. M. (2012). A general discrete-time modeling framework for animal movement using multistate random walks. *Ecological Monographs*, 82(3), 335–349.
- McClintock, B. T., London, J. M., Cameron, M. F., and Boveng, P. L. (2015). Modelling animal movement using the Argos satellite telemetry location error ellipse. *Methods in Ecology and Evolution*, 6(3), 266–277.
- McCulloch, C. E. and Cain, M. L. (1989). Analyzing discrete movement data as a correlated random walk. *Ecology*, 70(2), 383–388.
- McKellar, A. E., Kesler, D. C. and Walters, J. R. (2016). Resource selection in restored habitat. *Animal Conservation*, 19, 131–138.
- McKellar, A. E., Langrock, R., Walters, J. R., and Kesler, D. C. (2014). Using mixed hidden Markov models to examine behavioral states in a cooperatively breeding bird. *Behavioral Ecology*, 26(1), 148–157.
- McMahon, C. R., Collier, N., Northfield, J. K. and Glen, F. (2011). Taking the time to assess the effects of remote sensing and tracking devices on animals. *Animal Welfare-The UFAW Journal*, 20(4), 515.
- Metcalf, R.L. and Luckmann, W.H. (1994). *Introduction to Insect Pest Management*. John Wiley and Sons.
- Michelot, T., Langrock, R., and Patterson, T. A. (2016). moveHMM: an R package for the statistical modelling of animal movement data using hidden Markov models. *Methods in Ecology and Evolution*, 7(11), 1308–1315.
- Michelot, T., Langrock, R., Bestley, S., Jonsen, I. D., Photopoulou, T., and Patterson, T. A. (2017). Estimation and simulation of foraging trips in land-based marine predators. *Ecology*, 98(7), 1932–1944.

- Miller, H. J., Dodge, S., Miller, J. and Bohrer, G. (2019). Towards an integrated science of movement: converging research on animal movement ecology and human mobility science. *International Journal of Geographical Information Science*, 1-22.
- Miller, J. R., Turner, M. G., Smithwick, E. A., Dent, C. L. and Stanley, E. H. (2004). Spatial extrapolation: the science of predicting ecological patterns and processes. *BioScience*, 54(4), 310-320.
- Moorcroft P.R. (2012). Mechanistic approaches to understanding and predicting mammalian space use: recent advances, future directions. *Journal of Mammalogy*, 93(4), 903-916.
- Morales J.M. and Ellner S.P. (2002). Scaling up animal movements in heterogeneous landscapes: The importance of behavior. *Ecology*, 83(8), 2240-2247.
- Morales, J. M., Haydon, D. T., Frair, J., Holsinger, K. E. and Fryxell, J. M. (2004). Extracting more out of relocation data: building movement models as mixtures of random walks. *Ecology*, 85(9), 2436-2445.
- Movebank.org. (2019). Movebank. [online] Available at: <https://www.movebank.org/> [Accessed 9 Apr. 2019].
- Muheim, R., Schmaljohann, H. and Alerstam, T. (2018). Feasibility of sun and magnetic compass mechanisms in avian long-distance migration. *Movement Ecology*, 6(1), 8.
- Munden, R., Börger, L., Wilson, R. P., Redcliffe, J., Loison, A., Garel, M. and Potts, J. R. (2019). Making sense of ultrahigh-resolution movement data: A new algorithm for inferring sites of interest. *Ecology and Evolution*, 9(1), 265-274.
- Mundy, C.A., Allen-Williams, L.J., Underwood, N. and Warrington, S. (2000). Prey selection and foraging behaviour by *Pterostichus cupreus* L. (Col., Carabidae) under laboratory conditions. *Journal of Applied Entomology*, 124(9-10), 349-58.

- Mwaffo, V., Anderson, R. P., Butail, S. and Porfiri, M. (2015). A jump persistent turning walker to model zebrafish locomotion. *Journal of The Royal Society Interface*, 12(102), 20140884.
- Nakagawa, S. and Schielzeth, H. (2010). Repeatability for Gaussian and non-Gaussian data: a practical guide for biologists. *Biological Reviews*, 85(4), 935-956.
- Nakagawa, S. and Schielzeth, H. (2013). A general and simple method for obtaining R² from generalized linear mixed-effects models. *Methods in Ecology and Evolution*, 4(2), 133-142.
- Nams, V. O. (2013). Sampling animal movement paths causes turn autocorrelation. *Acta Biotheoretica*, 61(2), 269-284.
- Nams, V. O. (2014). Combining animal movements and behavioural data to detect behavioural states. *Ecology Letters*, 17(10), 1228–1237.
- Nathan, R., Getz, W.M., Revilla, E., Holyoak, M., Kadmon, R., Saltz, D. and Smouse, P.E. (2008). A movement ecology paradigm for unifying organismal movement research. *Proceedings of the National Academy of Sciences*, 105(49), 19052-19059.
- Nations, C., and Anderson-Sprecher, R. (2006). Estimation of animal location from radio telemetry data with temporal dependencies. *Journal of Agriculture, Biological, and Environmental Statistics*, 11(1), 87–105.
- Nelder, J. A., and Mead, R. (1965). A simplex method for function minimization. *The Computer Journal*, 7(4), 308-313.
- Nicosia, A., Duchesne, T., Rivest, L.-P., and Fortin, D. (2017). A general hidden state random walk model for animal movement. *Computational Statistics and Data Analysis*, 105, 76-95.
- Nilsen, C., Paige, J., Warner, O., Mayhew, B., Sutley, R., Lam, M., Bernoff, A. J., and Topaz, C. M. (2013). Social aggregation in pea aphids: Experiment and random walk modeling. *PLOS ONE*, 8(12), 1–11.

- Nilsson, J. Å., Bronmark, C., Hansson, L. A. and Chapman, B. B. (2014). Individuality in movement: The role of animal personality. *Animal Movement Across Scales*, 90-109.
- Niu, M., Blackwell, P. G. and Skarin, A. (2016). Modeling interdependent animal movement in continuous time. *Biometrics*, 72(2), 315-324.
- Offermans, R. (2004). *Gasterosteus aculeatus* https://commons.wikimedia.org/wiki/File:Gasterosteus_aculeatus.jpg
- Ose, N. J. and Ohmann, P. R. (2017). The selfish herd: Noise effects in Local Crowded Horizon and Voronoi models. *Journal of Theoretical Biology*, 424, 84-90.
- Parton, A. and Blackwell, P. G. (2017). Bayesian Inference for Multistate ‘Step and Turn’ Animal Movement in Continuous Time. *Journal of Agricultural, Biological and Environmental Statistics*, 22(3), 373–392.
- Patlak, C. S. (1953). Random walk with persistence and external bias. *The Bulletin of Mathematical Biophysics*, 15(3), 311-338.
- Patrick, S.C. and Weimerskirch, H. (2014). Personality, Foraging and Fitness Consequences in a Long Lived Seabird. *PLOS ONE* 9(2), e87269.
- Patterson, T. A., Basson, M., Bravington, M. V., and Gunn, J. S. (2009). Classifying movement behaviour in relation to environmental conditions using hidden Markov models. *Journal of Animal Ecology*, 78(6), 1113–1123.
- Patterson, T. A., McConnell, B. J., Fedak, M. A., Bravington, M. V., and Hindell, M. A. (2010). Using GPS data to evaluate the accuracy of state–space methods for correction of Argos satellite telemetry error. *Ecology*, 91(1), 273–285.
- Patterson, T. A., Thomas, L., Wilcox, C., Ovaskainen, O. and Matthiopoulos, J. (2008). State–space models of individual animal movement. *Trends in Ecology and Evolution*, 23(2), 87-94.

- Patterson, T.A., Parton, A., Langrock, R., Blackwell, P.G., Thomas, L. and King, R. (2017). Statistical modelling of individual animal movement: an overview of key methods and a discussion of practical challenges. *AStA Advances in Statistical Analysis*, 101(4), 399-438.
- Pearce, R.F., Giuggioli, L. and Rands, S.A. (2017). Bumblebees can discriminate between scent-marks deposited by conspecifics. *Scientific Reports*, 7, 43872.
- Pearson, K. (1905). The problem of the random walk. *Nature*, 72(1867), 342.
- Peck, S. B. (2001). *Smaller orders of insects of the Galápagos Islands, Ecuador: evolution, ecology, and diversity*. NRC Research Press.
- Peleg, O. and L. Mahadevan. (2016). Optimal switching between geocentric and egocentric strategies in navigation. *Royal Society Open Science*, 3(7), 160128.
- Penke, L., Denissen, J. J., and Miller, G. F. (2007). The evolutionary genetics of personality. *European Journal of Personality: Published for the European Association of Personality Psychology*, 21(5), 549-587.
- Pérez-Barbería, F.J., Small, M., Hooper, R.J., Aldezabal, A., Soriguer-Escofet, R., Bakken, G.S. and Gordon, I.J. (2015). State-space modelling of the drivers of movement behaviour in sympatric species. *PLOS ONE*, 10(11), e0142707.
- Pérez-Escudero, A., Vicente-Page, J., Hinz, R. C., Arganda, S. and De Polavieja, G. G. (2014). idTracker: tracking individuals in a group by automatic identification of unmarked animals. *Nature Methods*, 11(7), 743.
- Petrovskii, S., Mashanova, A. and Jansen, V.A.A. (2011). Variation in individual walking behavior creates the impression of a Lévy flight. *PNAS*, 108(21), 8704-8707.
- Petrovskii, S., Petrovskaya, N. and Bearup, D. (2014). Multiscale approach to pest insect monitoring: Random walks, pattern formation, synchronization, and networks. *Physics of Life Reviews*, 11(3), 467-525.

- Pettit, B., Perna, A., Biro, D. and Sumpter, D. J. (2013). Interaction rules underlying group decisions in homing pigeons. *Journal of the Royal Society Interface*, 10(89), 20130529.
- Pewsey, A., Lewis, T., and Jones, M. C. (2007). The Wrapped t Family of Circular Distributions. *Australian and New Zealand Journal of Statistics*, 49(1), 79–91.
- Pinaud, D. (2008). Quantifying search effort of moving animals at several spatial scales using first-passage time analysis: effect of the structure of environment and tracking systems. *Journal of Applied Ecology*, 45(1), 91-99.
- Pistorius, P., Hindell, M., Crawford, R., Makhado, A., Dyer, B., and Reisinger, R. (2017). At-sea distribution and habitat use in king penguins at sub-Antarctic Marion Island. *Ecology and Evolution*, 7(11), 3894–3903.
- Plank, M. J. and Codling, E. A. (2009). Sampling rate and misidentification of Lévy and non-Lévy movement paths. *Ecology*, 90(12), 3546-3553.
- Plank, M. J., Auger-Méthé, M., and Codling, E. A. (2013). Lévy or Not? Analysing Positional Data from Animal Movement Paths. In Lewis, M. A., Maini, P. K., and Petrovskii, S. V., editors, *Dispersal, Individual Movement and Spatial Ecology*, volume 2071, pages 33–52. Springer Berlin Heidelberg, Berlin, Heidelberg.
- Pocock, M.J.O. and Jennings, N. (2007). Testing biotic indicator taxa: the sensitivity of insectivorous mammals and their prey to the intensification of lowland agriculture. *Journal of Applied Ecology*, 45(1), 151–60.
- Polansky, L., Wittemyer, G., Cross, P.C., Tambling, C.J. and Getz, W.M. (2010). From moonlight to movement and synchronized randomness: Fourier and wavelet analyses of animal location time series data. *Ecology*, 91(5), 1506–1518.
- Postlethwaite, C. M. and Dennis, T. E. (2013). Effects of Temporal Resolution on an Inferential Model of Animal Movement. *PLOS ONE*, 8(5), e57640.

- Preisler, H. K., Brillinger, D. R., Ager, A. A., Kie, J. G. and Akers, R. P. (2001). Stochastic differential equations: a tool for studying animal movement. In Proc. IUFRO 4.11 Conference, Greenwich 26-29 June.
- Proulx, C. L., Proulx, L. and Blouin-Demers, G. (2013). Improving the realism of random walk movement analyses through the incorporation of habitat bias. *Ecological Modelling*, 269, 18-20.
- Pyke, G. H. (2015). Understanding movements of organisms: it's time to abandon the Lévy foraging hypothesis. *Methods in Ecology and Evolution*, 6(1), 1-16.
- R Core Team (2018). *R: A Language and Environment for Statistical Computing*. R Foundation for Statistical Computing, Vienna, Austria.
- Raichlen, D. A., Wood, B. M., Gordon, A. D., Mabulla, A. Z., Marlowe, F. W. and Pontzer, H. (2014). Evidence of Lévy walk foraging patterns in human hunter-gatherers. *Proceedings of the National Academy of Sciences*, 111(2), 728-733.
- Rainio, J. and Niemelä, J. (2003). Ground beetles (Coleoptera: Carabidae) as bioindicators. *Biodiversity and Conservation*, 12(3), 487-506.
- Ravindran, P. and Ghosh, S. K. (2011). Bayesian Analysis of Circular Data Using Wrapped Distributions. *Journal of Statistical Theory and Practice*, 5(4), 547-561.
- Rayleigh, J.W.S. (1905). The Problem of the Random Walk. *Nature*, 72, 318.
- Recio, M. R., Mathieu, R., Denys, P., Sirguy, P. and Seddon, P. J. (2011). Lightweight GPS-tags, one giant leap for wildlife tracking? An assessment approach. *PLOS ONE*, 6(12), e28225.
- Reynolds, A. M., Leprêtre, L. and Bohan, D. A. (2013). Movement patterns of *Tenebrio* beetles demonstrate empirically that correlated-random-walks have similitude with a Lévy walk. *Scientific reports*, 3, 3158.

- Reynolds, A.M. (2014). Towards a mechanistic framework that explains correlated random walk behaviour: Correlated random walkers can optimize their fitness when foraging under the risk of predation. *Ecological Complexity*, 19, 18-22.
- Rijnsdorp, A.D. (1980). Pattern of movement in and dispersal from a dutch forest of *Carabus problematicus* Hbst. (Coleoptera, Carabidae). *Oecologia*, 45(2), 274-81.
- Rivest, L.P., Duchesne, T., Nicosia, A. and Fortin, D. (2016). A general angular regression model for the analysis of data on animal movement in ecology. *Journal of the Royal Statistical Society: Series C (Applied Statistics)*, 65(3), 445-463.
- Robinson, W.D., Bowlin, M.S., Bisson, I., Shamoun-Baranes, J., Thorup, K., Diehl, R.H., Kunz, T.H., Mabey, S. and Winkler, D.W. (2010). Integrating concepts and technologies to advance the study of bird migration. *Frontiers in Ecology and the Environment*, 8(7), 354-361.
- Rodríguez, J.P., Fernández-Gracia, J., Thums, M., Hindell, M.A., Sequeira, A.M., Meekan, M.G., Costa, D.P., Guinet, C., Harcourt, R.G., McMahon, C.R. and Muelbert, M. (2017). Big data analyses reveal patterns and drivers of the movements of southern elephant seals. *Scientific reports*, 7(1), 112.
- Rosser, G., Fletcher, A.G., Maini, P.K. and Baker, R.E. (2013) The effect of sampling rate on observed statistics in a correlated random walk. *Journal of The Royal Society Interface*, 10(85), 20130273.
- Roy, S. and Adnan, M. A. S. (2012). Wrapped Generalized Gompertz distribution: an Application to Ornithology. *Journal of Biometrics and Biostatistics*, 3(6), 153-156.
- Sapiezynski, P., Stopczynski, A., Wind, D. K., Leskovec, J. and Lehmann, S. (2017). Inferring person-to-person proximity using WiFi signals. *Proceedings of the ACM on Interactive, Mobile, Wearable and Ubiquitous Technologies*, 1(2), 24.
- Schindler, D.W. (1998). Replication versus realism: the need for ecosystem-scale experiments. *Ecosystems*, 1(4), 323-334

- Schmidt, U. (2008). *Poecilus cupreus*. https://upload.wikimedia.org/wikipedia/commons/0/0c/Poecilus_cupreus_%28Linn%C3%A9%2C_1758%29_%282929073677%29.jpg. Accessed 5 May 2018.
- Schtickzelle, N., Joiris, A., Van Dyck, H., and Baguette, M. (2007). Quantitative analysis of changes in movement behaviour within and outside habitat in a specialist butterfly. *BMC Evolutionary Biology*, 7(1), 4.
- Schultz, C. B. and Crone, E. E. (2001). Edge-mediated dispersal behavior in a prairie butterfly. *Ecology*, 82(7), 1879–1892.
- Schütz, G. M. and Trimper, S. (2004). Elephants can always remember: Exact long-range memory effects in a non-Markovian random walk. *Physical Review E*, 70(4), 045101.
- Seoane, N. (2015). Modelling free-range cattle movements in forests using multistate random walks. *Journal of Biological Systems*, 23(supp01):S43–S54.
- Seuront, L. (2015). On uses, misuses and potential abuses of fractal analysis in zooplankton behavioral studies: A review, a critique and a few recommendations. *Physica A: Statistical Mechanics and its Applications*, 432, 410-434.
- Shimatani, I.K., Yoda, K., Katsumata, N. and Sato, K. (2012). Toward the Quantification of a Conceptual Framework for Movement Ecology Using Circular Statistical Modeling. *PLOS ONE* 7(11): e50309.
- Sih, A. and Bell, A.M. (2008). Insights for behavioural ecology from behavioural syndromes. *Advances in the Study of Behavior*, 38, 227-281.
- Sih, A., Cote, J., Evans, M., Fogarty, S. and Pruitt, J. (2012). Ecological implications of behavioural syndromes. *Ecology Letters*, 15(3), 278-289.
- Sih, A., Ferrari, M.C. and Harris, D.J. (2011). Evolution and behavioural responses to human-induced rapid environmental change. *Evolutionary Applications*, 4(2), 367-87.

- Sih, A., Spiegel, O., Godfrey, S., Leu, S. and Bull, C.M. (2018). Integrating social networks, animal personalities, movement ecology and parasites: a framework with examples from a lizard. *Animal Behaviour*, 136, 195-205.
- Sims, D. W., Humphries, N. E., Bradford, R. W. and Bruce, B. D. (2012). Lévy flight and Brownian search patterns of a free-ranging predator reflect different prey field characteristics. *Journal of Animal Ecology*, 81(2), 432-442.
- Sims, D. W., Queiroz, N., Humphries, N. E., Lima, F. P. and Hays, G. C. (2009). Long-term GPS tracking of ocean sunfish *Mola mola* offers a new direction in fish monitoring. *PLOS ONE*, 4(10), e7351
- Sims, D.W., Righton, D. and Pitchford, J.W. (2007). Minimizing errors in identifying Lévy flight behaviour of organisms. *Journal of Animal Ecology*, 76(2), 222-229.
- Šlachta, M. and Vokoun, J. (2011). Impact of a pyrethroid insecticide application on ground beetles (Coleoptera: Carabidae) in a winter rape stand. *Acta Universitatis Agriculturae et Silviculturae Mendelianae Brunensis*, 59(3), 179–84.
- Sokolov, I. M. (2012). Models of anomalous diffusion in crowded environments. *Soft Matter*, 8(35), 9043-9052.
- Souman, J. L., Frissen, I., Sreenivasa, M. N., Ernst, M. O. (2009). Walking straight into circles. *Current Biology*, 19(18), 1538-1542.
- Spiegel, O., Harel, R., Getz, W.M. and Nathan, R. (2013). Mixed strategies of griffon vultures' (*Gyps fulvus*) response to food deprivation lead to a hump-shaped movement pattern. *Movement ecology*, 1(1), 5.
- Spiegel, O., Leu, S.T., Bull, C.M. and Sih, A. (2017). What's your move? Movement as a link between personality and spatial dynamics in animal populations. *Ecology Letters* 20(1), 3-18.
- Srinivas, M and Sambasivarao, S. (2016). Importance of circular data in sports science – A review. *International Journal of Advanced and Applied Sciences*, 1, 37-44.

- Srivastava, D.S., Kolasa, J., Bengtsson, J., Gonzalez, A., Lawler, S.P., Miller, T.E., Munguia, P., Romanuk, T., Schneider, D.C. and Trzcinski, M.K. (2004). Are natural microcosms useful model systems for ecology?. *Trends in Ecology and Evolution*, 19(7), 379-384.
- Stanley, C. R., Mettke-Hofmann, C. and Preziosi, R. F. (2017). Personality in the cockroach *Diploptera punctata*: Evidence for stability across developmental stages despite age effects on boldness. *PLOS ONE*, 12(5), e0176564.
- Stephens, K., Pham, B., and Wardhani, A. (2003). Modelling fish behaviour. In Proceedings of the 1st international conference on computer graphics and interactive techniques in Australasia and South East Asia (pp. 71-78). ACM.
- Stephens, M. A. (1963). Random Walk on a Circle. *Biometrika*, 50(3-4), 385–390.
- Stevens, A., and Othmer, H. G. (1997). Aggregation, blowup, and collapse: the ABC's of taxis in reinforced random walks. *SIAM Journal on Applied Mathematics*, 57(4), 1044-1081.
- Stoffel, M. A., Nakagawa, S. and Schielzeth, H. (2017). rptR: Repeatability estimation and variance decomposition by generalized linear mixed-effects models. *Methods in Ecology and Evolution*, 8(11), 1639-1644.
- Sueur, C., King, A.J., Conradt, L., Kerth, G., Lusseau, D., Mettke-Hofmann, C., Schaffner, C.M., Williams, L., Zinner, D. and Aureli, F. (2011). Collective decision-making and fission-fusion dynamics: a conceptual framework. *Oikos*, 120(11), 1608-1617.
- Syntech. TrackSphere Locomotion Compensator Model LC-300. User guide. Syntech Hilversum, The Netherlands. 2004.
- Taylor-King, J. P., Loon, E. E. v., Rosser, G., and Chapman, S. J. (2015). From Birds to Bacteria: Generalised Velocity Jump Processes with Resting States. *Bulletin of Mathematical Biology*, 77(7), 1213–1236.

- Teimouri, M., Indahl, U., Sickel, H. and Tveite, H. (2018). Deriving animal movement behaviors using movement parameters extracted from location data. *ISPRS International Journal of Geo-Information*, 7(2), 78.
- Therrien, J. F., Pinaud, D., Gauthier, G., Lecomte, N., Bildstein, K. L. and Bety, J. (2015). Is pre-breeding prospecting behaviour affected by snow cover in the irruptive snowy owl? A test using state-space modelling and environmental data annotated via Movebank. *Movement Ecology*, 3(1), 1.
- Thiel, F., Schimansky-Geier, L. and Sokolov, I. M. (2012). Anomalous diffusion in run-and-tumble motion. *Physical Review E*, 86(2), 021117.
- Thomas, C.F.G., Green, F. and Marshall, E.J.P. (1997). Distribution, Dispersal and Population Size of the Ground Beetles, *Pterostichus melanarius* (Illiger) and *Harpalus rufipes* (Degeer) (Coleoptera, Carabidae), in Field Margin Habitats. *Biological Agriculture and Horticulture*, 15(1-4), 337–52.
- Thomas, C.F.G., Parkinson, L. and Marshall, E.J.P. (1998). Isolating the components of activity-density for the carabid beetle *Pterostichus melanarius* in farmland. *Oecologia*, 116(1-2), 103–12.
- Thomas, M.B., Wratten, S.D. and Sotherton, N.W. (1991). Creation of “Island” Habitats in Farmland to Manipulate Populations of Beneficial Arthropods: Predator Densities and Emigration. *Journal of Applied Ecology*, 28, 906–17.
- Thums, M., Fernández-Gracia, J., Sequeira, A. M., Eguíluz, V. M., Duarte, C. M. and Meekan, M. G. (2018). How big data fast tracked human mobility research and the lessons for animal movement ecology. *Frontiers in Marine Science*, 5, 21.
- Torres, L. G., Orben, R. A., Tolkova, I., and Thompson, D. R. (2017). Classification of Animal Movement Behavior through Residence in Space and Time. *PLOS ONE*, 12(1), e0168513.
- Tremblay, Y., Roberts, A. J. and Costa, D. P. (2007). Fractal landscape method: an

- alternative approach to measuring area-restricted searching behavior. *Journal of Experimental Biology*, 210(6), 935-945.
- Turchin, P. (1996). Fractal analyses of animal movement: a critique. *Ecology*, 77(7), 2086-2090.
- van de Kerk, M., Onorato, D. P., Criffield, M. A., Bolker, B. M., Augustine, B. C., McKinley, S. A., and Oli, M. K. (2015). Hidden semi-Markov models reveal multiphasic movement of the endangered Florida panther. *Journal of Animal Ecology*, 84(2), 576-585.
- Van Moorter, B., Rolandsen, C. M., Basille, M. and Gaillard, J. M. (2016). Movement is the glue connecting home ranges and habitat selection. *Journal of Animal Ecology*, 85(1), 21-31.
- Virkar, Y. and Clauset, A. (2014). Power-law distributions in binned empirical data. *The Annals of Applied Statistics*, 8(1), 89-119.
- Viswanathan, G. M., Afanasyev, V., Buldyrev, S. V., Murphy, E. J., Prince, P. A. and Stanley, H. E. (1996). Lévy flight search patterns of wandering albatrosses. *Nature*, 381(6581), 413.
- Viswanathan, G. M., Raposo, E. P. and Da Luz, M. G. E. (2008). Lévy flights and superdiffusion in the context of biological encounters and random searches. *Physics of Life Reviews*, 5(3), 133-150.
- Von Smoluchowski, M. (1906). Zur kinetischen theorie der brownschen molekularbewegung und der suspensionen. *Annalen der physik*, 326(14), 756-780.
- Wall, J., Wittemyer, G., LeMay, V., Douglas-Hamilton, I., and Klinkenberg, B. (2014a). Data from: Elliptical Time-Density model to estimate wildlife utilization distributions.
- Wall, J., Wittemyer, G., LeMay, V., Douglas-Hamilton, I., and Klinkenberg, B. (2014b).

- Elliptical Time-Density model to estimate wildlife utilization distributions. *Methods in Ecology and Evolution*, 5(8), 780–790.
- Wallin, H. and Ekbom, B. (1994). Influence of Hunger Level and Prey Densities on Movement Patterns in Three Species of Pterostichus Beetles (Coleoptera: Carabidae). *Environmental Entomology*, 23(5), 1171–81.
- Webster, M.M. and Hart, P.J. (2006). Subhabitat selection by foraging threespine stickleback (*Gasterosteus aculeatus*): previous experience and social conformity. *Behavioral Ecology and Sociobiology*, 60(1), 77-86.
- Weiss, G. H. (Ed.). (1994). *Contemporary problems in statistical physics*. Society for Industrial and Applied Mathematics.
- Westley, P.A.H., Berdahl, A.M., Torney, C.J. and Biro, D. (2018). Collective movement in ecology: from emerging technologies to conservation and management. *Philosophical Transactions of the Royal Society B-Biological Sciences* 373(1746).
- White, E.P., Enquist, B.J. and Green, J.L. (2008). On estimating the exponent of power-law frequency distributions. *Ecology*, 89(4), 905-912.
- Whoriskey, K., Auger-Méthé, M., Albertsen, C.M., Whoriskey, F.G., Binder, T.R., Krueger, C.C. and Mills Flemming, J. (2017). A hidden Markov movement model for rapidly identifying behavioral states from animal tracks. *Ecology and Evolution*, 7(7), 2112-2121.
- Williams, B. K., Nichols, J. D. and Conroy, M. J. (2002). *Analysis and management of animal populations*. Academic Press
- Wilson, D. S., Coleman, K., Clark, A. B. and Biederman, L. (1993). Shy-bold continuum in pumpkinseed sunfish (*Lepomis gibbosus*): An ecological study of a psychological trait. *Journal of Comparative Psychology*, 107(3), 250.
- With, K.A., Cadaret, S.J. and Davis C. (1999). Movement responses to patch structure in experimental fractal landscapes. *Ecology*, 80(4), 1340-1353.

- Wolf, M. and Weissing, F.J. (2012). Animal personalities: consequences for ecology and evolution. *Trends in Ecology and Evolution*, 27(8), 452-461.
- Wu, H.-i., Li, B.-L., Springer, T.A. and Neill, W.H. (2000). Modelling animal movement as a persistent random walk in two dimensions: expected magnitude of net displacement. *Ecological Modelling*, 132(1-2), 115-124.
- Young, H. C., Reid, T. G., Randall, L. A., Lachowsky, L. E., Foster, D. J., Pengelly, C. J., Latty, T., and Reid, M. L. (2013). Influences of Movement Behavior on Animal Distributions at Edges of Homogeneous Patches. *International Journal of Zoology*, 2013.
- Zaburdaev, V., Denisov, S. and Klafter, J. (2015). Lévy walks. *Reviews of Modern Physics*, 87(2), 483.
- Zienkiewicz, A., Barton, D. A., Porfiri, M. and Di Bernardo, M. (2015). Data-driven stochastic modelling of zebrafish locomotion. *Journal of Mathematical Biology*, 71(5), 1081-1105.